



**Effect of Histotripsy in decellularization of liver tissue &
Histotripsy-assisted stem cell derived 3D-hepatocyte
implantation for liver regeneration**

Saied Froghi

Thesis submitted for the degree of

Doctor of Philosophy (PhD)

Division of Surgery and Interventional Science

University College London

2024

Author's Declaration Statement

I, Saied Froghi, confirm that I have accomplished and written all the work explained in this thesis. This work is original, any parts that have been shown as part of teamwork are clearly indicated, and all external references are clearly cited.

Signed

Saied Froghi

Acknowledgements

I would like to extend my heartfelt gratitude to Professor Brian Davidson for his exceptional guidance, steadfast support, and mentorship during the entirety of my project and the development of this thesis. His expertise and insightful feedback have been pivotal to the success of my research. I am also deeply thankful to Professor Barry Fuller, my secondary supervisor, for his invaluable advice and expertise. Furthermore, I sincerely appreciate the contributions and support of our collaborators Professor Nader Saffari and Professor Alberto Quaglia throughout this project as their expertise has proven invaluable in the progression of the project. Also, I would like to thank contribution of Dr. Hasan Rashidi whose knowledge of stem cell and contribution has been pivotal to the key experiments and Dr Gelat whose expertise in histotripsy has been essential in the development of the projects.

Their collective dedication and assistance have been pivotal to my academic and personal growth, and I am profoundly thankful for their involvement in my journey.

I wish to also thank all the PhD students and colleagues whom I have had the pleasure of working alongside: Farid Froghi, Amjad Khalil, Alex Chiu, Carolina Ramos, Elena Zattera, Kelly Bokea, Maryam Hadi, Layla Hadi, Matheus de Andrades, Kurinchi Gurusamy, Reza Haghshenas, Amir Afrashteh, Guiseppe Fusai, Satya Bhattacharya & Hemant Kocher (The London Clinic Colleagues), Staff in Griffith's Institute, and HCA Wellington Hospital who kindly funded part of the PhD program and allowed participation in their fellowship program.

Dedication

This thesis is dedicated to my beloved parents, Mohammad and Maryam, whose unwavering support has been my guiding light throughout my PhD journey. I also dedicate it to my amazing wife, Mahad, and my daughters, Roya and Leyla. Their boundless love, patience, and encouragement have been the cornerstone of my strength and determination. Their presence fills my life with joy and inspiration, and I am profoundly grateful for their unwavering support during this academic pursuit.

Abstract

Chronic liver diseases, including cirrhosis and hepatocellular carcinoma, remain significant global health challenges due to their high morbidity and limited therapeutic options. This thesis investigates the potential of histotripsy, a non-invasive focused ultrasound technology, in two innovative applications: decellularization of liver tissue and facilitation of stem cell-derived 3D-hepatocyte transplantation for liver regeneration.

The first segment explores histotripsy's efficacy in generating acellular liver scaffolds, emphasizing its mechanical precision in preserving vascular structures while minimizing collateral damage. Experimental methods, including histological assessments and 3D tissue reconstructions, demonstrate the feasibility of histotripsy for creating biocompatible scaffolds, paving the way for advanced tissue engineering applications.

The second segment evaluates histotripsy-assisted implantation of stem cell-derived 3D hepatocyte spheroids in rodent models, aiming to overcome challenges in cell delivery, engraftment, and survival. Key findings include improved cell viability, enhanced tissue integration, and evidence of functional liver regeneration post-implantation. The thesis highlights histotripsy's potential to synergize with regenerative therapies, offering a transformative approach to address organ shortages and advance treatment strategies for end-stage liver diseases.

These findings underscore histotripsy's dual utility in liver tissue engineering and regenerative medicine, offering a foundation for future translational research and clinical applications.

Thesis Impact Statement

This thesis addresses critical challenges in the management of chronic liver diseases, including cirrhosis and hepatocellular carcinoma, which are among the leading causes of morbidity and mortality worldwide. The innovative use of histotripsy—a non-invasive, focused ultrasound technology—offers transformative potential in both liver tissue engineering and regenerative medicine. The thesis represents a number of packages of work carried across an interdisciplinary collaborative team including Surgeons, Engineers, Pathologists, Stem Cell biologist to name a few.

The research findings have significant implications across multiple domains:

1. **Advancing Liver Tissue Engineering:** The study demonstrates the feasibility of using histotripsy for the decellularization of liver tissues, creating biocompatible scaffolds while preserving essential vascular and biliary structures. This approach provides a novel, non-enzymatic alternative to traditional decellularization methods, overcoming key limitations such as enzymatic damage and suboptimal structural integrity. These insights pave the way for developing functional bioengineered liver grafts, addressing the critical organ shortage crisis.
2. **Enhancing Regenerative Medicine:** By leveraging histotripsy to facilitate the delivery and engraftment of stem cell-derived 3D hepatocytes, the research introduces a minimally invasive technique to improve cell viability, integration, and functionality in regenerating damaged liver tissues. This innovation has the potential to revolutionize cell therapy strategies for end-stage liver disease, reducing dependence on whole-organ transplantation.
3. **Clinical and Translational Impact:** The combined applications of histotripsy in decellularization and cell transplantation offer a scalable, non-invasive, and cost-

effective solution for addressing liver disease at various stages. These findings support the transition of histotripsy-based therapies from experimental models to clinical settings, benefiting patients with limited treatment options.

4. **Broader Scientific and Societal Implications:** The interdisciplinary methodologies and technologies developed in this research contribute to the broader fields of ultrasound-based therapies, regenerative medicine, and bioengineering. The successful translation of these approaches could catalyse advancements in the treatment of other organ systems, creating new paradigms for managing organ failure and chronic diseases.

By combining cutting-edge ultrasound technology with stem cell therapies, this thesis lays the groundwork for innovative, patient-centred solutions that could alleviate the global burden of liver disease. It highlights the potential of integrating emerging biomedical technologies to bridge the gap between basic science and clinical application.

Table of Contents

Author's Declaration Statement	2
Acknowledgements	3
Dedication	4
Abstract	5
Thesis Impact Statement	6
Table of Contents	8
Chapter 1 Clinical background to chronic liver disease and liver transplantation	14
1.1.1 Introduction:	15
1.1.2 Epidemiology.....	17
1.1.3 Aetiology of Cirrhosis	17
1.1.4 Pathophysiology of Chronic Liver disease/Cirrhosis:	18
1.1.5 Clinical Presentation	24
1.1.6 Diagnosis	29
1.1.7 Classifying severity of liver disease.....	32
1.1.8 Cirrhosis & Risk of HCC.....	34
1.1.9 Treatment Strategies	34
1.1.10 Liver Transplantation	37
1.2 <i>Cell therapy & other regenerative treatment strategies</i>	<i>37</i>
1.2.1 Primary Hepatocyte Transplantation (HTx):	38
1.2.2 Stem Cells:.....	40
1.2.3 Induced Pluripotent Stem Cells (iPSCs):.....	44
1.2.4 Bioengineering:	45
1.2.5 Organoids:	47
1.2.6 3D printing:	48
1.3 <i>Conclusion</i>	<i>48</i>
Chapter 2 Therapeutic Ultrasound and applications	50
2.1 <i>Introduction</i>	<i>51</i>
2.2 <i>High-Intensity Focused Ultrasound (HIFU)</i>	<i>55</i>
2.2.1 Biophysical effects.....	55
2.3 <i>Different modalities of focused ultrasound (FU).....</i>	<i>61</i>

2.4	<i>Clinical applications of focused Ultrasound</i>	62
2.4.1	Neurology:.....	62
2.4.2	Drug Delivery:.....	63
2.5	<i>Focused Ultrasound in hepatobiliary Malignancies</i>	65
2.5.1	Liver Cancer.....	65
2.5.2	Pancreatic cancer	71
2.6	<i>Histotripsy & its role in liver regeneration</i>	73
2.6.1	Experimental Models:	76
2.6.2	State of the art:	84
2.7	<i>Thesis hypothesis</i>	84
2.8	<i>Thesis aims</i>	85
2.9	<i>Thesis objectives</i>	85
Chapter 3	Methods	87
3.1	<i>Overall experimental method</i>	87
3.2	<i>Organ retrieval and transport</i>	88
3.3	<i>Modelling to define the histotripsy parameters</i>	89
3.4	<i>Histotripsy set up</i>	90
3.5	<i>Organ perfusion, histotripsy lesion formation and assessment</i>	92
	Perfusion set up:	92
3.6	<i>Tissue sampling</i>	93
3.7	<i>H&E and histochemical stains</i>	94
3.7.1	H&E Stain:	94
3.7.2	Picrosirius Red Stain:	94
3.7.3	Reticulin Stain:	95
3.8	<i>3D reconstruction of histotripsy site</i>	95
3.9	<i>Pre-culture light microscopy:</i>	98
3.10	<i>Cell culture: cell morphology and growth</i>	98
3.11	<i>Phalloidin/ Dapi staining</i>	98
3.12	<i>Live-Dead assay</i>	99
3.13	<i>Morphology assessment:</i>	100
3.14	<i>Cell Titre-Glo Metabolic Assay:</i>	100
3.15	<i>Histological evaluation of the excised histotripsy sites for 3D reconstruction</i>	101
3.15.1	Haematoxylin & Eosin (H&E) staining:	101
3.15.2	Picrosirius red stain:.....	101

3.15.3	Reticulin Stains:.....	102
3.16	<i>3D Hep generation, Differentiation & Maintenance</i>	102
3.16.1	Generation of self-aggregated hiPSC spheroids:	102
3.16.2	Differentiation into 3D Heps:.....	103
3.16.3	Maintenance of human induced pluripotent stem cells (hiPSCs):.....	103
3.16.4	Pre-implant evaluation: Functional characterisation.....	104
3.16.5	Immunofluorescence staining of the 3D Heps:.....	106
3.17	<i>Enzyme-Linked Immunosorbent Assay (ELISA)</i>	106
3.18	<i>Cytochrome P450 Assay</i>	107
3.19	<i>ImageJ Software:</i>	108
3.20	<i>Statistical methods:</i>	108
Chapter 4	Preliminary histological analysis of perfused versus non-perfused ex-vivo porcine liver and histotripsy calibration	109
4.1	<i>Introduction</i>	110
4.2	<i>Methods:</i>	113
4.2.1	Histotripsy setup (Full details in methods chapter)	113
4.2.2	Tissue sampling	116
4.2.3	Histology.....	118
4.2.4	Microscopy	118
4.2.5	Quantitative analysis.....	118
4.3	<i>Results</i>	120
4.3.1	Parameter analysis and histology correlation of BH liver lesions	120
4.3.2	Non-Perfused Samples	121
4.3.3	Perfused Samples	123
4.3.4	H&E staining	124
4.3.5	Picrosirius red staining	127
4.3.6	Polarised Sirius red staining	130
4.3.7	Quantitative analysis and variability	132
4.3.8	Reticulin staining.	134
4.4	<i>Discussion</i>	135
Chapter 5	Qualitative histological analysis of liver response to ultrasound histotripsy in ex-vivo perfused porcine liver including 3D histological reconstruction.	143
5.1	<i>Introduction</i>	144
5.2	<i>Material & Methods</i>	146

5.2.1	Histotripsy set-up	148
5.2.2	Tissue sampling	148
5.2.3	H&E and histochemical stains	148
5.2.4	3D reconstruction	148
5.3	<i>Results</i>	153
5.3.1	Descriptive Histology:	153
5.3.2	3D reconstruction	158
5.3.3	4.0 Discussion	158
5.4	<i>Conclusions</i>	161
Chapter 6 Liver ultrasound histotripsy: Novel analysis of the histotripsy site cell constituents with implications for histotripsy application in cell transplantation and cancer therapy 163		
6.1	<i>Introduction</i>	164
6.2	<i>Study Aims</i>	166
6.3	<i>Study Objectives</i>	166
6.4	<i>Hypothesis</i>	166
6.5	<i>Methods</i>	166
6.5.1	Pre-experiment trial with different tissues:	167
6.5.2	Overall Study design:	167
6.5.3	Histotripsy set up	167
6.5.4	Perfusion set up:	167
6.5.5	Pre-culture light microscopy:	169
6.5.6	Cell culture: cell morphology and growth	169
6.5.7	Phalloidin/ Dapi staining	169
6.5.8	Live-Dead assay	169
6.5.9	Morphology assessment:	169
6.5.10	Cell Titre-Glo Metabolic Assay	170
6.5.11	H&E and Picrosirius Red Staining:	170
6.5.12	ImageJ Software:	170
6.5.13	Statistical methods	170
6.6	<i>Results</i>	170
6.6.1	Preliminary study of histotripsy in liver tissue	171
6.7	<i>Detailed evaluation of liver histotripsy site aspirates (repeat liver experiment results) ...</i>	175
6.7.1	Organ perfusion, viability, and lesion creation & cell aspirate	175
6.7.2	Histology of lesions	175

6.7.3	Cell Culture:.....	177
6.7.4	Cell type, appearances, and numbers at baseline	178
6.7.5	Cell division and viability in culture.....	179
6.8	<i>Discussion:</i>	182
6.8.1	Preliminary liver studies.....	182
6.8.2	Other Organ Histotripsy	183
6.8.3	Histotripsy regime and the nature of the liver lesion based on histology.....	184
6.8.4	The use of the perfused organ as a model.....	186
6.8.5	Effect of perfusion & perfusate on cell harvest	186
6.8.6	The cell isolates, culture, and cell viability.....	188
6.8.7	Limitation of current study, further evaluation, and possible implications for therapy. 191	
6.8.8	Implications for future cell therapy	192
Chapter 7	Preliminary study on histotripsy assisted 3D-hepatocyte cell transplantation in in-vivo rat liver	193
7.1	<i>Background</i>	194
7.2	<i>Introduction</i>	195
7.3	<i>Study Aims</i>	197
7.4	<i>Study Objectives</i>	197
7.5	<i>Hypotheses</i>	197
7.6	<i>Methods:</i>	198
7.6.1	Overall Study design:.....	198
7.6.2	Regulatory Guidelines	199
7.6.3	Histotripsy set up & parameters	200
7.6.4	3D hepatospheres development and maturation	203
7.6.5	Animal Model & Husbandry details:	203
7.6.6	Experimental Procedure	205
7.6.7	Termination.....	211
7.6.8	Histopathology & Clinical Biochemistry	214
7.6.9	Histological Preparation.....	215
7.6.10	Biochemical analysis	216
7.7	<i>Results</i>	217
7.7.1	Functional assessment of the 3D Heps pre-implant	217
7.7.2	GA histotripsy.....	217

7.7.3	Histotripsy Lesions & Cell transplantation	218
7.7.4	Recovery (Cell implant vs control)	219
7.7.5	Weight gain	219
7.7.6	Termination and laparotomy findings	222
7.7.7	Histology.....	222
7.7.8	Cell function	225
7.8	<i>Discussion</i>	226
7.8.1	Safety of liver histotripsy in live rodent model:.....	226
7.8.2	Comparison of histotripsy sites with other protocols:.....	227
7.8.3	Feasibility and safety of 3D Hep implantation:.....	229
7.8.4	Evaluation of recovery and cause of post procedure termination (n=1):.....	230
7.8.5	Weight gain as surrogate of recovery	230
7.8.6	Tissue sampling, variability, liver and other organ injury, possibility of immune response	231
7.8.7	Implanted cell detection discussion.....	231
7.8.8	Implication for future studies, technique and assessment modification.	232
References		234
Supplement 1		264
Supplement 2		268
Supplement 3		269
Appendix 1. Manuscripts published during the time of PhD.....		270
<i>Published manuscripts:</i>		<i>270</i>
<i>Book chapters:</i>		<i>271</i>
<i>Published abstracts:.....</i>		<i>271</i>

Chapter 1 Clinical background to chronic liver disease and liver transplantation

1.1.1 Introduction:

Liver disease is a major global healthcare problem (**Figure 1**), affecting an estimated 844 million people worldwide (1). Despite this substantial burden, therapeutic options for the liver disease remain limited, in parts owing to a paucity of detailed analyses defining the cellular and molecular mechanisms that leads to chronic conditions in humans. New treatment strategies aim to alter the disease course and improve survival. The incidence of liver disease is on the rise and survival for many liver diseases is improving with new treatments. For example, recent advancements in hepatitis C virus (HCV) therapy have markedly enhanced results, particularly for patients with severe liver disease, including cirrhosis (2). In the last ten years, advancements in direct-acting antivirals (DAAs) have transformed HCV treatment, achieving elevated cure rates, including among patients with cirrhosis (2). Non-alcoholic fatty liver disease (NAFLD) and its advanced variant, non-alcoholic steatohepatitis (NASH), are emerging as significant worldwide health issues owing to their swift rise in prevalence and correlation with serious consequences. Their increasing influence is directly associated with escalating rates of obesity, diabetes, and metabolic syndrome globally. Non-alcoholic fatty liver disease (NAFLD) currently impacts approximately 25% of the worldwide population, with prevalence rates notably elevated in North America, the Middle East, and certain regions of Asia (3). Consequently, NAFLD is the predominant chronic liver disease globally. Approximately 20–30% of patients with NAFLD advance to NASH, a more severe condition marked by hepatic inflammation and fibrosis. This progression increases the likelihood of cirrhosis, liver failure, and hepatocellular carcinoma (HCC).

In Europe alone, around 29 million people are estimated to suffer from the chronic liver disease (4). Recent data suggests that about 0.1% of the European population is affected by cirrhosis, corresponding to 14-26 new cases per 100,000 inhabitants per year or an

estimated 170,000 deaths per year (5). Given no effective medical treatment is available for advanced cirrhosis to reverse disease state (6), prevention and early intervention are crucial in mitigating the increasing burden of NAFLD and NASH and halting disease progression to cirrhosis (7). Advocating for lifestyle modifications, reducing metabolic risks, enhancing public knowledge, and endorsing healthcare policies aimed at preventative strategies are essential actions in alleviating the effects of these illnesses. Both cirrhosis and primary liver cancer (incidence of 1-13 new cases) are representative of end-stage liver disease. With almost 10% of cirrhotic patients undergoing surgery during their last year of life (8), this translates into an ever-increasing cohort of patients with complex medical needs requiring a form of therapeutic intervention (i.e. surgery)(9).

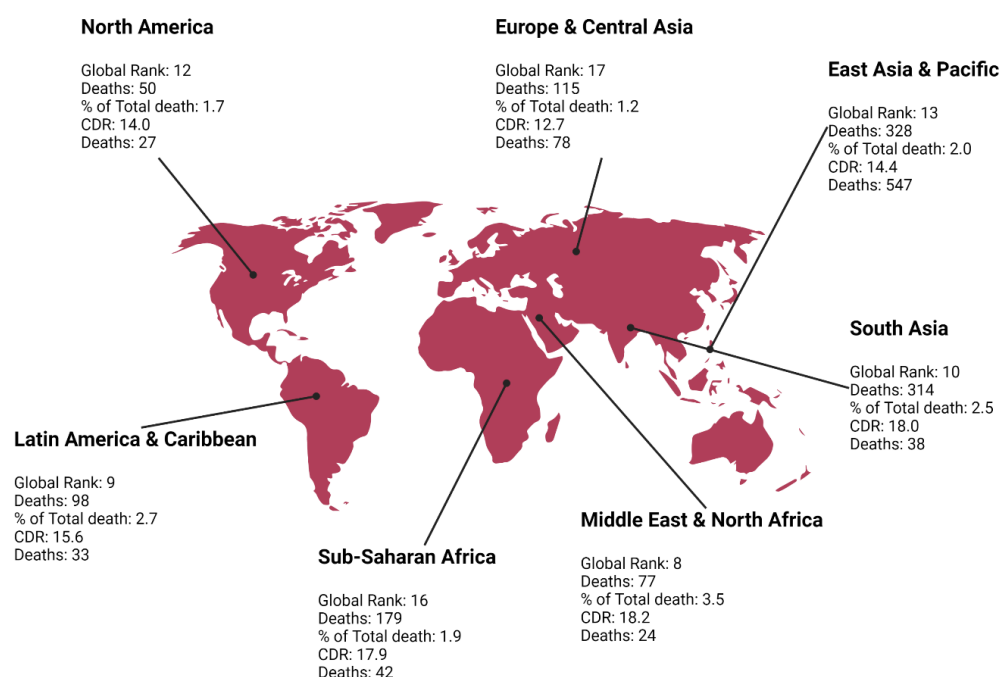


Figure 1 – Global mortality related to liver disease and liver cancer. Worldwide mortality from liver disease ranks 11th worldwide. Data from the Global Health Estimate 2015 is presented above and likely an underestimate as it does not account for deaths related to acute hepatitis. Death by Cause, Age, Sex, by Country and region, 2000-2015; Geneva, World Health Organisation. CDR: Crude death rates. [Figure adapted from data presented in Ref (10)]

1.1.2 Epidemiology

The exact prevalence of cirrhosis worldwide is unknown. In 2017, there were an estimated 112 million cases of compensated cirrhosis and 10.6 million cases of decompensated cirrhosis prevalent worldwide (11). This is thought to be an underestimation as we recognise the high prevalence of undiagnosed cirrhosis in both NASH and hepatitis C patients (12). A prior study revealed that an alarming 73% of patients experiencing their initial admission for cirrhosis or liver failure had never been referred to a liver clinic, highlighting a significant deficiency in the early identification of liver illness (13, 14).

Overall, the prevalence of liver cirrhosis has increased by 74.53% from 1990 to 2017 (11, 15) this is partly related to improved diagnostics (16). The highest age-standardised prevalence of both compensated (2455 per 100,000) and decompensated cirrhosis (267.4 per 100,000) was noted in the highest income Asia-Pacific region (11).

1.1.3 Aetiology of Cirrhosis

Cirrhosis can result from many different causes all leading to fibrosis and end stage liver disease (**Figure 2**). In some liver disease there is a single cause for example in cases of viral hepatitis or primary biliary sclerosis. However, in many cases cofactors may be important which increase or decrease susceptibility to a disease process. Factors such as age, sex, obesity, alcohol, iron intake play a significant role in determining the risk and rate of developing cirrhosis (17, 18). A genome wide analysis (19) revealed that variants of *FAF2*, *HSD17B13* and *SERPINA1* genes increase the chance of cirrhosis in the context of fatty liver disease and further genetic studies have shown mutations of *ANXA1* to increase the risk of cirrhosis too (20). This highlights an important role for the genetics, in addition to the environmental factors, can play that leads to development of or increases the chance of developing cirrhosis. More so, inherited liver illnesses comprise a collection

of metabolic and genetic disorders that generally lead to early chronic liver involvement (21, 22). The majority result from a deficiency in an enzyme or transport protein that modifies a metabolic pathway and has a pathogenic function primarily in the liver (23). The prevalence varies; however, the majority are uncommon conditions (24).

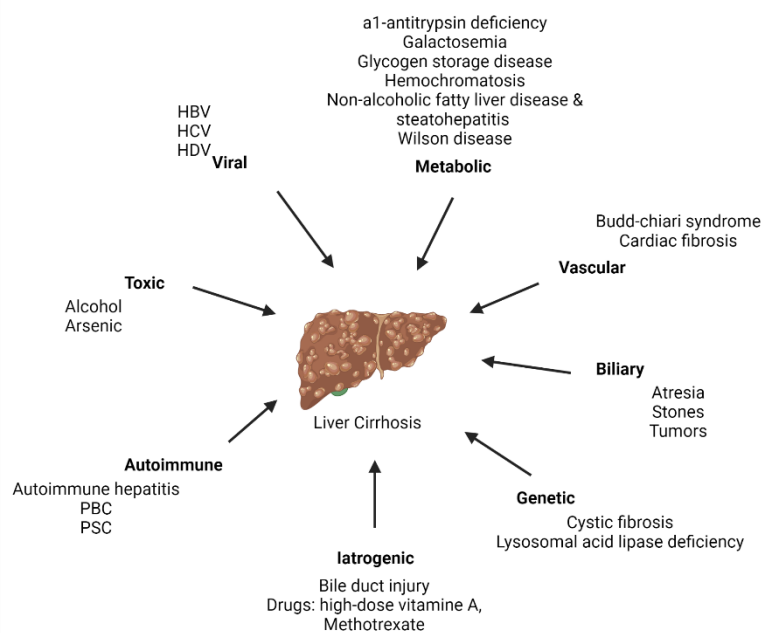


Figure 2 – Causes of cirrhosis

1.1.4 Pathophysiology of Chronic Liver disease/Cirrhosis:

As alluded before, chronic liver disease is one of the top 10 causes of death in the western world and causes severe morbidity (Figure 3). Cirrhosis is reversible in early stage and a progressive process. Cirrhosis is a result of a variety of liver diseases and is characterized by fibrosis and distortion to the architecture of the liver with the formation of regenerative nodules. Its major causes include chronic viral infections, alcoholic or

non-alcoholic liver steatohepatitis (NASH), autoimmune disorders of the liver and metabolic disorders. Cirrhosis can have varied clinical manifestations and complications.

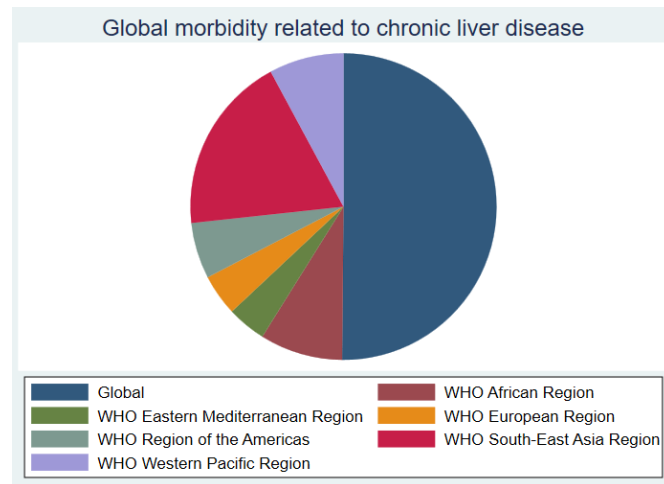


Figure 3 – Data available from the Global Health Estimate 2015; Figure adapted from data in Ref (10)

Frequent aetiologies of acute liver injury that typically resolve without advancing to chronic liver disease encompass: Hepatitis A, Drug-induced liver injury (DILI), Acute autoimmune hepatitis, ischemic hepatitis and hepatotoxin exposure. With these aetiologies when the offending agent is identified quickly and treated the liver's function tends to return to normal without the sequelae to progress to chronic liver disease. The entities mentioned can pose distinct cellular challenges that can disrupt normal liver function and lead to cellular injury (**Figure 4**). It's the ongoing or repetitive cellular injury that then leads to chronic liver disease. Therefore, advanced fibrosis and cirrhosis are regarded as the latter outcomes in the order of chronic liver damage, but they depend on the genetic and acquired etiological risks and factors. Most patients with chronic HCV progress slowly to cirrhosis at a rate of only 1-2% per year (25-28). Autopsy series have revealed that only 20-30% of patients with long-term HBV or HCV infection develop cirrhosis, and loaded HBV transgenic mice fail to progress normally to severe hepatic fibrosis (29-31). Further analysis of the nature and interaction of such risk factors will shed light on the development of novel therapeutic strategies. Only chronological

sequences of these rapidly progressive morphologic changes within well-defined stages of liver disease could detect the causal sequences (32). The present nine stages of chronic evolution were previously considered in discussions on distinct progression rates in patients with hepatitis C and alcoholics, who are also considered to develop advanced fibrosis and cirrhosis quite rapidly. These stages were also applied to patients with primary sclerosing cholangitis, and definitions conformed to data on specific distinct subpopulations of HCV patients, who are consistent with rapid progressors to cirrhosis. Chronic viral infections, especially with HCV, usually progress to end-stage fibrosis within 30 years, but these approximately 100-day intervals in the natural course of HCV are variable and depend on the interaction between viral and host factors, the amount of hepatocyte injury, and mild inflammation.



Figure 4 – Common aetiologies of acute liver injury and the possible cellular mechanism leading to injury summarised for each entity.

At cellular level the cell type most implicated in the pathogenesis of liver fibrosis is the hepatic stellate cells (HSC) (33). In normal liver tissue, the HSC resides in the space of Disse and are thought to play several key physiological roles including storage of vitamins (Vitamin A derivatives), help with maintenance of extracellular matrix (ECM), produce various growth factors (i.e. hepatocyte growth factor (HGF) and platelet-derived growth factor (PDGF)) and they have a role in immune regulation and response to injury and

activation (34, 35). HSC display a dual behaviour in that they support liver health under normal conditions but drive fibrosis if chronically activated due to the persistence of injury (34, 35). When activated they turn into myofibroblasts (**Figure 5**) (33, 36). This results in increased expression of smooth muscle actin, motility, and contractility (37). Progression to liver fibrosis is because of stellate cells beginning to generate different types of matrices (38). Fibronectin is thought to be the earliest form of matrix produced by HSC (39); later as fibrosis progresses matrix is thought to include type 1 collagen (40). This transition from early fibronectin production to collagen-rich matrix is a hallmark of fibrosis progression, where HSCs transform into myofibroblast-like cells, contributing to the dense, scar-like ECM that characterizes advanced liver fibrosis (41, 42). Not only HSC are involved in the ECM remodelling but are thought to play an important role in the pathogenesis of hepatocellular carcinoma (HCC) (33, 38). Several other players have been implicated in the pathogenesis of the fibrosis (**Figure 5**) and the development of cirrhosis including immune cells (i.e. Kupffer cells), endothelial cells and epithelial cells (37). Immune cells contribute significantly to the development of liver fibrosis by releasing cytokines that regulate HSC activation, proliferation, and ECM deposition, all of which are essential for fibrotic processes (43). Macrophages are among the primary regulators of fibrogenesis (44-46). They polarize into pro-fibrotic (M2) and pro-inflammatory (M1) types (47, 48), with M2 macrophages promoting fibrosis through cytokines like TGF- β , which activates HSCs (49). Kupffer cells, the liver's resident macrophages, play a similar role in liver-specific fibrosis by secreting pro-fibrotic cytokines (49). Other immune cells such as neutrophils promote the activation of the HSC through release of enzymes and reactive oxygen species (ROS) therefore enhances the process of fibrosis (49). T cells (Th2 and Th17) have been shown to release cytokines (IL-4, IL-13, IL-17) that enhance HSC activity and collagen production (50-52). B cells are

known to release cytokines but their role in the development of fibrosis is less understood. These immune cells, through complex signalling pathways such as TGF- β , JAK-STAT, and mTOR, actively regulate the fibrotic response, highlighting them as potential therapeutic targets for treating liver fibrosis (50). The consequential fibrosis and the remodelling of the ECM results in increased stiffness of the liver tissue. In turn the resultant cirrhosis will alter the liver's physiological roles – synthesis of most serum proteins, metabolism of nutrients and drugs, excretion and detoxification of toxins to name a few.

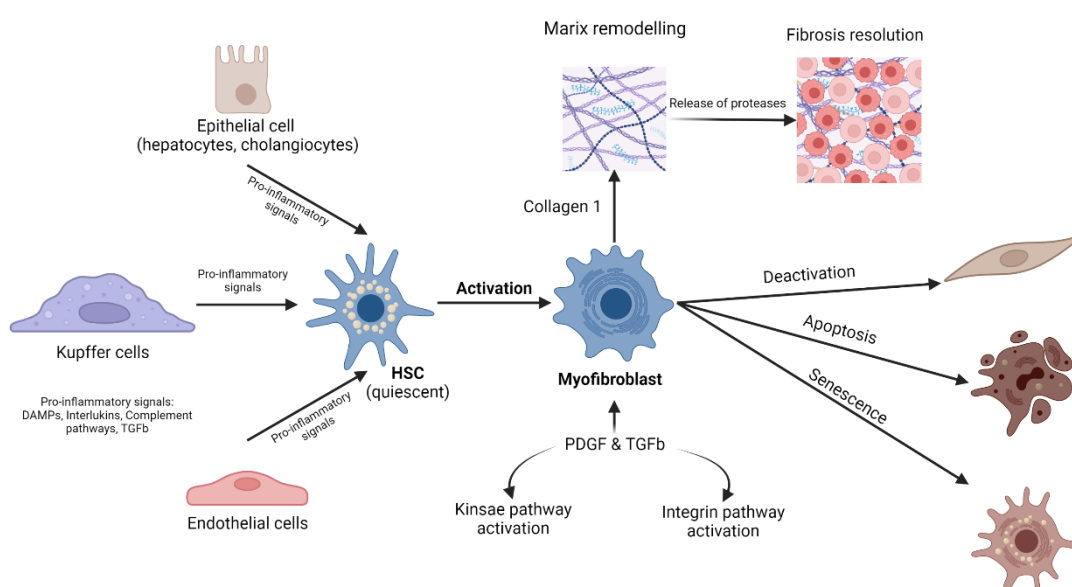


Figure 5 – Schematic diagram presenting overview of the process involved in development of fibrosis and cirrhosis. Injury to the epithelial cell results release of pro-inflammatory signals. In addition, activation of Kupffer cells results in further release of these pro-inflammatory signals and paracrine molecules being released from the sinusoidal endothelial cells. Combined effect is activation of HSC into myofibroblasts. Platelet derived growth factor (PDGF) and TGF β involving kinase pathway and integrin pathway activation are thought to play a significant role in the activation of myofibroblasts and ECM remodelling. Reversal of fibrosis results in deactivation of myofibroblasts, or its apoptosis or reverting to a senescence state. [Diagram adapted and modified from Ref(53)]

The repeated cycle of injury to hepatocytes results in cascade of ongoing inflammation and attempted regeneration. However, due to chronic injury, this regenerative process

becomes dysregulated, resulting in abnormal clusters of liver cells surrounded by scar tissue (54). The architectural change in the liver parenchyma brought about by the ongoing fibrotic process can lead to impaired blood flow and an increase in resistance in the vasculature particularly in the portal system. This is accompanied by impaired synthetic function and dysregulated endocrine pathways. Development of portal hypertension (PHT) is a hemodynamic abnormality due to the architectural changes in the cirrhotic liver that results in increased intrahepatic resistance to portal flow. Cirrhotic liver shows endothelial dysfunction, defined by a decrease in response to endothelium dependent vasodilators and by a lower generation of nitric oxide (NO) (55). This causes a higher portal pressure in response to flow and a more marked reaction to vasoconstrictors (56, 57). Several pathways have been implicated in the development of the PHT and endothelial dysregulation that highlights the complex cross talk between the endothelial cells and the HSC involved in development of fibrosis (58). Namely, ET-1 produced by HSC in response to injury can increase vascular tone by binding to ET-A and ET-B receptors (59, 60). In addition, loss of VEGF signalling leads to “capillarization” of liver sinusoidal endothelial cells (LSECs), increasing resistance and exacerbating portal hypertension (61). Pathological angiogenesis, supported by VEGF, increases splanchnic circulation, raising portal pressures (58). The Notch1 pathway is associated with abnormal intrahepatic vasculature (62).

PHT in turn can lead to splanchnic vasodilatation which can exacerbate hypovolemia resulting in activation of renin-angiotensin-aldosterone system as well as sympathetic nervous system activation. The clinical manifestation of this is ascites. The liver undergoes both functional and morphological changes with the development of cirrhosis that can manifest itself in different ways clinically.

1.1.5 Clinical Presentation

Cirrhosis may be classified as *compensated* or *decompensated*. Presence of variceal haemorrhage, ascites, encephalopathy, and jaundice characterises decompensated cirrhosis. In compensated cirrhosis these features are not present. Compensated patients have a median survival of 12 years compared to 2 years for decompensated patients (63). Compensated cirrhotic patients may be asymptomatic and may be diagnosed as an incidental finding on investigations for an unrelated condition. Commonly, there is evidence of deranged liver function test with radiological features such as replacement of

hepatic parenchyma with fibrotic tissue and evidence of regenerative nodules (64, 65). Decompensated patients on the other hand seek medical help due to presence of ascites or other complication of liver cirrhosis. Many complications seen in decompensated liver patients are thought to be due to a hyperdynamic circulation and peripheral vasodilatation altered systemic circulation (54) (Figure 6).

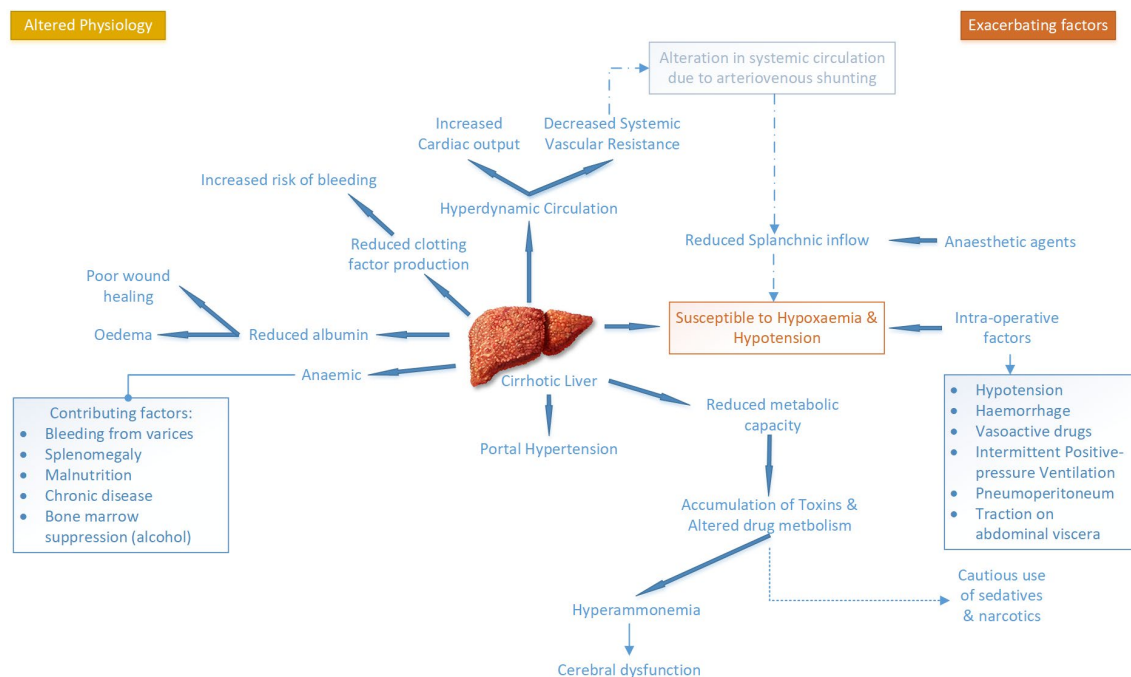


Figure 6 - Altered physiology in cirrhotic liver and consequential effects [Figure adapted from(9)]

1.1.5.1. Portal hypertension

PHT can clinically manifest itself with:

- **Oesophageal Varices:** Enlarged veins in the oesophagus are prone to rupture, leading to life-threatening gastrointestinal bleeding. The formation of varices serves as a surrogate indicator of PHT and denotes clinically significant portal hypertension. Hepatic venous pressure gradient (HVPG) serves as the most accurate surrogate marker for true portal pressure and PHT, with PHT defined as an HVPG over 5 mm Hg, and a value more than 10 mm Hg indicating clinically significant portal hypertension (54).

- **Splenomegaly:** Enlarged spleen due to increased portal venous pressure, often leading to low platelet counts (thrombocytopenia).
- **Ascites:** Fluid accumulation in the abdomen, resulting from increased hydrostatic pressure and reduced albumin synthesis, causing abdominal distension and discomfort.
- **Caput Medusae:** Visible distended veins around the umbilicus because of portosystemic shunting.

1.1.5.2. Hepatic encephalopathy (HE):

HE (**Figure 7**) is because of the failure of liver to eliminate toxins including ammonia causes neurotoxic buildup in the bloodstream, therefore affecting brain function (66). One contributing cause is portal hypertension-related shunting of blood around the liver. Symptoms range from subtle cognitive changes to severe confusion, lethargy, and coma. Early signs include personality changes, irritability, and poor concentration. HE can be classified according to underlying disease, severity of manifestation, its time course and according to precipitating factors (66).



Figure 7 – Classifications of HE according to cause, severity, time course and precipitating factors.

1.1.5.3. Jaundice & Pruritus:

Hepatocyte dysfunction leads to impaired bile synthesis and excretion, resulting in increased bilirubin levels in the bloodstream. Contributing factors encompass hepatic tissue degeneration and biliary duct blockage.

1.1.5.4. Coagulopathy & Hypoalbuminemia:

As liver function deteriorates, its ability to synthesise proteins, such as albumin and coagulation factors, is compromised. Low albumin levels contribute to oedema and ascites due to decreased oncotic pressure in blood vessels. There is increased bleeding tendency due to reduced clotting factors, presenting as easy bruising, prolonged bleeding

from minor injuries, or significant bleeding complications during medical procedures (67, 68). Although, prolonged bleeding time is not a reliable indicator of bleeding risk in these patients due to compensatory increases in von Willebrand factor (VWF), which helps counterbalance platelet deficits (69). Despite prolonged prothrombin time (PT) and activated partial thromboplastin time (APTT) in chronic liver disease, these metrics do not accurately predict bleeding risk (69). The function of fibrinolysis in chronic liver disease is contentious. Certain studies suggest hyperfibrinolysis, whilst others do not (70-73). There are imbalances in fibrinolytic activators and inhibitors, notably a decrease in thrombin-activatable fibrinolysis inhibitor (TAFI), however additional research is necessary to elucidate its function in bleeding problems.

1.1.5.5. Hepatorenal Syndrome (HRS):

HRS is a critical complication resulting from growing renal vasoconstriction and diminished renal blood flow in individuals with advanced cirrhosis and portal hypertension (74, 75). It remains a diagnosis of exclusion. Its pathophysiology is defined by a distinct triad: circulatory dysfunction, nitric oxide (NO) dysfunction, and systemic inflammation; however, specific renal damage has not been evidenced in clinicopathological studies (76). Kidney biopsies from patients with cirrhosis revealed a broad spectrum of renal impairment (76, 77). This presents with rapid decline in kidney function without structural kidney damage, leading to oliguria (low urine output) and azotaemia (elevated blood urea nitrogen and creatinine). Although there have been different studies evaluating role of biomarkers to aid diagnosis, no biomarkers demonstrate optimal performance in the differential diagnosis of AKI in patients with cirrhosis (77, 78). While the optimal biomarker would effectively differentiate between structural and functional AKI, additional validation studies are necessary for their generalised applicability.

1.1.5.6. Hepatopulmonary Syndrome:

This comes about because of abnormal vasodilation within the lungs associated with chronic liver disease creating ventilation-perfusion mismatches and thus leading to impaired oxygenation (79). Its clinical manifestations include symptoms of shortness of breath, cyanosis, and hypoxemia, often worsening when the patient is upright (platypnea-orthodeoxia).

1.1.5.7. Systemic manifestations:

The imbalanced hormones (i.e. increased oestrogen level), due to reduced liver metabolism, and hyperdynamic circulation contribute to systemic changes that can present with gynecomastia, spider angiomas and palmar erythema and muscle wasting.

1.1.6 Diagnosis

Liver disease can be diagnosed on histology, and therefore percutaneous liver biopsy is considered gold standard to assess liver fibrosis (80-82). However, liver biopsy is invasive, has a well-recognised risk, is costly and is associated with sampling error (17). Hence, a combination of clinical manifestation, laboratory findings, and radiological appearance can help the diagnostic process.

There is no single blood test that can evaluate all liver functions while also assessing the presence and severity of portal hypertension (83). Commonly available tests for assessing liver functions include blood bilirubin, liver enzymes (alanine [ALT] and aspartate aminotransferase [AST], serum alkaline phosphatase [ALP], gamma glutamyl transpeptidase [GGT]), serum albumin, and prothrombin time. Sometime these may not be reflective of the true extent of the disease. More recently, development of non-invasive tests such as metabolic breath tests (84) have been viewed with more interest as they have potential to be point-of-care tests in setting of acute or chronic liver failure. Quantitative liver functions such as indocyanine clearance tests [ICG-K] and methacetin breath tests [MBT] have been developed to examine the dynamic health of the liver, but each has its own limitations and availability (84, 85).

Imaging alone often lacks the sensitivity to differentiate between the various causes of cirrhosis. However, frequently in advanced cirrhosis there is hypertrophy of the caudate

lobe and lateral segments of the left lobe (segments 2 and 3) with concomitant atrophy of the posterior segments (6 and 7) of the right lobe (**Figure 8**) (65, 86, 87). The primary imaging challenge involves differentiating regenerative nodules, siderotic nodules, and dysplastic nodules from one another (65, 86).

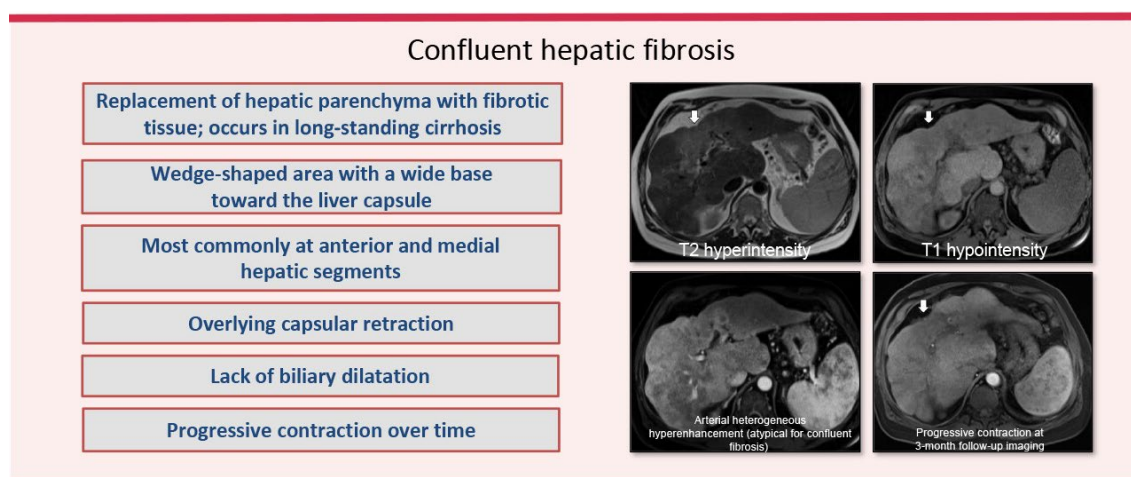


Figure 8 – Imaging findings in cirrhotic livers [Image adapted from Ref: (65)]

Tests such as transient elastography (TE) (88-90) can help stage the disease and through serial measurements disease progression can be tracked. Elastography methods, including Transient Elastography (TE), point-shear wave elastography (pSWE), bidimensional shear wave elastography (2D-SWE), and magnetic resonance elastography (MRE), provide liver stiffness measurements, which correlate with fibrosis and cirrhosis stages (90). TE has been reported to have a sensitivity of 87.5% and a specificity of 85.3% in its ability to predict clinically significant portal hypertension (89). All other modalities of TE have shown good sensitivity and specificity, however, due the limited number of studies conducted on heterogeneous populations, coupled with significant variability in cut-off values, indicates that pSWE is not currently advisable for routine screening of clinically significant PHT in patients with chronic liver disease (89, 91). Determining the extent of fibrosis may play an important role in clinical management of patients (89, 92). This helps guide the treatment strategy. While discussing all aspect of diagnostic tools for cirrhosis and liver fibrosis is beyond the scope of this chapter (see review (90)), we will briefly review the cut off point for TE in assessment of liver stiffness. Current recommendations for according to the Bevano VI consensus conference (93), liver stiffness measure of ≥ 10 kPa is suggestive of compensated advanced chronic liver disease (cACLD) and ≥ 15 kPa is highly suggestive of cACLD (89). Liver stiffness less than or

equal to 5 kPa (1.3 m/sec) has high probability of being normal, liver stiffness less than 9 kPa (1.7 m/sec), in the absence of other known clinical signs, rules out cACLD, and values greater than 13-15 kPa (2.1 m/sec) are highly suggestive of cACLD; in some patients with NAFLD, the cut-off values for cACLD may be lower and follow-up or additional testing in those with values between 7 and 9 kPa (94). While these non-invasive methods are used as adjunct to diagnosis of liver fibrosis, a more representative picture of fibrosis is through histology and there are several histological gradings developed (95-99). In clinical practice, three primary histological scoring systems are frequently used:

Metavir Scoring System: Commonly used for hepatitis C, this system grades fibrosis from F0 to F4 (95):

- F0: No fibrosis
- F1-F2: Mild to moderate fibrosis
- F3: Advanced fibrosis
- F4: Cirrhosis

Knodell Score: Used less frequently, the Knodell scoring system is part of the Histology Activity Index and grades fibrosis separately from necro-inflammatory activity (100).

Ishak Score: Provides a more detailed grading from 0 to 6 (Figure 9) (95):

- 0: No fibrosis
- 1-2: Mild fibrosis with expansion of portal areas
- 3-4: Bridging fibrosis (connecting different regions)
- 5-6: Cirrhosis








Appearance	Ishak stage: categorical description	Ishak	Metavir
	No fibrosis (normal)	0	F0
	Fibrosis expansion of some portal areas ± short fibrous septa	1	F1
	Fibrosis expansion of portal areas ± short fibrous septa	2	F2
	Fibrosis expansion of most portal areas with occasional portal to portal (P-P) bridging	3	
	Fibrosis expansion of portal areas with marked portal to portal (P-P) bridging as well as portal to central (P-C)	4	F3
	Marked bridging (P-P and / or P-C) with occasional nodules (incomplete cirrhosis)	5	
	Cirrhosis, probable or definite	6	F4

Figure 9 – Histological scoring system for liver fibrosis [adapted from: (96, 101)]

1.1.7 Classifying severity of liver disease

In addition to the assessment of the severity scores mentioned above, risk stratifications of patients to prioritise their treatment strategy is mandatory in patients with chronic liver disease. The Child-Turcotte-Pugh (CTP) score or model for end-stage liver disease (MELD) score may be used to determine the severity of liver disease and the operative risk for an individual patient. More generic assessment of surgical risk such as the American Society of Anaesthesiologist (ASA) classification is less helpful for this patient group as it is not specific to the liver disease. More useful are the new models for risk estimation in the context of liver disease.

CTP score (9)

The CTP score is easy to calculate and correlates well with severity of disease and survival. It was originally developed to predict operative risk in patients undergoing portosystemic shunt surgery for variceal bleeds. It has been found to be a useful indicator of operative risk for other surgical procedures in patients with chronic liver disease. CTP score is obtained by adding the score for five parameters: encephalopathy, ascites, bilirubin and albumin level and the degree of coagulopathy. The score ranges from 5 to 15 with a further classification of CTP scores into three classes: Class A (CTP score 5-

6), Class B (CTP score 7-9) and Class C (CTP score 10-15), the higher scores reflecting a more severe liver disease and hence higher operative risks. Overall general surgical risk of mortality is 10% for CTP classes A, 30% for class B and 82% for class C (102). This means while patients with mild chronic liver disease can tolerate surgery, those with higher scores should have a realistic discussion about the associated risk of mortality and non-surgical options. They tend to fall in CTP class C, presenting as an emergency, their risk of mortality is several folds, and surgery may have a detrimental effect. Risk of morbidity from surgical procedure also increases with higher classes of CTP classification and can have an impact on the quality of life of the patient. Hence, any intervention should be offered not only with mortality in mind but also with morbidity associated with the intervention and its short- and long-term impact on the quality of life of the patient.

MELD score (9)

The MELD score was originally developed to predict mortality after TIPS and now is implemented in risk assessment of patients awaiting liver transplantation, as well as, to predict perioperative mortality risk in abdominal surgery (103). It has been validated for the prediction of both short- and long-term survival of cirrhotic patients to allow anticipated survival without any interventions to be considered. When applied to the risk assessment of cirrhotic patients undergoing surgery A MELD score of 0-11 correlates with 5-10% 90-day mortality, a score of 12-25 with 25-54% mortality rate, and a score greater than 26 with a 90% postoperative mortality rate (104). In the non-transplant surgical group, there was approximately a 1% increase in mortality risk per MELD point below a score of 20, whereas there was a 2% increase in mortality risk per MELD point over 20 (105). A MELD score of greater than 8 in patients undergoing hepatic resection is associated with decreased long-term survival and correlates well with peri-operative mortality (106). Generally, a MELD score of 14 or greater should be considered as a replacement for CTP class C and as a predictor of being very high risk for abdominal surgery (107).

The above models provide an estimation of operative and post risk as well as an indicator for both short- and long-term survival. However, there are other factors that need to be considered for risk stratification and prediction in cirrhotic patients undergoing major surgery. For patients with cirrhosis undergoing either elective or emergency surgery, CTP and MELD scores provide a good measure of global liver function and patient's overall

risk. Any patient with CTP class B/C or a MELD score of >8 should be carefully assessed for surgery where possible the above risk stratification models should be accompanied with other methods of functional liver assessment. More so, when considering the risk of surgery patient's other comorbid conditions should be considered such as their age, BMI, the presence of diabetes, cardiovascular status, renal function and presence of sepsis. This will reveal more about the patient's physiological reserve and ability to cope with the insult of surgery.

1.1.8 Cirrhosis & Risk of HCC

Chronic liver disease and cirrhosis are the most important risk factors for development of hepatocellular carcinoma (HCC) (108) of which viral hepatitis and alcoholic liver cirrhosis are the leading cause globally. In USA, HCC is the ninth leading cause of mortality. It has a preponderance of male over female patients. The incidence of HCC is thought to rise as there is a rise in the non-alcoholic steatohepatitis (NASH) cases following rise of cases of obesity globally. Therefore, part of management of the compensated cirrhosis is screening for HCC with ultrasonography and tumour markers. Treatments for HCC can range from systemic therapy, local ablative therapy, and surgical resection as well as liver transplantation.

1.1.9 Treatment Strategies

In the context of liver cirrhosis, treatment would aim to reduce the progression of fibrosis and prevent the complications of end stage liver disease. Ultimately, when advanced cirrhosis is present with evidence of end stage liver disease suitable candidates are listed for liver transplantations. Although, anti-fibrosis treatment sounds like an ideal treatment strategy, several limitations have precluded its successful adaptation in human subjects. One limitation is the lack of effective tool to accurately measure fibrosis non-invasively (109). Despite advancement in the field of ultrasonography and MRI, most patients still require biopsy for diagnosis (110). Additionally, resolution of the fibrosis takes a long time, hence by the time a desired therapeutic effect is hoped to be achieved the fibrosis has progressed further. Lastly, liver fibrosis is a multifactorial process and therefore targeting a specific pathway may not necessarily halt disease progression, hence difficulty in appropriate pharmacological intervention. The complexity of hepatic fibrosis

necessitates a multifaceted approach in drug development, targeting various pathways involved in fibrosis progression, such as inflammation, stellate cell activation, and ECM deposition (111-113). While several agents show potential (**Figure 10**), many are in early trial stages, and no drugs have received full FDA approval solely for hepatic fibrosis (111, 112, 114). In a recent review *Shan et al* (111) suggested that combination therapies targeting multiple pathways may be the most effective strategy, reflecting the complex pathophysiology of hepatic fibrosis. Despite this, most of the clinical management is focused on screening for HCC and management of symptoms of decompensated liver disease.

The only curative treatment for those with end stage liver failure is liver transplantation.

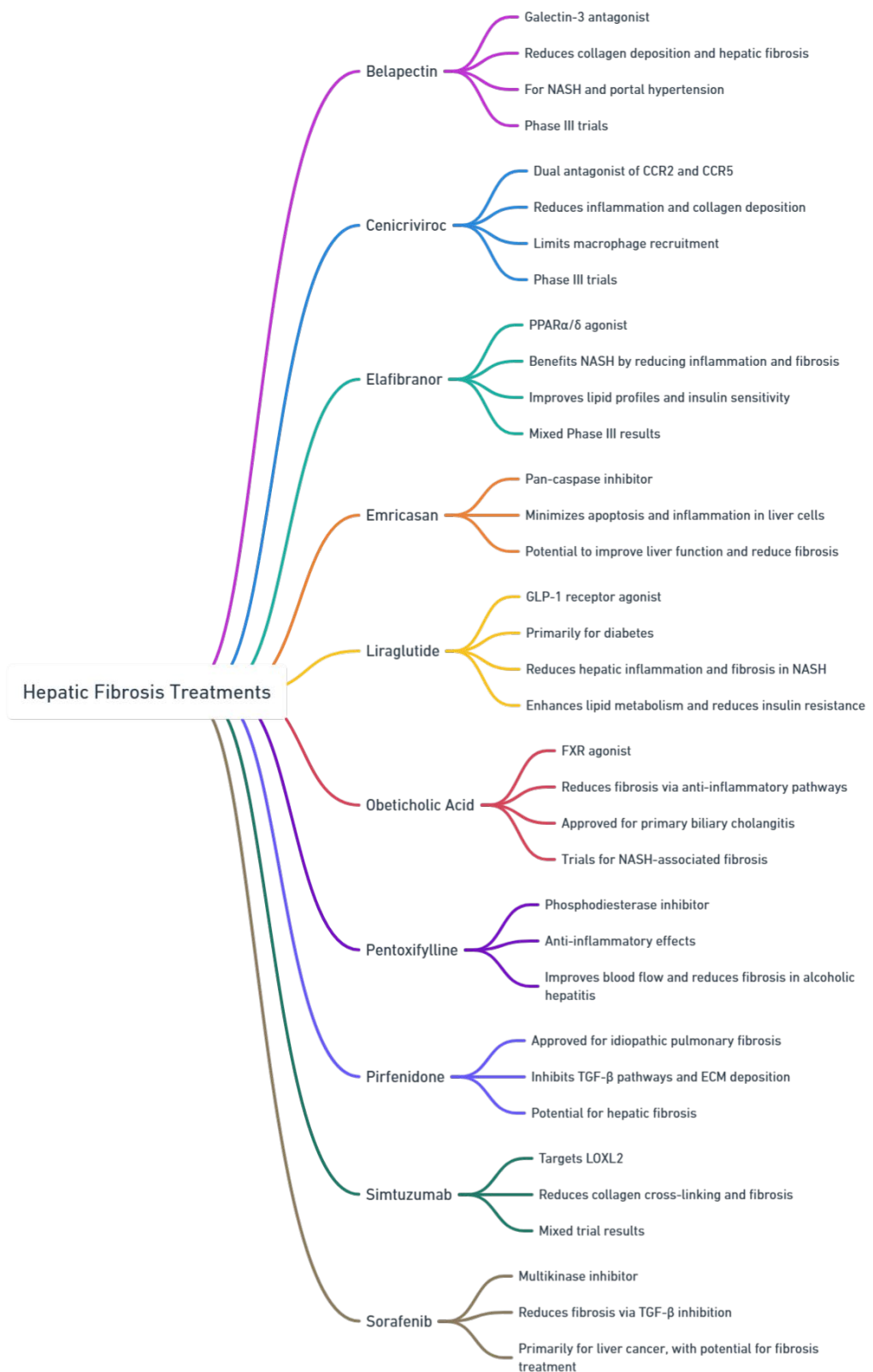


Figure 10 – Examples of the pharmacological agents with properties useful in treatment of hepatic fibrosis

1.1.10 Liver Transplantation

The first human orthotopic liver transplantation was reported by Thomas Starzl in United States and a year later the first successful case was reported by Sir Roy Calne in Europe (115, 116). Since then, liver transplantation has evolved rapidly becoming the standard therapy for acute and chronic liver failure of all aetiologies. With more than 80,000 procedures performed to date, survival rates have improved significantly in the last three decades, achieving rates of 96% and 71% at one and 10 years after liver transplantation, respectively (116). With the advent and introduction of new immunosuppression regimens rates as high as 96% 1-year post transplant was achievable as opposed to 65% before introduction of calcineurin inhibitors (117). Despite this success, there is still a high mortality related to patients with end stage liver disease on the waiting list. Greatest challenge to liver transplantation is the availability of organs for transplantation. More so, it's a complex procedure and costly to both the health care and patients. With the indications for liver transplantation expanding, this is unlikely to improve in the future and the demand for livers is predicted to increase in the next 20 years; thus, research has focused on regenerative strategies to overcome these limitations (i.e shortage of organs) (118, 119). As for indication for transplantation, due to the success of the new antiviral therapy a shift in the paradigm has taken place over the past decade. The indication for transplantation has now expanded to include certain cancers within strict criteria (120). In the last decade, this focus has shifted from techniques such as cellular therapy to novel engineering techniques (tissue engineering) as new ways to either expand donor pool or to halt disease process so that time can be bought on the waiting list (118).

1.2 Cell therapy & other regenerative treatment strategies

The most reported technique in liver regeneration is cellular therapy and the oldest form of cell therapy described is hepatocyte cell transplantation (HTx) (Figure 11) (118). However, the focus has now shifted to other sources of cells and other bioengineering techniques (i.e organoids and artificial liver support systems (121)). They can be used as bridging therapy to liver transplantation and can be reproduced using bioengineering techniques.

1.2.1 Primary Hepatocyte Transplantation (HTx):

Hepatocytes are the functional unit of the liver and are not only involved in physiological functions but also play an important part in liver regeneration making isolated primary hepatocytes the most obvious candidate for cell therapy. HTx (**Figure 11**) was viewed as an alternative to whole organ transplantation due to its presumed benefit of replacing lost hepatic function in the recipients (122). Initial experience of cellular therapy for liver disease involved infusing primary human hepatocytes via portal veins (123). The ideal candidates for this form of therapy are those with certain genetic or metabolic liver disorders. Patients with Crigler-Najjar Syndrome Type 1, Urea cycle defect, Factor VII deficiency and glycogen storage disease type 1 were among the first to receive hepatocyte transplantation (124). Apart from the factor VII deficiency were the requirement for factor VII reduced by 80%, the rest of the entities did not show a success rate more than 50% (125). Despite some successful cases, the authors note limitations such as inconsistent cell engraftment, viability, and the gradual loss of transplanted cell function over time. Future directions that were proposed included enhancing cell engraftment techniques, improving cryopreservation methods, and potentially utilizing stem cells or genetically modified hepatocytes to increase long-term efficacy and accessibility of the treatment (124, 126). Although intraportal injection is the preferred method of cell delivery, intrasplenic hepatocyte transplantation is under investigation as an alternative effective therapy for liver failure to overcome challenges with intraportal injection (i.e. cell engraftment & portal hypertension) (127, 128). The intraportal method entails measuring portal pressure prior to infusion of cells and can accommodate up to 100 million cells per kilogram of patient body weight infused over several sessions. While its minimally invasive and allows for repeated infusion, it can be associated with limitations such as poor cell engraftment, increased portal pressure and can result in thrombosis at times.

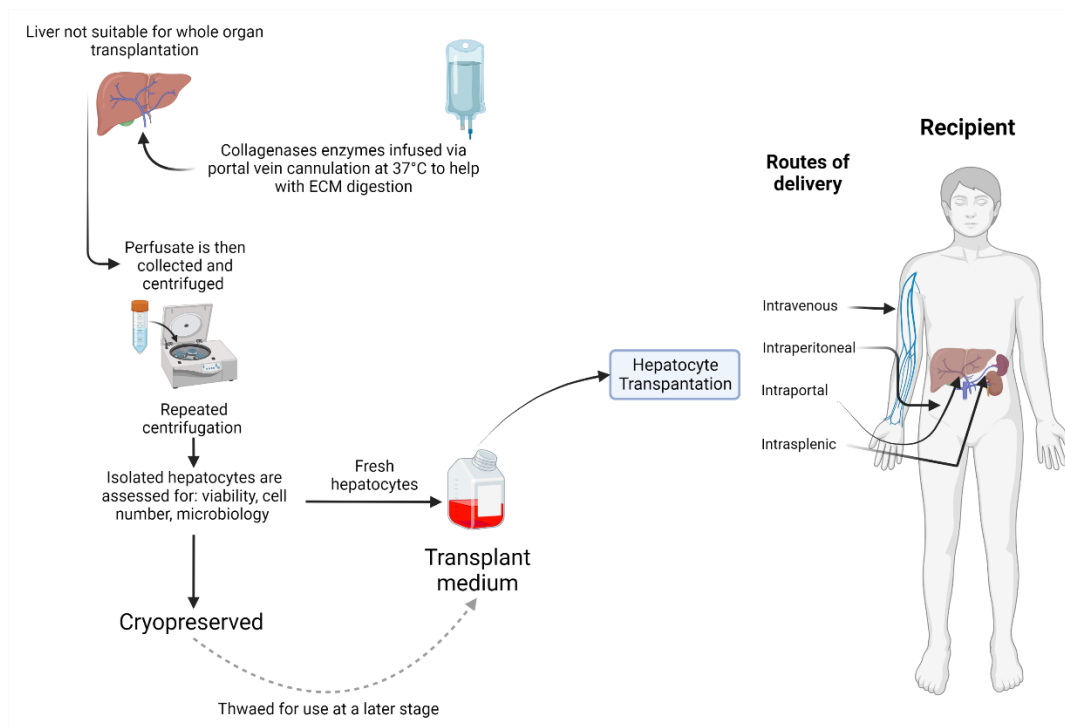


Figure 11 – Donor organs not suitable for whole organ transplantation are used to harvest hepatocytes for cell therapy. Often these donor organs tend to be of poorer quality as they have been declined for human transplant. The organs are subjected to an enzymatic digestion process to detach the hepatocyte from the ECM. The lysed cells are centrifuged several times to separate the cells from debris. Once isolated hepatocytes are assessed for quality and number, they can be transplanted fresh or can be cryopreserved for later implantation. Several routes of transplantation have been investigated. The entire process of enzymatic digestion and cryopreservation produces a loss of viable cells and a reduced cell function.

In a 5-year follow-up study of intrasplenic transplantation in 7 acute-on-chronic liver failure patients, Wang *et al.* reported clinical improvements in all patients following intrasplenic hepatocyte transplantation, with no splenic or liver infections or thrombotic complications (128). Three patients fully recovered, and one patient was bridged to transplantation. Although this is a small sample size and further studies are needed to evaluate the efficacy, this study suggests the possibility of intrasplenic hepatocyte transplantation as a promising therapy to decrease mortality rates in end-stage liver disease patients waiting for liver transplantation (128). While this route allows for hepatocytes to be deposited within the spleen's sinusoidal spaces, enabling them to function in a supportive role, it can be limited by efficacy of engraftment and within spleen hepatocytes can have limited function.

Foetal hepatocytes are a promising alternative to adult hepatocytes due to their high regenerative capacity. *Pietrosi et al.* assessed the safety and clinical efficacy of human foetal hepatocyte transplantation in 9 patients with the end-stage chronic liver disease through intrasplenic infusions (127). In this study, foetal hepatocytes were obtained from medically aborted fetuses aged 16 to 26 weeks of gestation. The foetal liver was obtained immediately post-abortion, preserved in University of Wisconsin storage solution, and transferred on ice to the laboratory for cell isolation. A vascular perfusion technique was employed to separate foetal hepatocytes, yielding around 1.5 billion cells with an average viability of 80%. Cells exhibiting vitality below 70% were excluded from transplantation. When compared to control patients on standard therapy, the treatment group showed improved Child-Pugh scores (10.1 to 9.1) with no adverse events related to the procedure. In addition, patients in the treatment group with a history of recurrent portosystemic encephalopathy had no further episodes during follow-up, whereas no improvement was observed in the control group. Due to the small sample size and non-randomized selection, the efficacy of foetal hepatocyte transplantation cannot be evaluated. However, the treated patients tolerated the procedure well and showed a stabilization in MELD score and positive effects on clinical scores, demonstrating that foetal hepatocyte transplantation is safe in end-stage liver disease patients (127).

The goal of hepatocyte transplantation is to aid regeneration of the native liver or to act as a bridge to liver transplantation (118). However, hepatocytes are often harvested from livers not suitable for transplantation, with the key limitation to hepatocyte transplantation being the poor availability of donor organs for the isolation of good quality hepatocytes (123, 129). In addition, necessary cryopreservation of cells affects viability and engraftment (130). Although, universal clinical guidelines for hepatocyte transplantation are not developed, numerous standards and best practices have been established by prominent research institutions and field professionals. These protocols include multiple facets of the procedure, such as: hepatocyte isolation and preparation (131), cryopreservation techniques (131), transplantation procedures (132), post-transplant monitoring (133). Therefore, alternative sources of cells have been investigated.

1.2.2 Stem Cells:

Stem cells can divide and renew themselves and can give rise to undifferentiated specialized cells (134). Liver stem cells are found in the Canals of Hering and are

considered to have the ability to differentiate into hepatocytes, however their true ability to transdifferentiate into mature hepatocytes is not fully known (135). Alternatively, researchers have generated hepatic progenitor cells from human embryonic stem cells through direct differentiation techniques. However, mesenchymal stromal/stem cells (MSC) are the most promising treatment for cirrhosis and have been identified as ideal candidates for cell therapy (130, 136). MSCs are a subtype of adult cells that have the capacity for self-renewal and the potential to differentiate into hepatocytes and hepatocyte-like cells (137). Although they are less effective than adult hepatocytes, MSCs can be isolated from multiple tissues, including bone marrow, adipose tissue, umbilical cord blood, and placenta (137). Additionally, they easily expand ex vivo and can selectively migrate to and engraft into damaged tissue following administration (136). In the past decade, multiple studies have utilized human embryonic stem cells and MSCs derived from different sources to treat patients (**Table 1**). Different routes of administration have been investigated. These studies demonstrated the safety of cells in treating liver disease, but no significant improvement was found in the treatment group. Despite the reported benefits from some studies, robust, randomized clinical studies are still required to gain confidence in the clinical efficacy of both stem cells and MSCs to treat liver disease (137). Additionally, a method to successfully track transplanted cells in the host liver is needed to collect quantitative data on repopulation, which is currently rare (129).

Table 1 - Clinical studies evaluating the use of stem cells and mesenchymal stem cells in liver disease. BM-MSC (bone-marrow-derived mesenchymal stem cell), SC (stem cell), MNC (mononuclear cell), G-CSF (granulocyte colony-stimulating factor), UC (umbilical cord), MELD (Model of End-Stage Liver Disease), AST (aspartate transaminase), ALT (alanine transaminase), INR (internationalized ratio) (138-150)

First Author (Date)	Type of Study	No. of patients treated	Controls (n)	Treatment received	Route of administration	Follow up (months)	Primary Outcome	Secondary Outcome / Results
Amer (2011)	RCT	20	Yes (20)	Autologous BM-MSC	Intrasplenic (10) Intrahepatic (10)	6	Safety and short term efficacy	Improvement in ascites + serum albumin. No significant

								nt differen ce between route of administ ration
Amin (2013)	Cohort Study	20	No	BM-MS	Injection	6	Safety and efficacy	Decreas ed bilirubin , AST, ALT, INR levels. Increase d albumin
Andreone (2015)	Phase I clinical study	12	No	BM-SC	Reinfusion	12	Safety	Signific ant improve ment within 2 months
El Ansary (2012)	Phase II clinical study	15	Yes (10)	MSC	IV injection	6	Safety and efficacy	Partial improve ment of liver function tests
Jang (2014)	Cohort Study	11	No	Autologous BM- MSC	Injection through hepatic artery	3	Improveme nt in patients' histological features	Liver histologi cal improve ments seen in 6/11 patients. Liver function
Mohamadn ejad (2013)	RCT	15	Yes (12)	Autologous BM- MSC	Infusion through cubital vein	12	Efficacy through absolute changes in MELD score	No significa nt changes in liver scores between two groups

Mohamadnejad (2016)	RCT	14	Yes (6)	Autologous BM-MNC	Intraportal infusion	6	Absolute changes in MELD score	
Nikeghbalian (2011)	Cohort Study	6	No	Autologous BM-SC	Intraportal	24	Safety and feasibility	
Park (2013)	Case series	5	No	BM-MNC	Hepatic artery infusion	4	Safety and feasibility	Serum albumin levels improved
Peng (2011)	Cas-control study	53	Yes (105)	Autologous MSC	Hepatic artery infusion	48	Safety, short and long-term efficacy	Albumin, MELD score significantly improved. No significant differences in incidence of HCC and mortality
Salama (2012)	Prospective cohort study	50	Yes (50)	SC	Portal vein or hepatic artery infusion	12	Health related quality of life	Greater survival seen in stem cell group. Grade of ascites improved
Sparh (2013)	RCT	28	Yes (30)	Autologous BM-MCT + G-CSF	Hepatic artery infusion	3	Absolute changes in MELD score (>3 point decrease)	MELD score improved in parallel in both groups. No significant

								improvements reported in treatment group
Zhang (2012)	Controlled study	30	Yes (15)	UC-MSC	IV infusion	12	Safety and efficacy	Some clinical signs/symptoms improved - reduced ascites volume, decreased levels of serum liver cirrhosis markers + improved liver function

In addition to direct administration, MSCs have been found to provide structural and trophic support to hepatocytes, improving the function and viability of transplanted primary human hepatocytes, irrespective of the route of administration (151). Fitzpatrick *et al.* found that direct co-culture of human MSCs isolated from the human umbilical cord or adipose tissue with primary human hepatocytes in-vitro improved production of both albumin and urea in comparison to hepatocyte monoculture (152). Additionally, the reported viability of cocultured hepatocytes was 16% greater than monocultured cells, demonstrating that coculture improved both function and viability, which could aid hepatocyte survival for cell therapy (152). Co-culturing with MSCs supports hepatocyte survival and function, making it a promising approach for enhancing cell-based therapies in liver disease and transplantation, however, it remains to be tested in clinical setting.

1.2.3 Induced Pluripotent Stem Cells (iPSCs):

In the last decade, advancements have been made in inducing terminally differentiated cells such as skin fibroblasts into pluripotent stem cells. These iPSCs can be sourced from

multiple cells and then induced to differentiate into liver-like cells (induced hepatocytes), providing yet another alternative source of cells (123). However, induced hepatocytes completely resembling the mature hepatocyte phenotype have yet to be reported, with cells more similar functionally to foetal hepatocytes (118, 153, 154). iPSCs yet are not viable to produce enough functional 2D hepatocytes for therapeutic applications (155). Additionally, they are restricted in their clinical application in human trials due to an associated risk of malignancy (156). Production of safe hepatocyte iPSCs is necessary before human clinical trials can be carried out. Despite this, iPSCs and induced hepatocytes have potential to aid pharmaceutical development in the future, as an unlimited source of cells to create cellular models of disease (118, 134). Rashid *et al.* successfully generated patient-specific human iPSCs from dermal fibroblasts of patients with different inherited metabolic diseases of the liver (157). Following differentiation of iPSCs into hepatocytes, they found that in 3 of the inherited conditions, generated hepatocytes recapitulated key pathological features of the disease, demonstrating how iPSCs can be used to model disease (157).

1.2.4 Bioengineering:

Modern liver tissue engineering has rapidly evolved in the last 10 years, and efforts now involve creating whole, implantable, and functional tissue-engineered liver construction (158). While U.S. Food and Drug Administration (FDA) has approved artificial skin and cartilage constructs, their clinical use remains limited. More so, there are no FDA or MHRA approved hepatic tissue engineered for tissue regeneration. Attempts to develop these platforms have been made mostly in in-vitro studies. Three-dimensional (3D) platforms include both scaffold-based systems and scaffold-free platforms that can provide support to cultured cells and allow the production and organization of cells in vitro (153). Scaffold-based systems offer structural support and mechanical properties needed for load-bearing tissues, while scaffold-free systems provide a more natural cell environment and are advantageous for soft tissues or applications where biocompatibility and immunogenicity are concerns (159, 160). In this way, the use of scaffolds can be combined with cell therapy to optimize hepatocyte transplantation. As mentioned previously, the main limitation of hepatocyte transplantation is insufficient cell survival following harvesting and isolation and then engraftment and immune clearance.

However, Török *et al.* found that by incorporating freshly isolated human hepatocytes onto a biodegradable polymer scaffold, hepatocyte function was preserved, and the initial cell loss seen in hepatocyte transplantation was reduced. These scaffolds were then cultured in a flow bioreactor that provided a pulsatile flow of nutrient-rich medium, promoting cell viability and function. In addition, a greater relative yield of hepatocytes with high viability was reported from smaller specimens of liver tissue, as opposed to an entire liver or lobe (161). This is significant considering the shortage of organs and tissues from which to culture cells, a key barrier limiting the advancements in cell therapy. While this is a useful step in advancing the technology, the study's six-day culture period, while useful for observing initial cell behaviour, may be insufficient to evaluate long-term hepatocyte function and the scaffold's support over extended periods, which are relevant for therapeutic applications.

Similarly, Yuan *et al.* were able to generate a scaffold from an acellular human amniotic membrane, which was combined with hepatocyte-like cells derived from human adipose stem cells to create a hepatic tissue graft, allowing effective engraftment of hepatocytes into the liver (162). Despite the short-term engraftment success, the paper was faced with a few challenges namely long-term engraftment, functionality, and immune compatibility. In this study use of 3D-AHAM scaffold supported hASC-HLCs with improved functional properties compared to traditional 2D cultures. While they did not provide an exact total cell mass transplanted, they demonstrated that hASC-HLCs cultured on the 3D-AHAM secreted higher levels of albumin (11 ng/10⁵ cells/day) and produced urea more effectively, indicating enhanced liver-specific function. The decellularized organs provide an ideal transplantable scaffold, however, there is limited availability and alternatives must be sought. Despite these scaffolds demonstrating improved liver function in animal models, they have yet to be trialled in humans. More recently, attempts have been made to provide a decellularized liver scaffold using a novel ultrasonic energy known as boiling histotripsy (163). Through mechanical disintegration of liver tissues while preserving the important structures like portal vein and bile duct, it provides a scaffold devoid of hepatocytes which can potentially be repopulated with cells. Although it is still an experimental entity it shows great promise for use in cell therapy as it does not have the negative effect collagenase enzymes pose on tissue and cells during cell isolation.

1.2.5 Organoids:

Organoids are 3D human micro-tissues that are generated in vitro, exploiting the general capacity of cells to self-organize and self-assemble into 3D spheroid structures known as liver buds(153, 164). Stem cells and primary human hepatocytes, as well as co-cultures of multiple and different cell types, can be used to form these transplantable organoids(153). Hu *et al.* successfully isolated human foetal liver cells to create hepatic organoids in vitro. Additionally, cryopreserved paediatric and adult primary human hepatocytes were used to establish organoids, but these were found to be more limited in expansion when compared to foetal cultures (165). Hu *et al.* demonstrated the ability to culture and expand human hepatocytes over long periods of time, which is significant since a key challenge in cell therapy has been maintaining viable and functional hepatocytes in culture for greater than two weeks (165). In fact, hepatocyte organoids derived from foetal liver cells were successfully cultured and expanded for an extended period, reaching over 11 months. It is hoped that, by providing a better understanding of the processes underlying mature hepatocyte expansion, novel therapeutic techniques in regenerative medicine can be designed (165). Liver organoids can be utilized to evaluate diseases including fibrosis, metabolic diseases, hepatitis, and malignancies (166).

One of the challenges with scaffolds is a lack of vascularity, resulting in cell necrosis and loss of function and failure of the graft to survive or function following transplantation in animal studies (158, 164). Takebe *et al.* successfully generated a functional and vascularized human liver from human iPSCs by transplanting liver buds that they created in vitro (167). Up to 48 hours after seeding, human iPSCs self-organized into 3D cell clusters which were mechanically stable and could be physically manipulated (167). Upon transplantation into a immune-deficient mouse model, human blood vessels within the liver bud connected to host vessels, forming functional vessels essential for successful engraftment (167). This process indicated that the host animal's vasculature and surrounding tissue provided the necessary stimuli for the differentiation and maturation of the hepatic organoids into a more complex, functional structure containing both hepatocytes and endothelial cells. While these findings are encouraging, administration of liver buds via blood vessels is currently not possible due to their large size, making routine use of organoids difficult (153). An alternative approach to tackle this limitation could be combining techniques by incorporating organoids into natural decellularized

liver scaffolds. Once repopulated, these scaffolds can recapitulate organ function, allowing for the formation of larger liver structures (164). This is one example of the barriers that need to be addressed prior to the successful application of organoids to human studies.

1.2.6 3D printing:

The introduction of 3D printing has allowed bioengineers to develop 3D tissue structures in which different types of cells can be organized, better preserving the function of cultures in vitro (164). Bio-printed tissue does not currently perfectly resemble the physical properties and function of the native liver. However, they do provide a better approximation of outcomes following injury than simple monocellular cultures, facilitating long-term assessment of liver toxicity and disease (164). It is unlikely that bioprinting and 3D fabrication techniques will be used to successfully treat patients with liver disease soon, but instead disease modelling will be the primary focus. As of today, bio-printed tissues are being used to model liver biology and disease and assess toxicity at a tissue level (164).

1.3 Conclusion

End stage liver disease of different aetiology is on the rise except for HCV which has reduced due to the success of new anti-viral. Despite the success of the liver transplantation, limitations of available donor pool, means mortality on the waiting list is unlikely to reduce in years to come. Effective anti-fibrosis therapies could transform the management of chronic liver disease by halting or reversing liver damage before cirrhosis sets in. For patients with significant fibrosis but without decompensated cirrhosis, such therapies could reduce the likelihood of needing a liver transplant. However, for advanced cirrhosis where fibrosis is extensive and liver architecture severely disrupted, anti-fibrosis therapy may only serve as a complementary approach, emphasizing the need for regenerative strategies or cell therapies to rebuild functional liver tissue. While still in experimental phase with no clinically approved regenerative technique, the proposed cell therapy and regenerative techniques have their own limitations. Lack of good quality donor organs, enzymatic digestion of the tissue that can affect the morphology of the cells and the invasive nature of the cell delivery are all common problems of cell therapy techniques.

Chapter 2 Therapeutic Ultrasound and applications

2.1 Introduction

Ultrasound (US), which is a first-line diagnostic investigation, as an energy source is now being adopted in various therapeutic applications e.g. drug delivery and ablation of small tumours (168-170). Its non-invasive nature and safe track record (171, 172) make it an appealing tool to be considered for therapeutic purposes. This is surmounted by the fact that it has real-time imaging capabilities; it's cost-effective as imaging modality and easily portable as a technology (173). Aside from advances in medical imaging, the US has shown potential for its use in wound healing, drug delivery, neural stimulation, bone healing, and use in orthodontic practice (**Figure 12**) (174-182). In addition to the above, its role in treating benign and cancerous lesions, as well as control of bleeding in a whole host of conditions is ever-expanding. More recently, the U.S. Food and Drug Administration (FDA) has approved histotripsy, a non-invasive technique that uses focused ultrasound waves to break down tumours, for the treatment of liver cancer (183). In addition, FDA has approved use of therapeutic focused ultrasound in treatment of essential tremor and Parkinson (184, 185). In UK, National Institute for Health & Care Excellence (NICE) has provided guidance on the use of ultrasound-guided high-intensity transcutaneous focused ultrasound for treating symptomatic uterine fibroids and in treatment of localised prostate cancer (186, 187). NICE has evaluated the EXOGEN ultrasound bone healing system for long bone fractures with non-union or delayed healing, providing guidance on its use (188).

Central to this expansion lies a better understanding of the fundamental properties of ultrasonic technology that can be harnessed in a safe manner. Ultrasound is described as a wave that can transport mechanical energy through the local vibration of particles (at frequencies of 22kHz or more), with no net transport of the particles themselves (172). Our understanding of this rather simplistic view of the US wave has changed greatly in medicine since its first experimental use as a diagnostic tool in the 1940s. Innovation of probes that can manipulate these frequencies beyond 30 MHz allows for greater penetration of tissues (**Table 2 & Table 3**)(in terms of depth and different tissue consistencies) and hence expands the range of tissues that can be targeted. High-frequency probes (shorter wavelength) provide better resolution but penetrate less deeply into the tissue; where as low-frequency probes (longer wavelength) but with reduced image resolution. Ultrasound probes used in therapeutic ultrasound (**Table 3**) focus the waves in one point/small area. In addition to depth of the tissue targeted, improved focus on target tissues through its small wavelength and precision control

over the shape and location of the energy position are considered advantages over other energy sources (189). However, it has challenges that needs to be addressed. Namely, injury can be sometime difficult to detect and its more difficult to monitor the effect and determine the adequacy of treatment. By tailoring therapeutic ultrasound probes to specific frequencies, power levels, and mechanisms, these devices can address a wide range of medical conditions non-invasively and with high precision.

Table 2 – This shows organized view of depth penetration, applications, and characteristics for different diagnostic ultrasound frequency ranges. These higher frequencies allow for: (1) greater depth penetration, (2) enhanced tissue differentiation, (3) expanded therapeutic application, (4) broadening diagnostic horizon, and (5) integration with emerging modalities (i.e. contrast enhanced US scans)

Frequency Range	Depth of Penetration	Applications	Characteristics	Reference
Low Frequency (2–5 MHz)	Up to 30 cm	<ul style="list-style-type: none"> - Imaging deep structures: abdomen, liver, kidney - Obstetric imaging: fetal anatomy - Cardiac imaging 	High penetration, lower resolution	Hedrick, et al. (190)
Mid Frequency (6–10 MHz)	3–10 cm	<ul style="list-style-type: none"> - Superficial organs: thyroid, breast - Vascular imaging: carotid arteries, deep vein thrombosis - Small-part imaging: testes, prostate 	Balanced resolution and penetration	Kremkau (191)
High Frequency (10–30 MHz)	1–5 cm	<ul style="list-style-type: none"> - Dermatological imaging: skin lesions - Ophthalmology: anterior eye segment - Musculoskeletal imaging: tendons, ligaments, nerves 	Excellent resolution, limited penetration	Kremkau (191)

Table 3 – Classification based on Frequency and Power Output of therapeutic ultrasound

Type	Frequency Range	Power Output	Applications
Histotripsy Probes	200 kHz–1 MHz	High (mechanical effects)	Non-invasive tissue ablation (e.g., liver tumours, thrombolysis).
HIFU Probes	0.5 MHz–10 MHz	High (thermal effects)	Tumour ablation, fibroid treatment, prostate cancer.
Low-Intensity Probes	<1 MHz	Low (non-thermal effects)	Neuromodulation, soft tissue healing, drug delivery.

Broadly speaking, US relies on two forms of energy to yield its desired effect: electromagnetic and mechanical energy. It is thought that the interaction of these energy forms with the tissue would result in thermal and non-thermal effects (192, 193). While the thermal and non-thermal effects of the US are considered separate entities (**Table 4**), but in reality, they are not separable (192). In practice, they are interrelated and typically occur simultaneously during therapeutic ultrasound applications. This interdependence means that isolating one effect from the other is challenging (192). However, by exploiting either form of these two effects (through manipulation of frequency range, power, & duration) one can achieve different therapeutic end results both *in-vitro* and *in-vivo* (194-196). These biological responses to the therapeutic effect of the US have played a major role in its current adoption (192). Hence, understanding how at the molecular or cellular level focused ultrasound can alter the properties of tissue can help in its better use and utilization leading to its translation into clinical endpoints. Here, we provide a summary of Focused Ultrasound and its other modalities with a particular focus on histotripsy and its potential clinical application.

Table 4 –Mechanisms involved in therapeutic ultrasound n both high and low frequency ultrasound

Mechanism	Description	Examples
Mechanical (Cavitation)	Uses focused ultrasound to create cavitation (microbubble formation and collapse) in targeted tissues, disrupting cell structures.	- Histotripsy for non-invasive tumor ablation.
Thermal (Focused Heating)	Ultrasound waves generate localized heating to coagulate or ablate tissues without damaging surrounding structures.	- HIFU for uterine fibroids and liver tumors.
Non-Thermal Effects	Low-energy ultrasound used to enhance cellular processes, stimulate healing, or facilitate drug delivery.	- Low-intensity ultrasound for neuromodulation

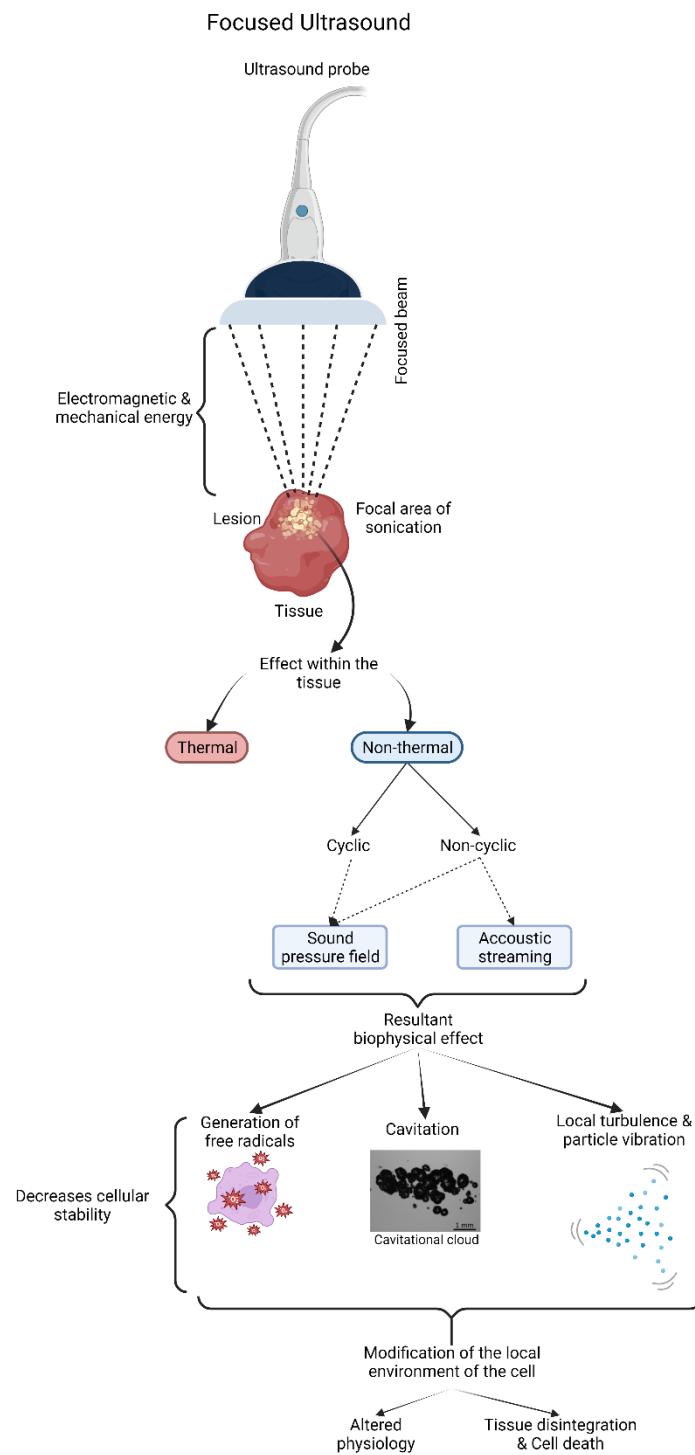


Figure 12 - General principle of mechanisms involved in the biophysical effect following sonication with focused ultrasound.

2.2 High-Intensity Focused Ultrasound (HIFU)

High intensity focused ultrasound (HIFU) is a non-invasive, non-ionizing energy modality that over the past decade has been under the spotlight of research as a promising technology in treatment of benign and cancerous lesions (189, 197). HIFU was first demonstrated for its therapeutic potential in central nervous system functional disorders (i.e. essential tremor and neuropathic pain) by Lindstrom and Fry in the 1950s (198, 199). Since then, its use has expanded in different areas of clinical practice. With recent advancement in MRI technology, HIFU targeting of the tissues can be more focused and the effect can be monitored (200). MRI can monitor tissue changes induced by HIFU through various parameters: (1) temperature mapping during treatment (real-time visualisation) which enables precise control of thermal dose to achieve effective ablation while minimizing damage to surrounding tissues (201); and (2) Post-treatment tissue characterisation which allows for evaluating tissue viability using parameters such as T1 and T2 relaxation times, diffusion-weighted imaging (DWI), and contrast enhancement patterns (202). Histological analysis obtained from resected surgical specimens post HIFU treatment are used to validate imaging findings and refine MRI protocols for better accuracy in assessing HIFU-induced tissue changes (203).

HIFU energy can pass through subcutaneous tissue without any damage and focus on a localised area in the deeper tissue. At the area where the beam is focused, temperature can rapidly reach 60°C or higher, leading to tissue changes that could range from thermal injury to coagulative necrosis with very sharp demarcations between the sonicated area and normal tissue (204).

2.2.1 Biophysical effects

The fundamental properties of the ultrasound technology rely on local particle vibrations (172). By altering the frequency between 0.7 MHz and 3.2 MHz, ultrasound can be manipulated for its mechanical and thermal effects. To a large extent evidence for these effects has been examined through in vitro studies (177, 192, 205-212) and only recently in vivo investigations have gained pace (182, 213-221). The molecular consequence of biophysical effects can be divided into the following categories: physical changes as a result of either heat or mechanical stress, chemical and stress-induced changes which can be either reversible or irreversible (**Figure 12**) (175, 222).

Rise of temperature in the focus of the sonication is dependent on a few important factors, which can be quantified by thermal index (Figure 2). Signal strength, area of targeted tissue,

amount of energy absorbed, medium/consistency of the tissue along with duration of exposure are all deemed important properties that affect the rate and extent of heat produced (172, 223, 224). Consequently, as the energy transported by ultrasound passes through tissue it gets attenuated, and its effect is far less in distant tissues. The attenuation of ultrasound energy as it passes through tissue is measured in decibels per centimetre (dB/cm) and depends on the tissue type, frequency of the ultrasound, and depth of penetration (225). For frequencies used in HIFU, attenuation can reduce intensity substantially within 2–10 cm (226). This means that for each centimetre the ultrasound wave travels through soft tissue, its intensity decreases by approximately 5 dB (227, 228). At a depth of 1 cm, the intensity drops by 5 dB, leaving about 31.6% of the original intensity (227, 228). Additionally, reduced heating occurs with pulsed ultrasound as opposed to continuous ultrasound. Hence, the heating produced by pulsed ultrasound is approximately dependent on the rate of on:off ratio (192, 229).

Draper et al (223) in a study examining the effect of continuous ultrasound (1.5W/cm² for 10 min) on temperature rise demonstrated the importance of depth and medium through which the energy is transferred. Comparing the temperature rise in human calf muscle following application of topical gel or underwater treatment, they were able to demonstrate ultrasound gel as a better conducting medium than water. The resultant temperature rise in topical gel group was 4.8°C compared to 2.1°C in water group (P<0.001). A suitable medium can help to reduce dissipation of the energy form in low frequency modalities. Also, the authors demonstrated the form of delivery of energy (continuous vs pulsed short wave) can affect the rate of rise of temperature. Thus, demonstrating this difference is due to the distinct energy delivery methods of each modality, rather than heat dissipation from the muscle.

Thermal:

Lesion size and tissue response

Typically, thermal effects are temporary unless they are used in increased orders of treatment and with a focused area of sonication. Whatever range frequency used, the extent of physiological response to heat may depend on several factors, including maximum temperature achieved, rate of temperature rise, time of heating and heated volume (193, 230). This is particularly relevant when considering clinical application of ultrasonic energy. Furthering the chain of variables, at lower number of sonication typically cellular function is altered via either (a) structural disruption (i.e. partial cell lysis) (231) or (b) enzymatic changes which respond to heat either via change of enzyme structure or by alteration of function (232).

At higher intensities similar effects occur but are more pronounced and lead to cell death or necrosis.

Currently, large-volume ablations (volume is relative and depends on target tissue i.e. for uterine fibroid 100-200 cubic centimetre (233) & for liver volumes exceeding 50 cubic centimetre (234)) are most efficient at frequencies of 500-700 kHz and depths of 100-150 mm (235). However, the limitation of such high frequency is an accumulation of near-field heat which prevents large-volume ablation. The rapid heating associated with high-frequency ablation can cause tissue charring or vaporization, creating an insulating layer that impedes further energy transmission and limits the size of the ablation zone (236). Because of this accumulated effect on healthy tissue / beyond the margins of ablation, lower frequencies are preferred (235). Additionally, if one is concerned with the preservation of blood vessels then pulsed HIFU has been shown to have better efficiency to induce tissue damage without affecting the blood vessels (237). While preservation of such structures is important to the regenerative applications, for cancer treatment the effect would have to get to the entire lesion, including the most distant from the transducer. Such understanding of the structural responses to HIFU is essential when considering the repair and regeneration of tissue. In studies demonstrating the effect of HIFU on tumour mass, the ultrasound beam is a focus to ablate the cancerous tissue along with the blood vessels that supply it. As demonstrated by *Guan et al* (238), the thermal effects of HIFU are not limited to cancerous cells only, the surrounding blood vessels that supply the malignant tissue are also destroyed. Using colour Doppler flow imaging, they were able to demonstrate the disappearance of peripheral and internal blood flow of the endometrial cancer tissue following HIFU therapy in the rabbit model.

HIFU and angiogenesis

Preventing angiogenesis may well be an important strategy in tumour growth suppression, however, at the other end of spectrum, tissue regeneration is a processes dependent on stimulation of angiogenesis (239). Thermal exposures equivalent to 41-45 °C for at least 5 minute has therapeutic consequences such as increased blood flow or reduction in muscle spasm as demonstrated in observational studies (182, 194, 240). In adipose tissue, thermal injury, following sonication, has been shown to result in coagulative necrosis and cell death (241). Consequently, there are reports of new collagen and elastin formation after thermoablation (242). Alteration of extracellular matrix seems to be a recognised thermal effect of HIFU demonstrated in use of therapeutic ultrasound in bone healing (230, 243).

Prevention of tissue hypoxia, hypovascularity, and hypocellularity in the context of sonication could not solely be explained by one property of the ultrasound and perhaps is a combination of ultrasonic properties that bring about the physiological change. What is clear however, is that tissue repair and regeneration is a complex process that involves interaction between different molecular machinery.

The non thermal effect of HIFU include acoustic cavitation, shearing and chemical changes because of free radical formation (**Figure 13**) (194).

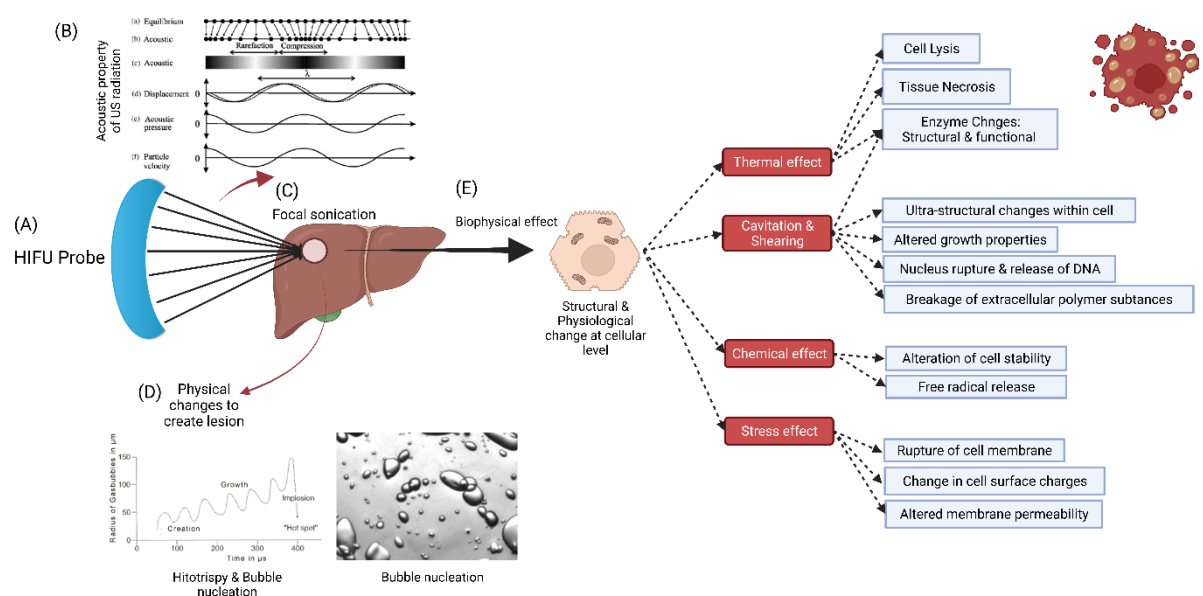


Figure 13 – Biophysical changes created by the sonication of High Intensity Focused Ultrasound. Depending on the modality of focused ultrasound used there are different biophysical changes brought about that can be either detrimental to the health of the cells within tissue or augment the process of regeneration and responses.

Cavitation & Acoustic streaming:

Perhaps the most important of the non-thermal effects is cavitation, a term first described by Sir John Thornycroft in the early 20th century (192). Historically, the term referred to formation and life of bubbles in liquids (192, 244). This is known as ‘bubble nucleation’. The phenomenon of nucleation is a thermodynamic process that is affected by both temperature and supersaturation levels of the liquid (244, 245). Their life cycle is dependent on several important factors: acoustic frequency, intensity, exposure time and availability of the

cavitation nuclei (182, 244-248). The acoustic pressure results in compression waves leading to formation of cavitation bubbles (**Figure 14**). The ongoing compression and rarefaction of the acoustic pressure results in the growth of the bubble. The size increases until it reaches an unstable size at which point it results in violent collapse. Ensuing this violent collapse is generation of free radicals due to high temperature and the pressure associated with collapse (245, 246, 249). Subsequently, if this occurs in the vicinity of living tissue it alters the tissue structure and function and can shatter cellular architecture. The extent of change is dependent on the amount of protein present in tissue (248, 250-252). Since absorption of ultrasound energy is dependent on the protein concentration and water content, tissues with greater protein concentration will have greater absorption capacity (248, 250). Ultimately, as the amount of energy absorbed increases, part of that mechanical energy is converted into heat. This is normally measured by attenuation coefficient (measured in decibels per centimetre per megahertz (dB/cm/MHz)) and higher values denote greater absorption and, consequently, more significant heating. For example, attenuation coefficient for fat is thought to be approximately 0.63 whereas liver is measured as ~0.5 and bone is close to 20 dB/cm/MHz (224, 229, 253). In theory, such changes in the temperature could occur in the micro-environment of the cells because of cavitation, however measuring such change in reality may not be possible (194).

Cavitation seems to be the main mechanism by which histotripsy interacts with tissue and results in the generation of acoustic cavitation and tissue breakdown (248, 254, 255). Results from different experiments have revealed the presence of nano meter-scale gas pockets in tissue that can function as cavitation nuclei (248, 254, 255). Once intrinsic threshold has exceeded, the resultant effect is the generation of cavitation during histotripsy sonication. This is achieved when microsecond length pulses reach negative pressures that exceed an intrinsic threshold and overcome the surface tension of existing nanometre gas pockets (255). This threshold has been measured in ex-vivo experiments to be 26–30 MPa for water-based tissues such as blood clots, liver, kidney, heart, brain, spleen, pancreas, as well as blood and water (255, 256). While intrinsic threshold does not change much with the changes in frequency, the consistency of the tissue changes the intrinsic threshold. As mentioned before the intrinsic threshold for cavitation within water-based tissues is between 26-30 MPa, whereas in the adipose tissue this is lower in the orders of 14-17 MPa (256, 257). This means the effectiveness of the histotripsy are determined by the viscoelasticity of the target tissue that in turn determines the dynamic of the cavitation bubbles (252).

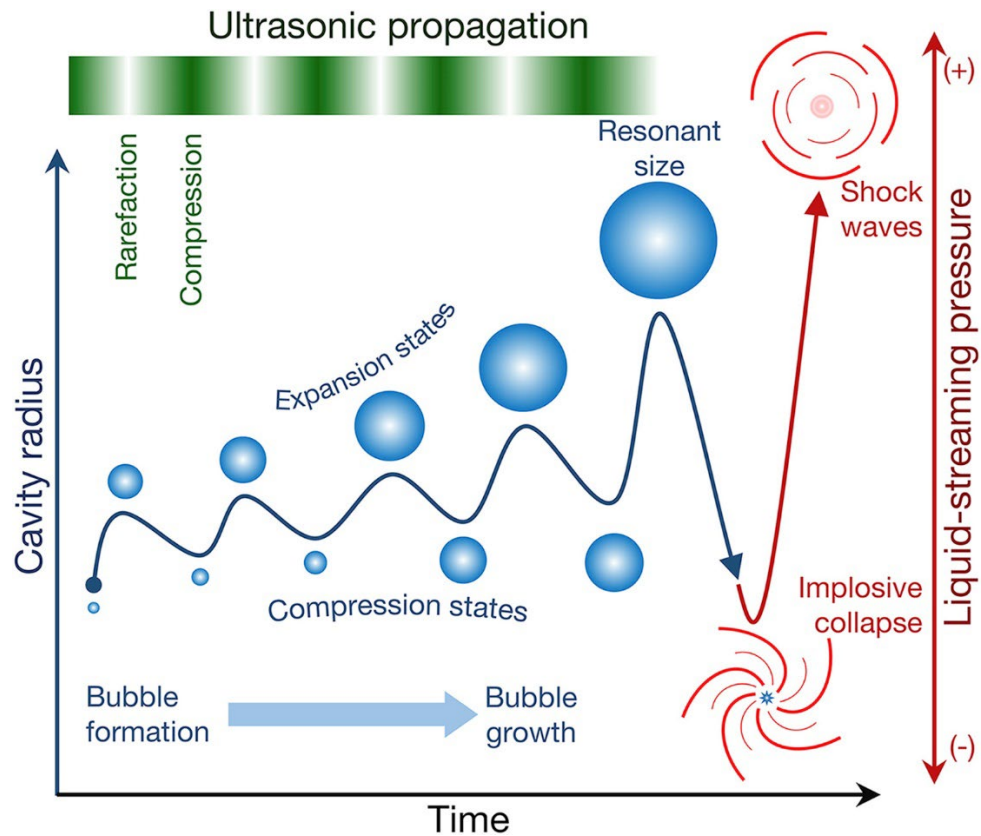


Figure 14 - Formation illustrations of acoustic cavitation throughout external ultrasonic propagation and of rebounding shock waves after implosive collapse (Figure from (246)). Cavitation microbubbles are thought to be generated in the extracellular matrix. Bubbles grow from 2–5nm to >100 μ m followed by energetic collapse within a few hundred microseconds(255). This rapid expansion and collapse of microbubbles produce very high strain and stress to immediately adjacent cells resulting in a precise mechanical disruption which can occasionally even disintegrate cells at the sonication site.

Another physical property of sound waves is acoustic streaming (**Figure 13**), a driving force capable of displacing ions and small molecules (182, 194, 258). In practice, it is very difficult to isolate and distinguish between the effects of cavitation and acoustic streaming. However, it is thought that acoustic streaming at cellular or molecular level can exert a unidirectional force on free floating ions and organelles that can lead to altered function and changes in structural integrity (259). Usually, these mechanical properties of ultrasound become more pronounced when the thermal effect is minimised (260). One way to achieve this is use of pulsed focused US (pFUS) rather than continuous focused US (cFUS), as this allows cooling of tissue in between pulses. In a recent study, *Burks et al* (261), revealed pFUS (peak rarefaction amplitude, 8.9 MPa; pulse repetition frequency, 5 Hz; duty cycle, 5%; number of pulses per site, 100) had little effect on the histological integrity of muscle and it did not

reveal cell death unlike cFUS. In addition, at cellular level pFUS resulted in increased cytokine release and increased expression of signalling molecules (e.g., ICAM-1 & V-CAM-1). The observed increase in repair signals in less damaged tissue could be due to an optimal balance of mechanotransduction-induced signalling without overwhelming tissue damage. In other words, severely damaged tissues may prioritize survival pathways (e.g., minimizing inflammation to prevent further injury) overactive repair. These findings have important implications for use of therapeutic ultrasound in inflammation and tissue regeneration.

Early studies investigating the gross effects of acoustic streaming and cavitation on cells revealed growth retardation of cells in vitro (230, 262), increased protein synthesis (230, 261, 262), and membrane alterations (194, 261). These properties which can be modulated in different clinic-pathological settings to alter the course of pathology and bring about desired physiological change.

2.3 Different modalities of focused ultrasound (FU)

Focused ultrasound can be delivered in the various intensities with different frequency ranges. It is important to note that the parameters of the HIFU are different to ones used in histotripsy (255). Histotripsy uses short ultrasound bursts (microseconds in length) with a low duty cycle (1%), higher peak pressure amplitudes, and endogenous gas in tissues to generate acoustic cavitation, whereas, thermal HIFU uses continuous or long bursts of ultrasound at moderately high intensity and high duty cycle (ultrasound on-time/total treatment time >10%) to heat tissue (255, 263, 264).

Types of histotripsy

Histotripsy is now distinguished into three different modalities based on its mechanistic properties (Intrinsic threshold histotripsy, Shock-scattering histotripsy, Boiling histotripsy) (Table 5). This is based on the difference between the frequency and the geometry of the transducer which in turn determines the size of the focal zone (255, 265).

Table 5 – Typical Histotripsy parameters used (255)

Parameters	Intrinsic Threshold Histotripsy	Shock-scattering Histotripsy	Boiling Histotripsy	HIFU
Frequency	250kHz–3MHz	500kHz–3MHz	1–3 MHz	1–5 MHz
Pulse duration	1–2 cycles (0.5-4ms)	3–10 cycles	100–200 (1–20 ms)	Continuous waves or high duty cycle
P-	>26 MPa	15–25 MPa	10–20 MPa	5–10 MPa
Pb	No requirement	>50MPa	>70MPa	5–30 Mpa
Duty cycle	1%	1%	2%	10–100%
PRF	1Hz – 1kHz	1Hz–1kHz	1Hz–2Hz	-
I _{SPPA}	>30 kW/cm ²	9–40 kW/cm ²	8–30 kW/cm ²	0.5–10 kW/cm ²
I _{SPTA}	0.5–300 W/cm ²	1–400 W/cm ²	50–600 W/cm ²	100–5000 W/cm ² –
Number of pulses	50–2000	50–2000	1–100	
Bioeffect	Mechanical tissue liquefaction		Mechanical tissue liquefaction	Thermal necrosis
Mechanism	Inertial cavitation		Boiling cavitation	Thermal

2.4 Clinical applications of focused Ultrasound

Histotripsy as well as other modalities of therapeutic ultrasound have been widely investigated in a range of pre-clinical and clinical settings. Below is a summary of some of its potential uses and the pre-clinical work leading to its potential clinical application with focus on histotripsy modality.

2.4.1 Neurology:

HIFU has been approved for clinical use in treatment of several neurological disorders (189, 266-273). Its use in essential tremor and Parkinson’s disease have been approved by FDA (274) within USA and elsewhere it has been used for neuropathic pain, obsessive compulsive disorder (272, 275). It is currently being trialled and investigated for treatment of entities such as Alzheimer’s disease or Epilepsy (276-278). HIFU has also been shown to have beneficial effect on brain tumours (i.e. glioblastoma) resulting in tumour thermocoagulation (273) as well as spinal cord lesions (279). The possible mechanism involves focused ablation with the resultant heat (typically above 60°C) produced at the tumour site that can induce protein denaturation and cell death within the tumour while sparing surrounding tissues (280, 281). The subsequent tumour cell death can release tumour antigens into the microenvironment,

potentially enhancing the immune system's recognition and attack of the remaining tumour cells (282).

More recently, histotripsy has been trialled for the treatment of different neurological conditions in pre-clinical settings, namely embolic stroke (283). Histotripsy has been shown in swine models to safely liquify clots without significant additional damage to the perihematoma region (284). The liquefied content of the clot could be easily evacuated, and the undrained clot had no effect on pig survival or neurological behaviour. Additionally, because of the property of histotripsy to be able to create cavitation bubble clouds that could lead to mechanical fractionation of tissue with sharp borders, it has also been subject to trial in animal models for treating cortical lesions. Sukovich et al (285) showed histotripsy can be used to generate sharply defined lesions of arbitrary shapes and sizes in the swine cortex. Lesions confined to within the gyri did not lead to significant haemorrhage or oedema responses at the treatment site in the acute or subacute time intervals. While this study indicates minimal haemorrhage and oedema, long-term safety, including effects on neural function and potential delayed complications, needs further validation. Data on chronic effects, including recovery, neural plasticity, and functional outcomes, remain limited.

2.4.2 Drug Delivery:

HIFU and other modalities of focused ultrasound have been used to increase drug delivery in various settings. Exposure to varying degree of a given frequency or intensity of ultrasound beam results in various biophysical effects in cells or tissues (286). In addition to cavitation and hyperthermia, the other well-known biophysical effects of ultrasound on cells is Sonoporation (**Figure 15**) (182, 286, 287). Each of the effects have different impacts on cell function and can be exploited for different therapeutic applications. Broadly speaking, focused ultrasound assisted drug delivery has been orientated on either of the two different aspects: (1) to increase local uptake of drug and reduce the systemic dose, (2) once nanoparticle drug is delivered to potentiate the effect of histotripsy dosage thus reducing the local side-effects related to the histotripsy dose but potentiating the therapeutic effect (288). In both approach the use of focused ultrasound and therapeutics have a synergistic effect.

Cavitation induced sonoporation occurs when ultrasonic beams/energy mechanically alters cell membrane molecules through micro bubble formation to enhance pore size and thus increase cell membrane fluidity (182, 286). This *ultrasound-mediated process temporarily permeabilizes the plasma membrane of living cells via mechanical forces generated by*

cavitation bubble dynamics, enabling the intracellular delivery of exogenous substances such as drugs and genes.. emulsions (capable of delivery of drugs or genes through a semi-permeable membranes) can enter cells passively through leaky membrane (**Figure 15**). Hence, ultrasound has been found useful in helping cells absorb small molecules, genes, and nanoparticles. Cavitation can also result in sonoporation through development of cavitating bubble nucleation (mechanism described in section 2.2). Cavitation-induced sonoporation (5) can then be used to deliver exogenous nano-emulsion particle that can be coated with surfactant and synthetic polymers to stabilise it as they can carry drugs, genes to the intracellular space (286, 289, 290). The use of exogenous particles can reduce the cavitation threshold (290). Sonoporation can temporarily increase the permeability of cell membranes, this has significant effects on cellular function and viability. This technique is widely studied in biomedical applications for not only drug delivery but also for gene transfections.

In addition to the effect on the cell membrane permeability, focused ultrasound is thought to alter local physiological conditions which can in turn alter cellular function. The force generated by the ultrasonic beam along with alteration in cell membrane permeability result in influx of ions from the extracellular space into the cellular cytoplasm (286).

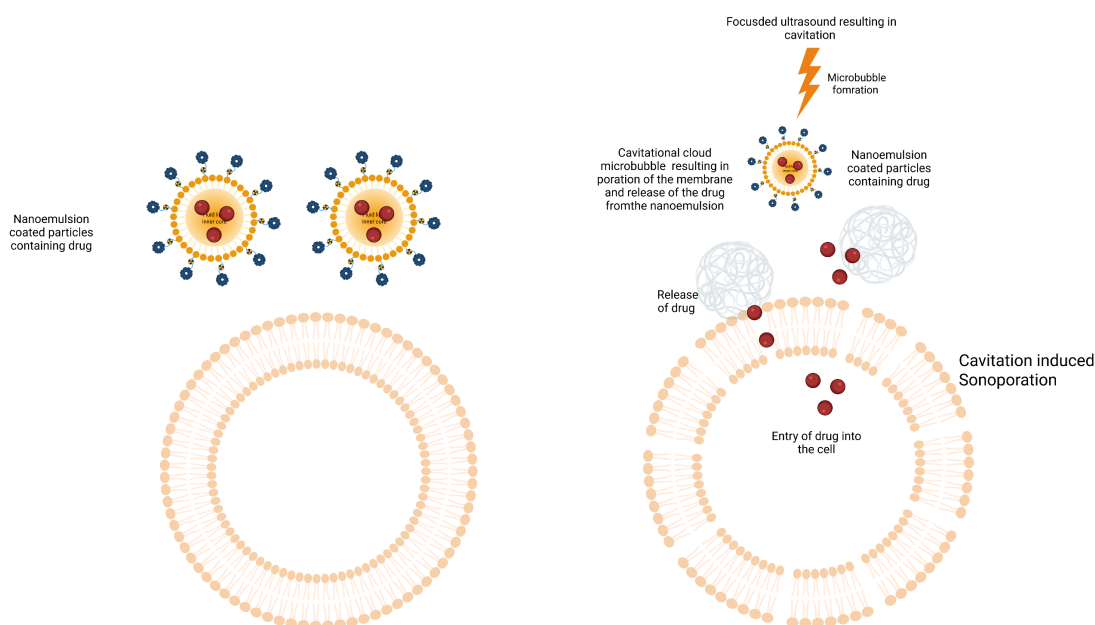


Figure 15 – Cavitation induced sonoporation

A good example for the use of sonoporation is in drug delivery into the central nervous system where the blood brain barrier must be negotiated. Presence of blood-brain barrier (BBB)

allows for selective entry of molecules into the central nervous system (**Figure 16**). While it has a protective role in normal physiology, it can be a barrier to therapeutic agents used for targets within the central nervous system. Available agents that can be used for different neurological disorders are usually not delivered to the brain because of the presence of the BBB or are delivered in sub-therapeutic level. Focused ultrasound combined with microbubbles can reversibly and temporarily open the BBB, thus enabling delivery of the therapeutic agents for the neurological disorder (291).

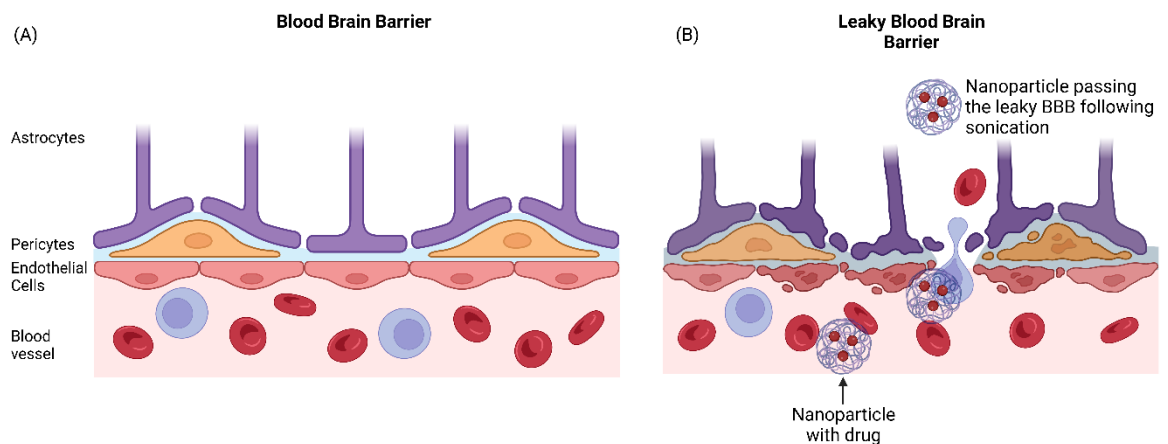


Figure 16 – BBB is a selective barrier that only allows certain molecules to pass. The selectivity of the BBB means drug delivery is often limited and sub-therapeutic concentrations of the drug in the CNS does not bring about the desired therapeutic effect. Focused ultrasound can result in poration of the BBB and makes it leaky, thus allowing drugs to pass readily across to the CNS from the blood stream. This is often a reversible change.

2.5 Focused Ultrasound in hepatobiliary Malignancies

Focused ultrasound and HIFU have been used both in the pre-clinical and clinical settings for the treatment of a wide variety of malignancies. The general applications have been reviewed:(204, 292)), Here we only focus on its use in treating hepatobiliary malignancies.

2.5.1 Liver Cancer

With the advent of modern imaging modalities, the potential applications for HIFU treatment have grown significantly; ultrasound and MRI are both used to guide and monitor HIFU beams (293). Because of its ability to target deep-seated tumours, HIFU

has become particularly appealing in cancer treatment, particularly in hepatobiliary tumours, where it has been used to ablate hepatocellular carcinomas.

HIFU has several potential advantages over other cancer treatment methods. HIFU is highly focused and spatially confined, resulting in less damage to surrounding tissues. Treatments are typically performed in a single session, often as a day case, avoiding prolonged hospital stays. Depending on the size, location, and patient preference, HIFU can be performed under general or epidural anaesthesia. Treatment time (**Table 6**) is comparable to other localised therapies, and systemic side effects are minimal.

Table 6 – Comparison of treatment time of different local therapy techniques with HIFU & Histotripsy

Therapy	Mechanism	Typical Treatment Time	Notes
HIFU	Thermal coagulation	30 minutes to 3 hours	Dependent on lesion size; requires slow energy deposition to avoid overheating. (294)
Histotripsy	Mechanical cavitation	10–30 minutes	Faster for larger lesions due to precise, localized energy application. (295)
Radiofrequency Ablation (RFA)	Thermal coagulation	30–90 minutes	Like HIFU but limited by thermal spread in surrounding tissues. (296)
Microwave Ablation (MWA)	Thermal coagulation	15–60 minutes	Quicker than HIFU due to higher energy deposition rates. (296)
Laser Ablation	Thermal ablation	30–90 minutes	Precision targeting for small lesions; longer for larger areas.(297)
Stereotactic Radiosurgery	Ionizing radiation	1–2 hours per session	May require multiple sessions over days or weeks.(298)

HIFU has potential advantage over surgery including the ability to target difficult-to-reach areas, lower risks of bleeding and infection, and less post-operative scarring and/or pain. In addition, unlike other ablative therapies, HIFU does not require an applicator to be placed directly on the target area (299). As a result, it does not pose the risk of cancer spread through seeding along the needle track that percutaneous ablation techniques do.

HIFU can target larger tumours (>3cm) than other ablative techniques such as RFA or MWA (300). Majority of the prior experience with HIFU is based on thermal ablation and tumour destruction in the context of liver tumours (293) (Table 7).

Table 7 – Summary of studies that have used HIFU to treat different hepatic lesions with the parameters used.

Study	Frequency (MHz)	Mean Total Exposure time (s)	Exposure time range (s)	Transducer aperture (mm)	Focal Length (mm)	Acoustic Power (W), median (Range)
Zhu 2008 (301)	0.8	10080	4260-22680	150	150	160-250
Zhang 2008 (302)	0.8	n/a	n/a	150	150	160-250
Numata 2009 (303)	1	833	401-1225	n/a	n/a	300-450
Jin 2010 (304)	0.8	n/a	3480-14520	120	135-155	160-350
Wang 2010 (305)	0.9	720	360-1260	200	120	200-400
Ng 2011 (306)	0.8	1560	180-7440	120	120	376 (155-473)
Xu 2011 (307)	0.8 / 1.6	4680	2700-9000	n/a	100-135	160-240
Cheung 2012 (308)	0.8	2864	n/a	n/a	n/a	391
Fukuda 2012 (309)	1	n/a	n/a	n/a	n/a	n/a
Leslie 2012 (310)	0.84 / 1.8	1260	12-2640	n/a	135/122	140-350
Kim 2012 (311)	0.8	3660	1380-16320	150	135	100-400
Ni 2012 (312)	0.8	n/a	n/a	120	150	n/a
TCheung 2012 (313)	0.8	1478	135-7487	n/a	120	371 (120-473)
Chan 2013 (314)	0.8	n/a	n/a	n/a	100-160	230-466
Cheung 2013 (315)	0.8	n/a	n/a	n/a	120	n/a
Fukuda 2013 (316)	1	n/a	n/a	200	150	300-450
TCheung 2013 (317)	0.8	n/a	n/a	n/a	120	n/a
Wang 2013 (318)	0.8	n/a	1800-12120	120	135-155	181-256
Zhu 2013 (319)	0.8	1985	611-4182	120	135 / 155	250-400
Cheung 2014 (300)	0.8	2606	338-7302	n/a	120	n/a
Chok 2014 (320)	0.8	1560	180-7440	n/a	150	376 (155-473)

QZhang 2019 (321)	0.96	n/a	n/a	n/a	n/a	n/a
Luo 2019 (322)	0.8	n/a	4946-16223	n/a	150	n/a
Average HIFU technical parameters	0.8 (mode)	2958 (mean)	n/a	120 (mode)	120 (mode)	323 (mean)

Sehmbi et al (293) review revealed 16 of 24 studies reported post-HIFU complications (**Table 7**) (300-302, 304, 306, 307, 310-315, 318, 319, 321, 322). The average HIFU frequency used in this study were 0.8 MHz with an average total exposure time of 2958 second (**Table 7**).

Outcomes

Tumour ablation rates for each study, as assessed by post-procedure imaging (MRI and/or CT), are presented in **Table 8**. There was great variability in tumour ablation rates, coupled with the inhomogeneous treatment protocols, HIFU technical parameters and patient characteristics no clear relationships could be established. Of all HIFU treatment procedures 51.68% resulted in complete tumour ablation, and 48.32% did not achieve complete tumour ablation.

Data on the survival of patient's post-procedure, both overall survival and disease-free survival, was only provided by some of the studies researched. Overall survival data, as a percentage of all patients treated with HIFU, was provided by ten studies reporting on 430 cases and is presented in **Table 9**. Mode of follow up was three years, however three studies followed up patients for 5 years. Survival data is difficult to compare across the cohort, as we cannot consider, stage, grade, size and position of tumour as well as comorbidities or patient demographic. Nonetheless we can see that overall survival at years one, three and five was 79.3%, 55.3% and 21.6% respectively.

In many of the studies HIFU was used as an adjuvant or secondary treatment (302, 304, 307, 308, 311, 312, 314, 318) and in a few studies as a bridging therapy (308, 317, 320). However, there were some studies which directly compared HIFU with RFA or TACE treatment. HIFU treatment alone has been compared with TACE by Cheung et al (300, 317), In both studies there was a higher rate of complete tumour ablation and increased survival in the HIFU group. Chan et al (314), performed a prospective clinical trial which directly compared HIFU against RFA in the treatment of recurrent HCC. This

study highlighted similar efficacy with both approaches, with slightly reduced side effects in the HIFU treatment group.

There is some evidence to suggest that the combination of HIFU with other ablative therapies, particularly TACE, is more effective than any alone. In combination studies, HIFU in conjunction with TACE, RFA or PEI, complete tumour ablation rate was higher at 58.72%.

Table 8: HIFU treatment outcomes

Study	Total Number Treated	Complete Tumour Ablation 100% (n)	Incomplete tumour Ablation <100% (n)
Chan2013 (314)	27	23	4
Cheung2012 (308)	1	1	0
Cheung2013 (315)	47	41	6
Cheung2014 (300)	26	13	13
Chok2014 (320)	21	7	14
Numata2009 (303)	21	18	3
Fukuda2012 (309)	14	11	3
Zhu2008 (301)	16	16	0
TCheung2013 (317)	10	9	1
Jin2010 (304)	73	33	40
Zhang2008 (302)	39	21	18
Leslie2012 (310)	31	28	3
Kim2012 (311)	25	5	20
Ng2011 (306)	49	39	10
Ni2012 (312)	120	0	120
TCheung2012 (313)	100	76	24
wang2010 (305)	9	9	0
Wang 2013 (318)	12	10	2
Xu2011 (307)	145	34	111
Zhang2011 (323)	39	28	11
Zhu2013 (319)	9	9	0
Total	834	431 (51.68%)	403 (48.32%)

Table 9: HIFU treatment overall five-year survival

Study	Overall Survival % (number of surviving patients)				
	1 year	2 years	3 years	4 years	5 years
Chan2013 (314)	96.3 (26)	76.1 (21)	64.2 (17)		
Cheung2012 (308)					
Cheung2013 (315)	97.4 (46)		81.2 (38)		
Cheung2014 (300)	84.6 (22)		49.2 (13)		32.3 (8)
Chok2014 (320)	100 (21)	100 (21)			
Numata2009 (303)					
Fukuda2012 (309)					
Fukuda2013 (316)					
Zhu2008 (301)	100 (16)	83.3 (13)	69.4 (11)	55.6 (9)	55.6 (9)
TCheung2013 (317)					
Jin2010 (304)	49.1 (36)	18.8 (14)	8.4 (6)		
Zhang2008 (302)	75.8 (30)	63.6 (25)	49.8 (19)	31.8 (12)	
Leslie2012 (310)					
Kim2012 (311)					
Ng2011 (306)	87.7 (43)		62.4 (31)		
Ni2012 (312)	75 (90)		35 (42)		15 (18)
TCheung2012 (313)					
wang2010 (305)					
Wang 2013 (318)	91.7 (11)	83.3 (10)			
Xu2011 (307)					
Zhang2011 (323)					
Zhu2013 (319)					
Mean	79.3 (341)	55.3 (104)	44.6 (177)	38.2 (21)	21.6 (35)

Eight articles reported no complications or did not specify the type(s) or frequency. Procedure-related deaths were unreported. Skin burns (15%), local pain (5%), and fever (2%) as well as post-HIFU pain were common reported complications, but some articles did not report pain or did not consider "mild" pain a complication. HIFU treatment of liver lesion has

been demonstrated to be a safe method and can be used either alone or in combination with chemotherapy or other local therapies.

Vidal-jove et al (324) published the first-in-man results of use of histotripsy in treatment of hepatic tumours (THERESA trial) in 2022. In this feasibility trial, 8 patients with a median age of 60.4 years with an average of targeted tumour diameter of 1.4cm were recruited to receive histotripsy. They demonstrated a safe and effective treatment of hepatic lesion with no evidence of tumour post 12 weeks after scan. Although this trial has several limitations (i.e., heterogenous pathologies, patients has received other forms of treatment prior to histotripsy), it on the other hand highlights the potential of histotripsy as a non-invasive and effective treatment modality in dealing with liver lesions and highlights the need for further clinical work. The gold standard for comparison in treating small HCCs is typically RFA, a widely used thermal ablation technique. Although no efficacy trial has directly compared HIFU and RFA in treating recurrent HCC, finding from several studies have shown similar efficacy between the two methods, with HIFU associated with slightly reduced side effects (293, 325).

2.5.2 Pancreatic cancer

Due to non-invasive nature HIFU has been considered in the treatment for advanced pancreatic malignancy. Although in clinical setting it has mostly been trialled for palliation, initial reports of HIFU use are encouraging and suggest that this technique is safe and can be used alone or in combination with systemic chemotherapy or radiation therapy (326-330). Analgesia is an essential aspect of quality of life in individuals with advanced pancreatic carcinoma. A meta-analysis of 23 studies involving 865 patients, 729 of whom had pancreatic cancer, revealed that HIFU treatment provided considerable pain alleviation for a significant number of patients (random effect: 0.81 (95% CI: 0.76–86)) (331) (**Figure 17**). On average a tumour reduction in size of ~50% has been reported (327, 332). However, notable side effects reported include Subcutaneous fat & vertebral necrosis, transient pancreatitis, pseudocyst, skin burns 1.1- 71%, tumour duodenal fistula, and third-degree burns. Other challenges associated with HIFU, and pancreatic cancer is the means of sonication of pancreas. Given its retroperitoneal location, other structures such as the bowel needs to be negotiated carefully to avoid injury.

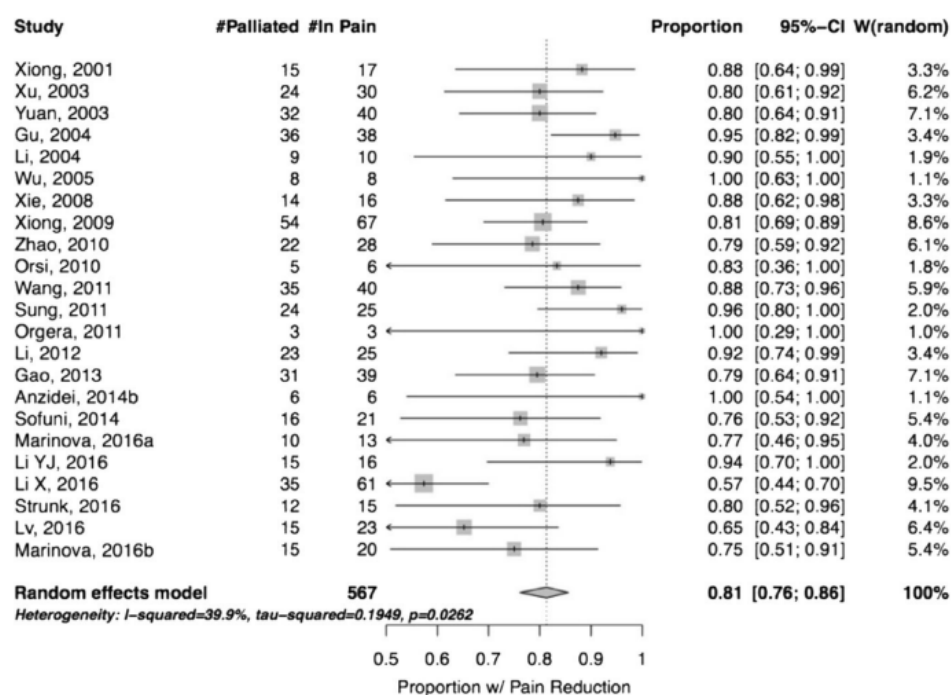


Figure 17 – Random effect model – studies included in the meta-analysis in study conducted by Dababou et al (331).
Proportion of patients with pain reduction. Random effect: 0.81 (95% CI: 0.76–86).

The destructive effect of the HIFU is brought about by its thermal effect mostly. Experimental cell culture results demonstrate cells die instantly at temperatures between 50–55°C (328, 333). Protein denaturation, membrane rupture, cell shrinkage, pyknosis, and hyperchromasia have been demonstrated in ex-vivo models between 60 and 100°C, causing practically rapid coagulation necrosis (328, 334). Delivery of focused ultrasound has been either in the form of continuous-wave or pulsed-wave HIFU sonication (328). The largest series of using HIFU for pancreatic cancer is reported by Wang et al (329). A total of 224 patient with pancreatic cancer were treated with HIFU to evaluate its safety. Although no severe complications were reported, post HIFU treatment there were reports of GI disturbance (abdominal distention, anorexia) in 4.5% of patients. In one patient obstructive jaundice was noted post treatment and a further 2 cases were noted to have vertebral injury evident on MRI scan. These finding showed that HIFU is a safe treatment strategy in carefully selected patient with stringent pre-treatment planning (327, 329). Aside from tumour volume reduction, an important aspect of HIFU treatment in unresectable pancreatic cancer is the symptomatic relief it offers after treatment. There is notable reduction in the tumour associated pain post treatment (332).

Studies have reported varying median overall survival (OS) times for patients undergoing HIFU treatment. For instance, a study involving 523 patients with unresectable pancreatic ductal adenocarcinoma found that those receiving HIFU combined with gemcitabine had a median OS of 7.4 months, compared to 6.0 months for those receiving gemcitabine alone (335). The same study reported 6-month and 1-year survival rates of 66.3% and 21.32% for the HIFU plus gemcitabine group, respectively, compared to 47.5% and 13.64% for the gemcitabine-only group. Moreso, a meta-analysis evaluating the role of HIFU in locally advanced pancreatic cancer indicated that patients treated with HIFU presented increased median OS, along with higher OS at 6 and 12 months after treatment compared with control groups ($p < 0.05$) (336).

2.6 Histotripsy & its role in liver regeneration

Histotripsy, a non-invasive ultrasound-based technique, has emerged as a promising method for not only liver tumour ablations but also for potentially facilitating liver regeneration. While the notion of employing concentrated ultrasound for therapeutic applications originated in the mid-20th century, the targeted use of histotripsy for hepatic therapy accelerated in the early 2000s. Researchers at the University of Michigan innovated this method, resulting in substantial advancements in non-invasive liver tumour therapies (337). In 2023, histotripsy obtained FDA approval for the treatment of liver tumours, signifying a significant advancement in its clinical use. Amongst more notable, the initial pre-clinical work carried out by Khokhlova, Vlaiaavljevich and their colleagues (264, 338-343) has significantly advanced the understanding and application of histotripsy in medical treatments, including its potential role in liver regeneration. Khokhlova investigated the precision of histotripsy in targeting liver tissues, aiming to minimize damage to surrounding healthy structures (264, 344). Her studies have demonstrated that histotripsy can effectively ablate liver tumours, leading to localized tissue destruction followed by regenerative responses. This suggests potential for liver regeneration post-treatment.

More recently, work carried out by Ki Joo Pahk has shown that histotripsy has anti-fibrotic properties in the liver tissues (345). His works showed boiling histotripsy sonicated liver tissue is accompanied by an increased hepatocyte specific marker expression and improved serological liver function markers without notable adverse effects. This shows potential role

for histotripsy in reducing fibrosis and promoting liver regeneration in liver fibrotic tissues. These experimental works have demonstrated histotripsy's attractive property to selectively target tissue whilst sparing structures such as blood vessels (**Figure 18**) (346). Moreso, histotripsy can produce a sharply demarcated margin between treated (fractionated tissue) and untreated (intact) regions with a transition distance of less than a cell length of the order of a micrometre (346, 347). In addition, further recent pre-clinical work on histotripsy have shown it may be of beneficial to use in benign prostatic hyperplasia (BPH), liver and kidney tumours, and kidney stone fragmentation, through enhancing anti-tumour immune response, and tissue decellularization for regenerative medicine applications (251, 264, 347, 348). These characteristics of histotripsy makes it a suitable tool for tissue engineering and regeneration. In addition, the possibility to modulate histotripsy parameters makes it more specific for targeting different tissues.

Pahk et al further studies long term healing response of the liver to boiling histotripsy treatment in vivo (347). Fourteen Sprague Dawley rats were treated with BH and sacrificed on days 0, 3, 7, 14, and 28 for morphological, histological, serological, and qPCR analyses. On day 0, the lesions produced were well-defined (approximately 1.44 cm²) with coagulated blood. The treatment site showed activated fibroblasts a week later, with newly formed extracellular matrix structure (ECM). ECM disruption lasted 7–28 days. At the BH site new blood vessels and normal hepatocytes regenerated without fibrosis. Although its an important finding, their work needs to be further evaluated in the setting of already established liver fibrosis or cirrhosis to demonstrate efficacy of histotripsy in liver regeneration.

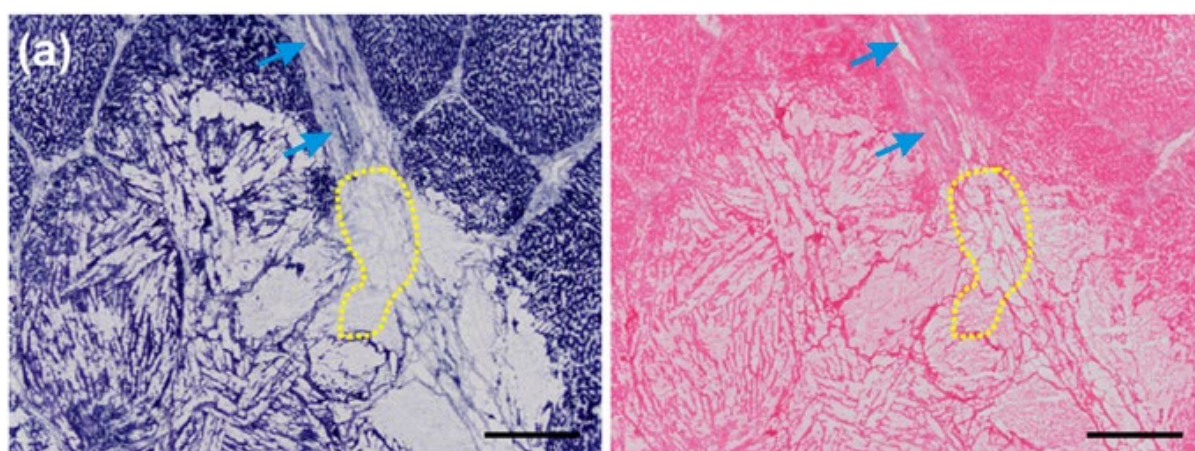


Figure 18 - Higher magnification histological images stained with NADH-d and H&E show the important details of boiling histotripsy-induced liquid lesions. (A) Liquid boiling histotripsy lesion histological images stained with H&E (left)

and NADH-d (right). Hepatocytes and their debris are not thermally denatured, but connective tissue in liquid boiling histotripsy lesions often is (dotted yellow line). However, a connective tissue structure (e.g., a blood vessel or biliary system element) immediately adjacent to the lesion is not affected mechanically or thermally (blue arrows). (Figure and legend adapted from (346)).

This is an important finding as it highlights the efficacy of histotripsy in developing cavitating lesions and activating local biological responses to help tissue regeneration and healing. Remodelling ECM is an important mechanism that can be used to govern the process of cell differentiation (349, 350). This includes the processes of establishing and maintaining stem cell niches, branching morphogenesis, angiogenesis, bone remodelling, and wound repair (349, 351). On the other hand, aberrant ECM dynamics can result in uncontrolled cell proliferation and invasion, a failure of cell death, and a loss of cell differentiation (352). This can lead to congenital abnormalities as well as pathological processes such as tissue fibrosis and cancer (350, 352). Heo et al (347) in their study demonstrated an upregulation of Matrix metalloproteases (MMP) enzyme in the treated area. MMPs are important player in ECM remodelling in health and disease (353). Particularly an important aspect to evaluate further when considering regeneration in the context of various liver disorders (steatosis and fibrosis).

Histotripsy has also been shown to be able to decellularize tissue while maintaining ECM (354). Histological evaluation post histotripsy revealed treatment conditions that produced decellularized lesions in which major fibrous structures such as stroma and vasculature remained intact while parenchymal cells were mostly lysed (354). Decellularization is a critical step for successful cell transplantation because it provides a biocompatible and functional scaffold that enhances cell engraftment, survival, and integration. The creation of bioartificial organs through histotripsy mediated decellularization is more likely to reach the clinic than the current chemical decellularization techniques that necessitate the employment of chemical and biological agents, frequently in conjunction with physical force, which may cause matrix damage.

Lastly, histotripsy has been shown to elicit different local and systemic immunological reactions post treatment (355, 356). Immune cells play an important role in tissue regeneration and expansion (357). Although, the pre-clinical studies of histotripsy focus most on immune response to histotripsy in the context of cancer treatment, very little has been shown to

demonstrate how histotripsy can modulate immune cascades that influence tissue regeneration.

2.6.1 Experimental Models:

Preclinical studies have employed various animal models to evaluate the efficacy and safety of histotripsy in liver applications. These studies demonstrated that histotripsy could effectively ablate liver tumours and, in some cases, promote regenerative processes. Most of the studies performed use different ultrasound parameters and experiments have been carried out on different animal models. This heterogeneity is reflective of the fact different tissues with different tensile strength require appropriate parameters to be used. This in turn make it difficult to reach a consensus on single optimised parameter to be used for all livers. In fact, every single liver depending on the intended aim of the histotripsy use would need to have its most optimum histotripsy parameters calculated and adjusted. This should be an area of focus for future research if histotripsy is going to be used for regenerative purposes.

On review of the literature and histotripsy use, previous experimental studies include both in-vitro and in-vivo models. Below is a summary of the use of focused ultrasound in in-vivo liver models so far.

In-vivo Studies

17 in-vivo models were used in 16 studies (213, 221, 343, 348, 358-369), with one study using two in-vivo models (221).

The types of tissue used in the in-vivo studies are summarised in **Table 10**. All 16 in-vivo models tested histotripsy on the animal's liver (n=16, 100%) (213, 221, 343, 348, 358-369). All studies reported the type of animal used for their model (213, 221, 343, 348, 358-369), with the most common being porcine (n = 10 models, 62.5%) (213, 221, 343, 358-362, 366, 367), followed by murine models (n = 4, 25%, with 3 of the 4 being rats and 1 being a mouse model) (348, 365, 368, 369) and sheep models (n = 2, 12.5%) (363, 364).

Table 10 - Summary of the Characteristics of In-Vivo Models

First Author, Date	Tissue Type	Animal Source	Model Type	Citation Number
Kim, 2011	Liver	Fetal Sheep	in-vivo	(364)
Kim, 2013	Liver	Ewes and Lambs	in-vivo	(363)
Vlaisavljevich, 2013	Liver	Porcine	In-vivo	(221)
Khokhlova, 2014	Liver	Porcine	In-vivo	(360)
Kim, 2014	Liver	Porcine	in-vivo	(361)
Vlaisavljevich, 2014	Liver	Porcine	In-vivo	(366)
Simon, 2015	Liver	Porcine	In-vivo	(358)
Vlaisavljevich, 2016	Liver	Murine (Rat)	In-vivo	(365)
Pahk, 2016	Liver	Murine (Rat)	In vivo	(348)
Arnal, 2017	Liver	Porcine	in-vivo	(213)
Vlaisavljevich, 2017	Liver	Porcine	In vivo	(343)
Smolock, 2018	Liver	Porcine	In vivo	(367)
Worlikar, 2018	Liver	Murine (Mouse)	In vivo	(369)
Khokhlova, 2019	Liver	Porcine	in-vivo	(359)
Longo, 2019	Liver	Porcine	in-vivo	(362)
Pahk, 2019	Liver	Murine (Rat)	In vivo	(368)

In-vivo model demographics are displayed in **Table 11**. 16 studies (213, 221, 343, 348, 358-369) reported the number of samples which histotripsy were performed on, with an average of 11 samples being tested (range: 2 to 22 samples). Sample weights and volumes were reported in 10 (343, 348, 359-362, 365-367, 369) and 2 (221, 360) studies respectively.

Pre-treatment imaging, histotripsy delivery device name and histotripsy imaging guidance were reported in all 16 studies (213, 221, 343, 348, 358-369). The most common method of pre-treatment imaging was US (n = 15 models, 88.2%) (213, 221, 343, 348, 358-369), and in the other two models, a high-speed digital camera was used (358, 368). Most commonly these transducer machines were designed in house and custom built for the study (n = 7, 41.2%), but some studies used transducers produced by companies such as Imasonic (n = 6, 35.3%), Sonic Concepts (n = 2, 11.8%) and HistoSonics (n = 2, 11.8%). The histotripsy settings for each model are discussed below.

The common form of imaging guidance in the in-vivo models was ultrasound (n = 14 models, 82.4%), followed by high-speed digital cameras (n = 2, 11.8%) and in-vivo MRI (n = 1, 5.9%).

Table 11 - Demographics of In-Vivo Models

First Date	Author,	Tissue Type	Animal Source	Cohort Size	Weight (kg)	Tissue Volume	Pre-Treatment Imaging	Delivery Device Name	Histotripsy Guidance
Kim, 2011		Liver	Fetal Sheep	9	-		US	Imasonic, Besancon, France	US
Kim, 2013		Liver	Ewes and Lambs	9 Ewes, 10 Lambs	-		B-mode US	Designed in House	US
Vlaisavljevich, 2013		Liver	Porcine	6	-		8 MHz phased array ultrasonic imaging probe	Imasonic, Besancon, France	US
Vlaisavljevich, 2013		Liver (Larger Therapy Regions)	Porcine	2	-	2.2×2.3×3.5 cm, 5×4×3 cm	8 MHz phased array ultrasonic imaging probe	Imasonic, Besancon, France	US
Vlaisavljevich, 2014		Liver	Porcine	2	29.9, 42.6	-	8 MHz phased array ultrasonic imaging probe	Imasonic, SAS, Voray sur l'Ognon, France	8 MHz phased array ultrasonic imaging probe
Khokhlova, 2014		Liver	Porcine		45.0-68.0	2x2x2cm	B-mode US	Designed in House	B-mode US
Kim, 2014		Liver	Porcine	8	40.0-50.0	-	B-mode US	Imasonic SAS, Voray sur l'Ognon, France	B-mode US
Simon, 2015		Liver	Porcine	-	-	-	High-speed digital camera	Designed in House	High-speed digital camera
Pahk, 2016		Liver	Murine (Rat)	11	0.200-0.250	-	US	H106; Sonic Concepts Inc., Bothell, WA, USA	US
Vlaisavljevich, 2016		Liver	Murine (Rat)	20	0.290-0.310	-	20 MHz imaging transducer (US)	Designed in House	In-vivo MRI

Arnal, 2017	Liver	Porcine	-	-	-	B-mode US	Imasonic, Voray-sur-l'Ognon, France + RITEC amplifier	US
Vlaisavljevich, 2017	Liver	Porcine	22	45.4	-	Sonos 7500 imaging system, Philips Electronics, Andover, MA, USA	Designed in House	Sonos 7500 imaging system, Philips Electronics, Andover, MA, USA
Smolock, 2018	Liver	Porcine	3 acute ⁺ , 7 chronic ⁺	70.0	-	US	VortxRx; HistoSonics	US
Worlikar, 2018	Liver	Murine (Mouse)	21		-	US	Custom Built	US
Longo, 2019	Liver	Porcine	6	55.0	-	B-mode US	VortxRx, HistoSonics, Inc., Ann Arbor, MI	B-mode US
Pahk, 2019	Liver	Murine (Rat)	-	0.200-0.250	-	High-speed digital camera	Sonic Concepts H106, Bothell, WA, US	High-speed digital camera
Khokhlova, 2019	Liver	Porcine	6	37.0-40.0	-	B-mode US	Designed in House	B-mode US

⁺ - acute models (-treatment, MR imaging, and immediate sacrifice) and chronic models (-treatment, MRI imaging, survival for 25–30 days, reimaging, and subsequent sacrifice)]

Each study used specific histotripsy parameters, which are displayed in **Table 12**. A range of transducer frequencies were used, from 0.700MHz (370) to 2.127MHz (368), but most common frequency used in histotripsy treatments was 1MHz (n = 6, 35.3%) (221, 363-365, 369). The total experiment sonication time was reported in four studies (221, 343, 361, 367). 6 studies reported on pulse length (n = 7 models, 41.2%), with three studies using a range of values in their experiments (338, 360, 361) and an overall range of

0.002ms (221) to 3000ms (361). 9 studies (n = 10 models) reported on the cycle number (221, 343, 348, 359, 363, 366-369), and a range of cycles were used, from 1 cycle (369) to 50 cycles (348). The most common cycle number used in the in vivo models was 10 (221, 366, 368). Eleven studies reported on pulse repetition frequency (n = 12 models) (364), with the most common PRF used being 500Hz (363), with a range from 1Hz (368) to 1000Hz (364). 9 studies (n=10 models) reported the transducer aperture of their transducer machine (363), with an average of 99.2mm (range of 64.0 – 150.0mm). 8 studies (n=9 models) reported the focal length of the machine (363), with an average of 89.5mm (range 62.6-120.0mm). 3 studies reported the acoustic power of their transducer machine (360), with two using a range of powers in their experiments (360). 11 studies (n = 12 models) reported the pressure amplitudes used in histotripsy, with the average peak negative amplitude being -22.9MPa (range -10.0 to -87.0MPa) and the average peak positive amplitude being 38.6MPa (range 16.0 to 102.0MPa) (363).

Table 12 – Focused Ultrasound Settings for In-Vivo Models

First Author, Date	Tissue Type	Animal Source	Transducer Frequency (MHz)	Total Sonication Time (mins)	Pulse Length (ms)	Number of Cycles	Number of Pulses Per Location	PRF (Hz)	Transducer Aperture (mm)	Focal Length (mm)	Acoustic Power (W)	Pressure amplitude (MPa) (P-, P+)
Kim, 2011	Liver	Fetal Sheep	1.000	-	0.005	-	-	200-1000	100.0	90.0	-	10, 16
Kim, 2013	Liver	Ewes and Lambs	1.000	-	0.005	5	-	500	100.0	90.0	-	10, 16
Vlaisavljevich, 2013	Liver	Porcine	1.000	-	0.002	10	-	500	100.0	90.0	-	23, 27
Vlaisavljevich, 2013	Liver (Larger Therapy Regions)	Porcine	1.000	26.7, 60.0	0.002	10	-	500	100.0	90.0	-	23, 27
Vlaisavljevich, 2014	Liver	Porcine	-	-	-	10	2000	500	100.0	90.0	-	17 (-)
Khokhlova, 2014	Liver	Porcine	-	-	1 - 500	-	-	-	64.0	-	-	240
Kim, 2014	Liver	Porcine	-	40.0	900 - 3000	-	4000	200	150.0	120.0	-	450-510
Simon, 2015	Liver	Porcine	2.127	-	-	-	-	-	-	-	-	-
Pahk, 2016	Liver	Murine (Rat)	2.000	-	-	50	-	-	64.0	62.6	-	-
Vlaisavljevich, 2016	Liver	Murine (Rat)	1.000	-	-	-	-	-	-	-	-	-
Arnal, 2017	Liver	Porcine	1.250	-	-	-	-	100	-	-	-	16, 18

Vlaisavljevich, 2017	Liver	Porcine	0.700	1.0, 15.0	-	5	-	50	-	110.0	-	16-20 (-)
Smolock, 2018	Liver	Porcine	0.700	24.3	-	4	-	300	-	-	-	14 (-)
Worlikar, 2018	Liver	Murine (Mouse)	1.000	-	-	1-2	50	100	-	-	-	30 (-)
Longo, 2019	Liver	Porcine	-	-	-	-	-	-	-	-	-	-
Pahk, 2019	Liver	Murine (Rat)	2.000	-	-	10	-	1	64.0	62.6	-	15.6, 85.4
Khokhlova, 2019	Liver	Porcine	1.500	-	1 - 10	5-30	-	1 - 10	150.0	-	88-380	-

Post-treatment imaging and histology results are displayed in **Table 13**. Post-treatment imaging was reported for all (213, 221, 343, 348, 358-369) but one study (213, 221, 343, 348, 358-369) and results depended on the aim of the original paper, but common findings were those of tissue ablation and fractionation following treatment with histotripsy. Additionally, studies identified that there is no additional damage to tissues in the focused ultrasound beam's path. Histology findings were reported in 14 studies (n = 15 models) (213, 221, 343, 348, 358-369) and all histology samples were analysed with hematoxylin and eosin (H&E) staining (n = 12 models, 70.6%), H&E and NADH-d staining (n = 1, 5.9%), NADH-d staining alone (n = 1, 5.9%), or H&E with Masson's trichrome staining (n = 1, 5.9%). Histological analysis revealed tissue fractionation and necrosis. Studies demonstrated that despite damage to the parenchyma, histological analysis found that blood vessels and biliary structures remained intact (n = 2, 11.8%).

Table 13 - Findings from studies using In-Vivo Models

First Author, Date	Tissue Type	Tissue Source	Post-Treatment Imaging	Post-Treatment Histology
Kim, 2011	Liver	Fetal Sheep	Bubble clouds were generated in 5/9 cases, generating identifiable lesions. Failure of generation of cavitation bubble was the primary cause of no lesion generation; this was most often due to increased depth to target and obstruction such as fetal limb.	H&E staining: confirmed lesion locations and sizes corresponding to regions where cavitation was monitored, with no lesions found when cavitation was absent.
Kim, 2013	Liver	Ewes and Lambs	generated lesions corresponded well with anticipated location and size.	H&E staining: distinct lesion created, no abnormal cells outside of treatment area,
Vlaisavljevich, 2013	Liver	Porcine	Ex vivo imaging (7T small animal scanner (7.0 Tesla, 310 mm bore, Varian, Inc, Walnut Creek, CA)): lesions observed as bright, hyper-	Gross morphology and H&E staining: fractionation of hepatic parenchyma inside the treated tissue volume, and staining demonstrated that blood vessels and

			intense regions on MRI, indicating fractionated homogenate	gallbladder structures remained intact inside the completely fractionated region i.e. blood vessels within the fractionated hepatic parenchyma were not perforated or visibly damaged. Large intact blood vessels (>1mm diameter) remained within the fractionated tissue.
Vlaisavljevich, 2013	Liver (Larger Therapy Regions)	Porcine	MRI: lesions (bright, hyper-intense regions on MRI, indicating fractionated homogenate) were of approximately 18 cm ³ and 60 cm ³ .	H&E staining: completely fractionated liver tissue throughout the treated volume
Vlaisavljevich, 2014	Liver	Porcine	MRI: in vivo lesions demonstrated lesion volumes with multiple large vessels remaining within the fractionated liver volumes	H&E staining: The damage to the liver, vessels, and bile ducts within and surrounding the treatment region was examined histologically under a microscope. To quantitatively assess the distribution of blood vessels remaining after histotripsy, the number of vessels was counted using three H&E slides for each lesion (total n=6). Histological evaluation of the lesion indicated hepatic parenchyma was completely fractionated into acellular debris while large vessels (>1 mm diameter) remained intact within the treated region.
Khokhlova, 2014	Liver	Porcine	Complete ablation of tissue to liquid/paste.	NADH-d staining
Kim, 2014	Liver	Porcine	Complete ablation possible and relatively unaffected by rib obstruction.	H&E staining
Simon, 2015	Liver	Porcine	US: the breathing motion of the pig resulted in erosion tracks rather than demarcated cavities on the liver surface. Some liver capsule damage observed with continued exposure.	H&E staining: indicated that cellular fractionation occurred NADH-d staining shows thermal damage with reduced enzymatic activity
Pahk, 2016	Liver	Murine (Rat)	Gross examination: histotripsy margins had sharp boundaries without thermal injury, and histotripsy cavities were filled with coagulated blood. Donor	H&E staining: confirmed cavity creation, with no signs of thermal damage.

			hepatocytes were injected into the cavity and identified with IVIS imaging.	
Vlaisavljevich, 2016	Liver	Murine (Rat)	MRI imaging showed sharp demarcation between the healthy liver and fractionated homogenate. Extracellular/extravasated blood products in the fractionated homogenate and surrounding oedema were the dominant finding on MRI after day 0 and day 3, respectively.	H&E staining and gross morphological examination: showed inflammation and an ingrowth of fibroblasts within the lesion and by day 28, the lesion was replaced by normal parenchyma with focal scarring
Arnal, 2017	Liver	Porcine	Not being investigated directly.	Not mentioned.
Vlaisavljevich, 2017	Liver	Porcine	Gross examination: indicates no visual damage to tissues in the path of HIFU. Additionally, well-defined lesions were observed in the liver.	H&E staining: there was complete fractionation within treated volume, with no recognizable cellular structures
Smolock, 2018	Liver	Porcine	Treatment appeared as a bubble cloud on US imaging during histotripsy. MRI showed spherical, well defined ablation zones.	Acute cases histology: central necrotic and fractionated zones surrounded by zones of partial necrosis (containing necrotic and viable hepatocytes). Outside of the necrotic areas, some ischemia was present secondary to portal and hepatic vein thrombosis, but the parenchyma was otherwise unaffected. Chronic cases histology - there is an area of central necrosis surrounded by a fibrous capsule.
Worlikar, 2018	Liver	Murine (Mouse)	US: histotripsy resulted in fractionation of tumour target regions, MRI: there was a reduction in tumour volume over time	H&E staining: confirmed the fractionation of treated sites, with complete fractionation into acellular debris. There was a sharp boundary around partially treated tumours, however, in these, some tumour cells remained. In the chronic murine models, histology confirmed some tumour regrowth.
Longo, 2019	Liver	Porcine	RAST achieved targeted tissue fractionation without body wall injury.	Not mentioned
Pahk, 2019	Liver	Murine (Rat)	On observation of tissues treated with histotripsy, the tadpole-shaped fractionated lesion is filled with blood.	H&E staining: In the tadpole shaped lesion, the 'head' margin consists of broken hepatocytes with ragged boundaries between the treated and untreated regions,

				whereas the 'tail' margins are demarcated with smooth edges.
Khokhlova, 2019	Liver	Porcine	Well demarcated lesions generated in liver using higher peak power. Indicates promise for technology in transabdominal and transcotal mechanical ablation	H&E and Masson's trichrome: completely homogenized hepatocytes while sparing the fibrous lobule boundary, capsule, blood vessels and biliary ducts.

2.6.2 State of the art:

As of November 2024, histotripsy is acknowledged as an effective non-invasive therapy for hepatic tumours (371). Clinical investigations, including the #HOPE4LIVER research (183), have established its safety and efficacy, resulting in its implementation in numerous medical centres. Although histotripsy has been approved for tumour treatment in clinical setting, its potential use in facilitating liver regeneration is still subject of future research. Current studies seek to enhance treatment regimens, examine combination therapies, and assess the efficacy of histotripsy in promoting liver regeneration. The technology's accuracy and non-thermal process provide benefits compared to conventional ablation techniques, establishing histotripsy as a potential asset in hepatology.

Overall, histotripsy is emerging as a new non-invasive, non-thermal energy source that can have a magnitude of uses in cancer treatment and in modulation of normal physiology such as tissue regeneration. Here we evaluate the role of boiling histotripsy in producing decellularized scaffolds of porcine liver and evaluate the lesions histologically and asses its constituents.

2.7 Thesis hypothesis

Histotripsy sonication can result in a decellularized cavity with preservation of the important structures in the liver, such as blood vessels and bile ducts. This facilitates implantation of stem cell derived 3D hepatocytes into the cavity that will then turn into a regenerative nidus to restore or augment liver function. Histotripsy can facilitate this by mechanical dissociation of the tissue and activation of local immune-humoral responses that initiate the regenerative process at the cellular level.

2.8 Thesis aims

- **To Develop a Novel Regenerative Approach for Liver Diseases:** Explore the potential of histotripsy to create a decellularized cavity in the liver, preserving critical structures like blood vessels and bile ducts, as a scaffold for hepatocyte implantation.
- **To Enhance Liver Regeneration:** Investigate the capacity of implanted 3D hepatocytes within the histotripsy-created cavity to act as a regenerative nidus for restoring or augmenting liver function.
- **To Activate and Utilize Local Regenerative Mechanisms:** Assess how histotripsy activates local humoral responses and cellular regenerative pathways to support liver healing and regrowth.
- **To facilitate the Development of Clinically Validated Tool:** Assess the efficacy of the histotripsy as a tool to be developed and validated within clinical settings for the treatment of the chronic liver disease and to assess the appropriate parameters to be used in different clinical settings.

2.9 Thesis objectives

- **Characterize the Decellularized Cavity:**
 - Evaluate the structure, dimensions, and functional integrity of histotripsy-created cavities using validated histological techniques
 - Confirm the preservation of critical liver structures such as blood vessels and bile ducts with the aid of histological analysis
- **Optimize Hepatocyte Implantation:**
 - Determine the optimal method for implanting 3D hepatocyte cultures into the decellularized cavity.
 - Assess the cavity constituents prior to implantation
 - Assess the viability, proliferation, and functional integration of implanted hepatocytes.

- **Assess Functional Outcomes:**
 - Measure liver function post-implantation (e.g., production of albumin).
 - Evaluate the improvement in liver function compared to controls or other regenerative approaches.
- **Study Regenerative Processes:**
 - Investigate the mechanical dissociation effects of histotripsy on liver tissue in both ex-vivo and in-vivo models
 - Examine the activation of local humoral responses (e.g., cytokines, growth factors) that promote regeneration.
- **Safety and Efficacy Analysis:**
 - Monitor for adverse effects, such as unintended tissue damage or immune reactions in the in-vivo model
 - Evaluate the long-term efficacy and sustainability of liver regeneration.
- **Preclinical Validation:**
 - Test the approach in relevant animal models to validate the technique and its outcomes before moving to clinical applications.
 - To analyse and validate in the pre-clinical stage the parameters suitable for decellularization of tissue and implantation of cells
- **Investigate Clinical Translation Potential:**
 - Assess feasibility, scalability, and reproducibility of the histotripsy-based approach for potential human clinical trials.

These aims and objectives provide a comprehensive framework for exploring and validating histotripsy's role in advancing liver regeneration therapies. In short term the objectives would be to evaluate the efficacy of histotripsy in liver tissue to develop a decellularized cavity that can foster hepatocytes once implanted. This thesis shows a body work that has been carried out to achieve these objectives in different models.

Chapter 3 Methods

To investigate the possible use of histotripsy in *ex-vivo* perfused porcine livers for their suitability as a nidus for cell transplantation as a novel technique and assessing lesions histologically and its constituents for viability. The lesions were reconstructed using simulation software to reproduce a 3D image of the lesions. In addition, the iPSC stem cell derived 3D hepatocytes were matured, and the histotripsy was trialed in-vivo rat models to assess for their viability after sonication. Below is the methodology used in each chapter to achieve the milestones related to the experiments in each chapter.

3.1 Overall experimental method

Porcine livers were retrieved fresh from the abattoir. They were obtained within 10 minutes of the termination (warm ischemia time) at the slaughterhouse. Following termination, the livers were rapidly retrieved using human organ retrieval techniques. These consisted of en-bloc retrieval of the pig's abdominal viscera followed by on-table isolation of the liver, with the major vessels and main bile duct. A subsequent on-table vessel perfusion was used to clear the remaining blood from the liver. This was achieved by perfusing the liver graft with 1000mL of heparin saline solution via the portal vein and transferred to the organ perfusion laboratory in an organ preservation solution (Saline was used as preservation solution for transport), on packed ice at about 5°C, in an insulated organ storage box (average cold storage time: 2 h). On arrival at the organ perfusion laboratory, the liver grafts were transferred to an organ perfusion circuit which maintained organ viability by perfusion with Soltran organ preservation solution (Baxter Healthcare, UK) using the protocol described in **Figure 19**.

Once established on the perfusion circuit, each liver was subjected to a histotripsy protocol. The site of histotripsy was selected at random, with both peripheral and central portions of the liver included for histological analysis and cell culture. Immediately following histotripsy treatment, lesion contents were aspirated from the core of each histotripsy lesion and were cultured in a 96-well plate. Aspirates were examined for cell content, quantity and viability of cells and were then cultured (**Figure 19**). Following culture, the cells were examined under light microscopy for morphology and

subsequently fixed for live-dead assay and alamarBlue™ stains. The experiments were repeated with 5 different porcine livers using the same histotripsy parameters and protocol.

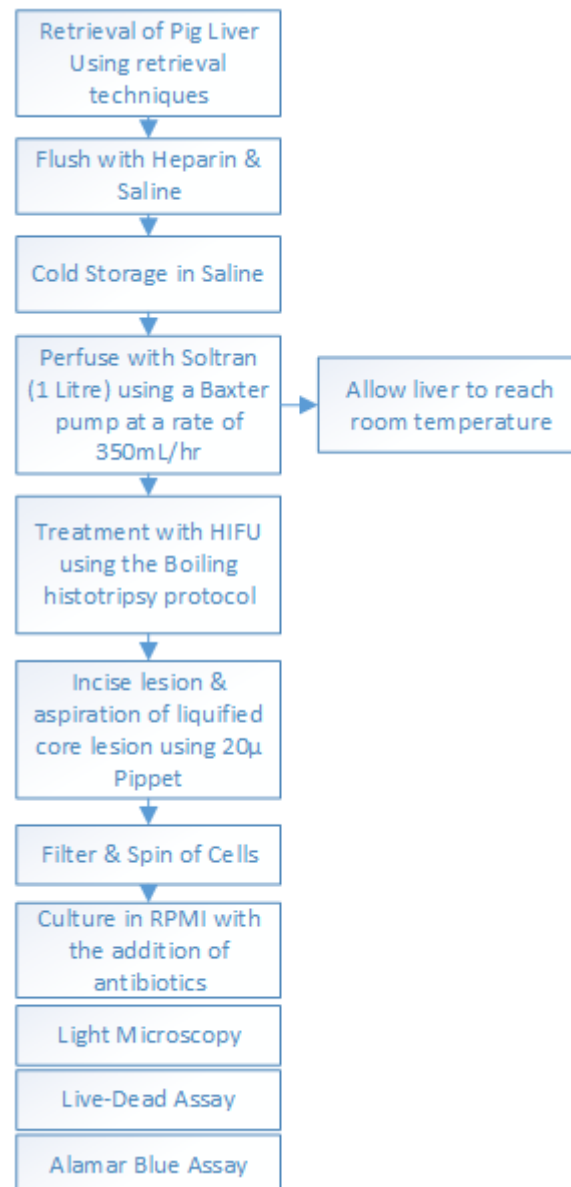


Figure 19 - Experimental protocol for the hepatocyte cell isolation from perfused pig livers using HIFU device.

3.2 Organ retrieval and transport

Pig livers were obtained fresh from the abattoir using human organ retrieval techniques. Livers were obtained within 10 minutes of the termination (equating to the warm ischemia time) at the slaughterhouse. Using organ transplant retrieval techniques, livers were

dissected from the complete set of abdominal viscera with isolation of the hepatic artery, portal vein and bile duct. At the abattoir, back table perfusion and flush of the livers was achieved following retrieval with 1000 mL of heparin saline solution via portal vein. They were packed in preservation solution and stored on crushed ice in insulated containers for transport at about 5° Celsius.

3.3 Modelling to define the histotripsy parameters

HIFU parameter modelling: (Work Carried by Prof Saffari & Dr Pier Gelat)

A modelling approach was used to estimate the HIFU pressure fields at the treatment zone. The HITU Simulator v2.0 (372), was used to solve the Khokhlov-Zabolotskaya-Kuznetsov (KZK) equation and obtain 2D axisymmetric pressure waveforms along the propagation axis and the radial direction. Both the KZK equation and the HITU Simulator have been extensively used to model boiling histotripsy pressure and temperature fields (251, 373-375).

The acoustic simulations were performed for a single-element bowl-shaped transducer operating at 2MHz (Sonic Concepts H-148) for input electrical powers of 150 W, assuming 85% transducer efficiency. Acoustic propagation was numerically evaluated in a domain consisting of 5.76cm of water along the axial direction followed by a semi-infinite region of liver tissue. To simulate the experimental set-up for histotripsy in perfused livers described in the sections below, acoustic field quantities were evaluated at 0.56 cm into the liver domain. The spatial grid for acoustics consisted of 10 elements per wavelength in the axial direction and 15 elements per wavelength in the radial direction. Peak focal pressures obtained were of $P^+ = 76.7\text{MPa}$ and $P^- = 13.4\text{MPa}$, with focal heating rates $935\text{W}\cdot\text{cm}^{-3}$ and maximum acoustic intensity $20.0\text{kW}\cdot\text{cm}^{-2}$.

3.4 Histotripsy set up

A 2 MHz single element spherically focused transducer (Sonic Concepts H-148, Bothell, WA, USA) with an aperture size of 64 mm, a radius of curvature of 63.2 mm and a 22.6 mm central opening was used with a transparent coupling cone (Sonic Concepts, C-101, Bothell, WA, USA) filled with degassed, de-ionized water. The transducer was driven by two function generators (Agilent 33220A, CA, USA) in series via a linear radiofrequency (RF) power amplifier (ENI 1040 L, Rochester, NY, USA). The first function generator was set to generate 50 pulses of a 1 Hz square wave with 1% duty cycle. This triggered the second function generator, which yielded a 2 MHz sinusoidal wave into the RF power amplifier. Therefore, the drive signal into the amplifier was 50 pulses of 10 ms duration containing 20k cycles. A power meter (Sonic Concepts 22A, Bothell, WA, USA) was connected between the RF amplifier and the ultrasound transducer, and the electrical power supplied to the transducer was monitored to be approximately 150 W. The pulse-averaged electrical power was 1.5 W (calculated using $P_{\text{averaged}} = P_{\text{peak}} \times \text{duty cycle}$). Assuming a nominal electrical to the acoustic power conversion efficiency of 85% (Sonic Concepts, Bothell, WA, USA) the acoustic peak positive (P+) and negative (P-) pressures at the HIFU focus on liver tissue were $P^+ = 77.7$ MPa and $P^- = -13.7$ MPa, obtained by numerically solving the Khokhlov-Zabolotskaya-Kuznetsov (KZK) parabolic nonlinear wave propagation equation for our input parameters using the HITFU Simulator v2 (Soneson 2017). The simulated acoustic waveforms and peak pressures at the HIFU focus are shown in **Figure 20**. During the experiments, a polyurethane rubber acoustic absorber (AptFlex F28, Precision Acoustics Ltd, UK) was placed under the liver samples to minimize ultrasonic reflections. This protocol was chosen because according to previous extensive work by the authors (348, 376, 377) and other groups (163, 360, 378) it leads to the production of a fully fractionated lesion in liver tissue with minimal thermal

denaturation. It was one of our aims to examine this assertion with more advanced histological analysis.

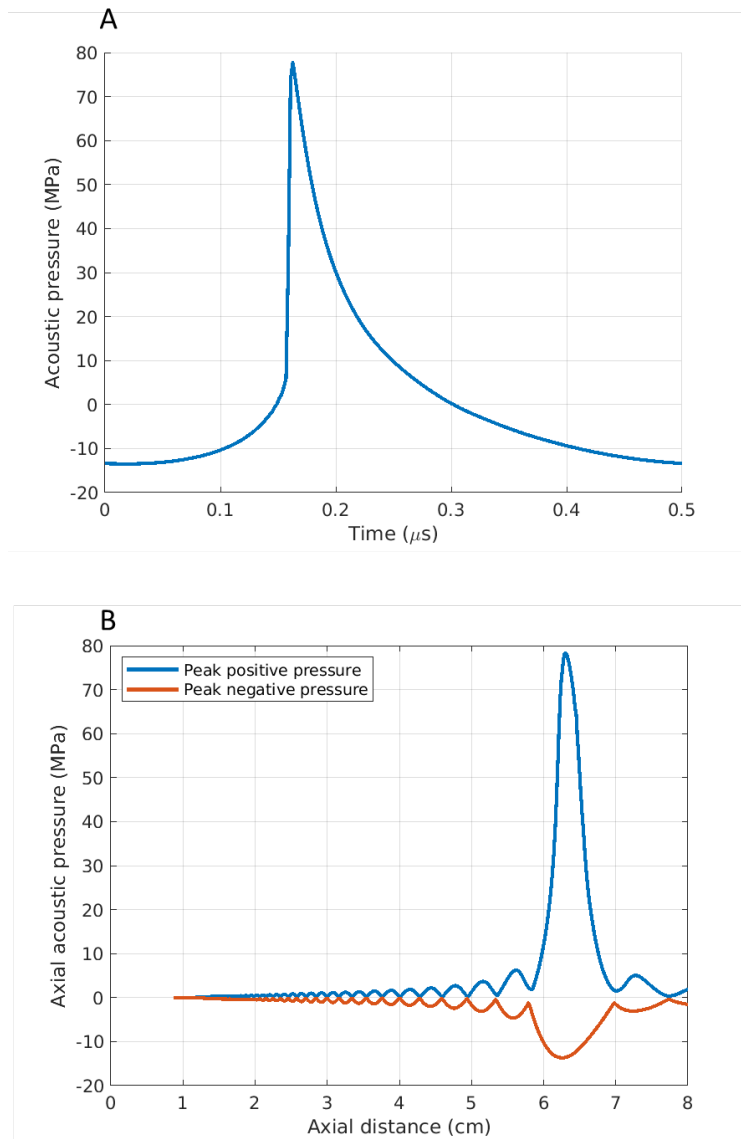


Figure 20 - Simulated acoustic waveforms at (a) the HIFU focus in liver tissue and (b) axial pressure distribution.

3.5 Organ perfusion, histotripsy lesion formation and assessment

Perfusion set up:

Upon arrival at the organ perfusion laboratory, the livers were placed in an organ bath lying over an ultrasound reflective layer and perfused with 1 L of preservation solution (Soltran, Baxter) and the core liver temperature was allowed to return to room temperature (ranging between 24 and 30°C) before being subjected to histotripsy insonation¹. Perfusion of the organ to maintain viability was administered via the portal vein (**Figure 21**) with the perfusate draining via the vena cava into an organ bath. The perfusate was not recycled. The perfusion solution was delivered using a perfusion pump (Baxter™, UK) to achieve constant flow rate of 350mL·h⁻¹ confirming vessel patency before lesions were created by US histotripsy. The HIFU probe was positioned in multiple sequential locations chosen at random over the surface of the perfused liver with 50 pulses applied over approximately one minute at each site. The focal histotripsy lesions could be identified by the puckering of the liver capsule, a pinpoint dimple. Once the lesions were created, these were incised with a surgical blade and the central liquefied core was aspirated using a 20µl single-channel gauge pipette. The aspirate was subject to pre-culture microscopy and then immediately transferred into culture medium for subsequent assessment of cell number and morphology.

¹ Insonation: Exposure to, or treatment with ultrasound

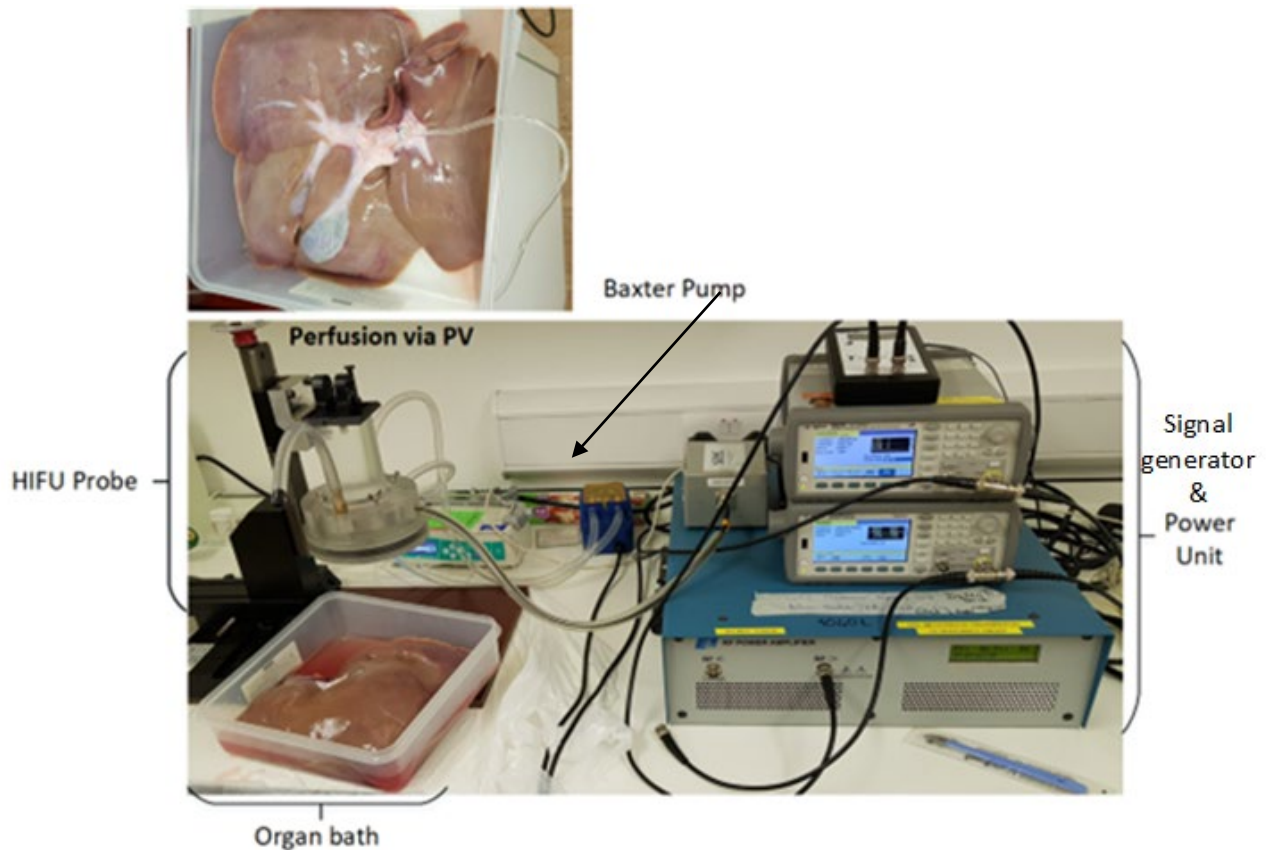


Figure 21 - Experimental set up for HIFU probe and histotripsy protocol. Retrieved pig liver is placed in an organ bath and cannulated via portal vein for perfusion with Soltran solution with a Baxter pump. The perfusate is collected in the organ bath which would be drained out of bath to ensure the probe is not submerged under perfusate fluid accumulating. The perfused liver is placed under the HIFU probe. The Signal generator & Power unit will be adjusted to a set parameter for this experiment.

3.6 Tissue sampling

After the application of BH the lesional site was resected with an approximate margin of 1cm and bisected using a surgical blade, to confirm the lesional site. Resection refers to an excision biopsy with a surgical blade with an approximate circumferential margin of 1cm from the core lesion or its surface landmark the liver capsule dimple; Bisection refers to the slicing of the resected sample in half, cutting through the middle and therefore dividing the lesion into two halves to gain access to the core content of the lesion. Then, a 20 μ m single-channel gauge pipette was only applied gently to the lesional surface to

aspirate the cavity content (results are presented in separate study). Although the protocol was specifically designed for cell harvesting from the core of the cavity in the perfused pig liver model, care was taken to minimize traumatic damage to the tissue. Lesions would only be aspirated if the cavity content were present at the time of bisecting the lesion. For a small number due to proximity to small vessels, as soon as the cavity was sliced open the content was washed away due to puncture of the vessels at the site and perfusate leaking through the vessel. These lesions were not aspirated and only biopsied. Both sides of the lesion were then removed in the form of wedge-shaped biopsy samples, which were placed immediately into a single formalin-filled container and submitted for paraffin embedding according to standard procedures.

3.7 H&E and histochemical stains

3.7.1 H&E Stain:

A single 4µm paraffin section from each sample (i.e., containing both wedge-shaped biopsy specimens) was stained with Haematoxylin (Harris Haematoxylin, Shandon, UK) and Eosin (Eosin Y, Shandon, UK) (H&E) using an autostainer (Leica, ST5020, UK).

3.7.2 Picrosirius Red Stain:

One additional section from each sample was stained with picro-Sirius red (SR) stain (Sigma-Aldrich, Direct Red 80, UK) with the following protocol: (1) Deparaffinize sections in 2 changes of xylene. (2) Rehydrate through 2 changes of alcohol, 70% alcohol and distilled water. (3) Apply SR solution to cover entire sections and incubate in humidified chamber for 60mins. (4) After 60 mins, rinse slides quickly in 2 changes of

Acetic Acid Solution. (5) Rinse slides in absolute alcohol and then dehydrate through 2 changes of alcohol, clear in 2 changes of xylene and mount with pertex mounting medium.

3.7.3 Reticulin Stain:

A further section from each sample was stained for reticulin. The staining procedure was carried out using the Reticulum II stainer kit (Roche catalogue number 860-024) and a Ventana BenchMark Special Stain system.

3.8 3D reconstruction of histotripsy site

(This work was carried out in collaboration with Prof Quaglia & Andrew Hall). Two additional histotripsy specimens were removed intact entirely sectioned at 4 μm into 368 and 408 serial sections, which were all stained with H&E and SR respectively. In the first sample the lesion was identified in sections 199 to 228 (cumulative section thickness of 116 μm). In the second specimen, minute lesional sites were identified in the full range of serial sections (1-408). The lesional serial sections were used for 3D reconstruction of the histotripsy sites using the specifically designed method illustrated in **Figure 45** and detailed below:

1. Sectioning: Serial sections of formalin-fixed paraffin-embedded (FFPE) liver was cut at 4 μm and any sections lost or missed were noted at the time of sectioning.

2. Images: The tissue was then stained with H&E in the first model and SR for the second and slides were imaged using a Zeiss AxioCamICc5 and Axiovision v2.8.1 (Zeiss, Oberkochen, Germany) and images saved in lossless TIFF format.

3. Mark-up: Each image was marked up using software that allows the altering of drawn pixels to a single RGB colour code (e.g., Microsoft Paint, Microsoft Corporation, Redmond, Washington, USA). Many image editing software packages can be used for this purpose however it is important to use a tool that allows editing the image so that the change to any pixel is to that of a set RGB colour value and all changed pixels are of that value. Many tools will feather or blend the edges of the marked area, and this will cause problems later on. This was used to define areas of interest such as portal tracts, capsule or lesions and the structures modelled in the final 3D reconstruction. Each RGB colour code defined an aspect of the final 3D model, e.g. red for blood vessels, green for capsule, blue for lesion.

A saturated blue (RGB, 0,0,255) rather than one similar to that of haematoxylin was used. Critical to this step was the use of lossless image formats as lossy formats, such as .jpeg, can cause image artefacts and loss of colour fidelity by reducing the accuracy of the model. In essence each image slice has been hand segmented according to the prevalent tissue morphology.

4. Registration: The images were registered using a custom MATLAB (The Mathworks, Natick, Massachusetts, USA) script. This script allows two images of serial sections to overlay each other and the alpha (transparency of the images) to be adjusted to visualize both images at once. Distinct features such as the liver capsule and the edge of the tissue can be used to align each image over one another and when a best fit is found the images are then automatically cropped and saved, forming a stack of registered images.

5. Extracting binary matrices: From the stack of registered images, we created a stack on binary matrices for each different type of feature i.e. Each colour is used in the Mark-up step. A 2D binary matrix is an image composed of solely 1 and 0s and can be visualized as a black and white image with no greyscale between. To create the binary matrix from the markup images we used a second custom MATLAB (The Mathworks, Natick, Massachusetts, USA) script in which a colour range is chosen and the pixels within the range are given a 1, and those without a 0, thus picking out a particular marked up feature. For example, the range chosen for the saturated blue mentioned in ‘Mark-up’ would be inclusive of only the pixels with a RGB value of 0,0,255, respectively. The range can be widened to pick out tissue features such as all the collagen in a SR-stained section if the stain is of sufficient quality. Each stack of 2D binary matrices when combined as a stack into a 3D binary matrix forms a 3D representation of each marked up feature.

6. 3D matrix: The segmented data of each morphological feature was subsequently rendered in 3D using an in-house developed MATLAB-script (The Mathworks, Massachusetts, USA). From this 3D binary matrix of voxels, a triangle mesh was formed on the outer surface of the voxels and the mesh was saved as a Standard Triangle Language (.stl) file. A separate .stl file was created for each feature, e.g., blood vessels, capsule, and lesion.

7. Mesh visualization: .stl files are a commonly used file format for 3D meshes. The images are from Meshlab (Cignoni et al 2008) open-source software. Meshlab is an open-source software created and maintained by the Visual Computing Lab, part of the ISTR-CNR in Pisa, Italy, www.meshlab.net. Multiple meshes, one for each feature, were loaded into the 3D space retaining their initial relative positions to one another and textured to create a final 3D model of the tissue.

3.9 Pre-culture light microscopy:

Prior to culture, the aspirates were examined under light microscopy and confirmed to have a mixture of cells and debris. As the aspirate underwent a spin process prior to culture, they were not stained at this stage to identify the cell type.

3.10 Cell culture: cell morphology and growth

Following aspiration of the histotripsy lesions the samples were placed immediately in cryovials to which 150 μ L of RPMI cell culture media (Gibco, Thermo Fisher Scientific) was added, supplemented with 10% FBS (Thermo Fisher Scientific) and 1% penicillin (5000 units/mL) and Streptomycin (5000 μ g \cdot mL⁻¹) (Thermo Fisher Scientific). Each sample was strained (40 μ m filter) to remove debris (VWR Collection, VWR, UK) and the cells within the sample were cultured in a 24-well plate (Corning Costar, Merck, UK) for up to 21 days. The cells were stained at different time points using live-dead assay and their growth was monitored using phalloidin/DAPI staining. Three aspirates were cultured in each well. Each lesion was aspirated once and then the lesion was excised for histological assessment. Before culture, a light microscopy assessment was carried out after suspension of the cell aspirate to ensure each well contained cell rather than debris.

3.11 Phalloidin/ Dapi staining

Cell morphology and growth at days 3 and 7 post seeding were examined using fluorescently labelled phalloidin which allowed filamentous actin to be visualised and DAPI which allowed the cell nuclei to be observed. Following the manufacturer's instructions, the cells were fixed using Formalin (10%) for 15 minutes and then washed with PBS. They then underwent permeabilisation with 1% BSA and 0.3% Triton-X solution for 30 minutes before being stained with phalloidin (2.5% in BSA) Triton-X

solution for 90 minutes. The cells were then washed with PBS (3X) and stained with Dapi for 10 minutes before imaging. The cells were imaged using an EVOS fluorescence inverted microscope (EVOS FL colour, Life Technologies) at wavelengths (Ex/Em 495/518 nm) for phalloidin and (Ex/Em 352/461 nm) for dapi. Phalloidin functions by binding and stabilising filamentous actin (F-actin) and effectively prevents the depolymerisation of actin fibres. It is used with a fluorescent tag to reveal the cell cytoskeleton. DAPI is a fluorescent stain that binds strongly to adenine–thymine rich regions in DNA and identifies active dividing cells. DAPI staining has 94% overall sensitivity for cell cycle profiling and therefore allows an integrative and simultaneous quantitative analysis of molecular and morphological parameters (379).

3.12 Live-Dead assay

The viability of the cells was assessed on days 3, 7 and 21 using a Live-dead imaging kit (Molecular Probes, Thermo Fisher Scientific). As per the manufacturer's guidelines, the cells underwent incubation with Live-dead solution containing 0.05% of 4 mM Calcein-AM (Ex/Em: 495/515 nm) and 0.2% of 2mM Ethidium homodimer-1 (Ex/Em 495/ 635 nm) at room temperature for 30 minutes prior to imaging them with an EVOS fluorescence inverted microscope (EVOS FL color, Life Technologies, US). The Live/Dead Cell Double Staining Kit is utilised for simultaneous fluorescence staining of viable and dead cells. This kit contains calcein-AM and Ethidium solutions, which stain viable and dead cells, respectively. Calcein-AM, acetoxymethyl ester of calcein, is highly lipophilic and cell membrane permeable. Though calcein-AM itself is not a fluorescent molecule, the calcein generated from Calcein-AM by esterase in a viable cell emits a strong green fluorescence (λ_{ex} 490 nm, λ_{em} 515 nm). Therefore, calcein-AM only stains viable cells. Alternatively, the nuclei staining dye Ethidium cannot pass through a viable

cell membrane. It reaches the nucleus by passing through disordered areas of dead cell membrane and intercalates with the DNA double helix of the cell to emit red fluorescence (λ_{ex} 535 nm, λ_{em} 617 nm). Since both calcein and Ethidium-DNA can be excited with 490 nm light, simultaneous monitoring of viable and dead cells is possible with a fluorescence microscope. The percentage of live and dead cells were calculated after staining.

3.13 Morphology assessment:

Once stained, the cells were examined under the microscope for morphology and confirmed as hepatocytes following review by two independent researchers and subsequently by an experienced hepato-pathologist (AQ).

3.14 Cell Titre-Glo Metabolic Assay:

Cell Titre-Glo (CTG) 3D cell (Promega) viability assay was used to measure ATP levels of the isolated hepatocytes in each well. The presence of metabolically active cells was quantified using the luminescence given off by the ATP produced. This assay was found to be appropriate since cells extracted from tissue have the tendency to generate ECM when cultured. This type of bioluminescence assay is found to be more sensitive in low density cell populations (380). In addition, this assay is known to have a high sensitivity for cell proliferation and cell toxicity. Given the low volume of cells we were working with, this assay proved to be ideal in assessing the metabolic activity of live cells. The cultures and CTG reagent were equilibrated to room temperature for 15 minutes before use. Cell culture supernatant was removed from each well to leave 50 μ l in each well prior to adding the reagent. 50 μ l of CTG reagent was then added to each well and the plate was placed on a shaker at 900 rpm for 30 s. The plate was then covered with foil

and incubated at room temperature for 30 minutes. Finally, the luminescence was measured using a plate reader (TECAN, Infinite® M200 PRO). One well containing only culture medium and no cells was used as control. Luminescence from each well containing cells was measured on days 7 and 21 post culture.

3.15 Histological evaluation of the excised histotripsy sites for 3D reconstruction

3.15.1 Haematoxylin & Eosin (H&E) staining:

H&E of the excised histotripsy sites was used to identify important structural information and any change following sonication to the liver parenchyma.

3.15.2 Picrosirius red stain:

Picrosirius red stain was used to demonstrate structural and architectural damage to collagen following histotripsy by staining for collagen type I & III. A single 4 µm paraffin section from each sample was stained with Haematoxylin (Harris Haematoxylin, Shandon, UK) and Eosin (Eosin Y, Shandon, UK) (H&E) using an auto-stainer (Leica, ST5020, UK).

One additional section from each sample was stained with Picrosirius red (SR) stain (Sigma-Aldrich, Direct Red 80, UK) with the following protocol: (1) Deparaffinise sections in 2 changes of xylene. (2) Rehydrate through 2 changes of alcohol, 70% alcohol and distilled water. (3) Apply SR solution to cover entire sections and incubate in humidified chamber for 60 min. (4) After 60 min, rinse slides quickly in 2 changes of Acetic Acid Solution. (5) Rinse slides in absolute alcohol and then dehydrate through 2 changes of alcohol, clear in 2 changes of xylene and mount with pertex mounting medium.

3.15.3 Reticulin Stains:

A further section from each sample was stained for reticulin. The staining procedure was carried out using the Reticulum II stainer kit (Roche catalogue number 860-024) and a Ventana BenchMark Special Stain system.

3.16 3D Hep generation, Differentiation & Maintenance

This work was carried in collaboration with Dr Hassan Rashidi who has developed and maintained the 3D Heps as per his previously published protocol.

3.16.1 Generation of self-aggregated hiPSC spheroids:

A previously published protocol was used to generate 3D Heps from hPSCs (Lucendo-Villarin et al., 2019 (381)). Initially, Agarose microplates were fabricated in 256-well format using the MicroTissues® 3D Petri Dish® mould (Sigma Aldrich) following the manufacturer's instructions and transferred to 12-well plates (Corning). hPSCs scaled up on laminin coated plasticware, were incubated with 1 ml of Gentle Dissociation Buffer (STEMCELL Technologies) for 7 min at 37° C. Following this, single cell suspensions were prepared by pipetting the buffer up and down gently. The cell suspension was centrifuged at 0.2 relative centrifugal force (rcf) for 5 min, discarded the supernatant and resuspended in mTeSR1™ supplemented with 10 µM Y-27,632 (Cayman Chemical Company) at a density of 2.0×10^6 live cells/ml. The agarose microplates were seeded by transferring 190 µl of cell suspension. After 2–3 h, 1 ml mTeSR1™ supplemented with 10 µM Y-27,632 was gently added to each well of the 12-well plate and incubated overnight to allow formation of self-aggregated spheroids as described elsewhere (Lucendo-Villarin et al., 2019).

3.16.2 Differentiation into 3D Heps:

Differentiation was initiated a day after generation of hiPSC spheroids by replacing mTeSR1™ with endoderm differentiation medium which consisted of RPMI 1640 containing 1 × B27 (Life Technologies), 100 ng/mL Activin A (PeproTech), and 50 ng/mL Wnt3a (R&D Systems). The medium was changed every 24 h for 72 h. On day 4, the endoderm differentiation medium was replaced with a hepatoblast differentiation medium. The medium consisted of knockout (KO)-DMEM (Life Technologies), knockout serum replacement (KOSR - Life Technologies), 0.5% Glutamax (Life Technologies), 1% non-essential amino acids (Life Technologies), 0.2% β-mercaptoethanol (Life Technologies), and 1% DMSO (Sigma), and was renewed every second day for a further 5 days. On day 9, the medium was replaced by a hepatocyte maturation medium HepatoZYME (Life Technologies) containing 1% Glutamax (Life Technologies), supplemented with 10 ng/ml hepatocyte growth factor (HGF; PeproTech) and 20 ng/ml oncostatin m (PeproTech). On day 21, cells were cultured in a maintenance medium consisting of William's E media (Life Technologies), supplemented with 10 ng/ml EGF (R&D Systems), 10 ng/ml VEGF (R&D Systems), 10 ng/ml HGF (PeproTech), 10 ng/ml bFGF (PeproTech), 10% KOSR, 1% Glutamax, and 1% penicillin–streptomycin (Thermo Fisher Scientific).

3.16.3 Maintenance of human induced pluripotent stem cells (hiPSCs):

An inhouse generated hiPSC line (GOS101B) was used in this study. GOS101B was cultured on laminin 521 (BioLamina) coated plates in serum-free mTeSR™1 medium (STEMCELL Technologies) as previously described (Rashidi et al., 2022). The cell lines were propagated in antibiotic free medium and were monitored regularly for mycoplasma infection using MycoAlert™ PLUS Mycoplasma Detection Kit (Lonza).

3.16.4 Pre-implant evaluation: Functional characterisation

(382, 383)

Aggregated hPSCs were differentiated toward the hepatocyte lineage using a stepwise differentiation protocol described above ((383); **Figure 22a**). To produce homogenous three-dimensional spheres (3D Heps) of defined size, the agarose multi-well plate technology was employed to form hPSC aggregates. By day 30 of differentiation, 3D Heps exhibited typical hepatic morphology with distinctive cell borders which was maintained until harvesting the organoids for transplantation on day 60 of differentiation. (**Figure 22a**). Differentiation to hepatic lineage was confirmed following detection of liver-specific genes by qPCR (**Figure 22b**). We also measured the level of AFP and ALB secretion using ELISA (**Figure 22c**) and CYP3A4 metabolic activity (**Figure 22d**).

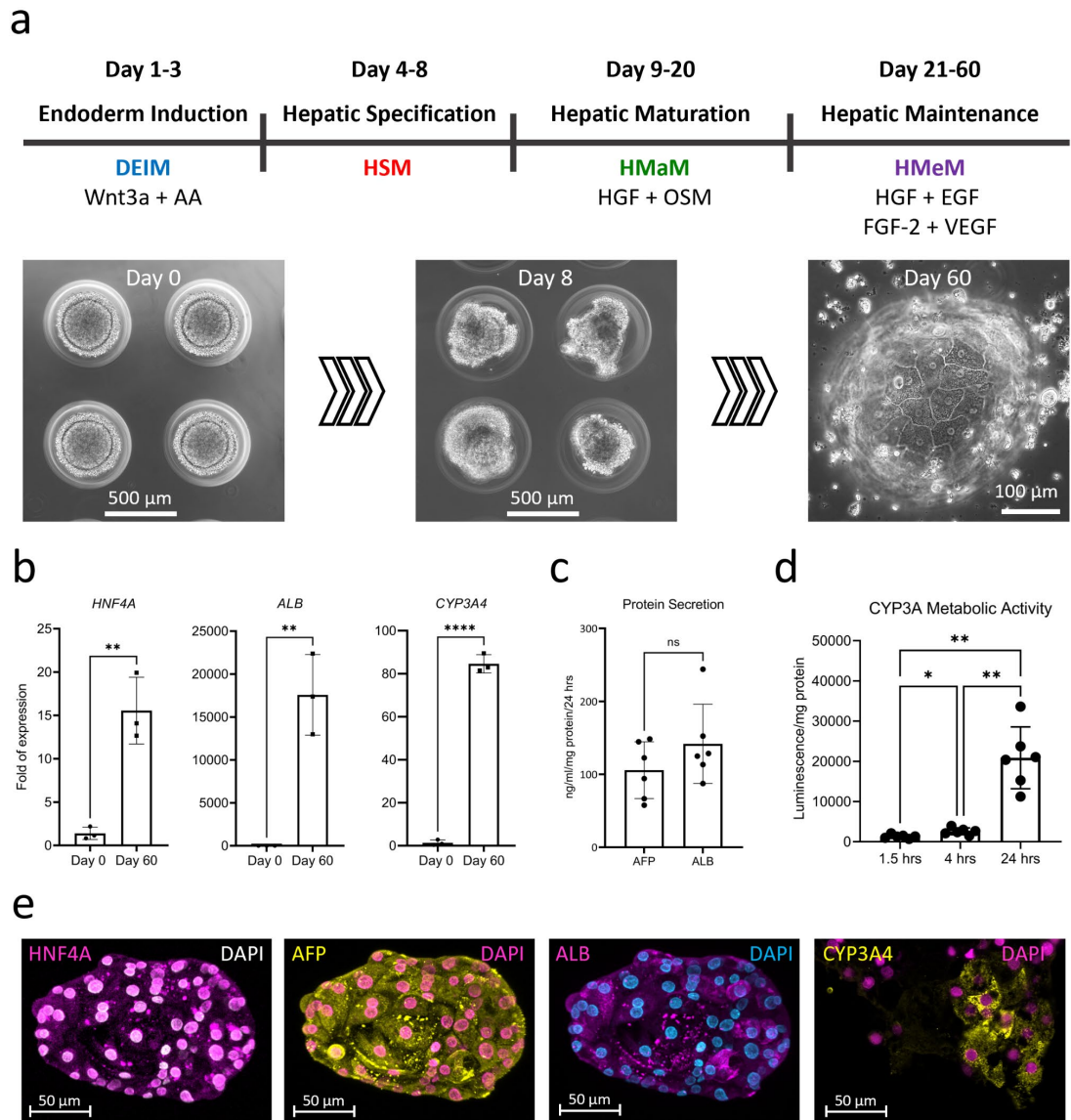


Figure 22 – Work carried by Dr Hassan Rashidi in assessing cell differentiation and viability of the 3D Hep Figure adapted from (382, 383). a) A stepwise differentiation protocol was used to generate 3D Heps from hiPSCs. b) Expression of liver-specific genes HNF4A, ALB and CYP3A4. c) ELISA was used to measure AFP and Alb secretion by generated 3D Heps. d) Bioluminescence assay was used to assess CYP3A4 metabolic activity of 3D Heps. e) Immunostaining was performed to detect liver-specific proteins. (Abbreviations: DEIM, Definitive Endoderm Induction Medium; HSM, Hepatic Specification Medium; HMaM, Hepatic Maturation Medium; HMeM, Hepatic Maintenance Medium)

3.16.5 Immunofluorescence staining of the 3D Heps:

Prior to implantation, 3D Heps were fixed in ice-cold methanol for 30 min, washed in PBS, and embedded in agarose before embedding in paraffin to obtain sections of 4 μ m thickness. Antigen retrieval was performed by heating dewaxed and rehydrated sections in $1 \times$ Tri-sodium Citrate buffer solution for 15 minutes in a microwave oven using defrosting option to avoid boiling of the buffer. Washed slides were used for subsequent staining to characterise generated cells. To perform immunostaining, stem cell-derived tissue was blocked with 10% BSA in PBS-tween (PBST) and incubated with primary antibody overnight at 4 °C and detected using species-specific fluorescent conjugated secondary antibody (Alexa Flour 488/Alexa Flour 568/Alexa Flour 680; Invitrogen). Sections were counterstained with DAPI (4',6-diamidino-2-phenylindole) and mounted with ClearMount™ mounting solution (Invitrogen). An extended staining protocol was developed and optimised to stain whole mount 3D Heps. Briefly, MeOH fixed spheroids were washed and rehydrated in PBS. Following overnight blocking in 10% BSA in PBST, the spheroids were incubated with primary antibody at desired concentration with gentle agitation at 4 °C overnight followed by 8 washes with 0.1% PBST (each wash 1 h) under gentle agitation at room temperature (RT). Secondary antibodies were incubated at 4 °C overnight and washed as described above. The nucleus was counterstained with DAPI (Life Technologies) before images were acquired using a Zeiss LSM 880 upright multiphoton confocal microscope.

3.17 Enzyme-Linked Immunosorbent Assay (ELISA)

Two dimensional and 3D mature hepatocytes derived from hiPSCs were incubated with HepatoZYME medium for 24 hours at different time points at 37°C in 5% (v/v) CO₂, 95% (v/v) O₂. The supernatants were collected after 24 hours and could be stored in -80

°C for later analysis. The ALB and AFP levels were measured, using commercially available microwell plates pre-coated with immobilized human anti-ALB and AFP antibodies (Alpha Diagnostic Intl. Inc., San Antonio, USA). The supernatant was diluted into 1:3 or 1:10 on the working sample diluent and transferred into wells in duplicate followed by 1-hour incubation at room temperature as per manufacturer's instructions. Following this step, microwells were washed with working wash solution four times and diluted anti-human ALB HRP conjugated was added to the microwells. The wells were incubated at room temperature for 30 minutes. Again, microwells were washed with working wash solution five times, and the substrate for the HRP enzyme TMB, was added and incubated for 15 minutes in the dark. Following this step, the stop solution was added to each well and the plates luminous activity was measured at 450 nm with a reference wavelength of 630 nm using a FLUOstart Omega plate reader (BMG LabTech, Germany). Plain tissue culture media which was incubated for 24 hours at 37°C was employed as a negative control. For data analysis, the collected data was normalised per ml per 24 mg protein as measured by the BCA Assay (Pierce, UK).

3.18 Cytochrome P450 Assay

2D and 3D hiPSC-derived HLCs were incubated for 5 hours, with the luciferin conjugated specific CYP3A (1:40) and CYP1A2 (1:50) substrate (P450 P-Glo Luminescence Kit, Promega, UK) at 37°C. The incubated supernatants were then collected and also could be stored at -80°C for later analysis. The Luciferin detection reagent was reconstituted by mixing the buffer into the bottle containing the lyophilised Luciferin detection reagent. For measurement, in a white 96 well plate 50 μ l of the supernatant sample mixed with 50 μ l of the detection reagent was added and incubated at room temperature in the dark for 20 minutes. The data was collected using a luminometer (POLARstar optima). For

data analysis, units of activity were measured as relative light units per ml per mg protein (RLU/ml/mg) as determined by the BCA assay.

3.19 ImageJ Software:

ImageJ 1.52 (National Institute of Health, USA) was used in processing and optimisation of the images acquired from histology and cell microscopy. The Cell Count plugin was used for counting cells in the Live-dead and DAPI microscopy images. The *Figure J* plugin was used in construction of optimized images for publication.

<https://imagej.nih.gov/ij/index.html>

3.20 Statistical methods:

GraphPad Prism© 6 software was used in the analysis of the data. Chi-squared test was used to compare the proportion of live cells on day 1 and day 7 post culture. Student's t-test or Mann–Whitney tests were used to determine the difference, which was set at $P < 0.05$. We did not use statistical methods to predetermine sample size, there was no randomization designed in the experiments, and the studies were not blinded. Data are represented as mean \pm SEM or median where appropriate.

Chapter 4 Preliminary histological analysis of perfused versus non-perfused ex-vivo porcine liver and histotripsy calibration

4.1 Introduction

Boiling histotripsy (BH) is an emerging technique for the mechanical disintegration of soft tissue (264) through the nucleation (384) and sustained activity of gas bubbles in the tissue (385) using high intensity focused ultrasound (HIFU). This methodology exploits and enhances bioeffects of HIFU propagation to non-invasively fractionate millimetric volumes of soft tissue in a few seconds.

Boiling histotripsy has been preclinically tested and parametrised for the disintegration of ex-vivo bovine liver, kidney and heart tissue, as well as in-vivo porcine and murine liver (163, 384, 386-388). Potential clinical applications of BH include the mechanical ablation of benign prostatic hyperplasia (BPH), liver, and kidney tumours, for inducing anti-tumour immune responses in cancer, for cell therapy. Comprehensive reviews on the clinical applications of histotripsy have been previously reported (264, 389).

A desirable feature of boiling histotripsy is that it requires acoustic pressures which are compatible with current clinical HIFU systems or more affordable and portable single-element bowl shaped HIFU transducers (264). In BH, millisecond long HIFU pulses containing strong shock fronts are periodically delivered to the target tissue. Such shocks are formed because of non-linear propagation effects, and their high harmonic components are readily absorbed by soft tissue and turned into heat (387).

The combined effects of rapid heating and large rarefactive ultrasound pressures at the focal volume is the induction of boiling bubble nucleation (384). These bubbles undergo rectified growth up to millimetric dimensions (390). Their interaction with the incoming acoustic field inflicts shear stresses which exceed the mechanical strength of the surrounding tissue (385). In addition to that, the incoming acoustic waves are reflected at the boiling bubble interface, creating a dense pre-focal cavitation cloud in regions of much lower temperature (391). The oscillation and violent collapse of these bubbles causes is also capable of effectively disintegrating soft tissue (264). This results in a small cavity (depending on the force used size can vary) that has debris of cells contained within it.

In recent years, there has been ongoing interest in the application of boiling histotripsy for the mechanical decellularization of soft tissue as well as cell therapy (163, 385). Histological analysis of BH lesions in rat liver displayed decellularized regions, achieving mechanical destruction of cells whilst sparing the surrounding vasculature (385). A later

study in ex-vivo non-perfused bovine liver demonstrated the ability of BH to disintegrate cells whilst preserving tissue structures such as vessels and ducts. This study also showed that the percent amount of denatured water-and-salt insoluble proteins increased with increasing pulse length (163).

In general, decellularization techniques (see section 2.6) aims to obtain volumes of three-dimensional extracellular matrix (ECM) scaffolds, which are primarily made of collagen, with preservation of the vascular network (386). In decellularization, it is important to achieve the removal of cells and genetic material whilst preserving the structural and biochemical properties of the ECM (387). Given the high susceptibility of collagen to thermal degradation (388) and the combined thermal/mechanical nature of boiling histotripsy (389), it is therefore of relevance to understand the extent of thermal damage around boiling histotripsy lesions. The effect of histotripsy on collagen fibres in the ECM of porcine liver has not been studied (see section 2.6.1) in the context of perfused versus non-perfused. Tissue perfusion can directly influence the heat dissipation and the biophysical property of the local environment (343) (see section 2.2.1). Non-perfused tissue may already exhibit compromised ECM integrity (392). This makes it difficult to evaluate the effectiveness of BH in preserving the ECM for subsequent cell transplantation. A direct comparison of how perfusion makes a difference to the histotripsy sonication of the tissue has not been previously examined.

In the present work, histological analysis of BH lesions produced in freshly retrieved porcine liver are analysed with H&E and picrosirius red staining, comparing the histopathology of perfused and non-perfused specimens. We perform numerical simulations of histotripsy propagation in soft tissue to quantify relevant acoustic quantities, predict histotripsy-induced temperature fields and understand temporal/spatial metrics of bubble nucleation. This ensures experiment repeatability and establishes a baseline for analysis of histological results. This work is an effort towards understanding the microscopical effects of perfusion in the application of boiling histotripsy to the decellularization of soft tissue.

Aim of chapter

- To develop a standardised BH algorithm and evaluate the tissue response to BH on liver.
- To investigate the effect of organ perfusion on the tissue response to BH

Hypothesis: histotripsy results in thermal injury in non-perfused tissue and results in mechanical disintegration in the perfused porcine samples with preservation of the extracellular matrix (ECM) as scaffold for future regeneration nidus.

4.2 Methods:

See Section 3.1 & 3.2

4.1.1 Organ procurement

As previously described in 3.1 of the methods section porcine livers were acquired using organ retrieval techniques. Retrieved organs were flushed of blood and were ready for perfusion and sonication on arrival to the lab ($n = 5$). In addition, a number ($n = 5$) of porcine livers were acquired using the same retrieval technique but were not subject to back bench flush and these livers were not perfused to maintain viability. Prior to these porcine experiments calibration of the histotripsy system was performed on fresh liver purchased from the market.

4.2.1 Histotripsy setup (Full details in methods chapter)

See Section 3.3 & 3.4

The Histotripsy probe was connected to a 3D positioner guided by a laser pointer (**Figure 23**). The probe was connected to a power unit and the signal generator that is monitored by the computer program. Under the probe is the organ bath where the porcine liver was be connected to the perfusion circuit. Prior to sonication the Histotripsy probe would be calibrated in a water tank containing distilled de-gassed water (**Figure 24**). The process of degassing entails removing dissolved gas in liquid which could take about one hour. The liver was cannulated via portal vein for perfusion and the IVC effusate would be collected in the organ bath (**Figure 25**).

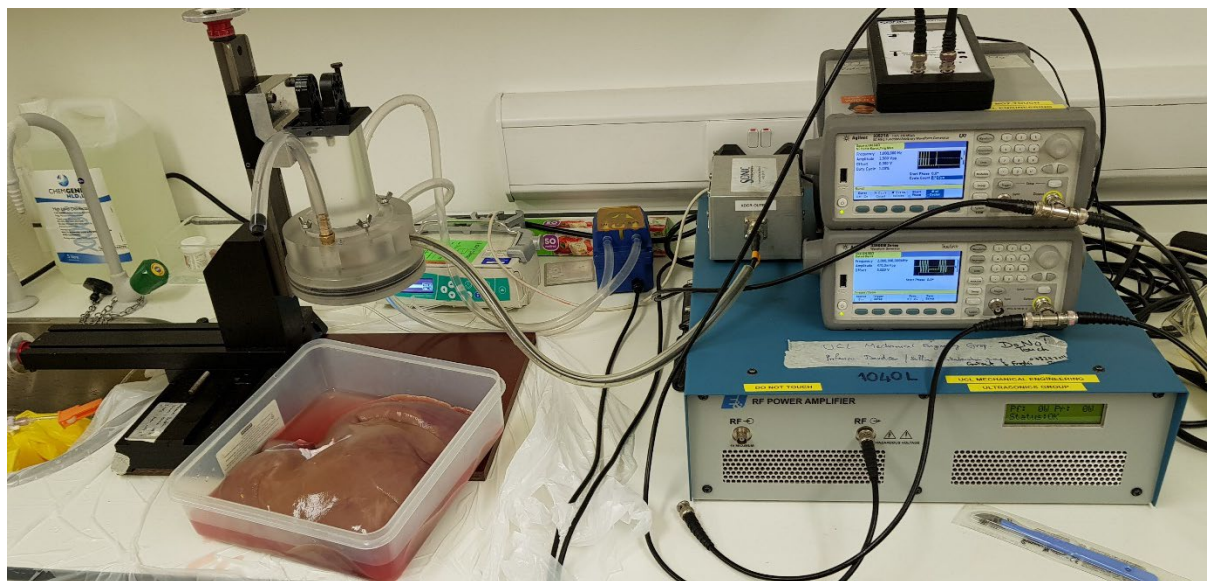
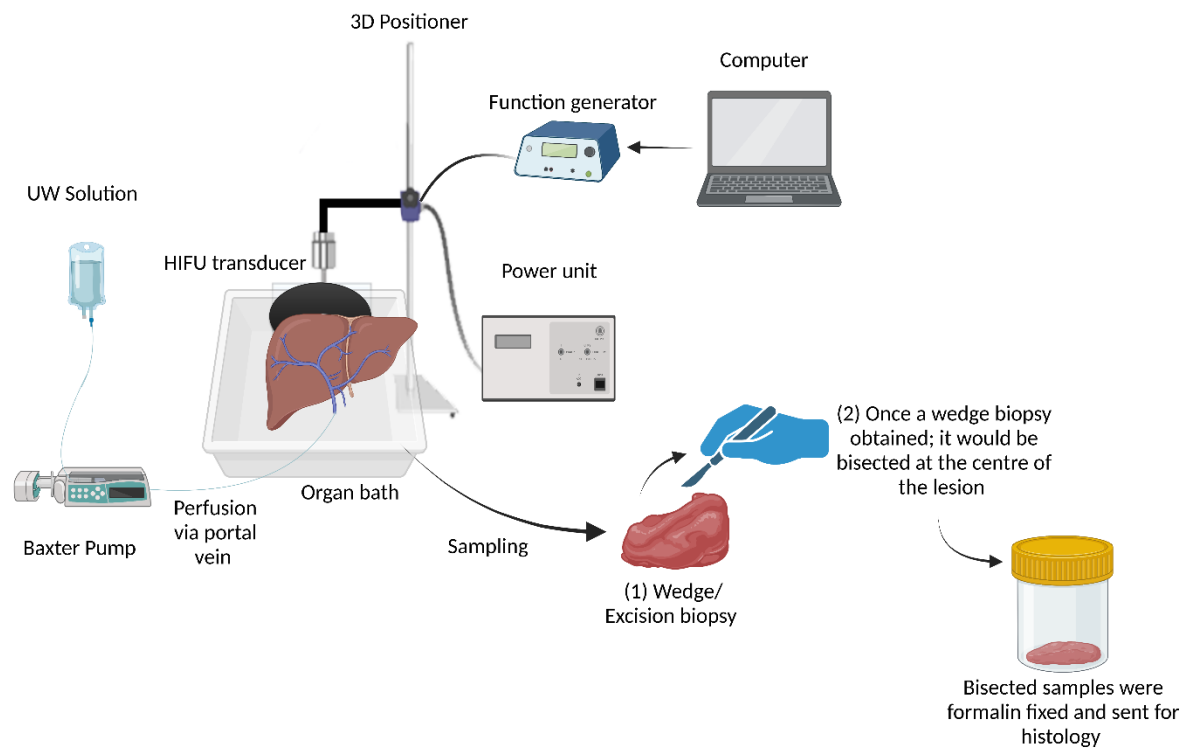


Figure 23 – Perfusion circuit and histotripsy set up along with organ bath that would keep the organ during experimentation.

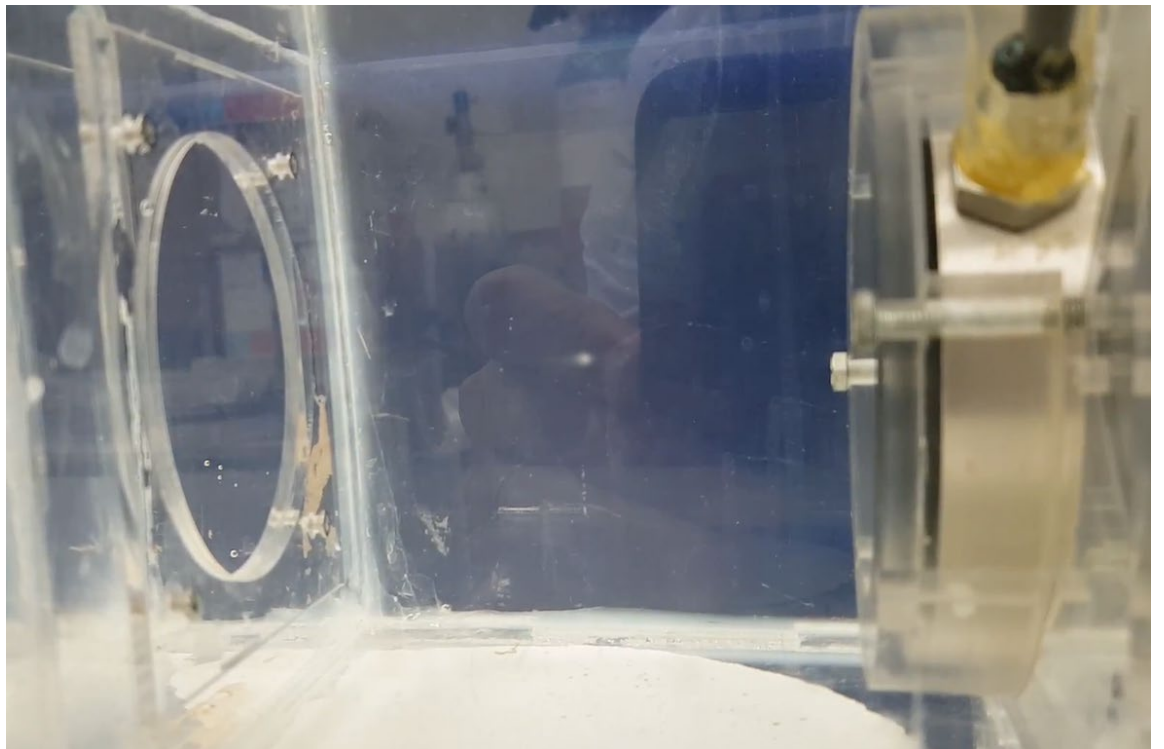
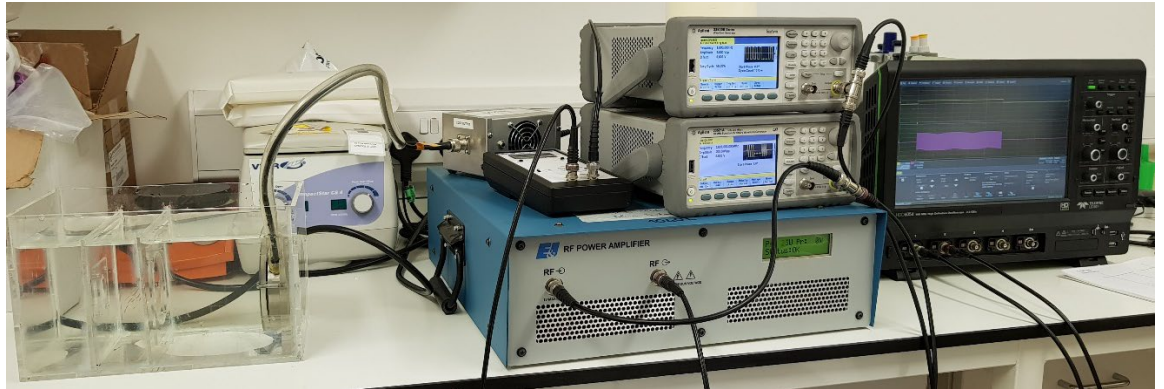


Figure 24 – Calibration tank showing the histotripsy probe and the sonication energy traversing through the distilled degassed water. Where the sonication happens is where the focus of the energy would be concentrated and hence in tissue this would be the point of maximal destruction/change.



Figure 25 - Left: Perfused porcine liver in the organ bath. The organ bath collects the perfusate draining via IVC during perfusion and sonication. Right: shows the PV cannulated just before its bifurcation to the left and right and secured in place using a stay suture. This allows perfusion of both lobes. As demonstrated in the picture this liver is relatively well perfused with only a few patchy areas that may not have flushed well following retrieval. well, (IVC: inferior vena cava; PV: portal vein)

4.2.2 Tissue sampling

Once histotripsy lesions were created, they were identified by the dimple impression left on the capsular surface of the liver. This would act as a rough guide as to where the centre of the lesion would be. The sample would then be excised as a wedge and bisected using a surgical blade to confirm the lesion in centre (**Figure 26**) and send for pathology in formalin containers (**Figure 27**).

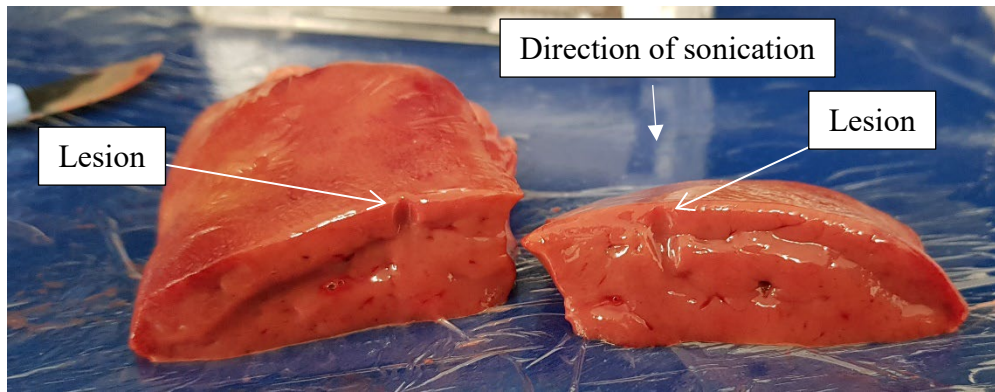


Figure 26 – Excised and bisected liver tissue following sonication. It demonstrates the lesion and the direction it takes passing inferiorly. The dimple at the capsular area would mark an approximate area of the lesion. The tissue is bisected using a surgical blade to examine the lesion and its contents.

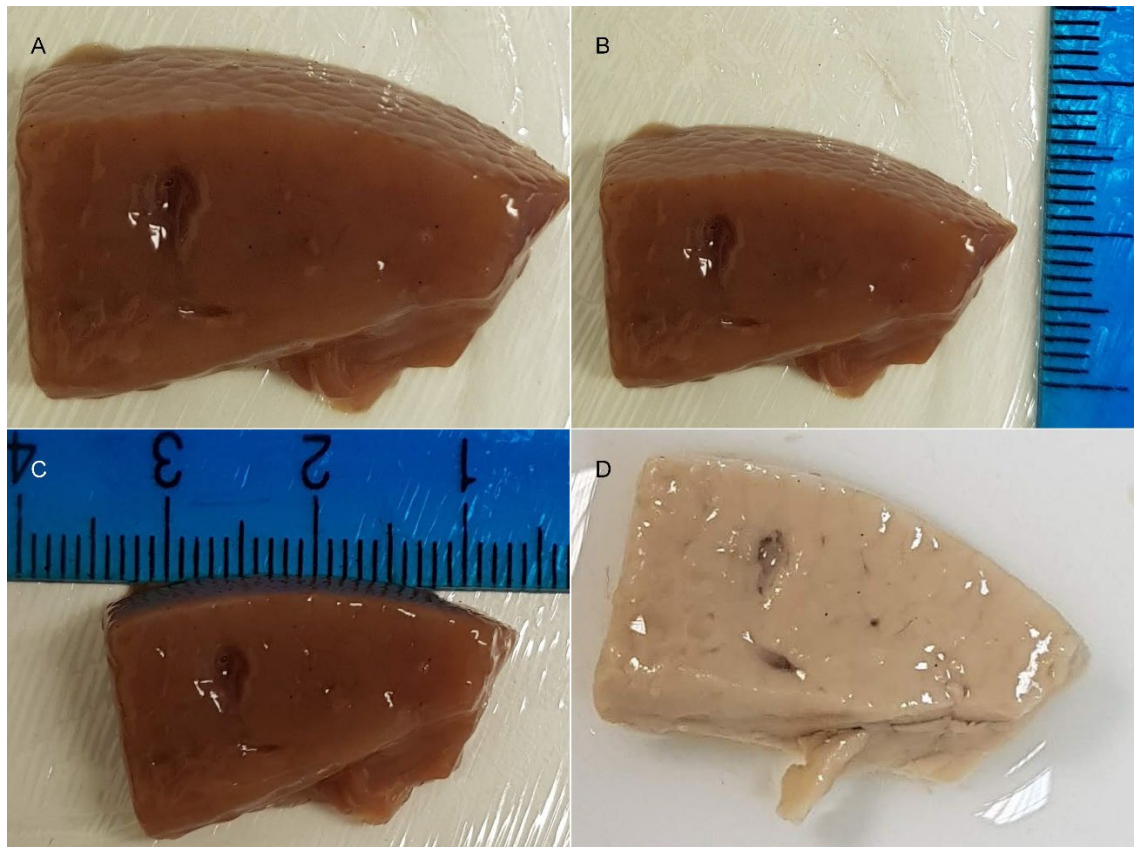


Figure 27 – example of wedge resection for tissue sampling. This is following 50p sonication and the tissue has been bisected through the lesion. The lesion is demonstrated in the top left image as a sharp-edged cavity which lies half a centimetre below the liver capsule. The bisected samples are sent for histology in formalin pots. Image shows a formalin fixed sample with the lesion clearly demonstrated on the cut surface.

4.2.3 Histology

H&E staining as well as picrosirius red staining was used to assess the ECM as well as the liver parenchyma in the sonicated area. The tissue is fixed in formalin and then processed with H&E and picrosirius red staining. The picrosirius red stained slides are selected and used for inverted light microscopy.

4.2.4 Microscopy

Microscopic evaluation of histotripsy lesions was performed using both brightfield and polarized light microscopy to assess tissue architecture and extracellular matrix (ECM) integrity. H&E staining enabled general histopathological assessment and identification of lesion demarcation, while picrosirius red staining under polarized light enhanced visualization of collagen birefringence, allowing qualitative and semi-quantitative analysis of ECM disruption.

4.2.5 Quantitative analysis

Statistical analysis was performed where relevant using two different software: STATA 16 (Copyright 1985-2019 StataCorp LLC, Texas, USA) and Python 3.9 program (Copyright ©2001-2024. Python Software Foundation). In this chapter, the Standard error of the mean is calculated using the STATA 16 program. The heatmap and the scatter plot are created with the following codes in the Python program.

Heatmap:

Seaborn's heatmap & Matplotlib library were used using the code below:

```
import matplotlib.pyplot as plt
import seaborn as sns

plt.figure(figsize=(10, 8))
sns.heatmap(correlation_matrix, annot=True, fmt=".2f", cmap="coolwarm",
cbar=True)
plt.title("Correlation Matrix Heatmap")
plt.show()
```

Scatter plot:

```
import pandas as pd
from scipy.stats import pearsonr
import matplotlib.pyplot as plt
import seaborn as sns
```

```

# Prepare the data
subset = sheet1_cleaned[[x_col, y_col]].dropna() # Drop rows with NaN values for
selected columns

# Perform Pearson correlation test
correlation_coefficient, p_value = pearsonr(subset[x_col], subset[y_col])

# Generate Scatter Plot
plt.figure(figsize=(8, 6))
sns.regplot(x=subset[x_col], y=subset[y_col], ci=95, scatter_kws={"alpha": 0.5})
plt.title(f"Scatter Plot: {x_col} vs. {y_col}\n"
          f"Correlation Coefficient = {correlation_coefficient:.2f}, p-value =
          {p_value:.4f}")
plt.xlabel(x_col)
plt.ylabel(y_col)
plt.show()

```

4.3 Results

4.3.1 Parameter analysis and histology correlation of BH liver lesions

A total of 120 lesions were created in both perfused and non-perfused tissue using different parameter settings as a trial and error to assess both on gross inspection the appearance of the lesion and under microscopy. Out of 120 of lesions were reviewed after initial histology inspection, 91 slides were sent to our expert pathologist (Prof Quaglia) to review and further comment. The 91 slides were confirmed to have a lesion present under microscope and hence sent for further review. The data presented in **Table 18 (Supplement 1)** is a summary of the review of the 91 selected slides. The parameter 50p at 1% duty cycle was used mostly for the lesion creation based on previously published studies and comparison was made with 100p and 150p at two different duty cycles. All the parameters could produce a lesion with varying degrees of thermal injury demonstrated (described below). The high the power and the duty cycle the higher the risk of thermal injury. The standard error of the mean (SEM) analysis of the reviewed slides shows perfused sample sonicated at 50p have a smaller SEM for the burns mark.

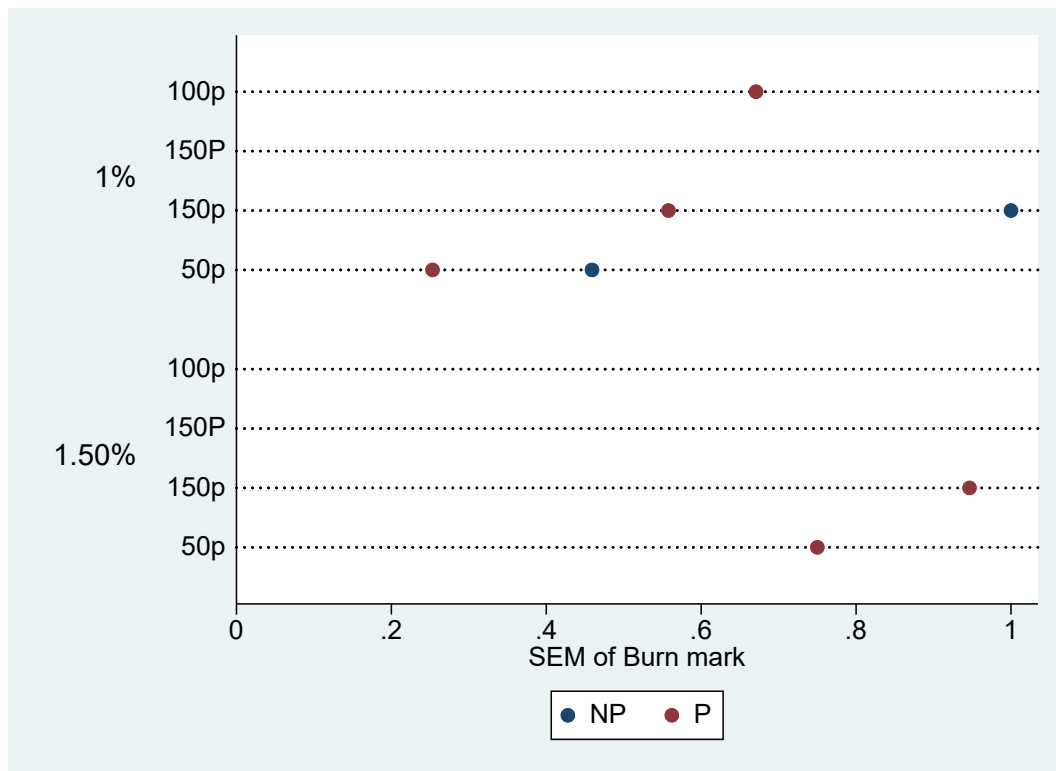


Figure 28 – Standard error of the mean (SEM) analysis of the burns mark created by different powers and different duty cycles for perfused and non-perfused samples. 50p sonicated lesion were more likely to represent absence of burns mark as demonstrated by their smaller SEM (P: perfused; NP: non-perfused; the pin the y axis denotes pulse duration)

Descriptive analysis of lesions:

4.3.2 Non-Perfused Samples

The non-perfused porcine livers were obtained in a similar manner as described in section 3.1 with a difference that they were not flushed in the abattoir and later were not perfused in the lab. The liver on gross inspection was red/blue in colour likely due to blood content in the tissues (**Figure 29a**). A total of 19 lesions in the non-perfused were selected for analysis. Sonication produced a dimple on the capsule of the liver that indicated the location of the lesion. There was no breach of the liver capsule.

On gross morphological examination, excised and bisected lesions showed a cavity. The cavity would lie about 5mm in the subcapsular space, and its typical length

would be between 0.5-1cm in size. In some cases, there would be a dense white tissue at the tail end of the lesion which would indicate thermal injury (**Figure 29b**). This was only demonstrated in higher duty cycles when we were calibrating the probe and identifying an appropriate parameter for porcine liver sonication. When same parameter (50p) was applied to a non-perfused dehydrated tissue, the degree of assumed thermal injury was higher. In fact, that cavity was not as clear as a non-perfused porcine liver. Following sonication, there is a white tract with breach of the liver capsule (**Figure 30c**). This highlights the importance of tissue water content.

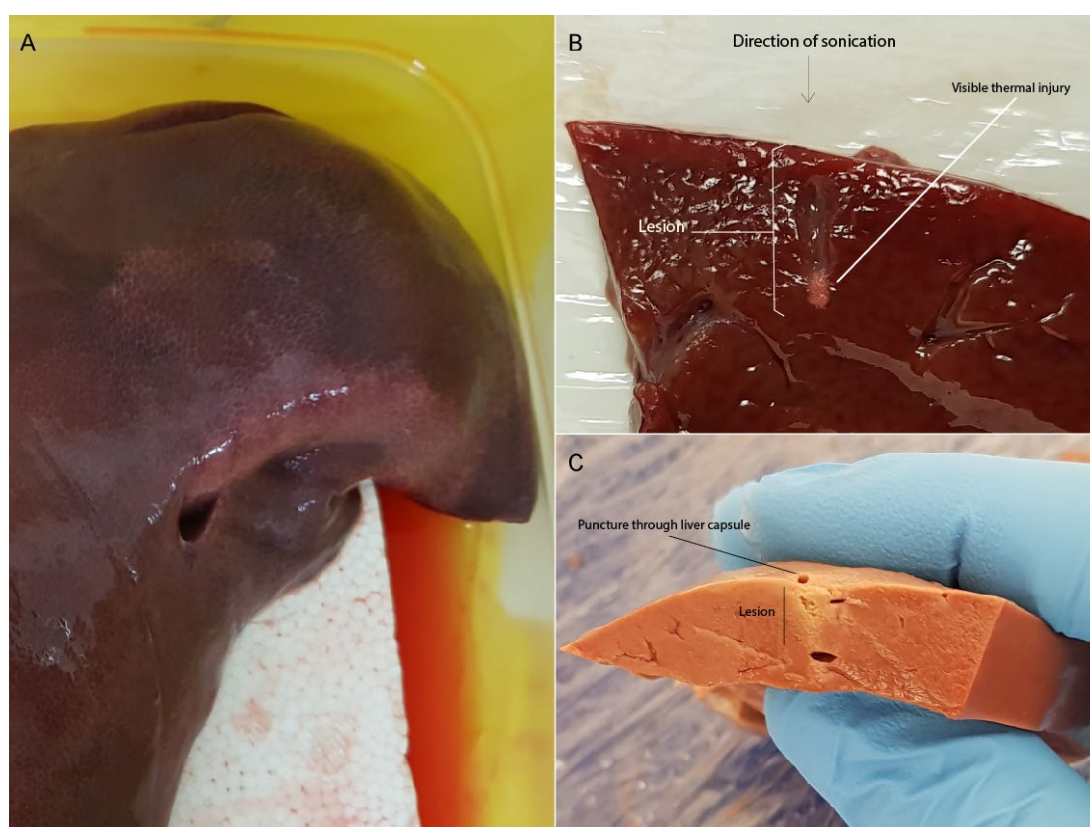


Figure 29 – (A) Non-perfused liver that demonstrates its still filled with the animal blood and clots. (B) Excised and bisected porcine lesion demonstrating a cavity produced by sonication which tends to be sub-capsular. In this specimen, there is evidence of possible thermal injury towards the tail end of the lesion appearing as a small dense white patch. (C) Dehydrated non-perfused cow liver that demonstrated following sonication there is a white tract form along the direction of the sonication. There was also breach of the liver capsule.

4.3.3 Perfused Samples

The method for obtaining the perfused livers is outlined in Section 3.1. All retrieved livers flushed well in the abattoir were subsequently re-perfused in a laboratory setting (**Figure 30a**). livers would be re-perfused at 350ml/hr; on gross inspection a satisfactory flow of the perfusate was observed through the perfusion circuit, entering the portal vein and exiting through the inferior vena cava and bile production was noted after reperfusion. A total of 72 lesions were selected for analysis from the perfused samples. Upon subjecting the organ to sonication, a discernible indentation would manifest, serving as a rough estimate of the lesion's location (**Figure 30b & c**). Lesions are commonly observed to have a diameter of 0.5 cm in the subcapsular region and are characterised by the presence of a fluid suspension.

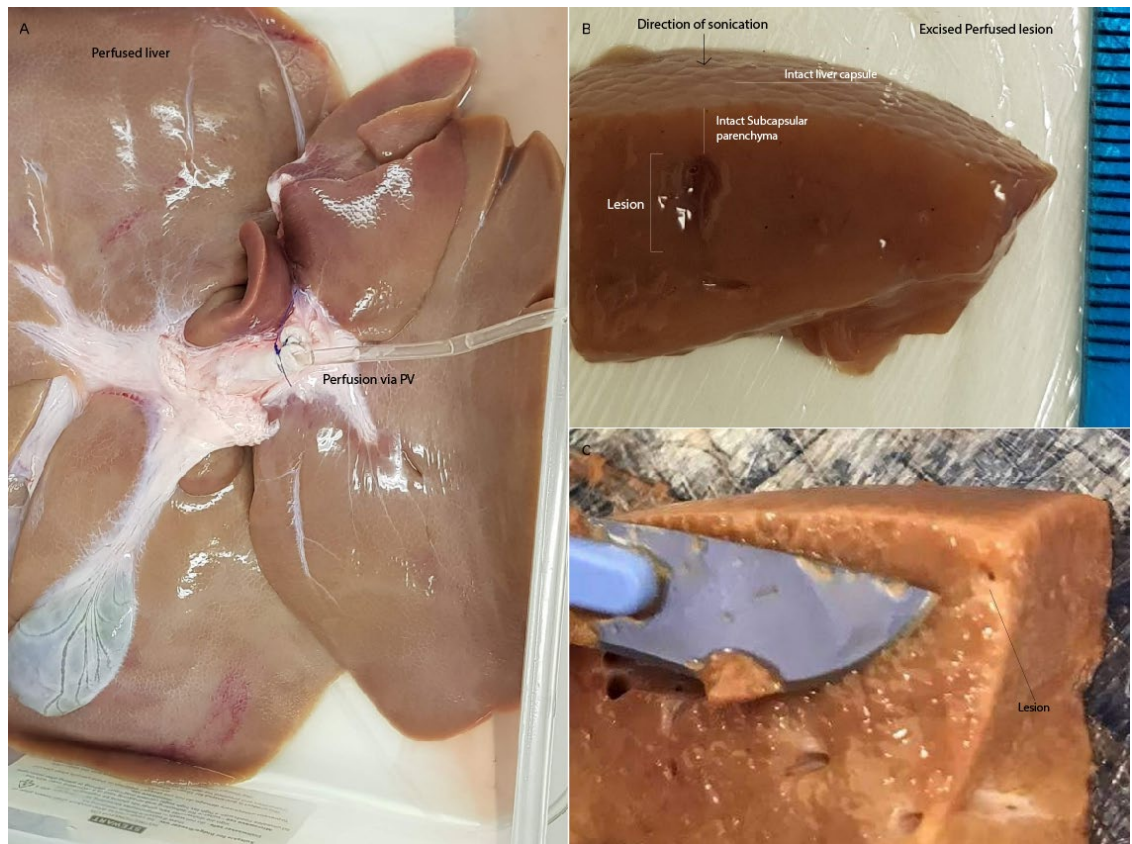


Figure 30 – (A) Perfused porcine liver connected to the Baxter pump perfusion circuit via portal vein. The liver is well perfused with sharp margins and gallbladder in situ. (B) Bisected perfused liver excision biopsy that shows the lesion

to be approximately 0.5cm below the capsular area and contains a core suspension of liquified material. (C) Another example of the histotripsy lesion in perfused sample that would lie approximately 0.5cm below the liver capsule. The core liquified suspension has been aspirated for culture and it reveals the cavity as a small hole indicated by the arrow.

4.3.4 H&E staining

Overall appearance of the lesions in both perfused and non-perfused tends to be of similar diameter and dimensions and in almost all sections the lesions appear subcapsular. Although there were tissue samples captured and cut in different orientations during sectioning, there is no breach of the capsule noted in either group. The lesions then to be in range of 0.5cm to just below a 1cm in length. In perfused group (**Figure 31a**), there is sharp demarcation between the lesion site and where normal hepatocyte, or tissue of unaffected site starts. The sharp boundary is also marked by loss of extracellular matrix septa in the core of the lesion. More so, in the perfused group the lesions contain a liquified suspension that was aspirated from majority of the samples to assess and examine the content later. In the non-perfused group (**Figure 31b**), a similar appearance was noted. Although on gross examination the lesions tend to have a higher degree of thermal injury but on histology there was no discernible difference between the two groups in terms of thermal injury (lesions size still 0.5-1cm and lie approx. 0.5 in subcapsular region). The non-perfused samples also displayed a demarcation between the edge of the lesion and the healthy tissue on H&E staining. As the core of the non-perfused group was not aspirated for cell culture, the core is identified by debris of sonicated cells and extracellular matrix. What's interesting is the loss of extra-cellular matrix in the core of the lesion like the perfused group. H&E is not a useful histological test to assess extracellular matrix damage and hence the need for further evaluation with picrosirius red and reticulin stains.

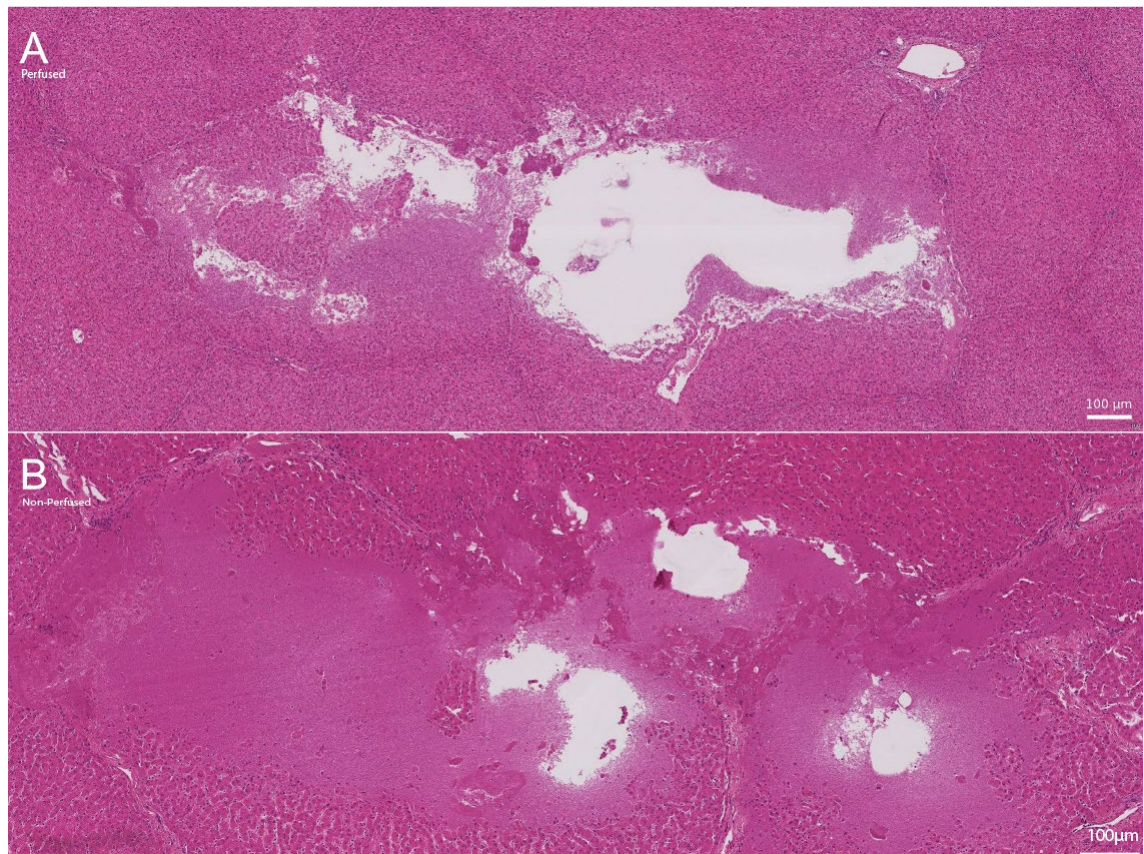


Figure 31 – example of 50p perfused and non-perfused sonicated porcine liver tissue. (A) This is an example of a perfused porcine liver subjected to the 50p pulse at 1% duty cycle. (10x zoom) (B) Demonstrates a non-perfused liver subjected to the same parameter as the perfused sample. (20x zoom) P: pulse duration

Quantitative analysis:

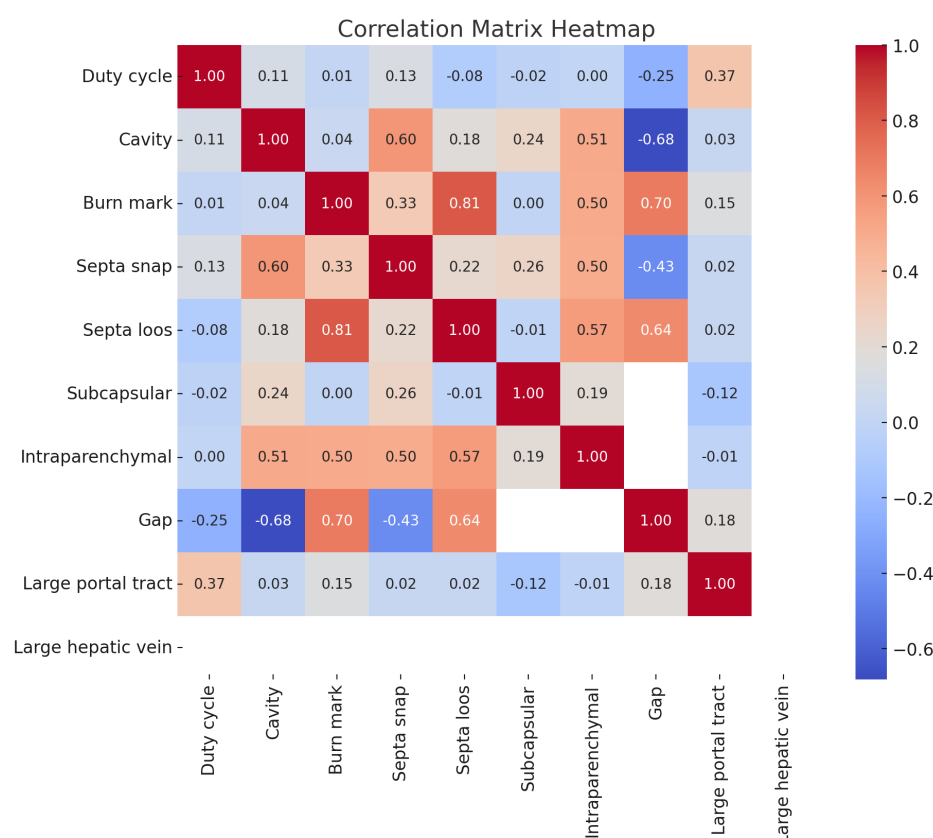


Figure 32 – Heatmap of the different parameters observed in the Table x. Correlation ranges from -1 to +1 where +1 indicates a perfect positive correlation (as one variable increases, the other also increases proportionally). Zero indicates no correlation (the variables are independent) and -1 indicates a perfect negative correlation (as one variable increases, the other decreases proportionally).

A heatmap (**Figure 32**) generated using the data in **Table 18** provides an overview of the relationship between the histological findings. Correlation ranges from -1 to +1 where +1 indicates a perfect positive correlation (as one variable increases, the other also increases proportionally). Zero indicates no correlation (the variables are independent) and -1 indicates a perfect negative correlation (as one variable increases, the other decreases proportionally). There is positive correlation between formation of a cavity and snapped septa (0.60). Also, a positive correlation between loose septa and possibility of observed burns exists. A scatter plot (**Figure 33**) of the observed burns area and the cavity formations of the reviewed histology slides reveals no significant relation between the cavity formation and burns injury (correlation coefficient: 0.04; p-value: 0.73).

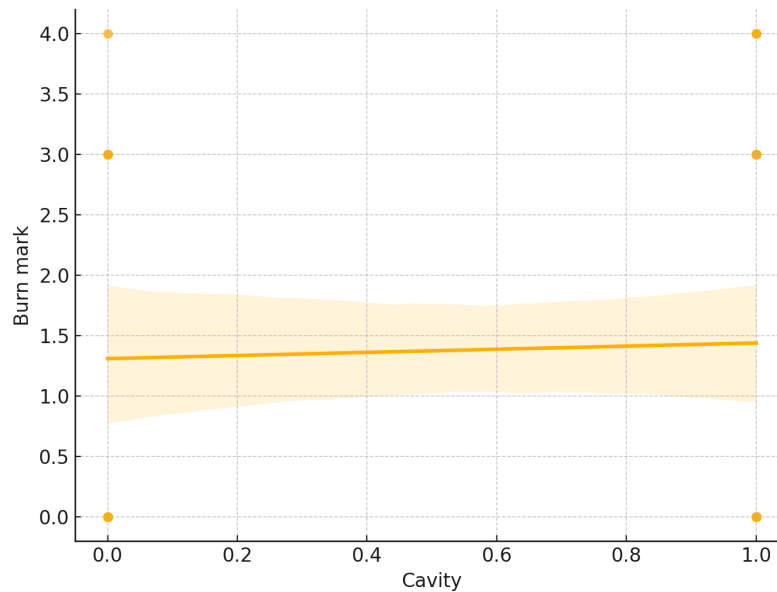


Figure 33 – Scatter plot of the cavity vs burns mark, correlation coefficient of 0.04 and a p-value of 0.736

4.3.5 Picrosirius red staining

Histological analysis was based on non- consecutive review of the slides selected after first round of review. A total of 22 slides were stained for picrosirius red. The slides are a mixture of perfused and non-perfused samples.

Descriptive histology

The same paraffin fixed samples were stained with picrosirius red to highlight the extracellular collagen matrix of the porcine liver. Picrosirius red stain highlights the natural birefringence of collagen fibres when exposed to polarized light, thus allowing for better visualisation of the collagen matrix than H&E staining. In perfused samples (**Figure 34a**), there is a disruption of the collagen matrix in the core of the lesion with a sharp demarcation at the edge of lesion. The collagen matrix is well persevered in the periphery of the lesion. In the centre of the lesion where a collagen septum traverses there seems to be a distortion of the collagen fibres (**Figure 35**). Vessels near the lesion, but not involved in the edge or centre, seems to be intact but those in the core of the lesion or at the edge are damaged due to the force of sonication (**Figure 35 & Figure 36**). Portal structures in the vicinity of the lesion or involved in the lesion are not preserved (**Figure 36 & Figure 38**).

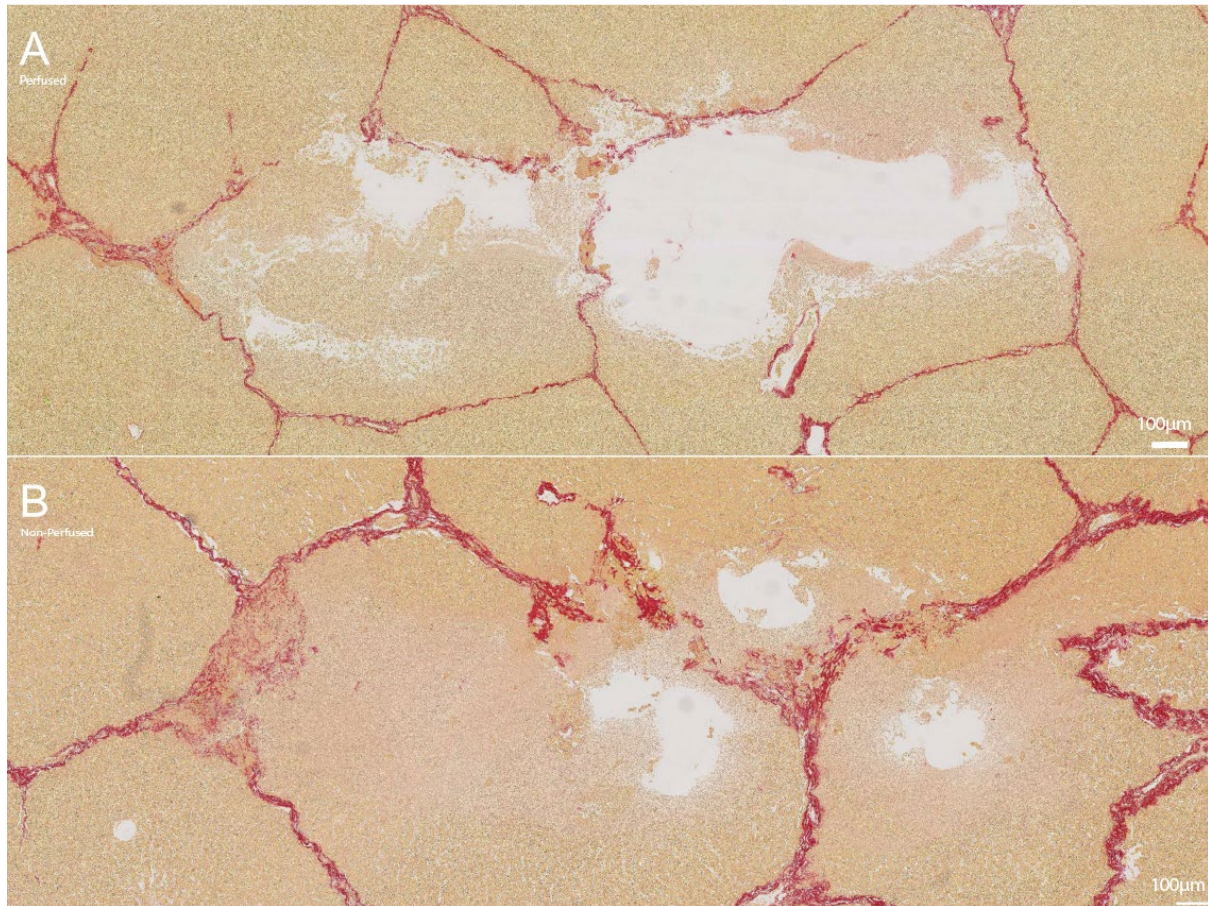


Figure 34 – Picrosirius red staining of the perfused (10x zoom) (A) and non-perfused (20x zoom) (B) group. The picrosirius red stain highlights the natural birefringence of collagen fibres when exposed to polarized light and hence they appear as bright red in the field. The collagen matrix of the septa in the perfused group seems preserved consistent with the sharp demarcation noted on the H&E stains. The non-perfused samples show more disorganization of the collagen following sonication. (50 pulse durations at 1% duty cycle)

In the non-perfused group similar distortion of the collagen septum is noted in the lesion territory (**Figure 34b**). The histotripsy sonication seems to affect the perfused and non-perfused in a similar way however, the extent of injury is difficult to assess and quantify just by H&E and picrosirius red staining. On first observation the extent of injury seems to be more in the collagen fibres of the non-perfused group compared to the perfused samples. Again, this does not reflect true extent as the picrosirius red staining relies on natural birefringence of collagen fibres and to reflect this better we have analysed some of the samples under polarised light microscopy.

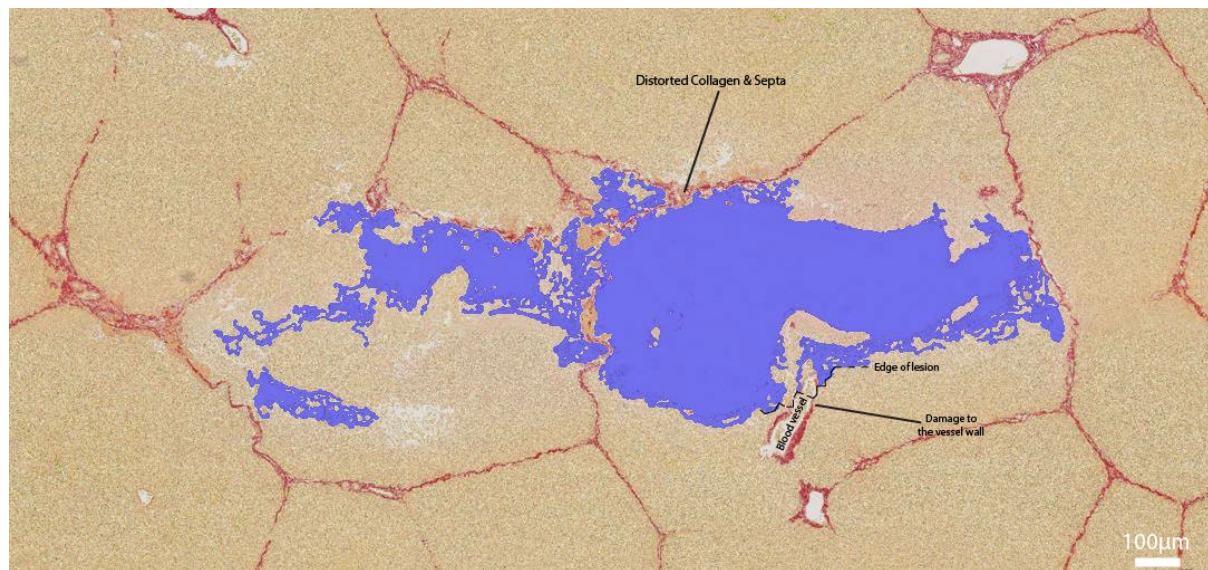


Figure 35 – This is a perfused sample, and the blue area represents the lesion and where sonication has resulted in tissue disruption. The collagen matrix that falls in the centre of the lesion is disorganised compared to the collagen of the same septa along its length suggesting damage to the ECM. Vessels and portal structures involved in the lesion or in the edge are damaged by the force of sonication. (50p at 1% duty cycle)

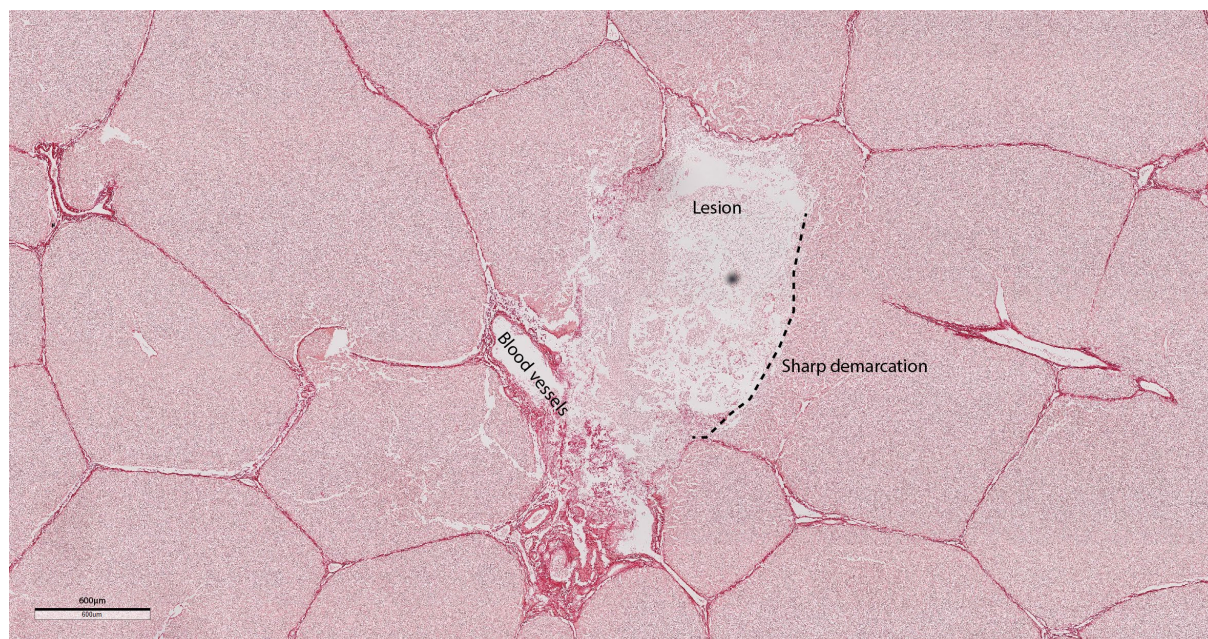


Figure 36 – 100p at 1% duty cycle sonication of a perfused porcine liver with sharp demarcation and disruption to blood vessels P: pulse duration

4.3.6 Polarised Sirius red staining

Descriptive histology (based on 22 samples)

To assess properly for collagen distortion the picrosirius red staining needs to be polarised through special polarisation filter (393). Further assessment of perfused versus non-perfused group was made through polarisation and quantitative dot assessment of affected area versus non-affected area by assessing the polarised intensity of the slides. On the basis that the birefringence intensity of the polarised slides are proportional to the orientation of the collagen fibres; the more intense areas are reflective of intact collagen and the less intense or lack of it is assumed to be due to disrupted collagen. In the perfused group the sharp demarcation is again observed in the polarised samples. There is no significant loss of bright birefringence at the edge or just close to the edge (**Figure 37A**). Where the collagen septum falls in the centre or is involved in the lesion there is loss of brightness indicating possible damage to the collagen matrix. On reverting the brightfield polarisation the brightness is retained which would make the damage to the collagen scaffold less likely (**Figure 37B**).

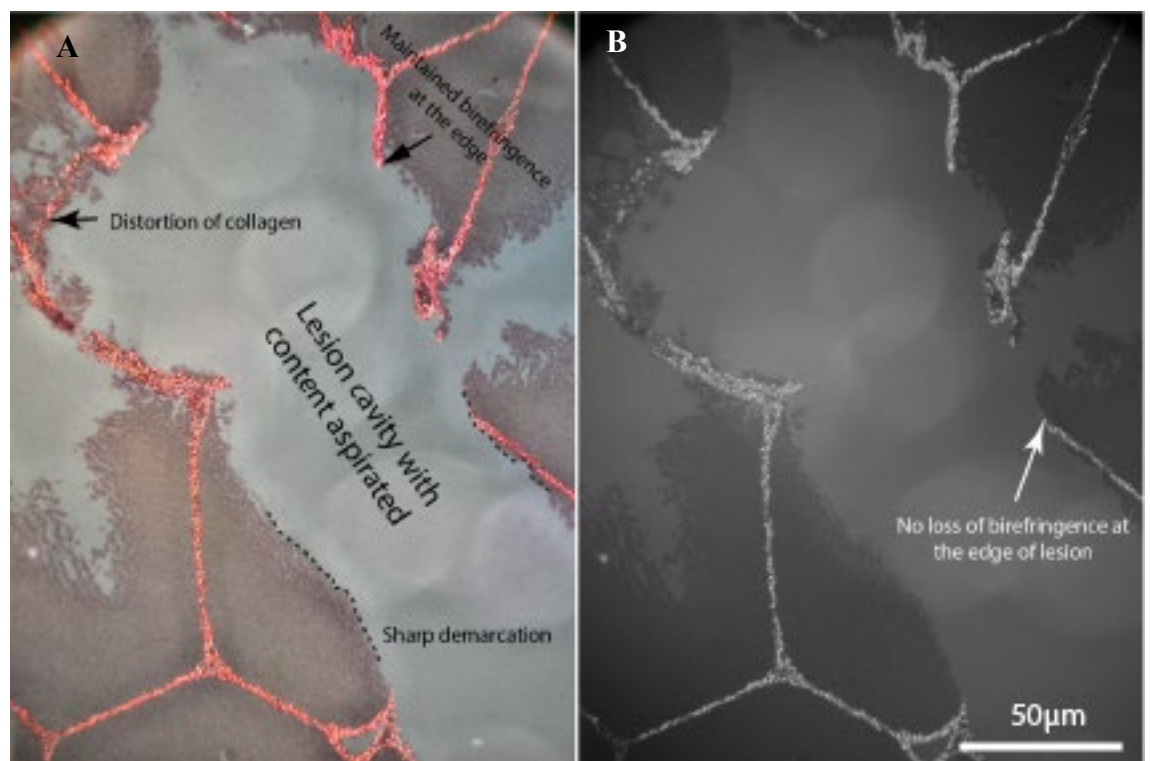


Figure 37 – (Left) Polarised perfused samples with show the natural birefringence of collagen fibres. Where this is assumed distortion, the birefringence would appear less, and the fibres would appear less bright. The inverted birefringence is used for quantitative analysis of brightness of places of interest along the collagen

septum. (Right) inverted bright field to black and white for quantitative dot analysis of brightness. (50p at 1% duty cycle)

Interestingly, the non-perfused samples show more collagen disruption on polarised light microscopy (**Figure 38A**). The collagen matrix is more disorganised and scatted in the area of sonication compared to perfused samples. There is less brightness on brightfield microscopy. This is better demonstrated on the reverting the brightfield to black & white images (**Figure 38B**). The areas with damage to the collagen matrix are not lighting up due to disorganisation and lack of brightfield on polarisation. More so, the greater area of disruption is in the centre of the lesion with smaller and lesser areas towards the periphery of the lesion. Although these results should be interpreted with much care, lack of brightness is thought to be indicative of the collagen damage following sonication. In **Figure 38**, even though there is greater disruption is noted there are areas that show some brightness in the core of the lesion.

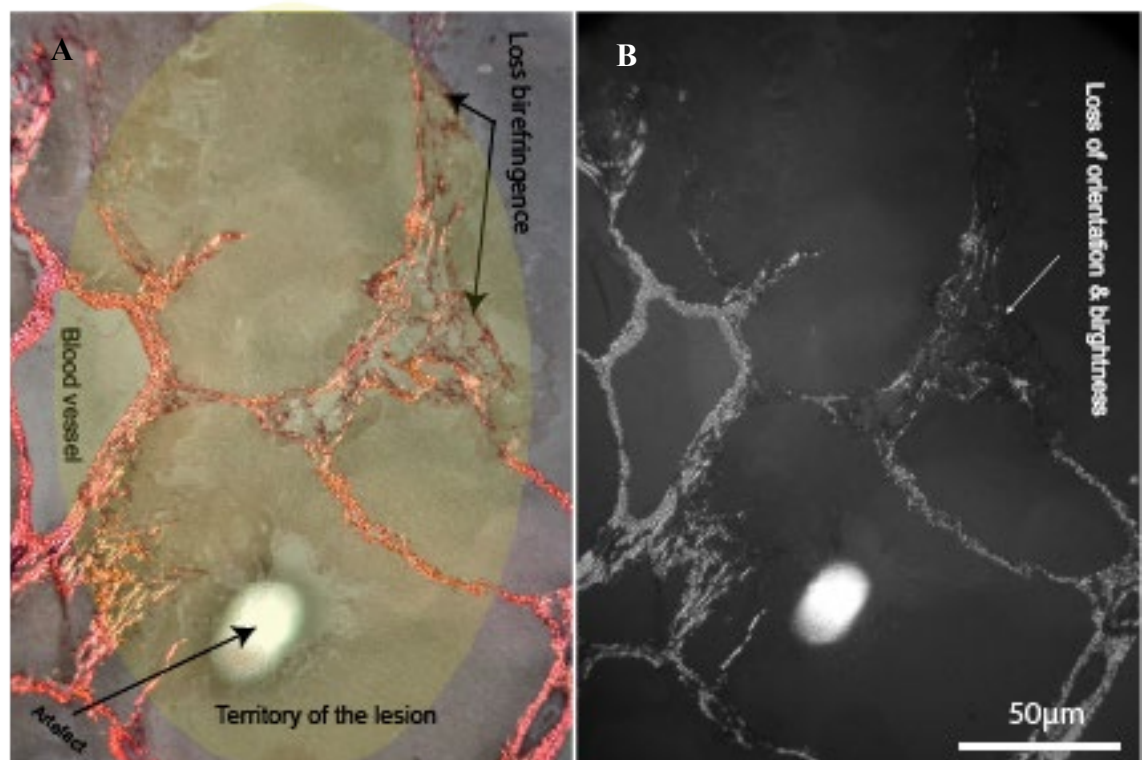


Figure 38 – non-perfused sample (sonicated at 50p). Greater degree of the collagen disruption is noted I the centre of the lesion. This is better demonstrated on the black & white image of the brightfield. Lack of brightness is thought to be indicative of damage to the collagen scaffold.

4.3.7 Quantitative analysis and variability

Table of samples analysed

To assess extent of the collagen disruption further we carried out quantitative analysis of the birefringence density of perfused and non-perfused samples. The density assessment is an estimate of the collagen density in the area of the lesion as well as the normal tissue adjacent to the lesion. In perfused samples a quantitative dot assessment of the mean density of birefringence at the edge of the lesion is compared with a normal area. The treated edge does not show any significant difference ($P = 0.2632$) in mean distribution of the collagen, thus confirming the sharp demarcation of the sonicated edge (**Figure 39**).

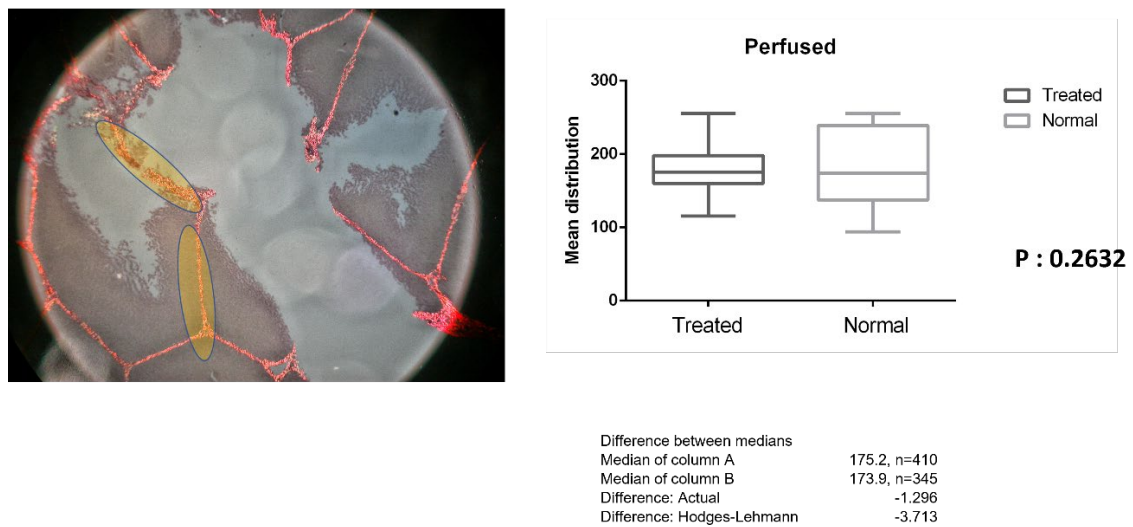


Figure 39 – Quantitative analysis of birefringence of the Sirius red staining following reversion to B&W images. The treated area is the edge of the BH lesion based on appearance under microscope and normal area that comparison is made is a well away from the treated lesion.

A similar assessment was carried for non-perfused samples (**Figure 40**). A quantitative mean density assessment of affected area versus non-affected area revealed a greater degree of collagen disruption ($P < 0.0001$).

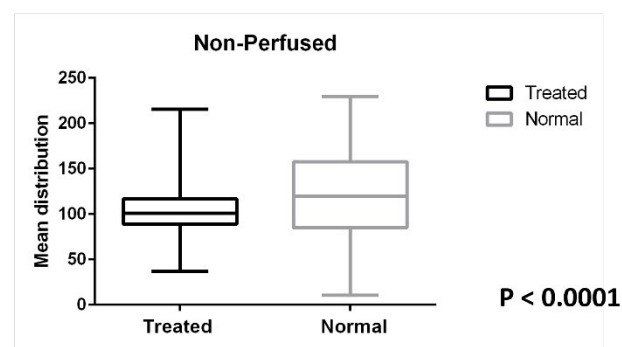


Figure 40 – Quantitative analysis of the collagen density in non-perfused samples. The loss of collagen density as reflected by birefringence density is significant in the treated area vs non-treated area.

On comparison of the affected area of the perfused samples with non-perfused samples, the mean distribution of the collagen density is significantly lower in the perfused group (Figure 41). Thus, indicating the collagen matrix is well preserved in the perfused group following sonication.

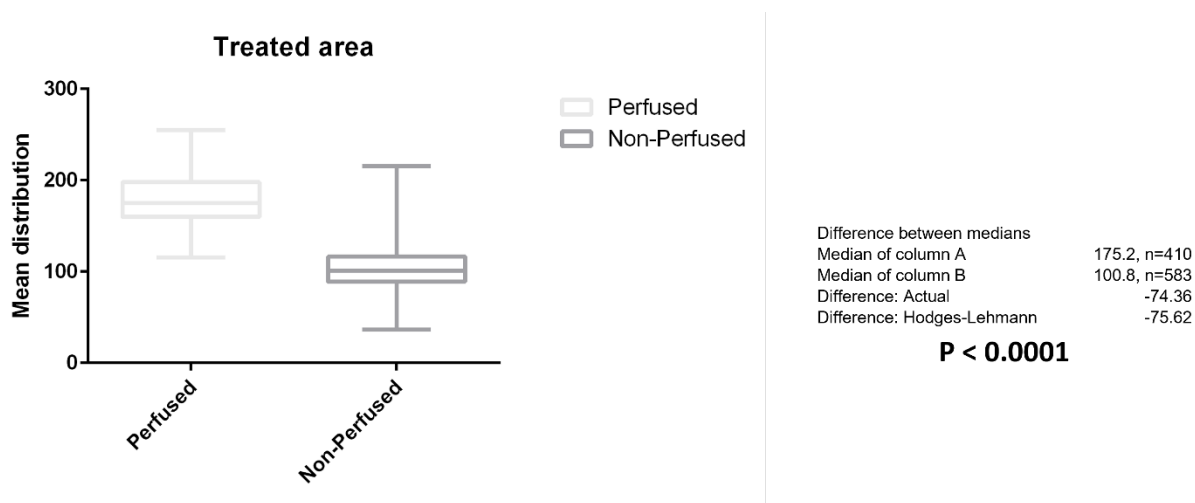


Figure 41 – Comparison of perfused vs non-perfused treated areas' collagen or birefringent mean density. The difference is significant with more preservation of the collagen matrix in the perfused samples.

Lastly, we analysed if the energy from sonication had dissipated into the periphery of the lesion seen macroscopically and thus resulting in a peripheral zone of tissue injury. This was assessed by arbitrarily dividing the tissue from edge to periphery into different zones

(Figure 42). An assessment of the birefringence of the perfused sample immediate zone, transition zone and peripheral zone revealed no significant difference.

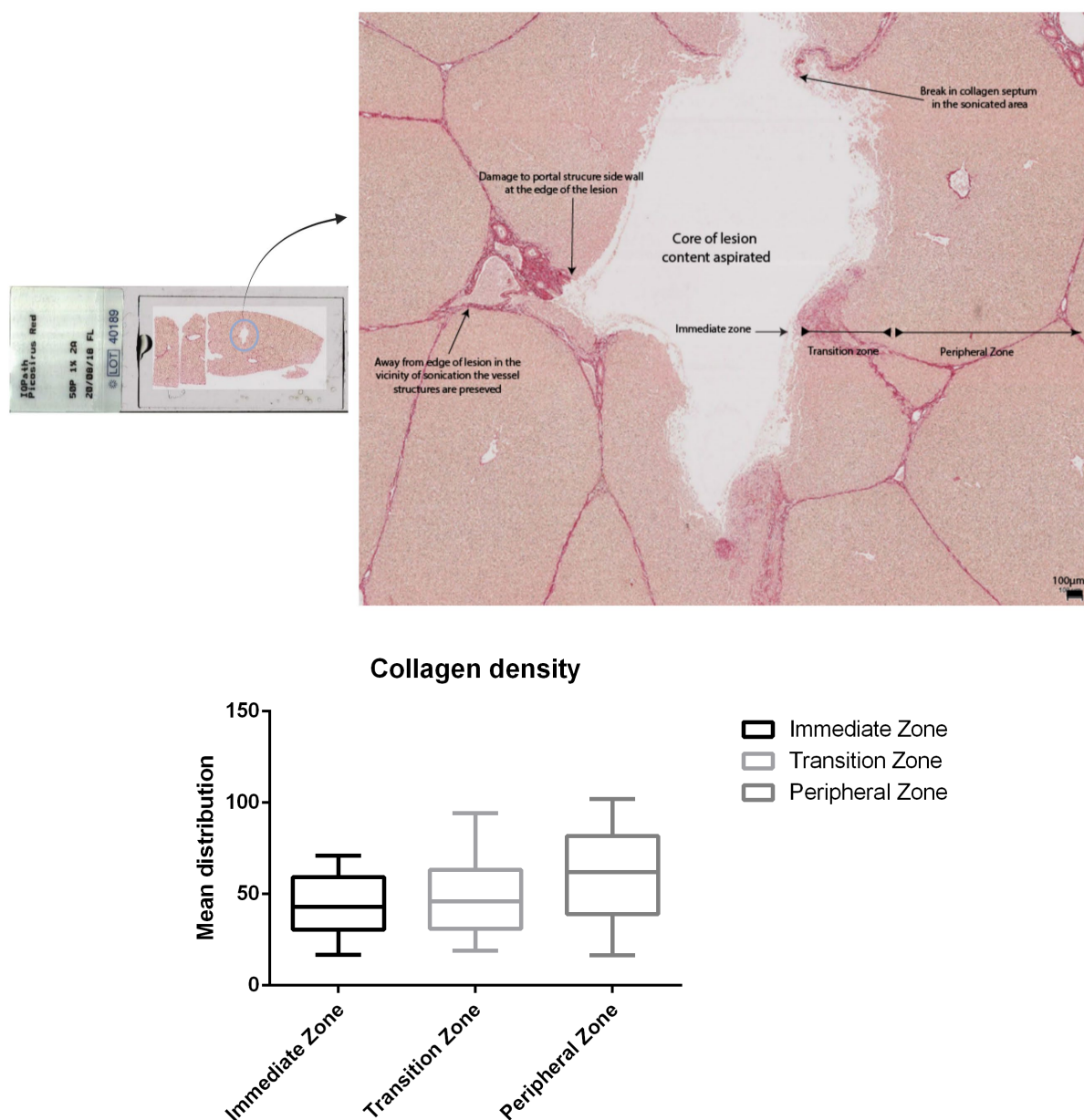


Figure 42 – Example of 50p lesion in a perfused sample with marked areas of energy dissipation and collagen disruption in graded zones. Small portal structures at the vicinity of the lesion are subject to damage by sonication whereas the structures away from the edge of the lesion seems to be well preserved.

4.3.8 Reticulin staining.

To further assess the collagen matrix integrity and demonstrated ECM, we performed reticulin staining and compared this with the same samples which had been stained with Sirius red. The reticulin stains in the perfused samples revealed complete destruction of

the collagen and ECM in the core of the lesion (**Figure 43**). The normal parenchyma was separated from the core of the lesion with a sharp demarcation. This set of result confirms the ECM disruption within the core of the lesion.

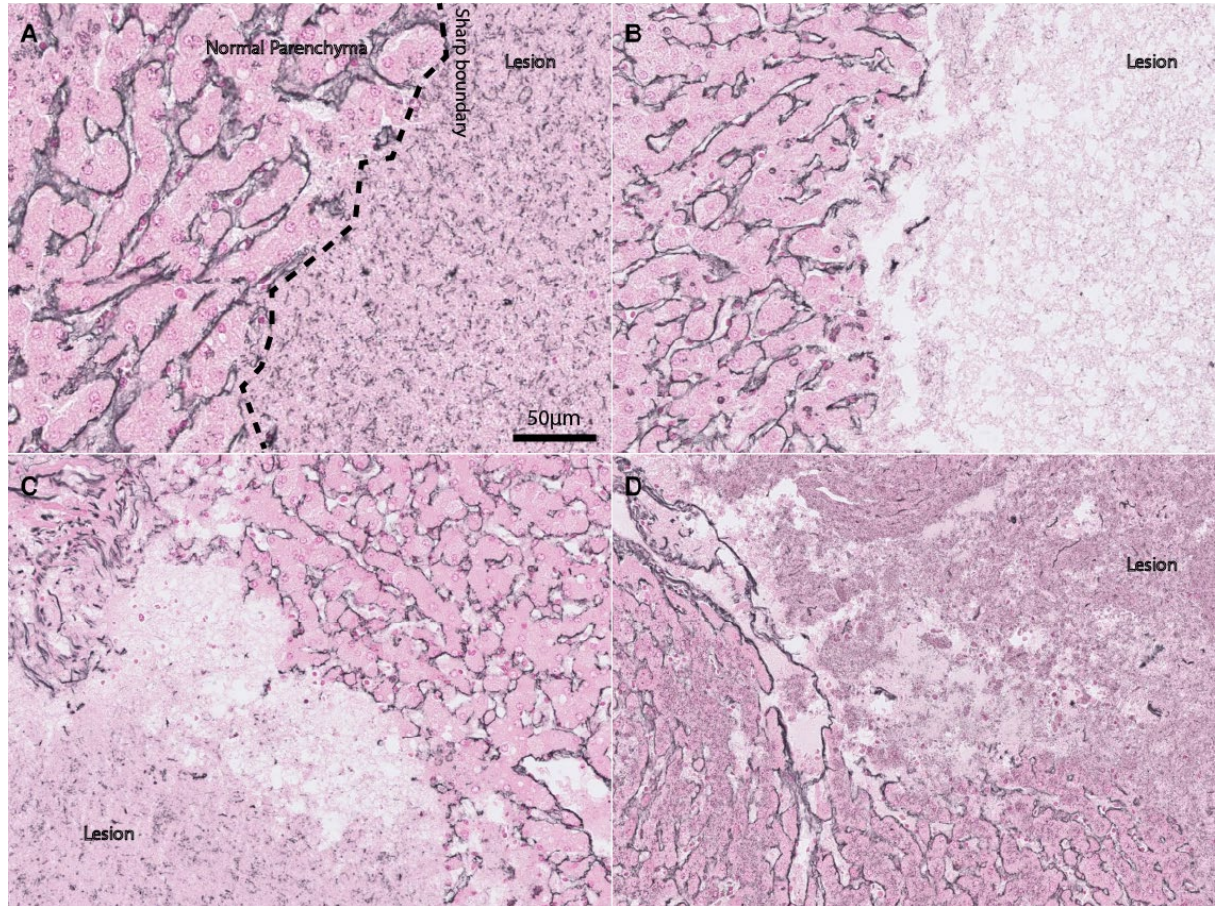


Figure 43 – Reticulin stains of the perfused samples (sonicated at 50p): reveal sharp demarcation between the normal liver and lesion. In addition, there is a loss of ECM in the core of the lesion with cellular debris remaining in the core. These samples are not aspirated and therefore have their core content still in situ. A) Demonstrates a lesion and normal parenchyma with sharp boundary; (B) demonstrate within the lesion there is no reticulin stain and the core of the lesion has ECM disruption. (C-D) Also demonstrate disruption of the reticulin fibres within the lesion.

4.4 Discussion

Histotripsy is a non-invasive therapeutic technique that involves using high-intensity ultrasound waves to liquefy or destroy targeted tissues with minimal damage to surrounding tissues (255). Histotripsy has shown great potential in a variety of clinical applications. The claim that it can selectively preserve the ECM (394) while resulting in

parenchymal disintegration has grasped much attention mostly for its potential clinical applications (391, 395).

Calibration of BH algorithm and histological features of the lesion: In calibration of the histotripsy, we used different pulse duration with different tissues. These were used as a trial and error to assess the closest protocol for ex-vivo porcine livers. Based on previously published data we used a similar pulse duration for our experiments which would closely resemble what would be used in clinical settings. The pulse duration of 50 was deemed more suitable for these experiments as it resulted in less injury and was assumed to lead to tissue decellularization with preservation of the architecture. The simulation carried out by (Prof Saffari & Dr Gelat, as described in the methods section 3.4) describes the details of the histotripsy protocol that was used. This protocol was chosen because according to previous extensive work by the authors (348, 376, 377) and other groups (163, 360, 378) it leads to the production of a fully fractionated lesion in liver tissue with minimal thermal denaturation. It was one of our aims to examine this assertion with more advanced histological analysis.

The Perfusion Model Used and Its Relevance to Clinical BH: Perfusion was modeled using a controlled circuit to simulate physiological conditions, ensuring tissue hydration and mimicking clinical scenarios. Perfused tissues demonstrated improved ECM preservation and reduced thermal injury compared to non-perfused samples. Out of the 72 perfused samples analyzed in **Table 18**, 37 samples showed no burns injury and the rest had possible burns mark that was confluent with the cavity and the decellularized area. Although this was not uniformly demonstrated on H&E slides, only the polarized picrosirius red samples showed a slight degree of difference between the perfused vs non-

perfused samples. These results should be interpreted with much care. Lack of brightness is thought to be indicative of the collagen damage following sonication but it also related to the orientation of the collagen fibers so it may not necessarily reflect a true collagen disruption. Albeit this model aligns with the principles of clinical BH, where perfusion could act as a heat sink, dissipating energy and preventing excessive localized heating. Similar findings have been reported in chemical decellularization studies, where perfusion under oscillating pressures enhanced ECM preservation (396-398).

In recent experiments, Struecker and colleagues (398) demonstrated the effect of perfusion on decellularization. Using chemical decellularization protocol they used a pulsed pressure perfusion system and compared the effect of decellularization to the non-perfused group. The perfusion device used to generate these pressure conditions replicates intra-abdominal conditions during respiration to optimize micro-perfusion within livers and thus the homogeneity of the decellularization procedure (398). Compared to livers perfused without oscillating pressure conditions, livers perfused under oscillating pressure conditions exhibited a more uniform course of decellularization and contained less DNA which has been demonstrated in other animal experiments too (397, 398). Perfusion under oscillating pressure seems to preserve the ECM better than chemical decellularization alone (399). In the setting of histotripsy where the decellularization process relies purely on the effect of ultrasonic energy, the perfusion circuit may function to create a heat-sink effect (400). Although the effect of perfusion in the setting of histotripsy has not previously been studied, the theory is that by achieving vessel patency and an active flow the degree of thermal injury is reduced. This theory is negated by the fact that the order of histotripsy sonication is in order of milliseconds duration, and it does not raise the temperature significantly. In fact, Khokhlova et al (400) makes a note of this in comparison to thermal ablation techniques, boiling histotripsy is not affected by the

heat-sink effect of the major blood vessels and is capable of treating the immediately adjacent tissue due to its tissue selectivity. Albeit this claim has not been directly compared in the setting of perfused versus non-perfused tissues. Additionally, tissue perfusion can alter tissue elasticity and stiffness. Our study uniquely demonstrates that perfusion has influences over lesion clarity and ECM integrity, though this is not shown to be statistically significantly different between the two groups as demonstrated by the scatter plot (Figure 30). The observed differences in thermal injury and collagen preservation between perfused and non-perfused samples provide critical insights into optimizing BH parameters for clinical applications.

Method of Histological Assessment: Histological assessment was conducted using H&E and picrosirius red staining under polarized light as well as reticulin stains. H&E staining provided an overview of lesion dimensions and architecture, while picrosirius red highlighted collagen integrity and disorganization. Although effective for initial assessments, these methods had limitations in quantifying collagen disruption, underscoring the need for complementary techniques such as Masson's trichrome staining or second harmonic generation (SHG) imaging.

To further evaluate this, we carried out a series of experiments looking at the effect of histotripsy in perfused versus non-perfused samples to objectively, through histological analysis demonstrate any difference. The ECM of the liver consists of collagen matrix that harbors hepatocytes and other cells in an organized fashion. Collagen, being the most abundant protein in vertebrates, forms the structural network of the ECM in biological tissues (401). It's worth noting, normal human livers contain roughly equal amounts of Type I, Type III, and basement membrane collagens; with Type III collagen predominance (402). In cirrhotic livers on the other hand, regardless of etiology, all types

of collagens are elevated with a predominance of Type I collagen (402-404). Collagen organization parameters, specifically fiber orientation and alignment, have been shown repeatedly to play an important role in the progression of several pathologies including metastasis of cancer (405-407). Pig liver has some similarity to the human liver in its architecture and lobule arrangements. However, differences exist in the collagen layout and orientation. In a study examining the liver three dimensional units in porcine liver, it was shown that collagen fibers were laid along the plane in which the portal venous branches and the hepatic venous radicles were distributed (408). They generated trabecula or septa of 10-25 μm thickness that delineated histologic lobules into irregular polygonal patches. These lobules measured 0.7-1.2 mm in diameter (408). This may be of relevance in the context of energy dissipation and heat deposition in boiling histotripsy. The proximity of the collagen trabeculae to the portal vessels may act as a heat sink effect and reduce the possibility of any thermal injury. This may explain the lack of any difference in the H&E stains we have carried in the perfused and non-perfused samples.

Our study shows disruption of the parenchyma and the ECM architecture in the core of the lesion. The extent of this requires more specialist stains to evaluate further.

Histological findings and alternative means of assessment: Although H&E stain is not the best stain to visual thermal injury it provides some insight about overall architecture of the lesion and parenchyma following sonication. There was no noticeable difference in the degree of burns injury in the perfused vs non-perfused group using H&E stains (as demonstrated by the scatter plot). H&E is not sensitive to subtle changes in collagen integrity or ECM composition, therefore, making it less effective for evaluating thermal or mechanical damage. Although there is no specific histological marker of thermal injury to assess the extent of thermal injury, perhaps the best way to visualize damage would be

to assess collagen damage. Even on picrosirius red stain the observed difference is not readily visible and requires birefringence. Although, this method highlights collagen fibres and allows differentiation between types based on birefringence it has significant limitations too. The observed difference noted on the birefringence slides needs to be interpreted with care as results can be influenced by sample orientation and thickness, leading to variability (409). Additionally, it does not provide detailed information about glycosaminoglycans or other ECM components.

Tissue collagen fibers can be seen using several ways. Some of these methods are only applicable to thin-sectioned histological samples, such as (1) Stains: picrosirius red (PSR), Movat's pentachrome, and Masson's trichrome; (2) Antibody detection; (3) Polarized microscopy, which enhances PSR-stained tissue visualization; and (4) SHG imaging (401, 410-413). Electron microscopy, atomic force microscopy, and scanning electron microscopy can visualize collagen, but their small fields of view, technical sample preparation, and high costs limit their use to non-routine, highly specialized applications (401).

Amongst these methods, polarization light microscopy has proven an effective method in qualitative and quantitative histological examination of the collagen (410). Particularly the birefringence of collagen is utilized to evaluate collagen organization and microstructure; the decomposition of collagen in pathologies (i.e. histotripsy related lesions) leads to disorganization and a loss of polarization sensitivity (413). In our picrosirius red staining we have demonstrated some difference in the extent of collagen injury when comparing perfused vs non-perfused. A noticeable difference which was significantly different between the collagen in the treated area ($P < 0.0001$). These results, however, should be interpreted with caution as there are several limitations to the polarization light microscopy (mentioned above), particularly linear polarization.

Although strong birefringence is normally suggestive of normal organized collagen (particularly thick collagen type I), the weaker birefringence is normally indicative of abnormal collagen orientation or presence of thinner fibers such as collagen type III (414). Different collagen fiber physical aggregation, polymerization, and three-dimensional organization can cause different interference colours and birefringence intensities (410, 414). This limitation is further evident when birefringent materials viewed with linearly polarized light look bright unless their optic axis is parallel to the transmission axis of either polarizing filter (410). In tissues with wavy fibers, some section of each fiber may be aligned parallel to the filters' transmission axis and appear dark, thus underestimating collagen content (410). This is reflected by the way the tissue is fixed and cut in preparation for the staining. When the histotripsy lesion is not captured or sliced in the center of lesion then the fibers may appear to be in different orientation and hence give an appearance of different intensity birefringence.

The addition of the reticulin stain only confirms disruption to the ECM in the treated area. Thus, it can be used as limited proof that in the sonicated area there is evidence of the ECM disruption. However, this is also limited by the fact that it primarily targets type III collagen and does not effectively stain other ECM components such as type I collagen, glycoproteins, or glycosaminoglycans. This limits its ability to provide a comprehensive view of the ECM architecture. It predominantly provides qualitative information and for quantitative analysis it requires further stains.

Quantitation of collagen: Although the quantitative analysis used here to assess for intensity of birefringence has been used previously (410, 411, 414, 415), in our study due to the limitations mentioned above about picrosirius red staining and polarization we can't rely on the quantitative results produced as it cannot be consistently reproduced. The difficulty in the consistency is probably since the histological examination was not done

in serial sectioning. Especially when the H&E and the non-polarized picrosirius red staining do not demonstrate any significant difference between the perfused and non-perfused group.

Conclusions

Although we have not been able to demonstrate a clear difference between the histological appearance of the perfused versus the non-perfused group, we have demonstrated that morphologically the lesions to some extent have similar appearance with sharp demarcations at the border of the lesion and the normal tissue. Our results are not suggestive of any thermal injury, either in the perfused or non-perfused group. The order of sonication is too short for thermal injury to ensue. Perhaps to evaluate collagen injury further, it requires additional histological analysis with stains such as Masson's trichrome. Within the core of the lesion the collagen fibers are damaged by the force of sonication with our protocol. This is important since regeneration relies on a healthy ECM scaffold (416). However, in our initial experiments we have not demonstrated preservation of the ECM and rather a sharp snap of the collagen fibers at the boundaries of the lesion. To further evaluate the efficacy of the histotripsy for creation of the lesions we need to further assess the lesions created in the perfused samples and to assess their core content along with histological assessment of ECM. The next step would be to further evaluate the perfused samples to create a 3D reconstruct of the lesion.

Chapter 5 Qualitative histological analysis of liver response to ultrasound histotripsy in ex-vivo perfused porcine liver including 3D histological reconstruction.

5.1 Introduction

Ultrasound histotripsy is a non-invasive procedure used to mechanically fractionate and liquefy soft tissue without causing thermal damage. Different ultrasound pulsing protocols can be used to cause mechanical tissue dissociation. The method employed in this study is referred to as boiling histotripsy (BH), where a series of millisecond-long ultrasound pulses are delivered to the treatment site. The nonlinear propagation of ultrasound waves results in the formation of shockwaves at the beam focus. High-amplitude shocks cause rapid and transient tissue heating, resulting in the nucleation of a boiling bubble (378, 417-419). The interaction of incident shocks with the boiling bubble causes tissue disruption and liquefaction without significant thermal injury to adjacent tissue because the millisecond pulses are so short lived that thermal conduction does not occur. The efficacy of mechanical fractionation, the ablation rate, and the reliability of boiling histotripsy depend on the correct choice of ultrasound frequency, focal peak pressure levels, pulse duration, the pulse duty cycle, and the number of BH pulses. The interplay between these parameters has been studied by many groups and extensively reported (338, 420). Possible applications of BH include the ablation of solid tumours (421-424), local drug delivery (425, 426), and cavity formation for direct intrahepatic cell delivery for cell therapy (348). We have carried out a series of studies using different US histotripsy protocols to create a nidus in the liver for transplantation of stem cell-derived 3D hepatocytes for the treatment of congenital and acquired liver disease.

The literature on the histological effects of histotripsy on liver tissue is limited and the results may vary with the experimental model used (408). There have been prior experiments involving bovine liver (378, 427-430). Simon et al. (428), for example, investigated how changes in static pressure and tissue wetness were shown to affect BH

injury. Increasing static pressure resulted in the formation of a mound on the cut surface of liver slices in contrast to the cavity generated at atmospheric pressure. The authors also applied their protocol to an in vivo porcine model and showed that wetting the liver surface targeted by BH with saline or surfactant increased tissue atomization and caused the rupture of the liver capsule in some instances. In experiments by Vlaisavljevich et al. (429), thermal pre-treatment affected liver stiffness and its susceptibility to histotripsy. Variations in the intensity of the trichrome stain (used to differentiate fine collagen fibers from other tissues, especially in the liver) depending on pre-treatment temperature were used as indicators of changes in collagen density. Macoskey et al. (430) examined the effect of different histotripsy dosages on collagen I and collagen III fibers on agarose-embedded 4 cm cube bovine liver samples using histochemical stains (Gordon and Sweet and trichrome stains) and showed that the cellular component was destroyed earlier than the extracellular matrix.

Other experiments have been carried out on pig liver. Cavitation cloud histotripsy on ex vivo and in vivo livers (221, 366, 429) caused complete fractionation of hepatic parenchyma and sharp lesional boundaries but no injury to large hepatic vessels or bile ducts. In a detailed histological examination of livers treated with BH, Wang et al. (163) described variations in tissue damage according to duty cycle. The authors assessed collagen fibres, vessels, bile ducts, and cellular function by NADH-diaphorase staining, protein content, and cellular components by electron microscopy on samples removed from the lesional area. An increase in duty cycles resulted in the formation of a macroscopically visible blanched border of up to 3 mm in width, which corresponded, microscopically, to a perilesional area of partial thermal denaturation with loss of NADH-diaphorase stain, an increased amount of intralesional nuclear debris, and the formation of heat-fixed eosinophilic tissue as the result of thermal coagulation. The damage to the

connective tissue framework was visible macroscopically and corresponded to microscopic changes in the configuration of collagen fibres, from fibrillary at lower duty cycles to globular at higher duty cycles, along with a concomitant reduction in the number of small-calibre vessels and bile ducts.

It's important to note, histotripsy responses have varied between publications and models possibly related to the treatment protocol (see section 2.6.1). Different animals have different degrees of collagen expression in the liver. Porcine liver has close similarity to the human liver in terms of architecture and collagen make up (431). Hence it makes a more reliable tissue to test histotripsy parameters and achieve clinically relevant data. More so, through perfusion circuit the porcine liver can provide data that is as close to the human physiological parameters during sonication.

In this chapter we provide a detailed description of the histological changes we have observed at 15 BH sites and the surrounding tissue. We have also carried out, for the first time, 3D reconstructions of two additional BH sites.

5.2 Material & Methods

The overall method is described in section 3.1 of methods chapter. Five pig livers were obtained fresh from the abattoir. Livers were obtained within 10 min of the termination, which was the period of liver warm ischemia. Using organ transplant retrieval techniques, livers were immediately dissected from the complete set of abdominal viscera, with isolation of the hepatic artery, portal vein, and bile duct (en bloc retrieval of the pig's abdominal viscera, followed by on-table retrieval of liver and its subsequent on-table flush). The isolation of the liver from the rest of the viscera took a total of 2 min. At the abattoir, back table perfusion and flush of the livers were achieved following retrieval with 1 L of heparin saline solution via the portal vein. Flushing was conducted as fast as

possible to drain the liver of any remaining blood (the flush would typically be complete in 10–15 min following cannulation of the portal vein). The livers were packed for transport from the abattoir using static cold storage in preservation with normal saline and stored in crushed ice containers for transport at an average temperature of 5 °C. Upon the arrival of the organ to the laboratory, the livers were placed in an organ bath lying over an ultrasound absorbing layer. The organ was re-perfused in two stages using an organ perfusion circuit with a pump. First, the liver was perfused via the main portal vein with a litre of Soltran organ preservation solution (Baxter Healthcare, UK), to allow the core temperature of the liver to slowly reach room temperature (ranging from 24 to 30 °C) before the histotripsy was performed. During the histotripsy period, the organ was further perfused with Soltran organ preservation solution to maintain viability. Perfusion occurred via the portal vein, with the perfusate draining via the vena cava into an organ bath. The perfusate was not recycled. During the perfusion, the livers would be placed in an organ bath lying over an ultrasound absorbing layer. The perfusion solution was delivered using a Baxter perfusion pump™ (Baxter Healthcare, UK) to achieve a constant flow rate of 350 mL/h, ensuring vessel patency before the histotripsy lesions were created. The setup of the histotripsy system is outlined below. The US transducer was applied to random positions (total sonication time per lesion was 50 s) on the perfused liver, and focal lesions could be identified by puckering of the capsule of the liver at the histotripsy site. Locations for histotripsy were chosen to include both central and peripheral portions of each liver. The depth of the lesion was estimated to be 0.5 cm below the liver capsule. Given that we used the same transducer, the depth was assumed to remain the same for every lesion. A total of 17 BH lesions were created over 5 liver and submitted for histological examination.

5.2.1 Histotripsy set-up

Histotripsy set up is described in section 3.2 - 3.4 of methods.

5.2.2 Tissue sampling

After the application of BH the lesional site was resected and bisected using a surgical blade, to reveal the lesional site. Resection refers to an excision biopsy with a surgical blade with an approximate circumferential margin of 1cm from the core lesion or its surface landmark the liver capsule dimple; Bisection refers to the slicing of the resected sample in half, cutting through the middle and therefore dividing the lesion into two halves to gain access to the core content of the lesion. A 20µm single-channel gauge pipette was used to aspirate the cavity content once the lesion had been bisected and the aspirate used for a separate study., Care was taken to minimise traumatic damage to the tissue.

Lesions would only be aspirated if the cavity content was liquid. For a small number due to proximity to small vessels, as soon as the cavity was sliced open the content was washed away due to puncture of the vessels at the site and perfusate leaking through the vessel. These lesions were not aspirated. Both sides of the lesion were then placed immediately into a single formalin-filled container and submitted for paraffin embedding according to standard procedures.

5.2.3 H&E and histochemical stains

See section 3.7

5.2.4 3D reconstruction

See section 3.8 images displayed here

Two additional histotripsy specimens were removed intact (not bisected or aspirated) and were entirely sectioned at 4 μm into 368 and 408 serial sections, which were all stained with H&E and SR respectively. In the first sample the lesion was identified in sections 199 to 228 (cumulative section thickness of 116 μm). In the second specimen minute lesional sites were identified in the full range of serial sections (1-408). The lesional serial sections were used for 3D reconstruction of the histotripsy sites using the specifically designed method illustrated in **Figure 44** and detailed below.

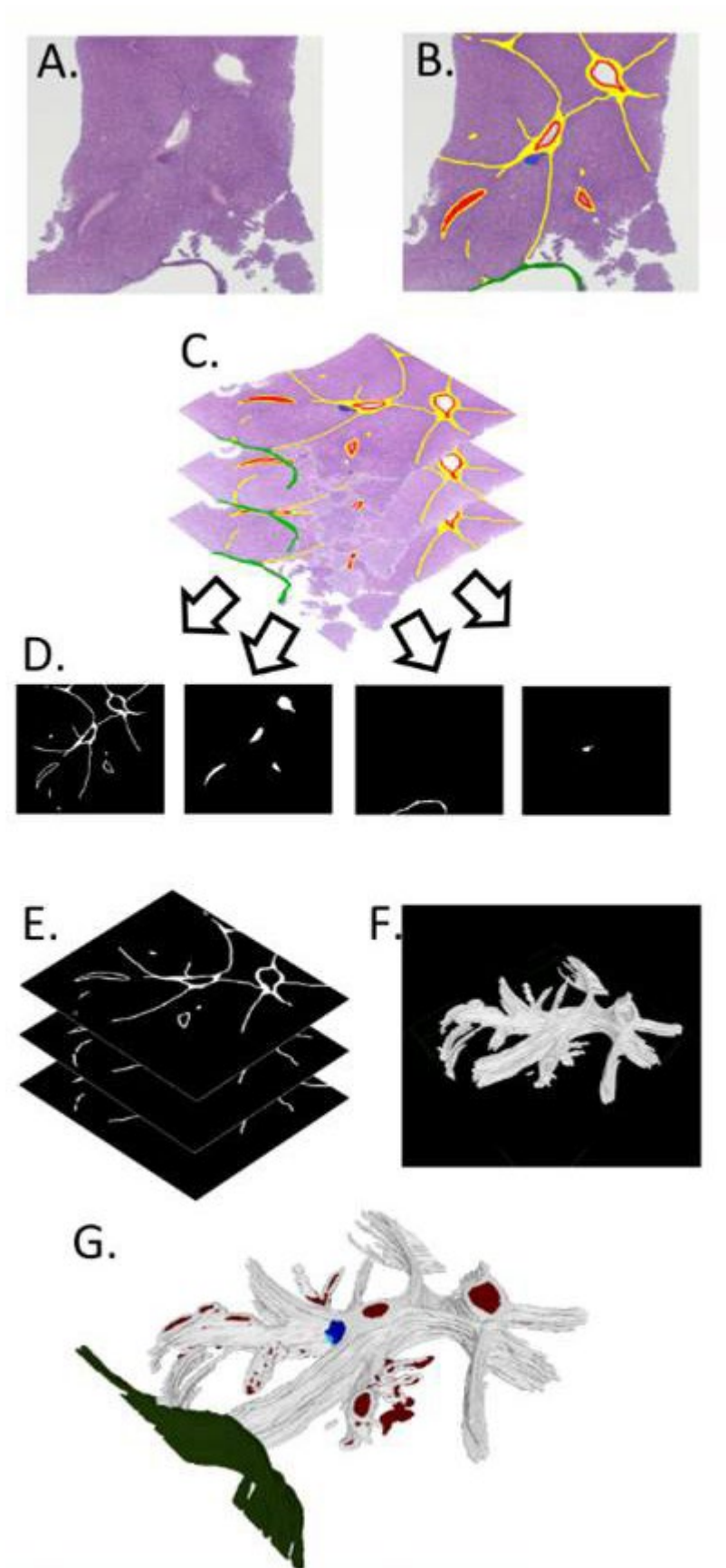


Figure 44 - Three-dimensional reconstruction steps from serial sections and image acquisition (A), identification of structures of interest (B), registered images (C), visualization of two-dimensional binary matrices (D), three-dimensional matrix formation (E), creation of a mesh over the voxels (F), and final three-dimensional mesh visualization (G).

Sectioning: Serial sections of formalin-fixed paraffin-embedded (FFPE) liver were cut at 4 μ m and any sections lost or missed were noted at the time of sectioning.

Images: The tissue was then stained with H&E in the first model and SR for the second and slides were imaged using a Zeiss AxioCam ICc5 and Axiovision v2.8.1 (Zeiss, Oberkochen, Germany) and images saved in lossless TIFF format (**Figure 44A**). This was done to demonstrate the parenchyma and the tract along with the lesion in different stains so then it can be superimposed.

Mark-up: Each image was marked up using software that allows the altering of drawn pixels to a single RGB colour code (e.g. Microsoft Paint, Microsoft Corporation, Redmond, Washington, USA). Many image editing software packages can be used for this purpose however it is important to use a tool that allows editing the image so that the change to any set pixel is to that of a set RGB colour value and all changed pixels are of that value. Many tools will feather or blend the edges of the marked area, and this will cause problems later on. This was used to define areas of interest such as portal tracts, capsule or lesions (**Figure 44B**) and the structures modelled in the final 3D reconstruction. Each RGB colour code defined an aspect of the final 3D model, e.g. red for blood vessels, green for capsule, blue for lesion. A saturated blue (RGB, 0,0,255) rather than one like that of haematoxylin was used. Critical to this step was the use of lossless image formats as lossy formats, such as .jpeg, can cause image artefacts and loss of colour fidelity reducing the accuracy of the model. In essence each image slice has been hand segmented according to the prevalent tissue morphology.

Registration: The images were registered using a custom MATLAB (The Mathworks, Natick, Massachusetts, USA) script. This script allows two images of serial sections to overlay each other and the alpha (transparency of the images) to be adjusted to visualise both images at once. Distinct features such as the liver capsule and the edge of the tissue can be used to align each image over one another and when a best fit is found the images are then automatically cropped and saved, (**Figure 44C**) forming a stack of registered images.

Extracting binary matrices: From the stack of registered images, we created a stack on binary matrices for each different type of feature i.e. Each colour used in the Mark-up step. A 2D binary matrix is an image composed of solely 1 and 0s and can be visualised as a black and white image with no greyscale between. To create the binary matrix from the markup images we used a second custom MATLAB (The Mathworks, Natick, Massachusetts, USA) script in which a colour range is chosen and the pixels within the range are given a 1, and those without a 0, thus picking out a particular marked up feature. For example, the range chosen for the saturated blue mentioned in ‘Mark-up’ would be inclusive of only the pixels with a RGB value of 0,0,255, respectively. The range can be widened to pick out tissue features such as all the collagen in a SR-stained section if the stain is of sufficient quality. Each stack of 2D binary matrices when combined as a stack into a 3D binary matrix forms a 3D representation of each marked up feature.

3D matrix: The segmented data of each morphological feature was subsequently rendered in 3D using an in-house developed MATLAB-script (The Mathworks, Massachusetts , USA). From this 3D binary matrix of voxels a triangle mesh was formed on the outer surface of the voxels and the mesh was saved as a Standard Triangle Language (.stl) file (**Figure 44F**– collagen). A separate .stl file was created for each feature, e.g. blood vessels, capsule, lesion.

Mesh visualization: .stl files are a commonly used file format for 3D meshes. The images in **Figure 44F** are from Meshlab (Cignoni et al 2008) open-source software. Meshlab is an open-source software created and maintained by the Visual Computing Lab, part of the ISTR-CNR in Pisa, Italy, www.meshlab.net. Multiple meshes, one for each feature were loaded into the 3D space retaining their initial relative positions to one another and textured to create a final 3D model of the tissue (**Figure 44G**).

5.3 Results

5.3.1 Descriptive Histology:

A total of 17 lesions were analysed for histology. Lesions were observed in subcapsular location, 0.5cm infracapsular. The histotripsy lesions consisted of an area of loss of hepatic plates within the hepatic parenchyma (**Figure 45**). The core of the lesion consisted of loose eosinophilic material (**Figure 46A**). Hepatocytes or other cell types could no longer be identified. Minute specks of basophilic material were also present in places in keeping with nuclear debris and scattered nuclei appeared to be morphologically intact (**Figure 46A inset**). These changes were designated as “type A lesions” and were present in all 15 samples. Smaller areas characterised by dense eosinophilia including eosinophilic clumps were also present in all 15 samples, usually at the periphery of type A lesions (**Figure 46A**). These areas were designated as “type B lesions”. The perisinusoidal extracellular matrix (ECM) marked by the reticulin stain in type A and type B lesions showed loss and fragmentation of reticulin fibres (**Figure 46B**). The perilesional hepatocytes and their supporting ECM were morphologically intact.

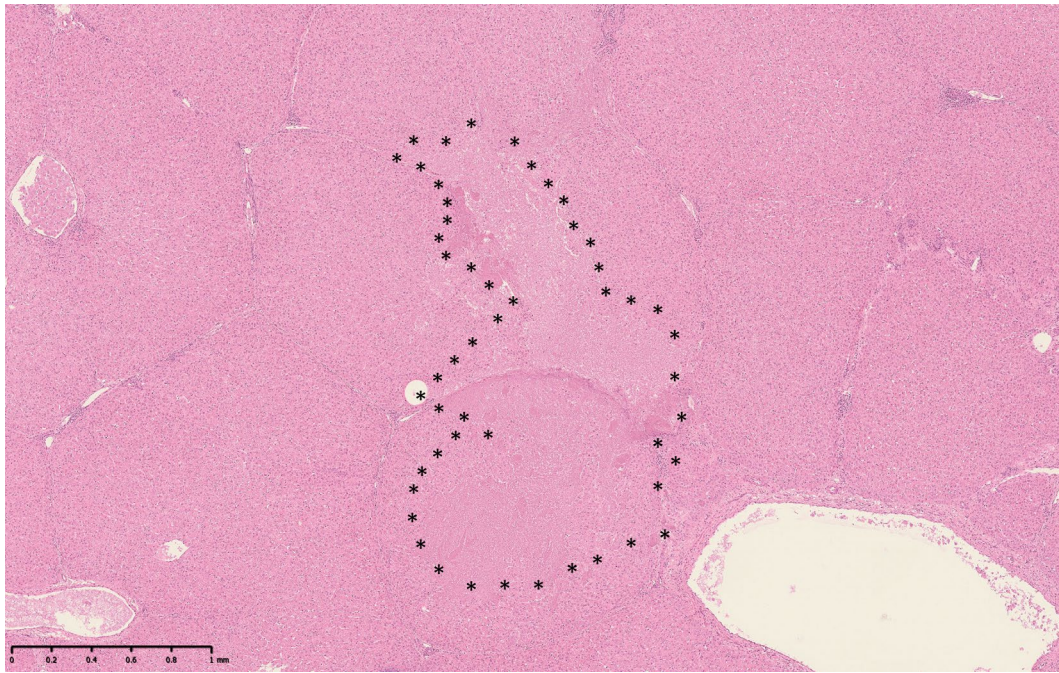


Figure 45 - An example of a well-demarcated BH lesional site, measuring at 2.34 mm by 1.19 mm in this plane of section (scale bar shown), delineated by asterisks, and composed of type A and type B lesions, with minimal formation of cavities. The lesional site spreads over adjacent lobules and is not demarcated by interlobular septa (H&E). The cellular contents appear not to be fully aspirated at the time of procedure. (The lesion was obtained as a wedge and not bisected through prior to histological analysis)

In all cases, ambient interlobular connective tissue septa within the histotripsy lesion showed distortion. In 10 out of 15 cases (67%) broken interlobular septa were also identified (**Figure 46C-F**). The collagen fibres in distorted septa retained their birefringence properties under polarized light (**Figure 46D-F**). This type of collagen fibre damage was designated as a “type C lesion”. Type C-lesions often co-localised with type B lesions. In some of the distorted septa collagen fibres appeared to have condensed into coarser bright red bundles or clumps showing reduced or no birefringence under polarised light (**Figure 46e and f**). This type of collagen damage was designated as “type D lesion”. Type D lesions also tended to co-localise with type B lesions.

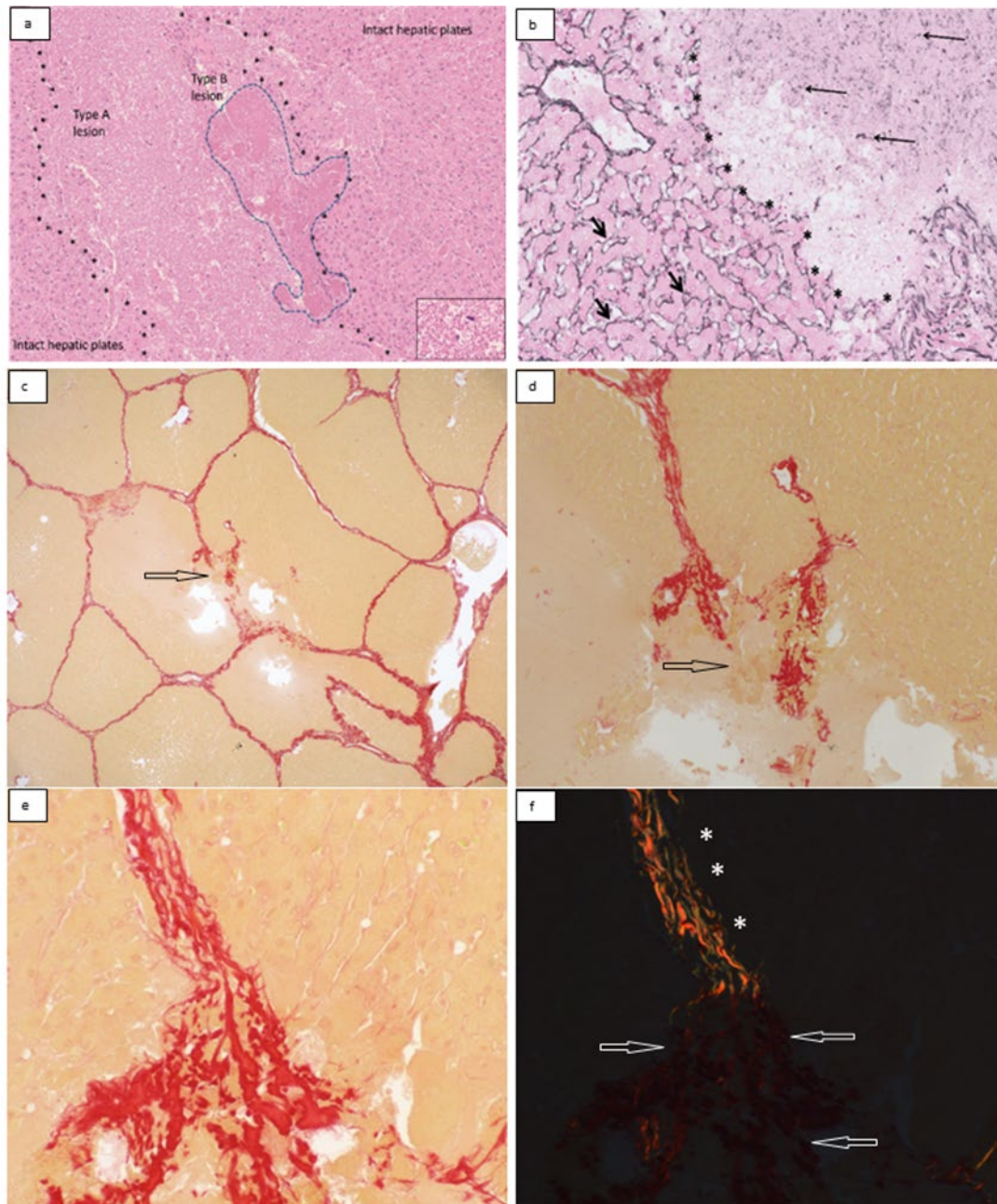


Figure 46 -(a) H&E: type A and B lesions. Nuclear debris and scattered nuclei were present in type A lesions (a, inset). (b) Reticulin stain: loss and fragmentation of reticulin fibres (long thin arrows) at lesional site. Please note sharp transition (asterisks), with nearby preserved hepatic plates showing an intact reticulin framework (short arrows). (c–f) Picro–Sirius red stain. (c,d) A broken interlobular septum is shown at lower (c, arrow) and higher (d) magnification. (e) and (f) show retention (asterisks) and loss (arrows) of collagen birefringence in type C and type D lesions, respectively.

In all cases damaged portal tracts were present at the periphery of the BH lesions (**Figure 47a**) with encasement and/or damage to local small portal biliary and/or vascular

structure-. In one case the BH lesion broke the wall of the branch of a portal vein of 800 μm cross sectional diameter (**Figure 47b**).

In 11 (73%) cases the core lesion included empty spaces. The liver surface capsule appeared intact in all cases. The BH lesion was more than 2 mm deep in most (11, 73%) specimens and affected the subcapsular parenchyma in 4 (27%) specimens. In these 4 specimens one or more deeper BH lesions were separated from the subcapsular lesion by intact liver parenchyma.

Figure 5a

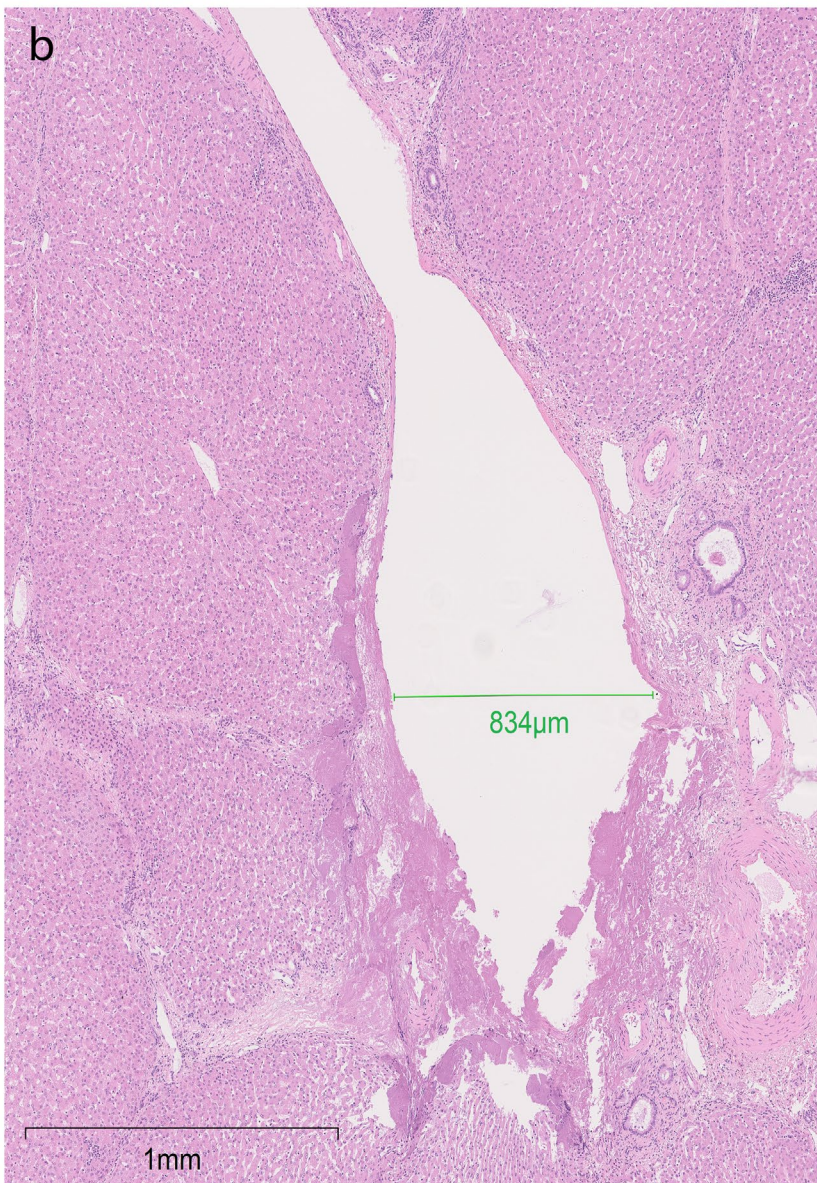
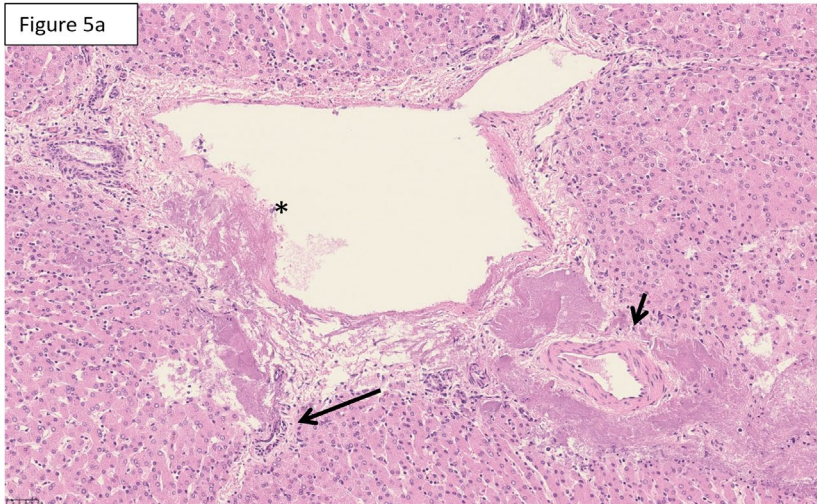


Figure 47 - (a) BH lesion extending to a nearby portal tract with injury to portal vein (asterisk), bile duct (long arrow), and encasement of an arterial branch (short arrow) (H&E). (b) Injury to a portal vein that is 834 μm in diameter (green bar).

5.3.2 3D reconstruction

The 3D reconstruction of two histotripsy sites was successful. Two lesions are created using similar parameters but have different appearance. The first reconstruction showed an ovoid lesion resting onto porto-septal connective tissue and approximately 1 mm deep of the liver capsule without a connecting track (Figure 48a). The second reconstruction showed that the lesion was composed of several minute spots of hepatic plate injury aligned on an oblique axis to the liver capsule plane (Figure 48b) and scattered to a depth of 6 mm from the liver capsule.

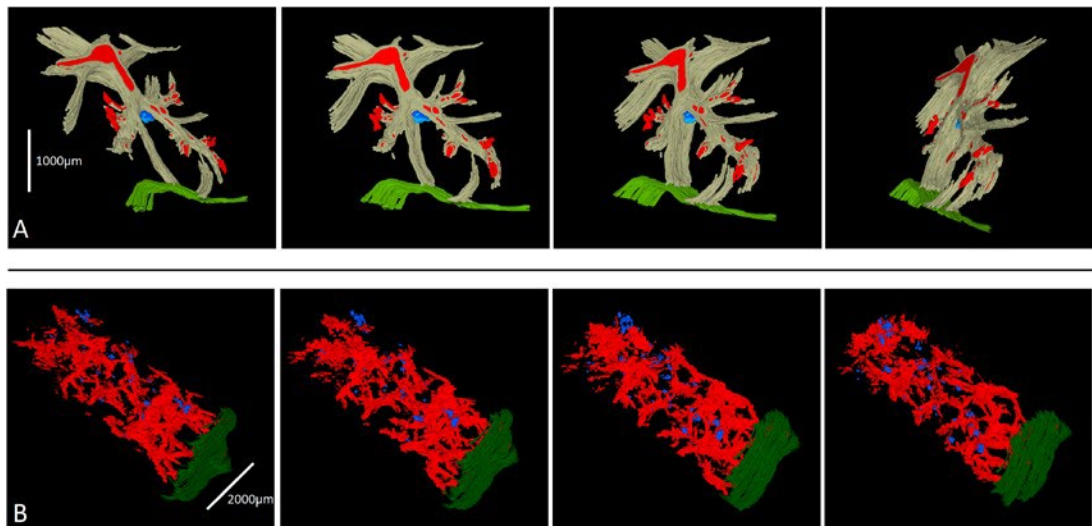


Figure 48 - Three-dimensional reconstruction of two HT lesions. (A) The first HT lesion is shown as a blue nodular area resting against the convergence of two fibro-connective vascularized (red) septa (grey) and well away from the capsule (green). The second HT lesion (B) is shown as multiple blue lesional foci aligned on an oblique axis to the liver capsule plane (green). Vasculature is in red.

5.3.3 4.0 Discussion

We have evaluated the effect of histotripsy in a viable perfused porcine liver ex vivo model with a histological evaluation of 15 excised lesions.

Perilesional liver parenchyma: The BH lesion was sharply demarcated and the hepatocytes and their supportive ECM facing the edge of the BH site appeared intact, histologically. We could not confirm, however, whether their enzymatic activity was preserved, using techniques such as the nicotinamide dinucleotide diaphorase (NADH-d) (428, 432), because we used formalin-fixed and paraffin-embedded sections. Apoptosis has been described in the liver parenchyma surrounding areas of necrosis caused by in-vivo radiofrequency ablation in pig livers (433) or by in vivo conventional thermal high intensity focused ultrasound (HIFU) in rabbit livers (434). In both these other models, there was a time interval of a few days for the apoptotic process to develop fully, possibly due to reperfusion of the ablated tissue (433) and the effect of reactive oxygen species released locally (434). Whereas we removed the specimens for analysis immediately after completing the histotripsy.

Portal tract involvement: The border of the lesion extended to portal tracts, usually of small size, although, in one instance, a larger portal vein branch was involved and damaged, suggesting that vessels larger than the 300µm threshold, proposed by Khokhlova et al.(435), may be susceptible to histotripsy damage. Of note, rupture of vessels ranging in size from approximately 50 to 500 (343) and portal and hepatic vein thrombosis (367) have been observed in specimens from two in-vivo histotripsy porcine models.

Effect of BH on collagen and reticulin fibers: Loss of SR-stained collagen birefringence (is a sign of collagen disruption) has been observed in rodent aorta treated with laser welding (436) and in laser irradiated bovine tendons (437), but, to our knowledge, it is a novel finding in BH sites in pig liver. The loss of the reticulin framework inside the BH site indicates that BH does not affect the cellular component exclusively, but it disrupts the ECM scaffolding of the hepatic plates. This is in line with the findings by Macoskey

et al.(430), who showed a progressive deterioration of the ECM with increasing number of histotripsy pulses and followed by a loss of the cellular component. The presence of type D lesions away from the main histotripsy site are similar to the narrow regions of thermal damage described by Khokhlova et al. (338)in an in vivo porcine liver model. This observation suggests that thermal energy may be transmitted along connective tissue septa, a feature previously reported using liver microwave ablation (438). However, it is possible that the margin of the cellular liquefactive area reaches these points in the deeper parts of the specimen that are not included in the planes of the sections examined. Regardless of the precise mechanism involved, the histotripsy track releases sufficient energy to break the connective tissue septa present physiologically in porcine liver, and the same effect would be expected on the pathological septa forming in chronically diseased hepatic tissue in humans as part of fibrosis progression secondary to chronic liver disease.

Liver capsule: The BH site was subcapsular in some instances, but the liver capsule remained intact in our series despite the direct contact with the BH probe. The presence of an intact capsule is likely to reduce the impact of focal damage to vessels or biliary radicals following in vivo histotripsy, as any bleeding or bile leakage would be contained.

Limitations: There are technical limitations that need to be considered when interpreting our results. The specimens were obtained as part of a protocol that also involved cell harvesting from the histotripsy sites. The aspiration of the lesion liquid center or cell analysis may have partially affected the lesion appearances, particularly the formation of cavity-like spaces in some of the specimens. It is therefore not possible to confirm or exclude whether these cavities are due to boiling bubble nucleation or cavitation.

Our study design did not allow us to make a precise and reliable quantitative correlation between the type and extent of tissue damage and the BH parameters, including the effect

of perfusion. The value of this histological review is to give information about the type of tissue damage observed, lesional boundaries, and the relationship with nearby hepatic parenchyma, portal structures, and connective tissue septa. The lesional area may not be fully represented in the two-dimensional assessment performed in each specimen.

Three-dimensional reconstruction. The purpose of the 3D reconstruction of two additional specimens was to address this limitation. Our two models showed that 3D reconstruction is feasible and gives valuable insight into the size, shape, and localization of the BH lesional site and its precise relationships to ambient anatomical structures. The first model, in particular (**Figure 47a**), shows that the lesional site rests against a portal tract and fibrous septa, suggesting that the connective tissue interface could reflect at least part of the energy. Further work is necessary to confirm this observation, but future studies aimed at refining the BH protocol (is to optimize the size, location, and nature of the BH lesions should consider the use of 3D reconstruction and correlate the 3D appearance, size, and location of the BH lesions with the BH procedure ultrasound parameters.

5.4 Conclusions

In summary, we describe in detail the effects of BH on a series of viable perfused porcine liver specimens. BH produces well-demarcated lesions, causing damage to both cellular and ECM components of the hepatic plates, and delivers sufficient energy to alter the configuration of collagen bundles, break ambient fibrous septa, and damage portal tract structures, including relatively large portal vein branches. The lesion is well demarcated with a very sharp border, where both the cellular and ECM components of the perilesional hepatic plates appear morphologically intact. The liver capsule is not affected by direct contact with the BH probe. A 3D reconstruction of BH sites is feasible and has great

potential to correlate the BH parameters with the site, size, and nature of the BH liver lesions created.

As a result of these findings, we set to analyze the core content of the cavity created by the BH further.

Chapter 6 Liver ultrasound histotripsy: Novel analysis of the histotripsy site cell constituents with implications for histotripsy application in cell transplantation and cancer therapy

6.1 Introduction

Only liver transplantation can cure end-stage liver disease and liver-based metabolic diseases. However, donor organ shortages have limited treatment (439, 440). Allogenic hepatocyte transplantation may replace liver transplantation. Over the past two decades, hepatocyte transplantation has moved from bench to bedside. Standardised methods for human hepatocyte isolation, culture, and cryopreservation have expanded clinical programs (439, 440). Standardized techniques have been established for isolation, culture, and cryopreservation of human hepatocytes that have led to the expansion of the clinical programs (441). Clinical hepatocyte transplantation safety and short-term efficacy have been proven (125, 442, 443). However, a major problem is the shortage of donor organs from which to isolate hepatocytes as viable organs are utilised for whole organ transplant. Only sub optimal grafts which have been declined for whole organ transplants are currently being offered for cell isolation. This may partly explain why hepatocyte transplantation has failed to achieve a major clinical role in the treatment of liver failure as the grafts used for hepatocyte transplant have low cell yields and methods for engraftment are currently inadequate to justify wider clinical application (444). In addition to above, the major limitation to hepatocyte transplantation by portal perfusion is portal vein thrombosis.

Current techniques for isolation of hepatocytes from liver tissue usually involve a combination of mechanical disruption and the perfusion of collagenase via major hepatic veins (444-446). The mechanical and chemical treatment damages the harvested cells and has resulted in low cell yields. Current success of cell engraftment is dependent on the number of viable cells extracted and implanted. Repeated hepatocyte transplantation has been shown to increase the number of engrafted cells above 5% (recipients liver cell mass), a level sufficient to correct some metabolic defects (447). Primary adult

hepatocytes lose function and viability following isolation and culture and have limited proliferation potential in vitro (447). Thus, a new approach is required for both isolation and engraftment to improve the outcome of cell therapies for both acute and chronic liver disease. Apart from cell transplantation, availability of viable human hepatocytes is essential for testing new systemic therapies to evaluate hepatotoxicity and could help accelerate scientific studies in other disciplines. Hence, the need to expand and improve techniques for viability of isolated hepatocytes could range from use of iPSc to novel technologies such as histotripsy.

Histotripsy has been investigated as a method for decellularization and in treating cancers. In boiling histotripsy (BH), localized, high-amplitude shock waves cause rapid tissue heating, resulting in the formation of a boiling bubble within the tissue (373). The interaction of incident US shocks with the boiling bubble results in tissue disruption and liquefaction without significant thermal injury to the tissue. This happens because the timescales of heat diffusion and thermal injury are much longer than those of the mechanical action of oscillating bubbles (375, 376, 419).

This property of histotripsy led to experimental work on the decellularization of tissue while maintaining a degree of extracellular structure (i.e., preserved blood vessels at the site of HIFU insonation) (344, 448, 449). Histotripsy has not previously been applied to hepatocyte isolation from liver tissue or as a potential technique to facilitate cell transplantation. Moreso, the vast majority of current cell extraction techniques (125, 440-445) have been based on the collagenase digestion technique [originally developed by Berry & Friend (450)] , which of itself is time consuming and expensive. Use of histotripsy to extract cells in the perfused whole organ system provides an alternative to collagenase cell extraction. Histotripsy not only can help in cell extraction but also in implantation of extracted cells by creating a niche environment for the cells. In this paper

we demonstrate a novel method for hepatocyte isolation using histotripsy in a perfused liver model. Perfusion of the isolated liver maintains tissue viability and vessel patency and has been shown to influence the quality of the lesion created by the HIFU system (451).

6.2 Study Aims

To assess the contents of the cavity produced by BH in normal liver and characterise the content of the cavity.

6.3 Study Objectives

- To establish a protocol for porcine liver harvesting and perfusion to allow ex vivo histotripsy on viable perfused liver.
- To use an established BH protocol to produce focal liver lesions
- To study the fluid core produced by BH for cell content.
- To culture the cell content and establish cell morphology and viability

6.4 Hypothesis

The action of BH when applied to minimise thermal effects could result in viable cells within the histotripsy core.

6.5 Methods:

To investigate the possible use of histotripsy we used porcine livers retrieved in the manner described below and perfused in a simple perfusion circuit in the lab. The content of the sonicated lesions was then aspirated, cultured and analysed.

6.5.1 Pre-experiment trial with different tissues:

To assess the ability of the histotripsy parameter used previously, we trialled the parameters in several different tissues including perfused porcine liver, kidney, and pancreas. This was to test the feasibility of cell isolation and to assess the cells in a culture medium.

The preliminary work on porcine liver was to isolate cells and culture for 7 days. The cells would be assessed with light microscopy for morphology. Targeted kidney and pancreas tissues were also cultured and only one lesion from each were sent for histological analysis. Following the trial period the experiment was repeated as described below.

6.5.2 Overall Study design:

See Section 3.1

6.5.3 Histotripsy set up

See Section 3.3-3.4

6.5.4 Perfusion set up:

6.5.4.1. Organ retrieval – see **section 3.2**

6.5.4.2. Lab based organ perfusion – see **section 3.5**

Upon arrival at the organ perfusion laboratory the livers were perfused with 1 litre of preservation solution (Soltran, Baxter) and the core liver temperature was allowed to return to room temperature (ranging between 24-30 °C) before being subjected to histotripsy insonation. Perfusion of the organ to maintain viability was via the portal vein (**Figure 50**) with the perfusate draining via the vena cava into an organ bath. The perfusate was not recycled. At the beginning of the perfusion, the liver was placed in an organ bath lying over an ultrasound reflective layer. The perfusion solution was delivered using a

perfusion pump (Baxter™, UK) to achieve constant flow rate of 350ml/hr confirming vessel patency before lesions are created by US histotripsy. The HIFU probe was positioned in multiple sequential locations chosen at random over the surface of the perfused liver with 50 pulses applied (in approximately one minute) at each site. The focal histotripsy lesions could be identified by the puckering of the liver capsule, a pinpoint dimple. Once the lesions were created the lesion was incised with a surgical blade and the central liquefied core was aspirated using a 20µl single-channel gauge pipette. The aspirate was then immediately transferred into culture medium for subsequent assessment of cell number and morphology.

At the preliminary experiment we perfused liver with the perfusion circuit described above using 2 livers and then the repeat experiment with 5 new porcine livers. At the stage of the preliminary perfusion experiments we also used pig kidney and pancreas to perfuse and subject to BH before aspirating the lesions.

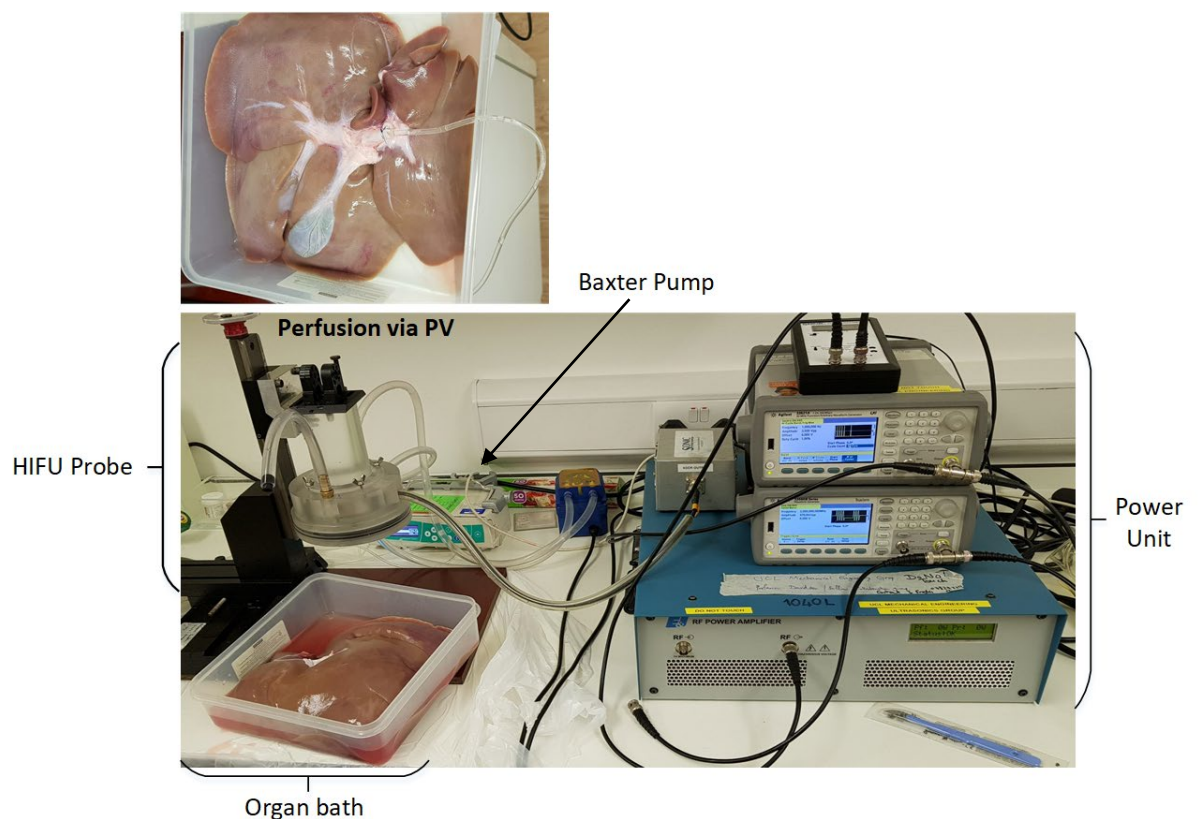


Figure 49 – Experimental set up for HIFU probe and histotripsy protocol. Retrieved pig liver is placed in an organ bag and cannulated via portal vein for perfusion with Soltran solution with a Baxter pump. The perfusate is collected in the organ bath. The perfused liver is placed under the HIFU probe. The transducer is powered by high DC power supply. The Power unit will be adjusted to a set parameter for the cell isolation protocol. The probe was driven by a high voltage pulser designed to generate short single pulses seen in photo sitting above the transducer.

6.5.5 Pre-culture light microscopy:

Prior to culture, the aspirates were examined under light microscope and confirmed to have a mixture of cells and debris. As aspirate underwent a spin process prior to culture, they were not stained at this stage to identify the cell type.

6.5.6 Cell culture: cell morphology and growth

See Section 3.10

6.5.7 Phalloidin/ Dapi staining

Cell morphology and growth at days 3 and 7 post seeding were examined using fluorescently labelled phalloidin which allowed filamentous actin to be visualised and Dapi which allowed the cell nuclei to be observed. Following manufacturer's instructions (see methods chapter – Section 3.11)

6.5.8 Live-Dead assay

The viability of the cells was assessed on days 3, 7 and 21 using a Live-dead imaging kit (Molecular Probes, Thermo Fisher Scientific) as per manufacturer's guidelines. See Section 3.11

6.5.9 Morphology assessment:

Once stained as above, the cells were examined under microscope for morphology and confirmed as hepatocytes following review by two independent observers and subsequently by an experienced hepato-pathologist.

6.5.10 Cell Titre-Glo Metabolic Assay

See Section 3.14

6.5.11 H&E and Picrosirius Red Staining:

See section 3.7

6.5.12 ImageJ Software:

ImageJ 1.52 (National Institute of Health, USA) was used in processing and optimisation of the images acquired from histology and cell microscopy. Cell Count plugin was used for counting cells in the Live-dead and DAPI microscopy images. *Figure J* plugin was used in construction of optimised images for publication.

<https://imagej.nih.gov/ij/index.html>

6.5.13 Statistical methods

GraphPad Prism© 6 software was used in the analysis of the data. Chi-squared test was used to compare the proportion of live cells on day 1 and day 7 post culture. Student's t test or Mann–Whitney tests were used to determine the difference, which was set at $P < 0.05$. We did not use statistical methods to predetermine sample size, there was no randomization designed in the experiments, and the studies were not blinded. Data are represented as mean \pm SEM or median where appropriated.

6.6 Results:

The result of the preliminary study is presented here first followed by the results of the repeat experiment.

6.6.1 Preliminary study of histotripsy in liver tissue

Initially two pig livers retrieved in the same manner as described in section 3.2 were perfused in the perfusion lab (Section 3.5) and were subjected to the same US histotripsy parameters described in section 3.3-3.4. There were 10 lesions that were aspirated for the cell suspension and the initial aspirate were analysed under microscopy without spinning the sample. This revealed a supernatant of suspended cells and debris.

Once the suspension examined under microscopy the aspirates were cultured in a cell medium as described in **section 6.5.6**.

Figure 50a shows the microscopy results of the trialled culture cells at 17 hours after culture. There were lots of cells visible under the light microscopy after 12 hours. The cultured aspirate not only contained cells but also cells and debris (**Figure 50**) and this was because we did not spin the aspirates to purify for cells. The cultured cells were examined at day 7 to see if they have survived the culture medium conditions. It's worth noting the culture medium was un-optimised and the medium would only receive top up with addition of antibiotics. On day 7, the number of cells has clearly decreased to a very few scattered cells. Interestingly, there was evidence of cells clumped together (**Figure 50D** - 3D asterisk). However, whether these cells were alive, or dead was not evident from the light microscopy result and required further assessment on repeat experiment.

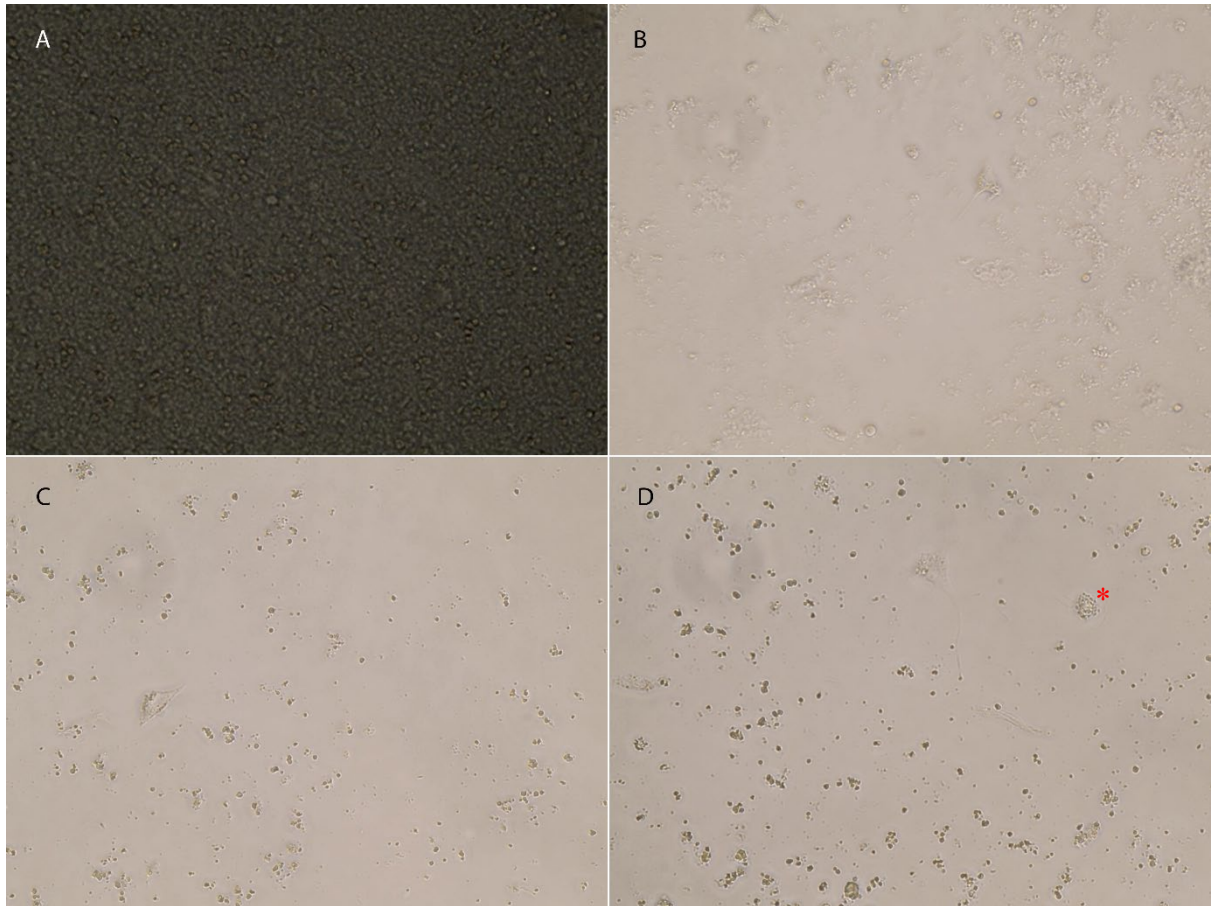


Figure 50 – Light microscopy analysis of the aspirated cells following culture. (A) shows the cultured aspirates 24 hours after aspiration and after culture in the cell medium. (B), (C) & (D) are light microscopy analysis of three different plates at day 7 post culture. It shows the number of cells has reduced significantly but there are a few scattered entities that could represent cells clumped together. Red asterisk in (D) denotes possible clumped cells.

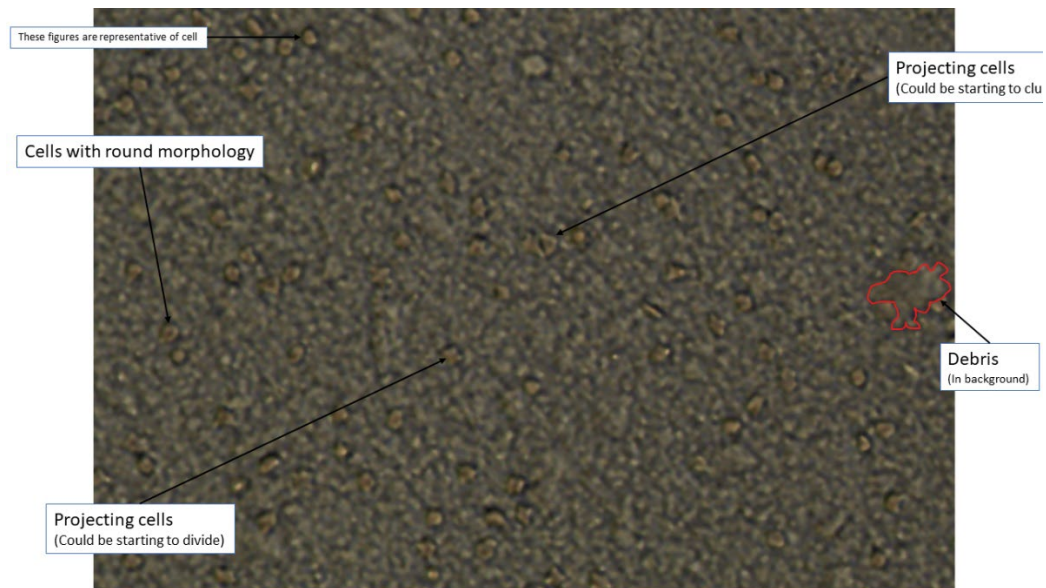


Figure 51 – A closer look at the cultured aspirates at 17 hours (Zoomed in Figure 4a) revealed interesting observations that prompted further investigations to characterise the aspirates. There was evidence of round bodies which could represent cells as well as projecting cells that may represent dividing cells.

6.6.1.3. Results of histotripsy in other porcine organs

We also targeted porcine kidney and pancreas to assess and examine the utility of the histotripsy for cell isolation within these tissues. These were used with the same treatment protocol as described in **section 6.5.3** but different tissues. Four aspirates from four different kidney lesions (**Figure 52**), produced a few scattered cells, however they were too few and they were not cultured. Similarly, pig pancreas (**Figure 53**) was subjected to same parameters of the histotripsy that was used for liver and again it produced a core with cells and debris. This was not cultured as it was not the aim of the study, more so it was difficult to identify the lesion for aspiration as the tissue consistency was different to the liver tissue.

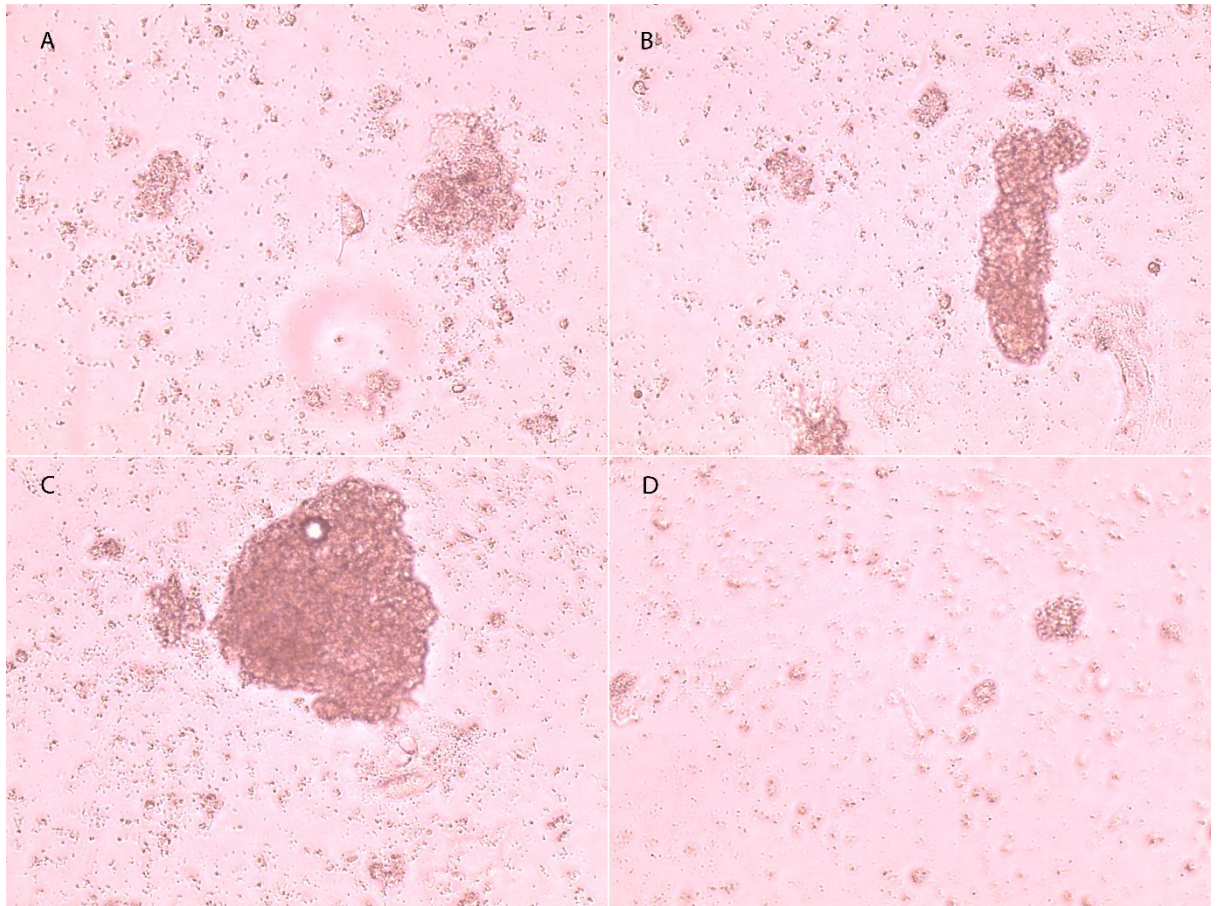


Figure 52 – Images A-D represent the initial microscopy of the aspirates from the 4 kidney lesions produced. The initial aspirates show very few scatter cells. However, their characteristic remains to be further examined.

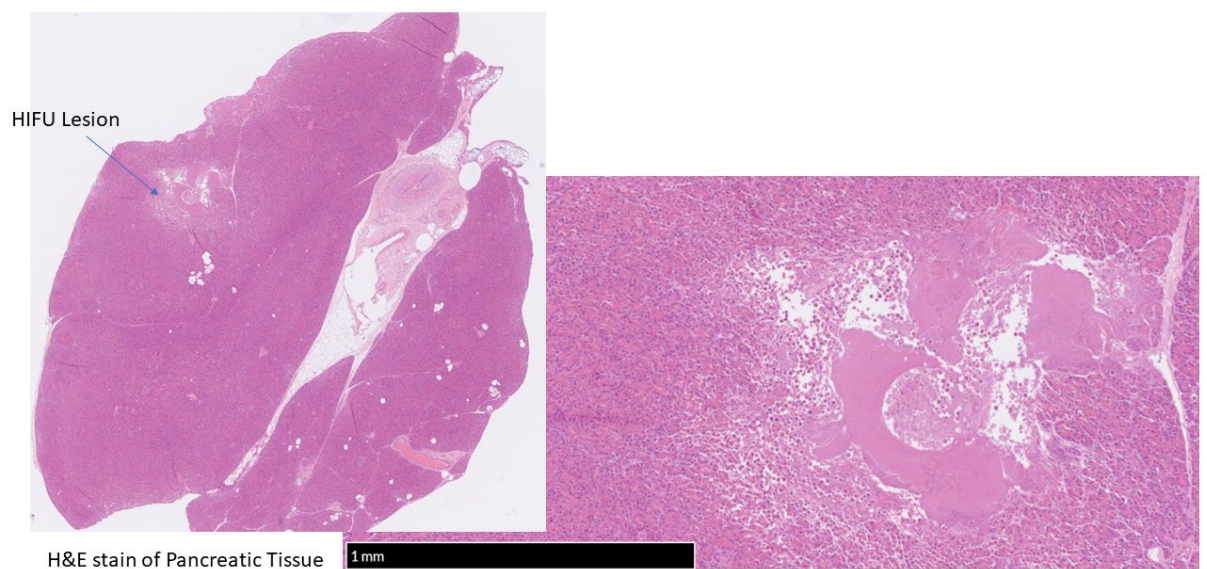


Figure 53 – Pig pancreatic tissue subjected to histotripsy sonication. The H&E staining reveals a lesion with core suspension of cells and debris. However, as the pancreatic tissue is more fatty and less vascular than the liver tissue there is more architectural distortion noted in the lesion.

Following our initial trial attempt to test the idea of histotripsy assisted cell aspiration and culture we conducted a refined method with perfused pig liver only. The results are as follows.

6.7 Detailed evaluation of liver histotripsy site aspirates (repeat liver experiment results)

6.7.1 Organ perfusion, viability, and lesion creation & cell aspirate

All livers were successfully flushed and achieved uniform perfusion based on the visual appearance of the organ. Livers were perfused with non-oxygenated perfusion fluids at 350mL/hr (as described in **section 6.5.4**) via the portal vein and the median starting temperature of the perfusate was 29°C. The experiments were repeated with 5 different porcine livers and similar histotripsy parameters of the HIFU machine was used. We analysed 130 individual lesions from these 5 livers using this protocol. After perfusion all livers maintained a degree of bile production confirming viable livers capable of bile production and excretion. Following treatment with histotripsy each lesion was bisected and the contained cell suspension in the core of lesion was then aspirated. Time taken to aspirate each lesion is less than a minute. To increase the volume of cell suspension the aspirate from three sequential lesion was combined in each well of the 96 well culture plate resulting in 43 plates/wells in culture.

6.7.2 Histology of lesions

The histotripsy lesions were evaluated by an experienced liver histopathologist (AQ). They were typically about 0.5 cm below the surface of the liver capsule (**Figure 54**). The core of the lesion contained a suspension of cells mixed with extracellular matrix debris (**Figure 54 & Figure 55**). The typical histotripsy site appeared histologically to track from the subcapsular region to an

intraparenchymal depth of about 0.5-1 cm. Except for sampling and embedding artefacts the liver capsule was intact. The histotripsy site consisted of an area of loss of hepatic plates and supporting matrix, with rupture of intervening interlobular septa and in a few instances of portal structures. In two cases the ruptured portal, biliary and vascular structures were small (artery and bile duct of 125micron diameter, and portal vein maximum diameter 250 micron) but in one case the histotripsy broke the wall of a branch of the portal vein 800µm-diameter. The histotripsy area was sharply demarcated with hepatocytes a few microns away from its edge appearing intact morphologically. There was no difference in description of histological appearance of the lesions obtained from the periphery of the liver or more central lesion.

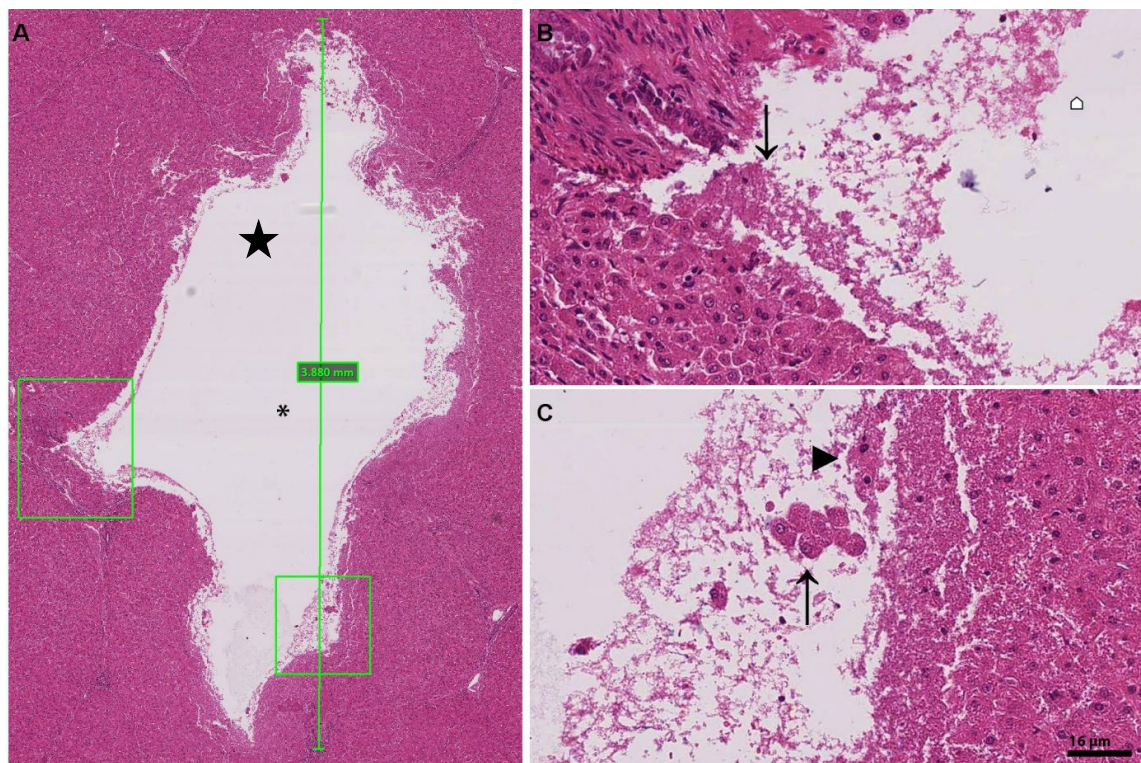


Figure 54 – H&E cross section staining of the HIFU histotripsy lesion. (A) Example of a lesion with its core suspension aspirated for analysis. The * marks the core of lesion where cell suspension would have been and HIFU creates a cavity of about 3.8mm in size. The two square areas are zoomed in, left box corresponds to (B) and right box corresponds to (C) which show intact hepatocytes detached by the force of histotripsy. The force generated is focused and the adjacent cellular and extracellular components are preserved. (B) Reveals the impact of the histotripsy force resulting in fragmenting cells into fine fragments (*) and causing in mechanical disturbance of adjacent cells. The arrow marks damage to a nearby vessel. (C) The force not only results in destruction of cellular and extracellular components into fine granules, but it can also result in burst of the cell membrane (►) whereas other cells escape (↑) the full impact of the force generated and are either in clusters of intact cells or as individual cells in the core suspension.

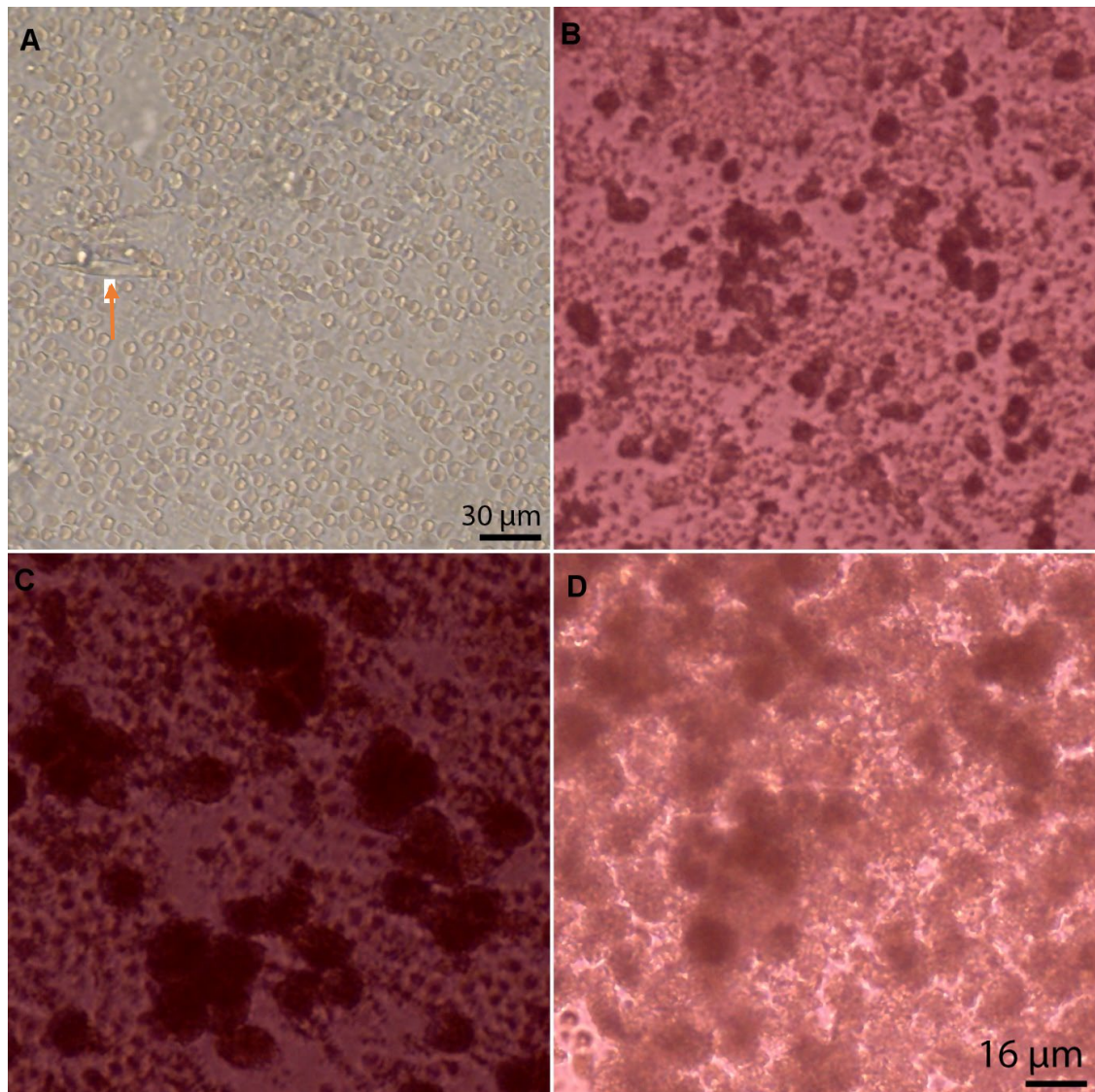


Figure 55 – Harvest from each lesion demonstrating different quantity and type of cells being extracted. (A) Cell extracts 24 hours post culture prior to spin reveals a mixture of different cell types. Arrow points towards a fibroblast, (B) 2 days post culture (C) 4 days post culture (D) 6 days post culture

6.7.3 Cell Culture:

Immediate after cells were passed the centrifugation stage and filtering as described in methods, cells were cultured in the 96 well plate with RPMI and antibiotics. Wells remained free of florid infection and no well was discarded due to infection.

6.7.4 Cell type, appearances, and numbers at baseline

An initial manual count of the cells within the aspirate revealed approximately 2446 cells/aspirate equating to 61×10^4 cells per mL. Although the number of cells aspirated from each lesion was variable (**Figure 55**), the count was approximately 36.6×10^4 cells in 600 μ l of aspirate. Given each well contains 3 aspirates then the total number of cells cultured per well was approximately 1.86×10^6 . Initial cell aspirates contained cell debris along with a mixture of possible different cells (based on microscopic morphological appearance). Extracellular matrix components were also present (**Figure 55**). A live-dead staining analysis along with manual count of cells on day 1 revealed viable cells to be between 12-16% (approximately 1520 cells per well) of the cell population and mixed with several dead cells (approx. 7680 cells per well) (**Figure 56**).

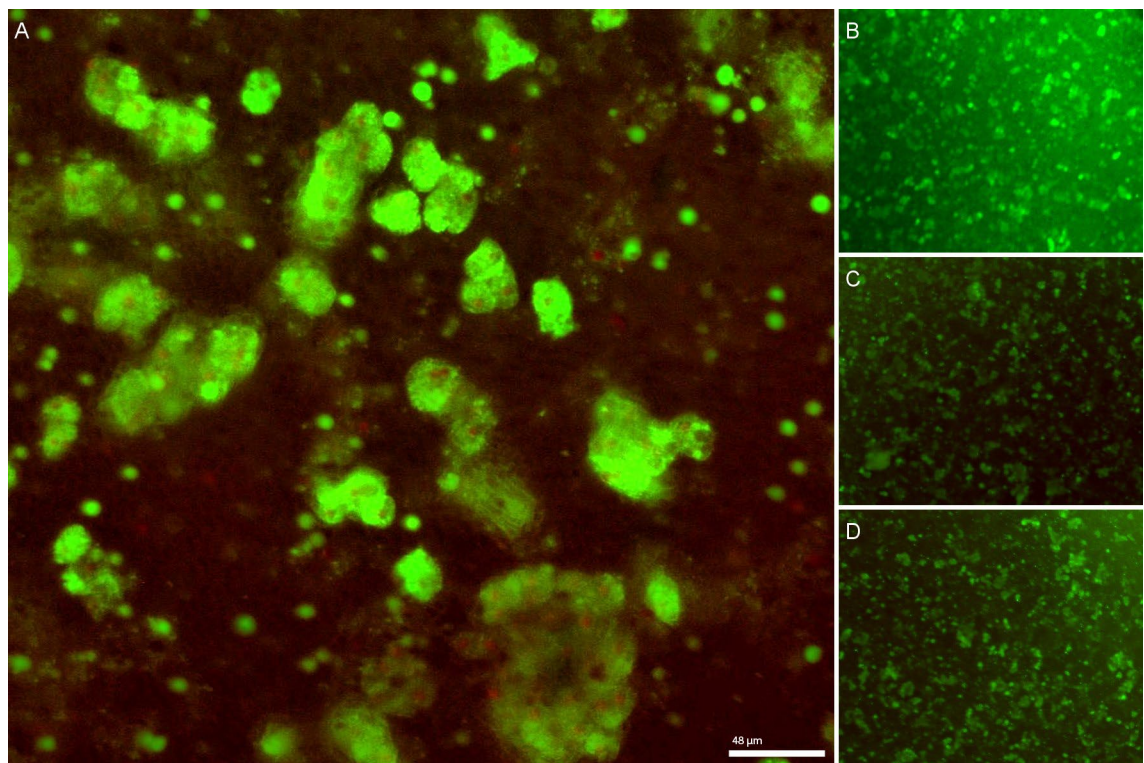


Figure 56 – Live-Dead staining 24 hours post culture reveals several liver cells (Green fluorescence) along with debris and dead cell (red stains) (20x zoom). (B, C, D) Cells in other well plates also show a mixture of live and dead of different quantity.

6.7.5 Cell division and viability in culture

DAPI staining of cells 7 days post culture revealed live cells that have started to clump together (**Figure 57**). The cells have an intact cytoskeleton and have started to form a network. The number of live cells per well almost doubled between baseline and day 7 (Day 1: 1206 cells to Day 7: 2022 per well) (**Figure 58**) and there is a change from 12% to 45% live cell after 7 days of culture. The increase in viable cell numbers was statistically significant ($P < 0.0001$) (**Table 14**). Morphological analysis of the live cells on the 7th day confirms adult hepatocyte replication and survival. Metabolic activity of the cultured cells analysed using cell titre-Glo assay showed an activity peak 7 days post culture (**Figure 59**). This was a significant increase when compared to control (medium alone) ($P < 0.0001$); Luminescence: 3.57 RLU²). This assay is known to have a high sensitivity for cell proliferation and cell toxicity. Given the low volume of cells we were working with this assay proved to be ideal in assessing the metabolic activity of live cells. Although there was a decline in average activity per well from the first week onwards (Average Luminescence: 24.6 RLU), cultured cells also displayed metabolic activity 21 days post culture (Average Luminescence: 7.85 RLU) when compared to control group. Metabolic activity was demonstrated across all wells over the 21 days of culture monitoring.

² RLU: Relative Light Units; measure of luminescence to measure Cell Titre-Glo activity

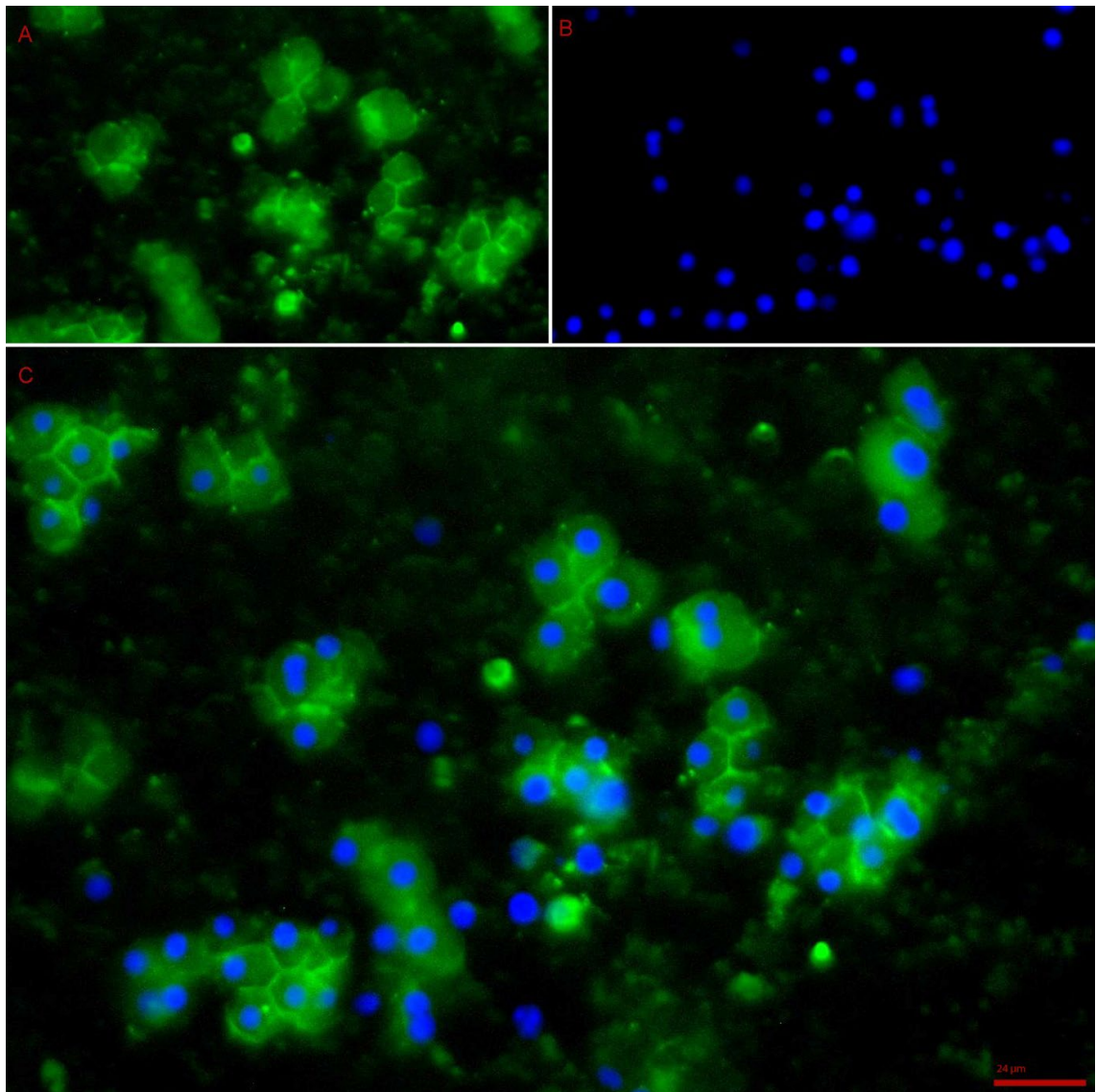


Figure 57 – Phalloidin & DAPI stain 7 days post culture revealing clusters of live cells with preserved cytoskeleton. Blue: live cell nuclei; Green: cytoskeleton of hepatocytes. (A) Green fluorescence showing the cytoskeleton of the hepatocytes, revealing intact cytoskeleton network and clumped group of cells at 7 days post culture. (B) Blue fluorescence revealing nuclei of live hepatocytes. (C) Combined fluorescence of the superimposed nuclei and cytoskeletal staining, revealing live cells clumped together at 7 days post culture while preserving their skeletal integrity. The cells seem to conform to a 3D structure and bound to a natural matrix. (40x Zoom EVOS microscopy)

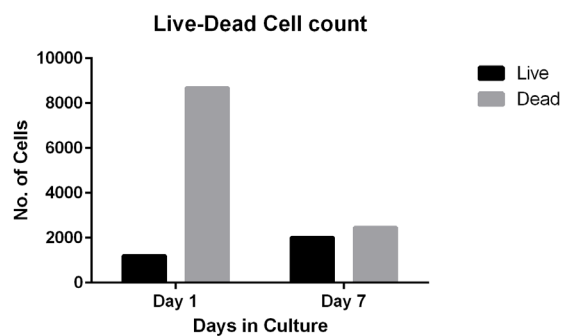


Figure 58 – Live-dead cell count analysis. Using ImageJ software (live-dead plugin) number of liver cells were quantified on Day 1 and Day 7. There is an increase in the number of live cells 7 days post culture. Almost double the number of live cells observed a week after culture and this indicates replication and cell activity.

Table 14 – Analysis of Live & Dead cell of cell culture day 1 and day 7 post culture

	Live	Dead	Total	% Live
D1	1206	8690	9896	12.2
D7	2022	2460	4482	45.1

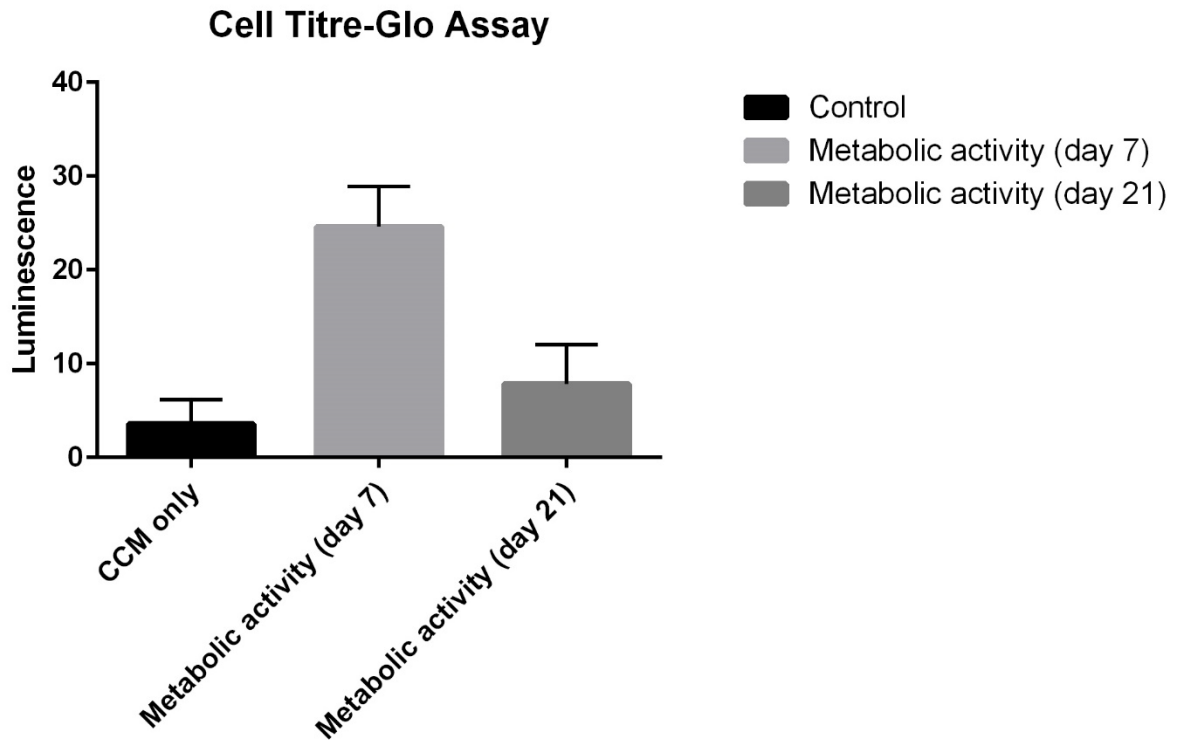


Figure 59 – Cell Titre-Glo Metabolic assay. Showing a significantly high metabolic activity a week post culture and this reduces 21 days post culture. Albeit a reduced activity has been shown 21 days post culture, this is still higher than control group that contain no cell.

6.8 Discussion:

We report the first detailed analysis of the cell aspirate and culture and its correlation with local histological changes following liver histotripsy of viable whole liver organs in vitro using an isolated perfused organ system. Here we discuss our preliminary cell experiment results along with factors influencing cell harvest and viability as well as factors influencing the success of harvested cells to remain alive and functional in culture medium.

6.8.1 Preliminary liver studies

The study established that histotripsy could effectively generate localized lesions in perfused porcine livers similar to the previously described lesion in the previous chapters and the can be aspirated can be further analysed. Our initial analysis of the lesion cores

revealed a mixture of cells and ECM debris. The application of histotripsy at a frequency of 1 Hz and a 1% duty cycle minimized thermal effects while maintaining tissue viability. The method demonstrated the feasibility of liver cell isolation. However, the preliminary results are limited by a number of factors: (1) limited number of lesions created and bisected to be aspirated for cell analysis; (2) this meant the volume of cells per well would be very low; (3) the culture medium was not optimised for culture as we did not expect to find cells with intact morphology. The preliminary results of the liver culture revealed that sonication can result in a lesion that its core can have viable cells. Given there were viable cells even at day 7, necessitated a repeat experiment to assess viability of the cells further. Especially when, there was evidence of round bodies which could represent cells as well as projecting cells that may represent dividing cells (**Figure 51**). Lastly, our preliminary experiment lacked histological correlation and functional study of the cultured cells.

6.8.2 Other Organ Histotripsy

Histotripsy applied to perfused porcine kidneys and pancreas revealed limitations due to tissue consistency differences. Kidney lesions produced fewer cells, while pancreatic lesions showed greater architectural disruption. The fatty and less vascular nature of pancreatic tissue posed challenges in lesion identification and cell aspiration. There was more damage noted in the pancreas tissue due to the higher fat content and the fact it is a less vascularised organ compared to liver (**Figure 53**). These are in line with the work previous in-vivo observation and findings that the water content and vascularity of the tissue affected the degree of injury (252). The findings also suggest that organ-specific parameters might need optimization to achieve comparable outcomes across different tissues. These early observations of cell isolation and culture following histotripsy have not been shown before. Thus, highlights the potentials of histotripsy in cell isolation in pancreatic tissue (i.e. islet cell extraction). We did not repeat the experiments in pancreatic

and kidney as the parameters we had selected were specific for liver tissue and our aims and objectives were to focus in liver cell therapy.

6.8.3 Histotripsy regime and the nature of the liver lesion based on histology.

There are several factors that affect the extent and nature of the histotripsy lesion in the liver. The histotripsy treatment dose applied is important in creating a lesion in which the core consist of a liquified suspension. *Khokhlova et al (264)* noted that the histotripsy area is sharply demarcated and hepatocytes a few microns away from the lesion edge appear morphologically intact. We have noted similar findings in our study. However, with our treatment protocol we have seen damage to branches of a portal vein larger than those observed by *Khokhlova et al (264)*. This finding may have important clinical implications as it highlights the importance of appropriate dose adjustment for the tissue being sonicated (424) as well as appropriate adjustment for the aim of the sonication (i.e. Tumour ablation vs mechanical decellularization). For example, dose applied for cell harvest would be different for those applied for tumour ablation. Break in vasculature in the clinical setting could of concern in terms of bleeding and dissemination of tumour cells when using histotripsy to treat neoplastic lesions. *Worlikar et al (369)*, demonstrated tumour regrowth following treatment of murine HCC with histotripsy. Our study revealing for the first time the presence of live cells within the core lesion post histotripsy could explain the finding of tumour regrowth due to the persistence of viable cancer cells in the liquified lesion core. Although the focus of this paper is not cancer treatment this finding may be highly relevant to tumour treatment using histotripsy.

It should be noted, however, that the process of liver perfusion with Soltran might introduce stabilised gas microbubbles in the vasculature which are likely to oscillate as a

response to the incoming acoustic field (452, 453). These pre-existing bubbles could then cause mechanical damage to the vascular wall to a higher extent than bubbles that nucleate “from scratch”, I.e. solely as a response to the acoustic field, like those observed in intrinsic histotripsy and boiling histotripsy protocols (264).

The histotripsy set-up used in these experiments was based on previous boiling histotripsy protocols for the mechanical disintegration of bovine, porcine and murine liver tissue (435). Fifty histotripsy pulses were used to achieve mechanical ablation of the treatment area. Previous works have used 5 to 50 pulses and reported complete tissue emulsification upon further histological analysis (449, 454). *Khokhlova et al.* (359) in experiments sonicating in-vivo porcine liver also demonstrated on histology disruption of the core with sharp demarcations. Previous experiments in tissue phantoms show that the degree of mechanical fractionation of the treatment zone increases with increasing pulses (375). None of the previous studies have analysed content of the histotripsy lesions.

In our study, a Pulse repetition frequency (PRF) of 1 Hz was used so that the focal region had time to cool down before subsequent pulses and avoid thermal damage. Following from simulation results a 1% duty cycle was used in order to raise the focal temperature so that focal peak-negative pressures surpass the temperature-dependent nucleation threshold of soft tissue (373) for sonication at an ultrasound frequency of 2 MHz. By optimising the duty cycle of our experiments in terms of the minimal pulse lengths required for bubble nucleation, it is also possible that thermal damage inflicted by HIFU heat deposition is minimised, contributing to increased viability of cells within the treatment zone. These results highlight the importance of HIFU parameters in relation to the biophysical effect required.

A future formal comparison in the protocol used with different range would substantiate these results and help further with parameterisation for different purposes.

6.8.4 The use of the perfused organ as a model

Ex-vivo perfusion systems cannot perfectly replicate the physiological conditions of a living organism, such as dynamic blood flow, oxygenation, and metabolic processes. However, our simple perfusion circuit maintained a degree of viability to allow for intervention and evaluation like the circumstances in-vivo, most notably the vessel patency (455). Even though the perfusion circuit aim was to allow perfusate to pass through and keep the vessels patent, achieving consistent perfusion across the entire organ can be challenging, potentially leading to under-perfused areas that may affect cell viability and yield. Lack of an oxygenated circuit and lack of nutrient in the perfusate can also impact viable cell harvest. Presence of oxygenated perfusion can have an impact on the oxidative stress and energy status of the cells and organ (456). The presence of perfusion would have an impact in preservation of the ECM and increasing chance of mechanical dissociation of cells by increasing water content of the tissue. This is better reflected by our previous histological experiments on the effect of BH in perfused vs non-perfused porcine liver.

6.8.5 Effect of perfusion & perfusate on cell harvest

Perfusion and organ viability may in part explain the presence of viable cells in the histotripsy cavity. In our study, perfused livers produced a lesion with core suspension that was aspirated and cultured successfully which was repeatable from every lesion. The liver is a highly vascular organ, and the circulation creates a heat-sink effect for thermal injury. The heat-sink effect of the perfusion in the setting of histotripsy may play an important role in the viability and success of the cells isolates (264). Although, the heat-

sink effect is an important factor to consider in the success of cell extraction, one should bear in mind that the timescales of histotripsy are of the order of milliseconds, whilst the timescales of perfusion are of the order of seconds. Hence, other factors in the perfused model could influence the cell isolation. Since the histotripsy mechanism is non-thermal, the heat-sink effect from blood vessels adjacent to the histotripsy site is unlikely to be a significant factor (341). The cavitation cloud initiation threshold changes with temperature as well as the tissue's strength, density, and water content (457, 458). The water content of the tissue in the perfused model will be higher than that of a non-perfused liver. *Vlaisavljevich et al* (458), demonstrated in 43 types of harvested porcine tissue the importance of tissue density, water content, ultimate stress, and ultimate fractional strain in determining tissue erosion after sonication. This affects the histotripsy profile and rates of heat deposition/transfer around the lesion and makes parametrisation tailored to the tissue an important aspect to consider (457). Such factors attributed to the organ perfusion could explain the success of extracting viable cells from the core lesion. The role of perfusion is more so highlighted by the fact the retrieved liver would become less viable as time passes prior to perfusion. Studies from normothermic machine perfusion of the liver reveal once liver is perfused the viability of the organ is also improved (459).

The organ perfusion system utilised Soltran clinical organ preservation solution (also known as Hypertonic Citrate solution) which may have been an advantage for the cell isolation. This simple solution is based on high concentrations of citrate as the major anion (460) which is also an efficient chelator of calcium ions. The standard collagenase digestion systems are based on two-step perfusions in which an initial perfusion is made with calcium-free solutions (461), on the basis that this starts the process of weakening attachments between the liver cells and extracellular matrix components. Removal of the Ca^{2+} in the first step helps to disrupt desmosomes, while the addition of the Ca^{2+} in the

second step is required for the optimum collagenases' activity (462). Although we didn't use enzymatic digestion, in our model of experimental set-up, the presence of calcium chelators (Soltran Solution) may have a synergistic effect on the histotripsy sonication in tissue dissociation and thus aiding cell harvest.

To our knowledge, our group is first to describe the use of a perfused organ system for evaluating liver histotripsy and the analysis of the histotripsy cavity constituents. The advantage of the perfusion system for cell histotripsy directed cell isolation includes the ability to change perfusate fluid according to the type of liver (463) and alteration of the temperature to adjust for cavitation with the intention of optimising hepatocyte viability.

6.8.6 The cell isolates, culture, and cell viability

Our study reveals that, following treatment with histotripsy, the core lesion contains several live cells that when cultured not only retain their morphology and structure but also retain metabolic activity and divide in standard culture medium. The initial isolate contains a mixture of cells and extracellular debris with the debris being removed following centrifugation.

The subsequent cell isolate would contain hepatocytes and a small number of other cells such as sinusoidal endothelial cells, biliary canalicular cells and fibroblasts. These small cells could be separated from mature hepatocytes by low-speed centrifugal washes (125, 440-445, 464). This was not done in the current experiments as we considered that mixed cell cultures might sustain mature hepatocytes. The cultured cells were alive on day one (average of 16% viability) but remained alive beyond 7 days in standard culture conditions. Overall, the number of isolated liver cells almost doubles by day seven and metabolic activity peaks a week post culture. After a week, the number of live cells starts to decrease in number, most probably reflective of the lack of space in the plate. Mature

hepatocytes could be identified in the cultures as typical large hexagonal cells which by day seven have aggregated in areas of the culture forming a natural 3D network.

It's known that primary hepatocyte culture in-vitro can rapidly lose their cuboidal morphology and liver specific function over a few days (465). In our experimental culture hepatocytes retain morphology & function for longer period. We considered that the success of culturing hepatocytes from the histotripsy aspirate may be related to the aspirate containing some extracellular matrix and some non-parenchymal cells (NPC). The effect of the co-culture of the hepatocytes with endothelial cells and other NPCs has been shown to significantly improve liver specific function of the hepatocytes, and the co-culture system could further promote angiogenesis at a later stage in in-vivo tissue (466). Additionally, hepatocyte and NPC in-vitro co-cultivation can mimic the native hepatic microenvironment (467, 468). Additionally, in-vitro cocultivation of hepatocytes and nonparenchymal cells has been used to preserve and modulate the hepatocyte phenotype and function (469, 470). In our cell culture experiments, there might be limited natural deposition of collagen by the mixed small cell components present along with hepatocytes, thus aiding the natural extra-cellular matrix (ECM) deposition and cell network formation. In contrast the conventional hepatocyte isolation techniques discard non-parenchymal cells through post enzymatic digestion washing steps. Our isolation and culturing method allows both parenchymal and non-parenchymal cells to survive the process and in turn contribute towards the synthesis of ECM post culturing. Non-parenchymal cells such as sinusoidal endothelial cells and Kupffer cells are involved in secretion of bioactive factors and ECM components (471-474). Kupffer cells not only enhance hepatocyte growth factor expression but can also produce growth factors, metalloproteinases, elastase, collagenase and fibronectin (474). As the cell number in the current experiments were insufficient for flow cytometry immunofluorescence staining

will be used in future experiments to further quantify and characterise the cultured cells. Immunofluorescence would allow better identification of cell types isolated and provides a more accurate count of cells cultured.

The CTG assay used in this study has been specifically designed to measure ATP levels in 3D cell cultures, therefore the results obtained after the application of this assay further support the possibility of an ECM being present. The fact we had observed cell clumping together may reflect the cells in culture were organising into 3D clusters of cells. This structuring in-vitro allows for interaction with the cell-ECM cross talk and may have an impact on the longevity of culture, as previously demonstrated 3D hepatospheres retain morphology, live longer, and have increased functionality compared with single layer or 2D in-vitro hepatocyte cultures ([470](#), [475](#)).

CTG measure mitochondrial activity and ATP production; hence the degree of luminescence is proportional to the live cells within the wells. The fact that these cells show metabolic activity almost 21 days post histotripsy and culture mean cells can remain alive beyond a week with their metabolic activity intact using this method. This is an important finding in terms of hepatocyte preservation. Even though the culture medium was not optimised beyond 2 weeks, liver-derived cells were alive 21 days post culture. Longevity is important in cell transplantation especially when dealing with adult hepatocytes. Historically, methods such as supplementation of culture medium with non-physiological inducers (i.e dimethyl sulfoxide or phenobarbital), as well as co-culture with other cell types have been used to enhance longevity of hepatocytes in cell culture([476](#)). This method doesn't require supplementation with non-physiological inducers. Additionally, the Phalloidin & DAPI staining revealed intact cytoskeleton network and clumped group of cells at 7 days post culture. This may reflect connection of hepatocytes via intermediate filaments of cell cytoskeleton with their adjacent cell.

Cells that have formed a network while maintaining their cytoskeleton maybe more stable in maintaining their morphology in cell culture. Hepatocytes are rich in gap junctions and cell proximity improves their interaction. In liver, gap junctions are predominantly found in hepatocytes and play critical roles in virtually all phases of the hepatic life cycle, including cell growth, differentiation, liver-specific functionality, and cell death (477, 478).

6.8.7 Limitation of current study, further evaluation, and possible implications for therapy.

There are several limitations of the current study that could affect quantity of the cell extracted as well as its quality. To name parameters used could be optimised further to yield higher number of cells; use of human liver instead of pig liver makes the parameters more translatable and more suited for clinical use. The ultrasonic probe used targets a small area and hence to gain a high yield of cell it requires repetitive sonication of different areas to accumulate enough extract for cell culture. Whilst relatively low yields were produced by one application of histotripsy, the technique could be repeated rapidly across liver segments to liberate more cells. Limited cells available meant we could not perform flow cytometry to quantify and characterise the cultured cell through a more objective and robust mean. The use of flow cytometry is further limited when the cells clump together in later stages of the culture. The cells harvested showed varying degree of metabolic activity. Future work would entail modifying this model to extract larger numbers of human liver cells, identifying in detail the component in the mixed cell isolates and optimising the conditions required for long term cell culture. Subsequent characterisation of autocrine activity and albumin production would define the functionality of the isolated hepatocytes (479).

6.8.8 Implications for future cell therapy

This technique may be suitable for hepatocyte isolation and subsequent auto-transplantation, which has been demonstrated to be successful in both animal (480) and clinical studies (481). New technologies in gene therapy or gene editing may increase the importance of hepatocyte auto-transplantation. Compared to conventional isolation techniques, this method provides a means of cell harvest and isolation without use of detergents or enzymes. The enzymes used in degradation and decellularization of liver tissue potentially have a cytotoxic effect on the functionality of the isolated cells that can alter the mechanical or genetic property of the cells (387). With the above method a small tissue can be targeted repeatedly without the need for any detergent to yield cells for harvest over a period of less than a minute. The reproducibility of the technique along with fast cell harvest makes it a unique technique to consider in regenerative medicine and cell transplantation.

In summary, this is the first time that histotripsy is used for cell isolation with reproducible results in a perfused liver model. Results from our study present a novel method for cell isolation and tissue decellularization that can be devoid of chemicals and is faster than conventional chemical decellularization and harvesting techniques. Its implication in clinical transplantation and regenerative medicine are substantial. Further optimisation of the technique is required to ensure higher quality yield with increased number of cells harvested. Future studies should aim to answer the limitations of the study and assess suitability of the harvested cells for transplantation. Although this is a pilot study has yielded novel results, it requires validation of the technique in human tissue for clinical use. In addition, with adjustment of the parameters the technique can be applied to other tissues for cell harvest and culture such as kidney and pancreatic tissue.

Chapter 7 Preliminary study on histotripsy assisted 3D-hepatocyte cell transplantation in in- vivo rat liver

7.1 Background

The human liver has the greatest regenerative capacity of any organ (482). Hepatocytes account for more than 80% of liver mass and are key in liver regeneration (483). Viral infections, metabolic disorders, excess alcohol consumption, and when chronic, can progress to end-stage liver disease (484). In chronic liver disease, a chronic loss of hepatocytes occurs, as well as diffuse inflammation, leading to fibrosis and cirrhosis (135, 483). During fibrosis, the proportion of senescent hepatocytes increases, and the progression of the disease to liver fibrosis is associated with liver regeneration impairment (135). Chronic liver disease and fibrosis are associated with high mortality and morbidity rates, highlighting the need for effective treatment.

Liver transplantation (LT) is the only life-saving cure for end-stage liver disease but is limited to a select number of patients due to a severe shortage of organ donors (484). Since this is unlikely to improve in the future and the demand for liver transplant is predicted to increase in the next 20 years, research has focused on regenerative rather than replacement strategies to overcome these limitations (118, 164). In the last decade, this focus has shifted from traditional techniques such as cellular therapy to novel engineering of tissue scaffolds, 3D printing of tissues and novel approaches such as histotripsy-assisted cell implantation (348). The success of these strategies to clinical practice remains to be established and further research is needed to address the barriers limiting their incorporation into clinical practice. Nonetheless, regenerative medicine could provide a needed alternative to liver transplantation.

7.2 Introduction

The liver is essential to life as it produces key proteins and removes harmful toxins from the blood. Despite enormous regenerative capacity, if the liver fails, transplantation is the only hope for survival. Due to the shortage of donor organs, cell therapy is an attractive alternative (485, 486). Cell therapy can be used to add cells to the liver or to remodel and repair the damaged liver (486). While functioning liver cells can be generated from stem cells in the lab, the current inefficient method of cell transplantation is the major bottleneck (486).

In our previous studies we have shown that histotripsy can produce discernible lesion in perfused porcine livers. The histology of which revealed lesions with subcapsular location (0.5cm typically) and a length between 0.5 to 1cm with sharp boundaries. The preservation of parenchyma at the edge of the lesion. The cavity created with greater degree of ECM preservation in perfused models makes it a nidus for implantation. Our 3D reconstruction of the images revealed the morphology of the lesion that and its relationship to the vasculature and biliary tree. More so, our analysis of the cell aspirates from the core of the lesions revealed viability of the cells that had retained its morphology and regenerative capacity. Our prior work has led us to set experiment to analyse effect of histotripsy in in-vivo animal models.

Amongst several animals that can be used for in-vivo study of histotripsy and liver regeneration, rat is a suitable model. Rats have been widely used in liver regeneration research due to the well-characterized surgical procedures, such as the 70% partial hepatectomy introduced by Higgins and Anderson in 1931 (487). In addition, the regenerative responses in rat mimics human liver regeneration in many physiological and molecular aspects making them an ideal cost-effective model to study liver regeneration process (483, 488). Previously, histotripsy parameters were optimised for rat livers in

Prof Saffari's group (449). They demonstrated in their that direct injection of cells inside the cavity in the in-vivo rat model can facilitate successful uptake, proliferation and integration of the transplanted hepatocytes in the recipient liver with restoration of plasma albumin level to 50% of the normal level in Nagase analbuminemic rats.

Here, we aimed to test a new method for cell transplantation by using boiling histotripsy parameters to create small cavities in the liver into which stem cell-derived 3D hepatocytes were transplanted.

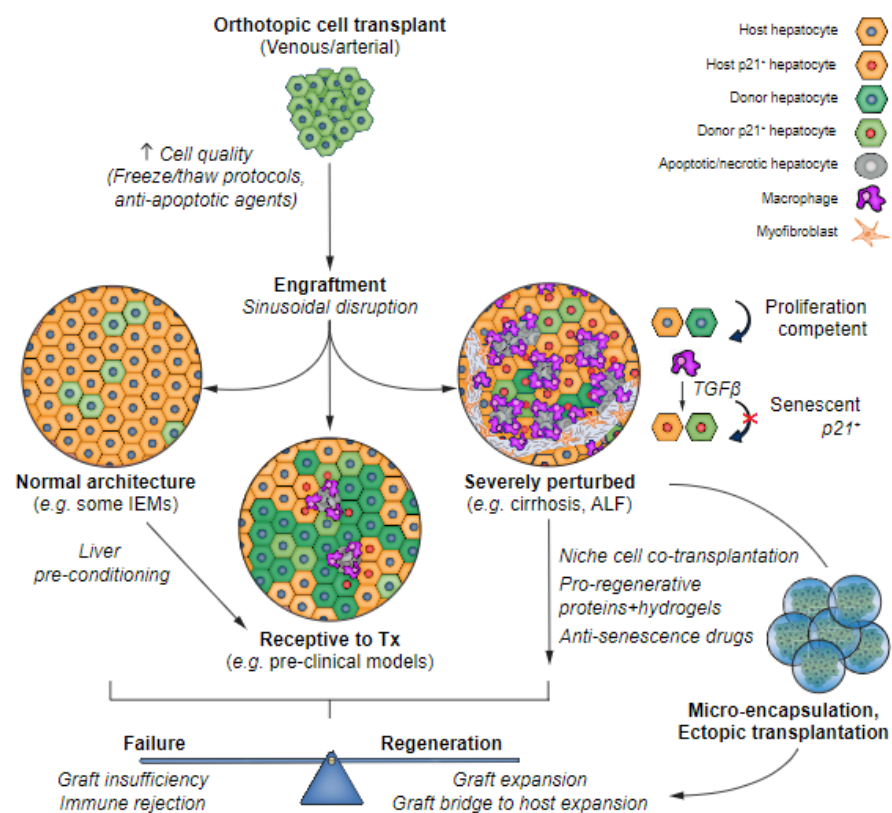


Figure 60 - The first barrier to successful hepatocyte transplant is cell quality, which has been improved by optimising cryopreservation/thawing techniques. Liver preconditioning induces endothelial cell apoptosis, allowing donor cell integration into hepatic cords. The distorted microenvironment of severe injury is challenging for donor engraftment/proliferation. Macrophage TGFb spreads p21-induced senescence in host and donor hepatocytes. Strategies to mitigate the severe niche include co-transplantation of immunomodulatory cells, inhibiting senescence, or growth factor treatment. Hepatocytes can be encapsulated and transplanted extrahepatically to circumvent the liver injury niche and avoid immune destruction. Successful cell transplant currently provides a functional bridge to host regeneration/orthotopic liver transplantation. ALF, acute liver failure; TGFb, transforming growth factor-b (486)

7.3 Study Aims

The aim of the study was to demonstrate successful creation of histotripsy lesion which could act as nidus for implantation and successful engraftment of stem-cell derived 3D hepatocytes in rat model. In addition, we aimed to assess the short-term safety of injected 3D heps in the immunocompetent rats.

7.4 Study Objectives

- Evaluate the effects of histotripsy treatment on liver tissue in a rat model.
- Assess the feasibility and efficacy of 3D hepatocyte transplantation into histotripsy-induced liver lesions.
- Monitor the biochemical and physiological changes post-treatment through blood analysis.
- Investigate the histological outcomes of histotripsy and cell transplantation on liver tissue regeneration.
- Compare the outcomes of histotripsy alone versus histotripsy combined with cell transplantation.
- Determine the viability, integration, and functionality of transplanted 3D hepatocytes at the lesion site over a one-month period.

7.5 Hypotheses

Histotripsy creates lesions suitable for 3D-hepatocyte implantation and cells can be implanted successfully and safely without any problems for up to a month.

7.6 Methods:

We utilised 16 healthy male rats with 6 allocated to the control group and 10 to the experimental group. The control group was only subjected to histotripsy treatment. The experimental group had cell transplantation (3D heps) immediately after treatment with histotripsy. 3D hepatocytes were directly injected into the lesion site. Post treatment the animals were recovered and then sacrificed in timed intervals of up to a month. Prior to termination a blood sample was collected to monitor biochemistry. The liver was harvested and divided into two parts: one part was sent in formaldehyde and the other part was immersed in isopentane and then frozen with liquid nitrogen.

7.6.1 Overall Study design:

Immunocompetent healthy Sprague Dawley rats were randomly grouped into control (n=6) & an experimental group (n=10) (**Figure 61**). The animals were housed in The Griffin Institute (Northwick Park Hospital, London) animal facility and allowed two weeks of acclimatization prior to commencing experiments. Following the two weeks the animals had their weight measured and their health checked by the in-house vet.

The control group underwent histotripsy to the liver and the test group underwent histotripsy to the liver + 3D hep transplantation. Both groups had a laparotomy, and the liver was exteriorised so that the ultrasound probe had direct contact with the liver. Each animal liver had formation of a single histotripsy lesion. For the intervention group, following histotripsy, the site was marked, and the cells injected into the histotripsy cavity.

After the intervention a 5 min observation was performed before closure of the abdomen, to ensure no immediate complication (eg., bleeding). After closure, the animals were

recovered, and some were culled after Day 15 and the rest on day 28 (depending on group allocation). Termination points discussed in subsequent sections. Prior to termination, blood samples are taken for functional correlation after histotripsy treatment for both groups and animals health would be monitored throughout up to the point of termination. Post termination, an autopsy is performed with the whole liver explant for histological analysis.

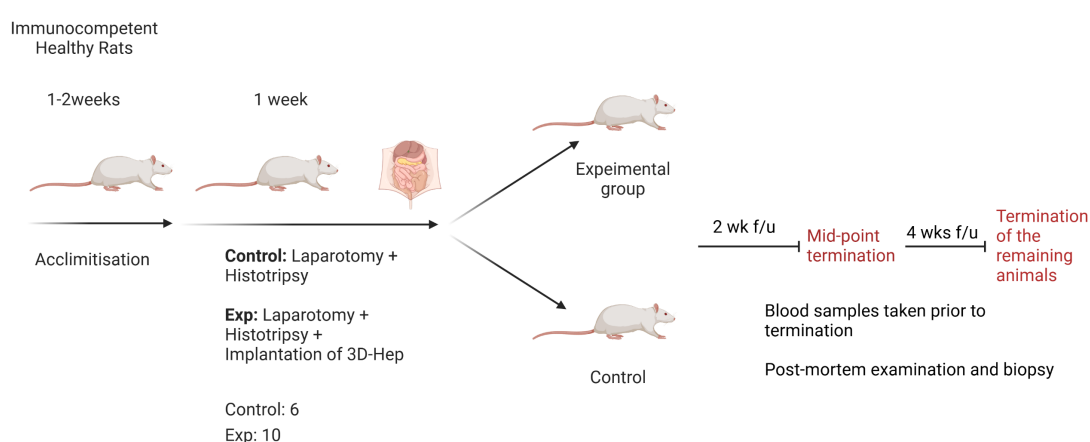


Figure 61 – Overall experimental design, allocating 16 healthy, immunocompetent rats to two groups: control & experimental arm. Control arm had 6 rats and experimental arm had 10 rats that were both subjected to laparotomy and histotripsy sonication. The experimental group received injection of the 3D-Hep into the lesion site. Animals were terminated at specific time point: 2 weeks (mid-point) and 28 days post sonication.

7.6.2 Regulatory Guidelines

The UK (United Kingdom) Home Office controls scientific procedures on animals in the UK and does so by the issue of licences under the Animal (Scientific Procedures) Act 1986. The regulations conform to the European Convention for the Protection of Vertebrate Animals Used for Experimental and Other Scientific Purposes (Strasbourg, Council of Europe) and achieves the standard of care required by the US Department of Health and Human Services Guide for the Care and the Use of Laboratory Animals.

The Home Office Project Licence governing this study (Project Licence - PPL: P0FCC1CA1; Protocol Number: 01; Project Licence Title: Prevention of post-surgical adhesions; Project Licence Holder: S Vara) directly specifies the regulated procedures required on this project, severity limits and possible adverse effects on the animals.

As part of our local practices and in accordance with Home Office Guidelines, this study has been presented and reviewed at our AWERB. Specifically, AWERB_17.

No formal claim of Good Laboratory Practice (GLP) compliance is made. The study was conducted in accordance with the standards of the Test Facility. Test Facility study number SF.UCL.08.21.

7.6.3 Histotripsy set up & parameters

A schematic representation of the histotripsy unit is shown below (**Figure 62**). A 2 MHz single element bowl shaped transducer (Sonic Concepts H-148, Bothell, WA, USA) with an aperture size of 64 mm and a 22.6 mm central opening was used with a transparent coupling cone (Sonic Concepts, C-101, Bothell, WA, USA) filled with degassed, de-ionised water (**Figure 63**). The transducer was driven by two function generators (Agilent 33220A, CA, USA) in series via a linear radiofrequency (RF) power amplifier (ENI 1040 L, Rochester, NY, USA). The first function generator was set to generate 50 cycles of a 1 Hz square wave with 1% duty cycle. This triggered the second function generator, that outputted a 2 MHz sinusoidal wave into the RF power amplifier. A power meter (Sonic Concepts 22A, Bothell, WA, USA) was connected between the RF amplifier and the HIFU source, and the electrical power P_{elec} supplied to the transducer was monitored to be approximately 150 W. During the experiments, a polyurethane rubber acoustic absorber (AptFlex F28, Precision Acoustics Ltd, UK) was placed under the rat to

minimise ultrasonic reflections. The parameters and setup were previously validated by Prof Saffari's Group (449). The parameters were expected to create subcapsular lesions that were approximately 0.5cm in size. The amplitude of the 2MHz voltage was 561 mv peak-to-peak (Table 15).

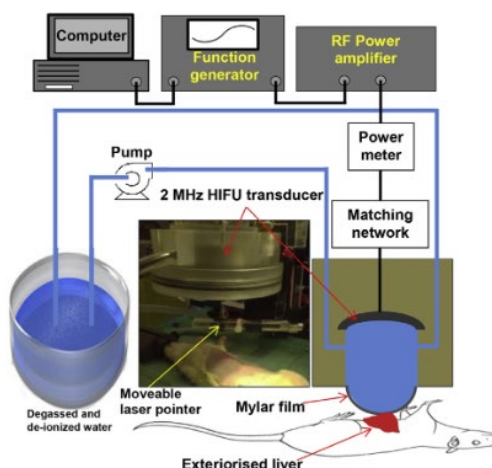


Figure 62 – Schematic representation of the experimental set up of the histotripsy unit. The HIFU transducer probe is placed directly above the rat liver and positioned with an x,y,z manual positioner guided by a laser pointer (adapted from Pahk et al (449))

To achieve consistency, the propagation distance in the liver was set to 5 mm during the experiments. The rat liver was partly exteriorised to maximise the contact with the US probe, to help localisation of the lesion and to allow direct delivery of the 3D Heps into the created lesion. For the duration of sonication, the probe was in contact with the surface of the liver. After the sonication process +/- delivery of the cells the liver was returned to the abdomen and after a 5-minute observation period the abdomen was closed with sutures.

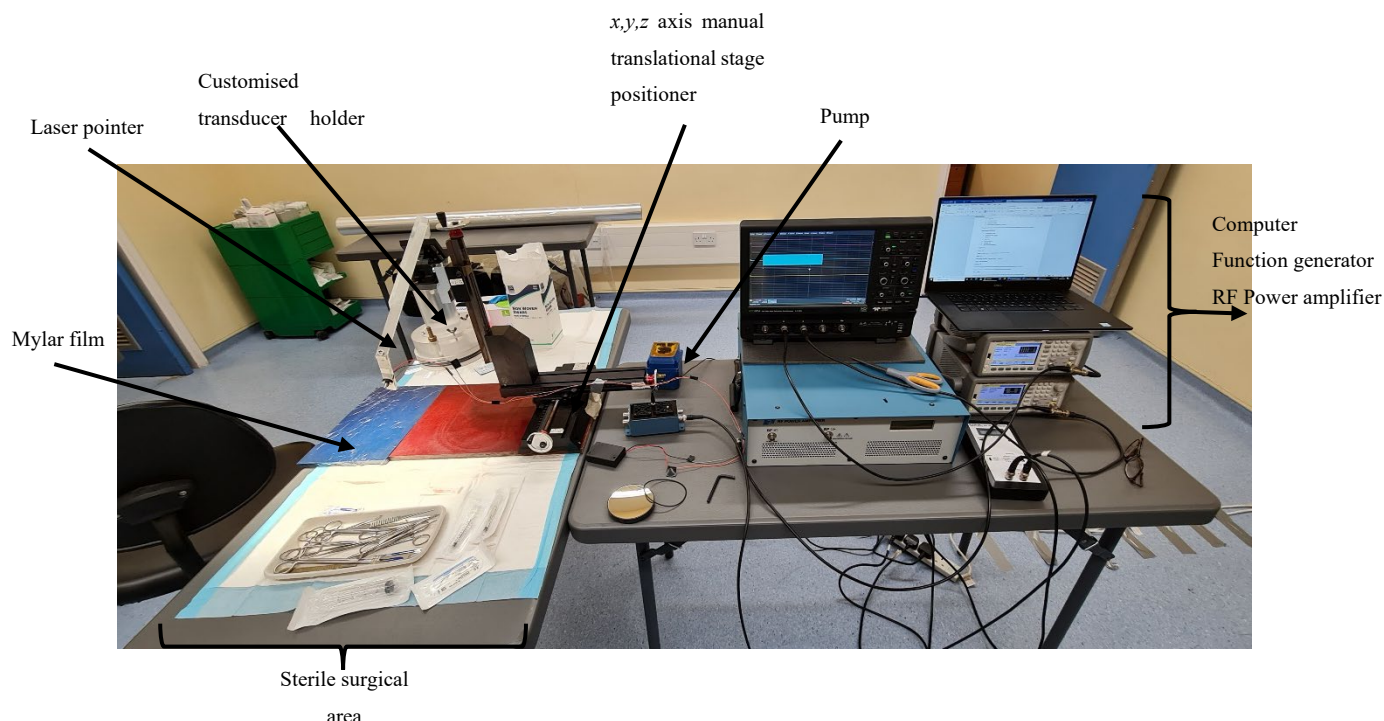


Figure 63 – HIFU experimental set up for sonication of rats in the animal facility. The transducer is held in position with the aid of an x,y,z axis manual translational stage positioner which allows positioning of the transducer over the liver. The pump delivers de-gassed water to the customised transducer holder. The computer and the function generator are set to the pre-defined parameters and the RF power amplifier delivers the histotripsy dose via the 2.0 MHz probe. With the aid of the laser pointer the probe is positioned in the correct area over the rat liver.

Table 15 – Parameters & setting used for the for the 2 MHz Transducer to apply the histotripsy

2 MHz Transducer					
Master Agilent			Slave Agilent		
Frequency	1Hz		Frequency	2 MHz	
Amplitude	2Vpp		Amplitude	561 mVpp	
Offset	0 V		Offset	0 V	
Duty Cycle	1 %				
Cycle Count	50 cycles				

7.6.4 3D hepatospheres development and maturation

The stem cell derived 3D hepatocytes were developed by Dr H. Rashidi as per his published protocol (489). The process for maturation and derivation of the 3D Heps began approximately 30 days prior the sonication of the rat liver (Figure 64). This is because the hepatoblast formation and maturation takes place around day 20 and subsequently are maintained in special medium with growth factors. These 3D Hep have been shown previously to remain stable for up to one year and maintain their function for around 365 days (383). The 3D Heps were developed and matured in the Institute of Child Health, GOSH and then stored in dry ice to be delivered to the animal facility on the day of the experiments.

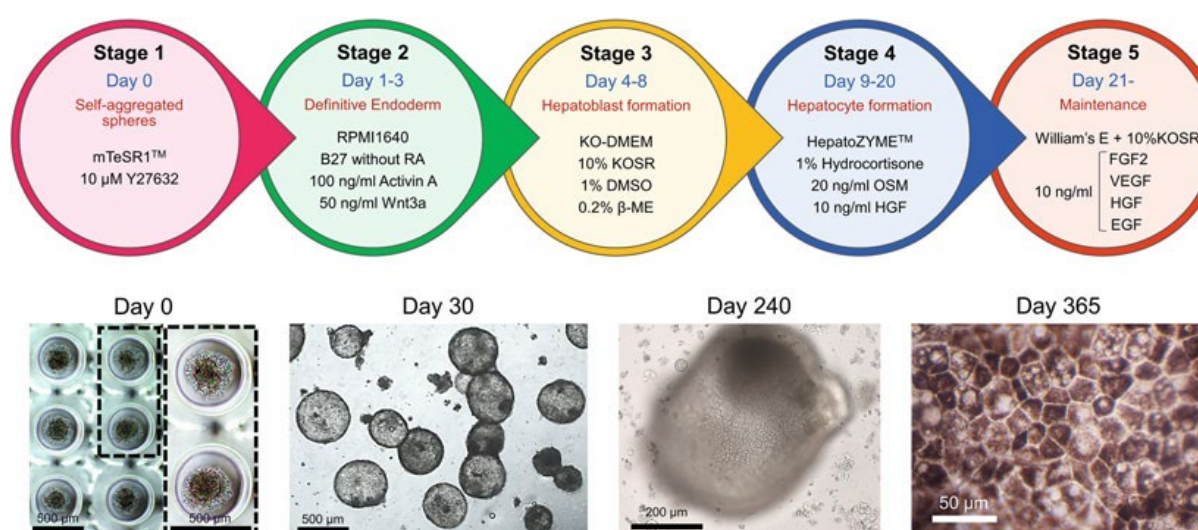


Figure 64 – Schematic representation detailing the stepwise differentiation protocol to generate 3D hepatospheres (3D Heps) from hPSCs. The hPSCs are sequentially directed through different stages to yield 3D Heps which maintained their phenotypes for an extended period in culture (383).

7.6.5 Animal Model & Husbandry details:

Immunocompetent Sprague Dawley rats (Supplier: Envigo, 3 Sovereign Ct, Huntingdon PE29 6YL) were used for this experiment. 16 healthy male rats were allocated in to arms randomly as described before. Male rats will be used to avoid hormonal fluctuations. The

average weight of the animals at day 0 (arrival in the facility) was 260 grams (151-175g). The weight of the animals was then closely monitored at days 9, 16, and 29. Upon arrival to the facility (arrival date: 2nd Jun 2021) the animals were allowed a 10-day acclimatisation period. The animals were examined for general health by the NACWO shortly after arrival and before inclusion in the study. The general health of the animals was observed prior to, and post-surgery and findings were reported on animal record as per study protocol. Also, upon arrival animals were marked at the tail with animal number in black felt-tip pen. Animal cages were identified by a label containing study specific information including study number, animal ID and sex.

The animals were paired in plastic boxes with wire lids (**Figure 65**), containing wood chip bedding prior to and following surgery. Animals will receive standard feed and water and will be housed in standard temperature-controlled room 20-24°C, relative humidity of 50+/- 10% with an alternating light/dark cycle 12/12 hours. The animals were kept on the basal diet of RM1 (P) pellets (Special Diet Services, Essex) available *ad libitum*. Similarly, water (supplied by Three Valleys Water) was available *ad libitum*. No known substances were expected in the diet or in the drinking water which might adversely affect the result of the study.



Figure 65 – animals were paired into one cage pre- and post-surgery. The remained on the basal diet of pellet throughout the period of the experiment.

7.6.6 Experimental Procedure

7.6.6.1. Procedures Pre-Surgery

The animals were weighed on the day of surgery. The general health of the animals was observed as per protocol. The in-house vet confirmed inclusion. Blood (2 mL) was collected in the week prior to surgery from a superficial caudal vein for clinical pathology.

7.6.6.2. Anaesthesia & Preparation

For each animal, the animal was placed into an anaesthetic induction chamber. Flow of Isoflurane with oxygen was gradually increased until anaesthesia is induced. The animal was then removed from the chamber and general anaesthesia maintained with Isoflurane and oxygen via a close-fitting mask. The fur of the abdomen was removed with clippers. The identification number was marked on the base of the tail with a marker pen. The analgesic Carprofen (0.1 mL/kg) and Buprenorphine (0.02 mL/kg) was administered subcutaneously. The animal was transferred to the operating theatre (**Figure 66**). The animal was placed in the appropriate position on the operating table. Anaesthesia was

maintained with Isoflurane and oxygen via a close-fitting mask. The exposed skin was cleaned with Chlorhexidine (Animal Care Ltd). The animal was covered with sterile drapes in such a way, to leave only the operative site exposed. All procedures were performed using aseptic technique from this point on.

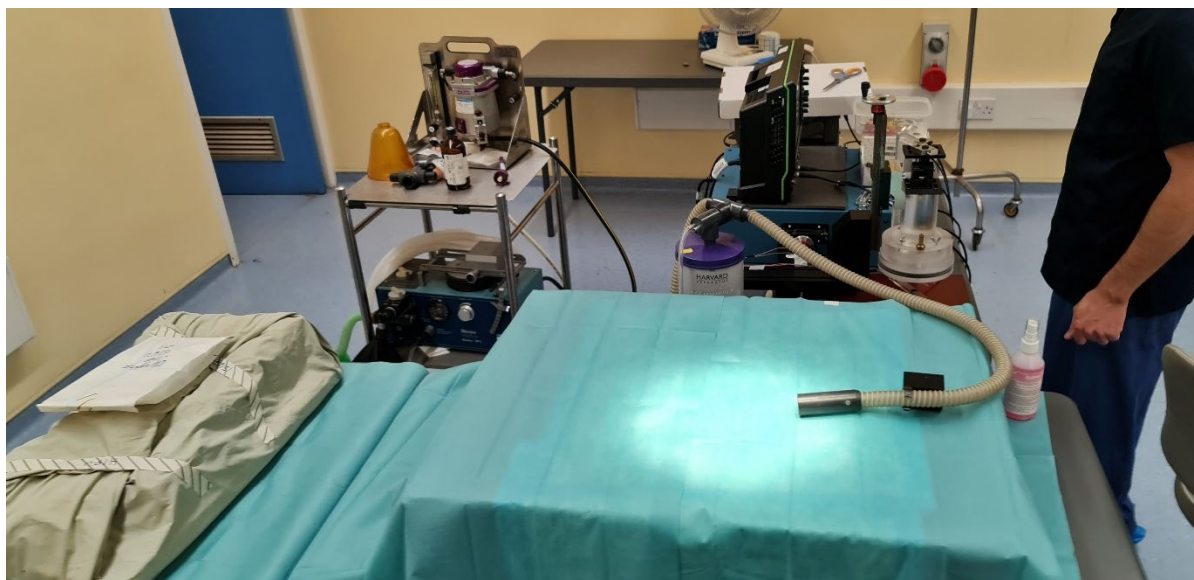


Figure 66 - Demonstrates the sterile field were test subjects would be placed along with the anaesthetic circuit used for the delivery oxygen and Isoflurane for the period of the surgery.

7.6.6.3. Surgical Procedure, Sonication & Cell transplantation

Surgery:

The day of surgery was considered as study day 0. The surgical procedure for each animal was performed as follows: 2 drops of lidocaine 2% were applied topically to the incision site, as local anaesthetic. An upper midline laparotomy was performed to expose the liver and the skin retracted using 4-0 prolene sutures and weighted down with mosquito forceps (**Figure 69**). The right lobe of the liver was then exteriorised (**Figure 68**).

Sonication:

The Histotripsy probe was then lowered onto the exposed liver (**Figure 69**), so the centre of the probe was in contact with the exposed area of the liver. The positioning was guided

by the laser pointer and the aid of the manual positioner. Once placement was confirmed, the histotripsy was applied to create a lesion.



Figure 67 – Operative field, sterile drapes and aseptic technique used throughout the procedure. Following mid-line laparotomy traction suture were used to maximise exposure to the surface of the liver.



Figure 68 – Following laparotomy the right lobe of the liver was exteriorised by mobilising the anterior ligamentous attachment. The liver was pulled out and down slightly so its anterior surface is maximally exposed, and the probe can be placed directly over the right lobe.



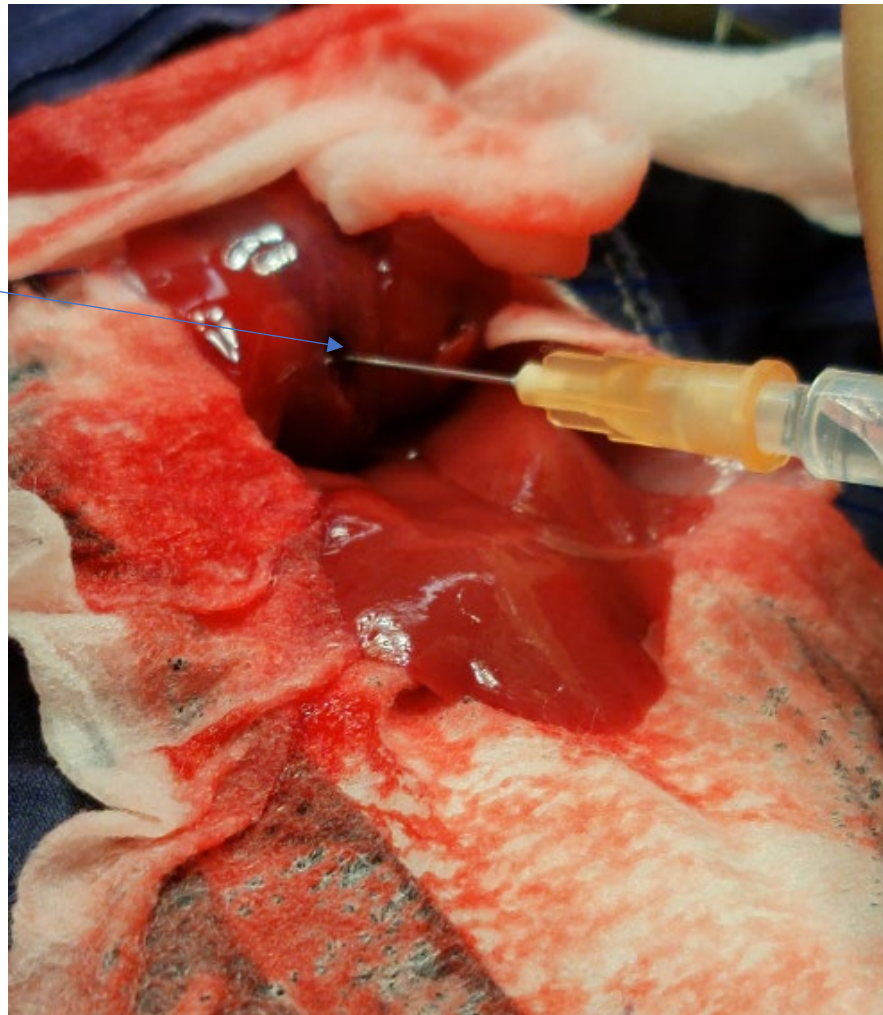
Figure 69 – Demonstrating the positioning of the rat and the probe directly over the liver. A sterile syringe was placed behind the lumbar spine prior to draping to accentuate the curvature and bring the liver further to the surface. (Above picture is only a demonstration of how positioning would be done prior to draping).

For the control group, after the exposure to histotripsy there was a period of 3-5 min observation for any point of bleeding. If there were no adverse events, then the abdomen was closed in layers with 3-0 vicryl first and then 3-0 prolene to the skin.

Cell Transplantation:

For the test group, after the exposure to the histotripsy, 3D hepatocyte cells were injected into the lesion using an orange needle (**Figure 70**). Once injection was completed there was a period of observation prior to closure of the abdomen. Veterinary Wound Powder and Opsite were administered to the closed wound sites all subjects. The animal was allowed to recover, collars placed on each animal to prevent cutting sutures and taken back to the accommodation area.

Posterior aspect of the Right lobe of the liver, the histotripsy has puncture through the posterior capsule. The defect is the lesion site.



Pre-loaded syringe with 3D Heps with a hypodermic orange needle

Figure 70 - Reveals a lesion site. The histotripsy has gone through the lobe and punctured the posterior capsule of the right lobe thus exposing the lesion site. The 3D Heps were injected directly into the cavity using a hypodermic orange needle.

7.6.6.4. Post-Surgery

Observations

Assessments of general appearance, physical activity, appetite, urination, urine appearance, defaecation, and faeces appearance. Water and food consumption were not measured. We monitored for any post op bleeding from day 1 up to week 1. Post-surgery animal weight was measured at day 9, day 16, day 23 and day of termination. Animals were observed for any evidence of wound infection.

Post-Surgery Analgesia

Carprofen (0.1mL/Kg) was administered for 3 days, and then as required.

Suture and collar removal

After a conversation with the Study Director and NACWO, it was decided that sutures were to remain for the duration of the study.

7.6.7 Termination

The procedure for the scheduled (or unscheduled; if animals were critically ill then they would be terminated) termination (study day 28) for each animal was as follows: Each animal was anaesthetised as per section 7.6.6.2. An intracardiac blood sample (up to 5mL) was taken for processing. The samples were then packed in a polystyrene box, packed with ice, for transport. The animal was then euthanised using an intraperitoneal Sodium Pentobarbitone overdose. A femoral stab was carried after overdose to ensure termination. All observations were recorded on the post-mortem examination. After termination, the liver was exposed, and the right liver lobe or the entire liver was harvested. The territory of the lesion was marked with 4 needles, for ease of identification. In addition, any suspicious organ or lesion was retrieved for further histological assessment. Termination was carried at mid-point of the study and on the last day, break down as described in section 7.6.7.

Termination Date	Animal ID
Mid-point	1/2/3/4/5/9/10
Last day	6/8/11/12/13/14/15/16*

Post-mortem examination & biopsy

After termination and confirmation of death as per section 7.6.7, the animal was placed on the operating table and a thoraco-laparotomy incision was made to expose all the internal organs (**Figure 71**). A careful incision and inspection were performed so the liver and the other abdominal organs remain intact and any abnormality on gross inspection was documented. After the incision the skin edges were retracted using artery clips. After general inspection, liver was retrieved as a whole organ. If the upper aspect of the right lobe of the liver was adhered to the diaphragm, then liver along with a patch of diaphragmatic muscle was harvested for histological examination (**Figure 72**). A stepwise inspection was performed: first liver and the histotripsy site examined, then peritoneum and omental inspection; followed by inspection of the bowel and lungs. Any other organ of interest was removed en-bloc for further histological examination. The tissues were preserved in formaldehyde with the remaining 5 being preserved as frozen specimen as per (**Table 16**).



Figure 71 – Post-mortem examination of the internal organs was performed via a thoraco-laparotomy incision. This exposed the liver, abdominal organs including the spleen and the kidneys, as well as the lung and heart.

Liver
capsule
adherent to
diaphragm

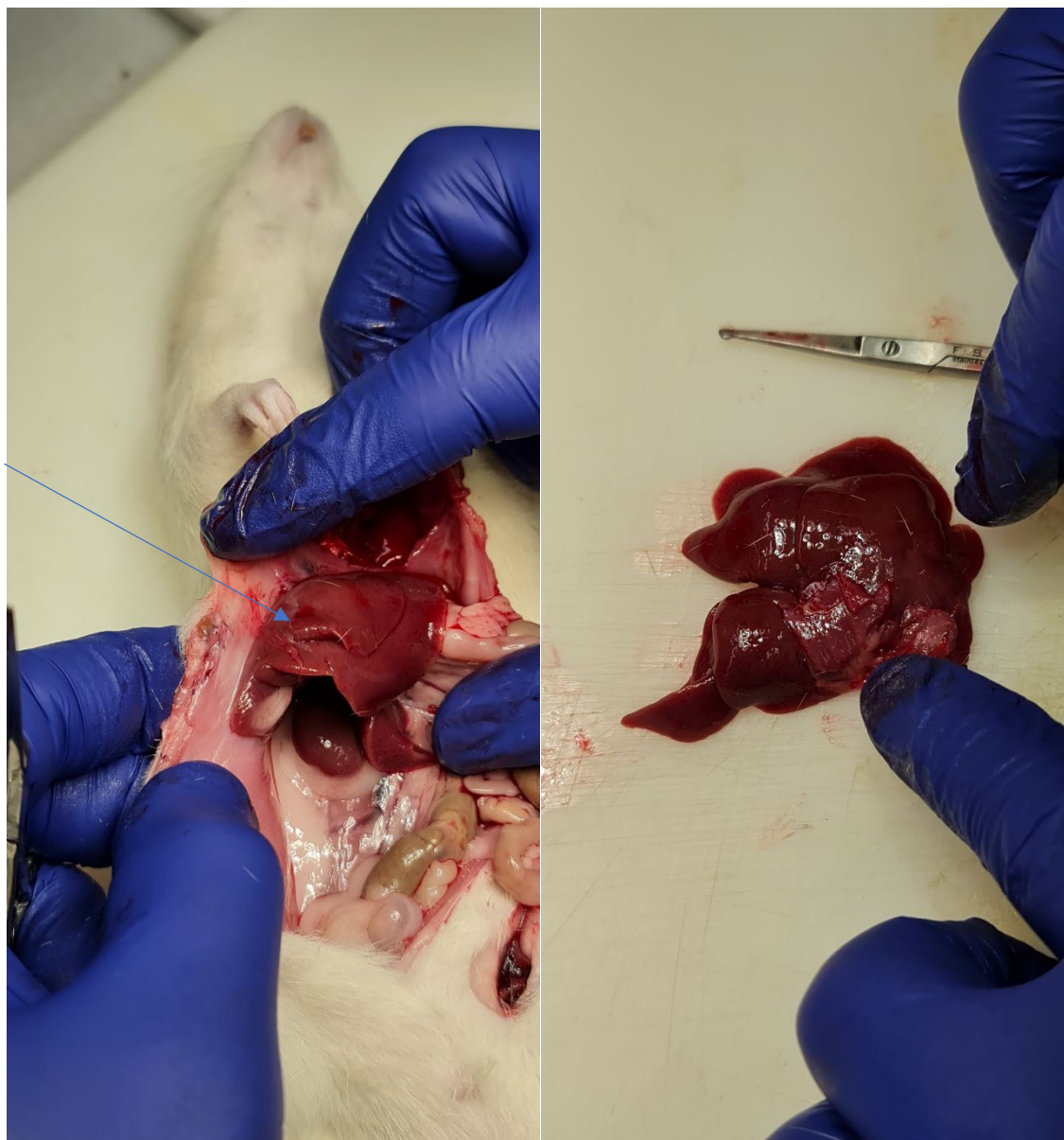


Figure 72 – Demonstrating adherent liver to the diaphragm and the excision biopsy entailed retrieval of the whole liver along with the patch of the diaphragm. This ensured minimal damage to the liver.

7.6.8 Histopathology & Clinical Biochemistry

Histology and histopathological evaluation were arranged by a dedicated liver pathologist (Prof Quaglia). Livers were retrieved at specific time point and would be persevered in formaldehyde solution or preserved as frozen tissue for H&E staining and histological examination. As per allocation below (**Table 16**), lobes were either taken for immersion in formaldehyde. Only 2 test samples from each group would be used to be immersed in isopentane first before being frozen by liquid nitrogen. The mid-point termination group

have three frozen samples taken. All samples were transported on dry ice, for processing outside of the test facility. Blood samples (5-10 mL) were collected prior to termination for processing outside of the test facility. Animal 7 was terminated prior to the scheduled termination date and no blood was taken. All the frozen samples were stored in the cryofreezer at the pathology lab. The frozen samples were stored in -80°C freezer until analysis.

Table 16 – Histology allocation for sample collection and preservation at mid-point and end of the experiment.

Termination Date	Animal ID	Treatment group	Preparation for Histology
Termination at 28 th day	1	Control	Formaldehyde
	2	Control	Formaldehyde
	3	Control	Formaldehyde
	4	Test	Formaldehyde
	5	Test	Frozen
	9	Test	Formaldehyde
	10	Test	Frozen
Mid-point termination	6	Control	Formaldehyde
	8	Control	Formaldehyde
	11	Test	Frozen
	12	Test	Formaldehyde
	13	Test	Formaldehyde
	14	Test	Frozen
	15	Test	Formaldehyde
	16	Test	Frozen

7.6.9 Histological Preparation

Preserved tissues in the formaldehyde were taken to pathology lab for further examination and cross-sectioning. Prior to cutting using a microtome, the organs were examined by

expert liver pathologist (Prof. Albert Quaglia), and the organs were sliced into thinner slicer for better formaldehyde immersion and fixation (**Figure 73**). The tissues were labelled and further treated with formaldehyde.

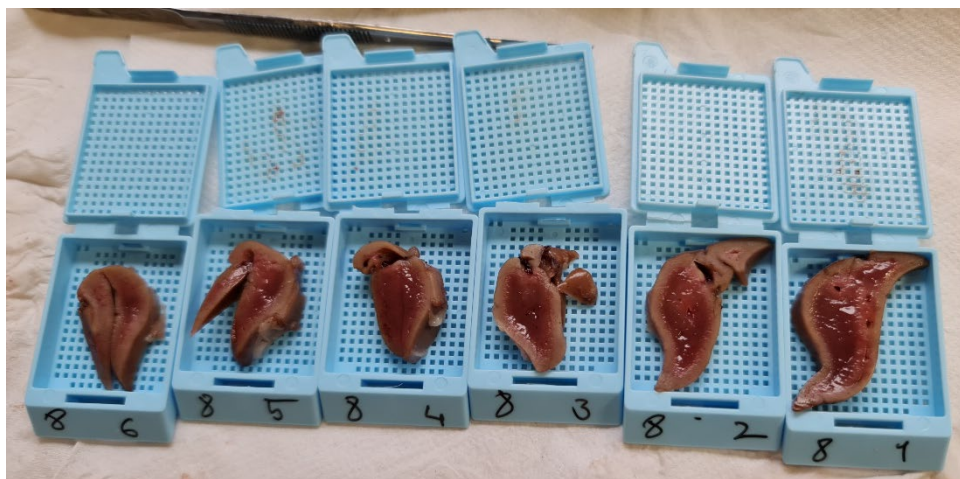


Figure 73 – Example of a rat liver divided into thin slices and each slice preserved in a separate cassette for further fixation with formaldehyde. Each cassette is then labelled according to the rat ID number and number of slices recorded (i.e. rat number 8 with the whole liver divided into 6 slices).

7.6.10 Biochemical analysis

Routine blood tests were taken to termination as described 7.6.6.1

7.6.10.5. Enzyme-Linked Immunosorbent Assay (ELISA)

Two dimensional and 3D mature hepatocytes (for differentiation methods see **section: 3.16**) derived from hiPSCs were incubated with HepatoZYME™ medium for 24 hours at different time points. For ELISA methodology see **section 3.17**.

7.6.10.6. Cytochrome P450 Assay

Cytochrome P450 was measured using the Luciferase assay as described in **section 3.18**.

7.7 Results

7.7.1 Functional assessment of the 3D Heps pre-implant

A pre-culture analysis of CYP3A metabolic activity was carried for characterisation of the 3D Hep cells in vitro. CYP3A activity was recorded over the 24-hour period. The cells showed an increasing CYP3A activity at 1.5 hrs and 4 hrs pre-culture (**Figure 74**), indicating no external or endogenous influence on the cell's metabolic capacity.

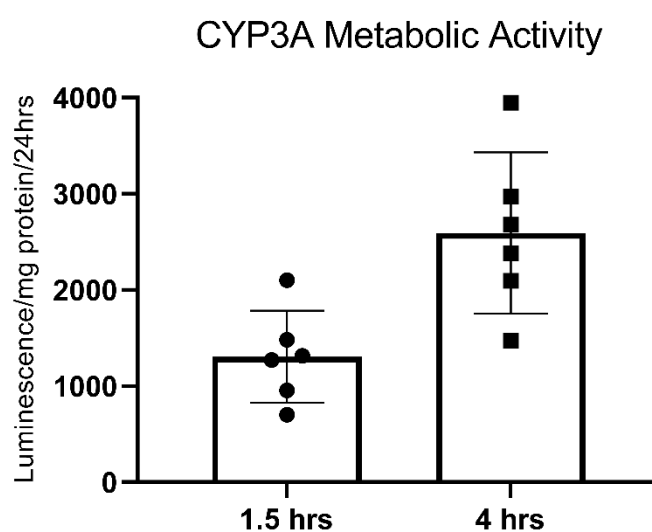


Figure 74 – CYP3A metabolic assay of the cell prior to culture indicates cells to be metabolically active

7.7.2 GA histotripsy

All subjects were successfully received GA, laparotomised and treated with histotripsy. There were no intra-op complications following histotripsy. All 16 rats, but one, were successfully recovered after the operation.

7.7.3 Histotripsy Lesions & Cell transplantation

Histotripsy sonication

In both groups liver was exteriorised without any damage and histotripsy probe was placed successfully over the right lobe of the liver using laser guidance. Placement was successful in all cases without any crush injuries to the liver.

Capsular breach

Following histotripsy sonication majority tolerated it well and, in all circumstances apart from two, the posterior capsule was breached without any damage to the structures sitting posterior to the liver (**Figure 75**). No immediate significant haemorrhage following sonication noted and any small bleed was controlled using pressure with a gauze. Haemostasis was achieved prior to cell injection and closure. No damage or breach of the other organs was noted intra-operatively after sonication.

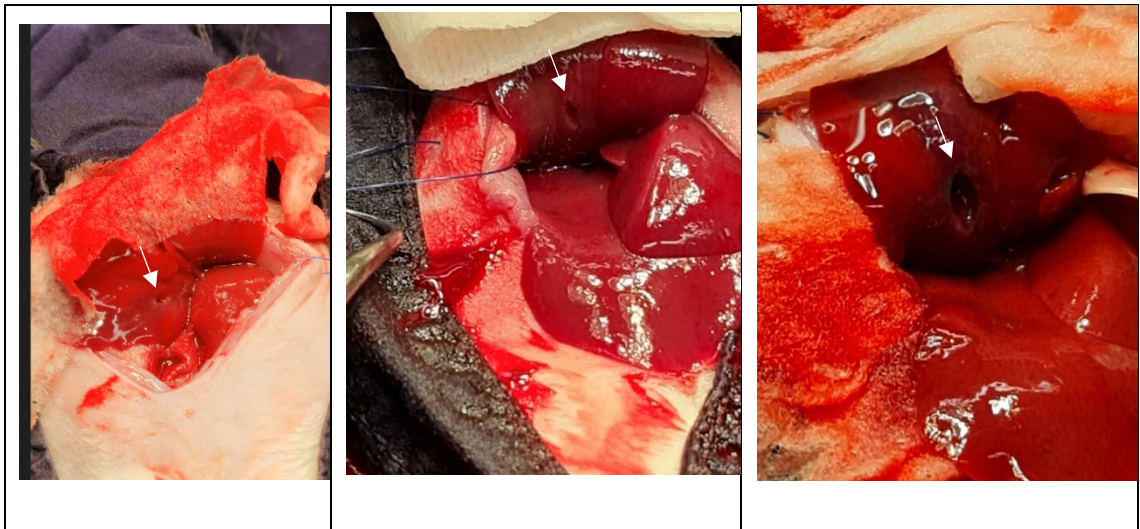


Figure 75 – Post sonication, there was a breach of the posterior capsule of the right lobe. The lesion was evident to gross examination. There was no significant immediate bleed from the lesion site. Haemostasis was achieved prior to cell injection and closure of the abdomen. The white arrow points to the lesion site and shows breach of the posterior capsule of the liver.

Cell implant

In all the cases a successful dose of 3D Heps were injected into cavity. In instances of the capsular breach, the cells were delivered directly into the cavity area under direct vision.

There was no note of the cells being washed out of the cavity during the operation.

Bleeding

There was no major bleeding that would compromise animals hemodynamic and physiology of the animals intra-op. Any small bleeding point was controlled with gauze and pressure. All animals had haemostasis achieved at the end of the 5 min haemostatic break prior to closure.

7.7.4 Recovery (Cell implant vs control)

All animals were recovered successfully immediate after the laparotomy. Only one animal had an unscheduled termination. Test subject (Rat ID 7) had unscheduled early termination following surgery. This animal had a prolonged recovery and took longer to wake up from anaesthesia. The animal appeared unwell and was terminated 12 hours after surgery. No postmortem was performed for Rat ID 7.

7.7.5 Weight gain

Weight gain post-surgery was considered a surrogate for a healthy animal (raw data in supplement 3). The variability in weight is shown in **Figure 76**. Comparison of the weight at day 0 between the subjects in the midpoint termination group and the full-term termination revealed no significant differences (mean: 262.1 vs 257.3; P-value < 0.72). Similarly, there was no statistically significant difference between the mid and full termination group at Day 9 (281 vs 262.3; P-value<0.93). The gain of weight in the mid termination group between day 0 and day 9 was shown to be significant (262.1 vs 281; P-value<0.0048). the difference in gain of weight in the full termination group from day

0 today 9 was not significant ($P\text{-value}<0.36$). For the animals remaining in the experiment after the mid-point termination there was a significant change of weight from their base line of day zero on days 23 (262.1 vs 332) and 29 (262.1 vs 350.8) ($P\text{-values}<0.0001$ for both). No significant difference was observed between the control and the test group of the mid- or full-point termination (**Figure 77 & Figure 78**).

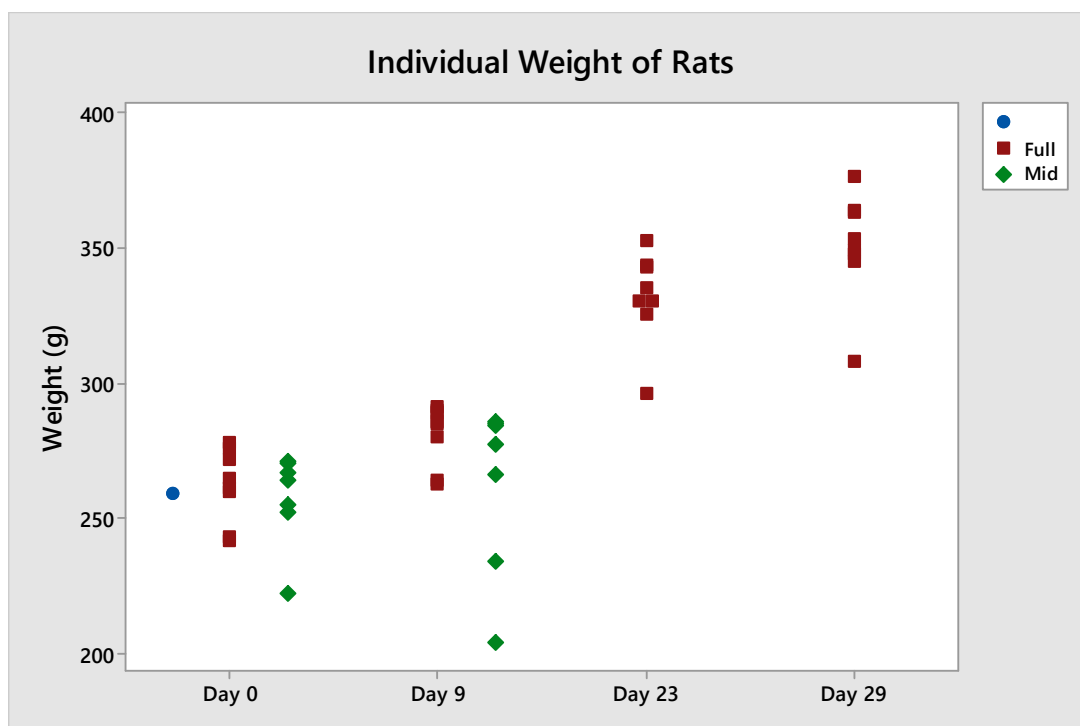


Figure 76 – Record of the weight of the individual test subjects at time intervals: Day 0, 9, 23, and 29th day. Animals were weighed prior to surgery and post-surgery. Green diamond indicates the weight of the animals terminated mid-experiment. Red squares are the individual weight of the rats in both control and experimental groups terminated at full term of the experiment date. Blue circle is the weight of the Rat ID 7 culled on day 0 post-surgery due to complication.

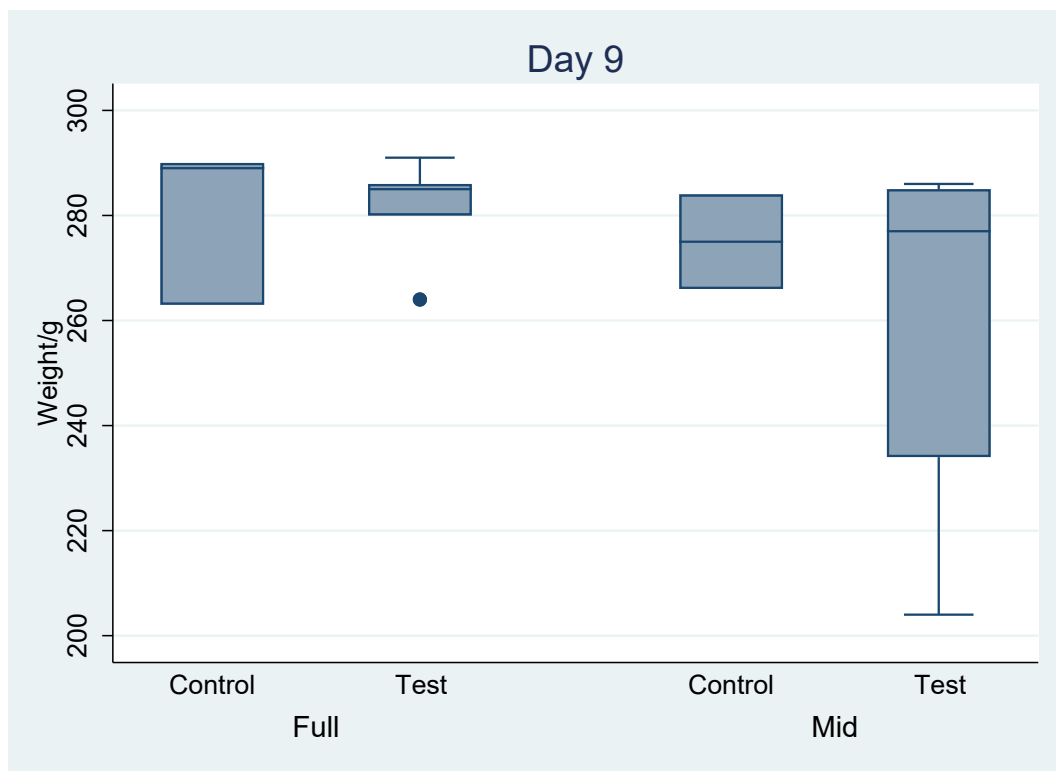


Figure 77 – Weight of the animals post sonication on day 9 between control vs test group of mid-termination and full termination group

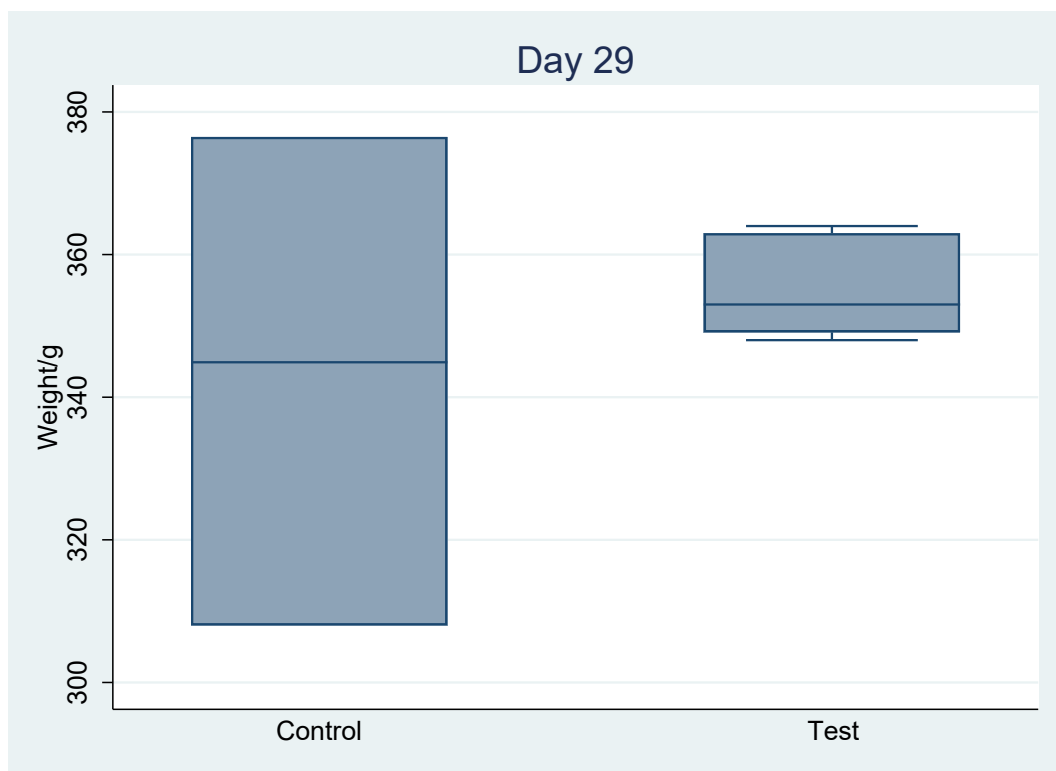


Figure 78 – weight of the subjects on day 29 comparison between the control and test group.

7.7.6 Termination and laparotomy findings

Termination of the animals was carried out successfully without any complications as described in protocol. On macroscopic examination at post-mortem all subject after histotripsy sonication had visible inflammatory changes around the right lobe of the liver. In the 3D Hep injected group there was evidence of more severe reaction where the right lobe was adhered to the peritoneal reflection and diaphragm above it. In animal ID 4, the adhesion was very strong that the liver and the rib had to be resected en-bloc to avoid damage to the liver capsule or parenchyma. In ten subjects (apart from animal ID 1 & 2), there was evidence of obvious change in the base of the right lung on gross inspection and hence the lung tissue was harvested. In test subject number 13 and 16 there was a white patch noted on the small bowel hence these were taken further histological analysis. In all circumstance the right kidney was also taken further histological analysis to examine if breach of the liver capsule has resulted in any damage to structures below. There was obvious hypertrophy of the left lobe in all the sonicated subjects.

7.7.7 Histology

A total of 235 slides of different tissues were stained for human nuclear hepatocyte and H&E and reviewed by our expert pathologist (AQ). Out of a total of 235 samples, 152 were of the liver tissues, 29 of lung tissue, 21 of the kidneys, 11 from spleens, 2 small bowel, 1 lymph node and 1 rib was stained and analysed. 4 slides were failed stained. **Table 17** summarises the number of histology slides analysed per organ animal.

Histological staining for human nuclear hepatocyte and H&E staining revealed no evidence of implanted 3D Heps (**Figure 79**). All the slides in the text group were negative for human nuclear staining. Further the H&E stains revealed no architectural disturbance at the time of sacrifice which would correspond to either 2 weeks or more than 3 weeks

post sonication. There are scattered immune cells suggestive of an inflammatory episode, but no evidence of scar tissue was observed. Analysis of the tissues other than the liver revealed no seeding of the 3D Heps locally or at distant.

Table 17 – Summary of the organs retrieved and number of slides per organ analysed for each animal

Termination Date	Animal ID	Treatment group	Organs stained and analysed
Termination at 28 th day	1	Control	9 Livers 1 Kidney
	2	Control	6 Livers 1 Kidney
	3	Control	7 Liver; 1 Lung; 1 Kidney
	4	Test	7 Liver; 1 Rib; 1 Lung; 3 Kidney
	5	Test	37 Livers; 2 Lungs 2 Kidney; 1 Spleen
	9	Test	8 Livers; 7 lungs; 2 spleens; 3 Kidney
	10	Test	14 Liver; 1 Node; 1 Kidney; 6 Lung
Mid-point termination	6	Control	6 Livers; 1 Lung
	8	Control	7 Livers; 1 Lung
	11	Test	12 Livers; 1 Lung; 1 Spleen
	12	Test	7 Liver; 2 Kidney; 1 Spleen; 1 Lung
	13	Test	19 Livers; 1 Lung; 2 Kidney; 1 Spleen; 1 Small bowel
	14	Test	7 Livers; 3 Kidneys; 4 Lungs; 3 Spleen
	15	Test	6 Livers; 1 Spleen; 3 Lungs
	16	Test	12 Livers; 1 Small bowel; 2 Lung; 2 Kidney; 1 Spleen

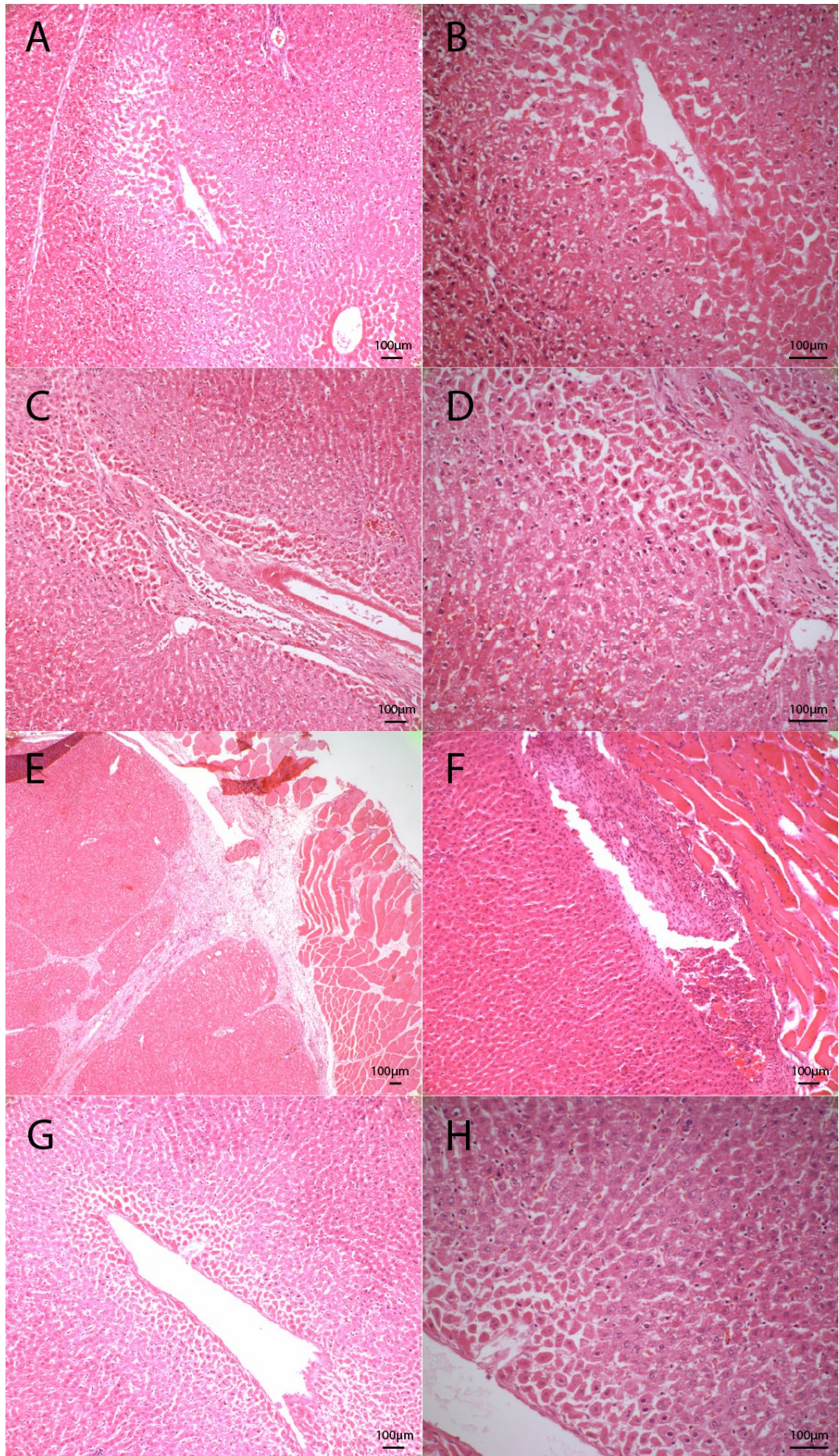


Figure 79 - Histology of the rodent livers – This shows the histological analysis of the Rat 2, 3, 5 & 10. Two and three are control rats; 5 and 10 are experimental rats. **A & B:** Rat 2 10x & 20x respectively. **C & D:** Rat 3 10x & 20x respectively. **E & F:** Rat 5 4x & 10x respectively. **G & H:** Rat 10 10x & 20x respectively. None of the histology slides revealed human hepatocyte on nuclear staining. All reveal normal rat liver architecture.

7.7.8 Cell function

We performed blood biochemistry on plasma collected from two controls and ten cell transplanted rats at the time of termination to detect human AFP and ALB. There was no human AFP or ALB production detected in neither the control group nor the experimental group (**Figure 80 & Figure 81**). The control group (Ctrl in vivo) denotes the group where no human cells were transplanted. The kits for the AFP and ALB are human specific and therefore, there should not be any level detected in the control group which is demonstrated in the figures below. The experimental group on the other hand had human derived 3D hepatospheres transplanted and therefore the kit would have picked up any level produced by the rats after transplantation. This is negative for both the AFP and ALB in the experimental group.

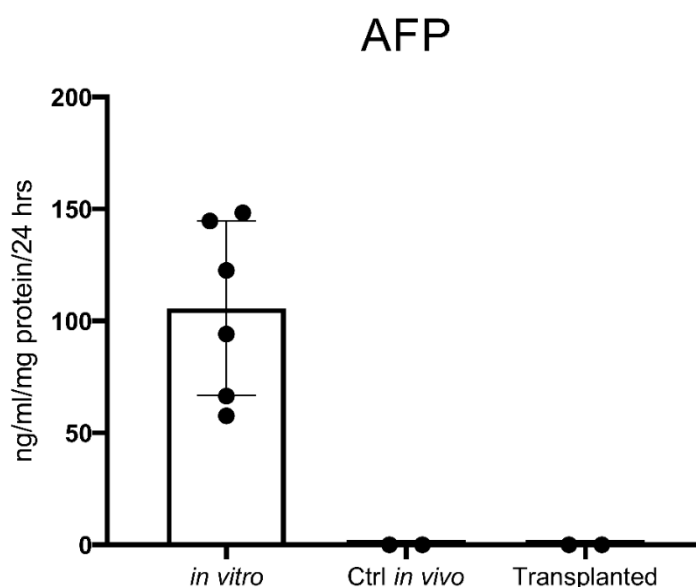


Figure 80 – AFP assay measuring level produced in both control and experimental group. In vitro is the control base mark against which the levels in the Control (rats that didn't have the cell transplanted: Ctrl in-vivo) vs Experimental group (Rats that had cells transplanted: Transplanted) are measured.

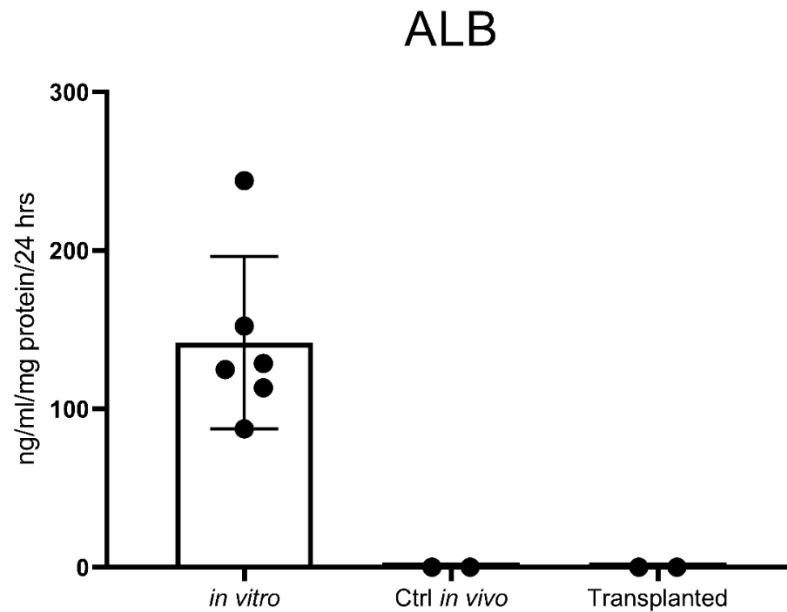


Figure 81 - ALB assay measuring level produced in both control and experimental group. In vitro is the control base mark against which the levels in the Control (rats that didn't have the cell transplanted: Ctrl in-vivo) vs Experimental group (Rats that had cells transplanted: Transplanted) are measured.

7.8 Discussion

7.8.1 Safety of liver histotripsy in live rodent model:

In this study, we have demonstrated that the histotripsy can be successfully used in a small animal models. Histotripsy has been demonstrated as a non-invasive technique capable of mechanically ablating liver tissue with precision. In rodent models, it effectively creates subcapsular lesions with well-defined boundaries suitable for transplantation. Notably, capsular breaches have been observed in some cases, underscoring the necessity for precise control of energy parameters and probe positioning. Despite these breaches, studies have reported minimal bleeding and no significant compromise to the subjects, indicating the relative safety of the procedure. Prior studies have confirmed histotripsy's safety in both therapeutic and preclinical applications, with minimal off-target damage under optimized conditions (490).

7.8.2 Comparison of histotripsy sites with other protocols:

Histotripsy-induced lesions differed from those created by other modalities (e.g., thermal ablation or cryotherapy) in their precise architecture and minimal peripheral tissue damage. Capsular breaches, while minor, pose challenges for cell retention. Further refinement in probe design and parameter optimization is needed to address this issue and ensure successful cell engraftment.

In our study, the focus is more on creating a lesion with maximal tissue destruction in the core of lesion to create a nidus with minimal damage to the periphery of the lesion and maximal tissue or architectural preservation that would later facilitate tissue regeneration. This makes parametrisation of the histotripsy a more dynamic process. For our study, we used parameters previously described by Ki Joo Pahk (449) and combined with simulated parameters from our cell work study in the ex-vivo model (491). The parameters used did produce a cavity in the rat livers, however, in some instances the force resulted in the puncture of the posterior capsule of the liver. Despite using the right lobe of the liver for sonication as it has the greatest thickness, the force produced resulted in the puncture of the liver capsule. This indicates two factors that needs to be further adjusted: (1) the positioning of the probe; (2) the calculated depth of the focus for sonication which can depend on the shape of the probe. The positioning of the probe needs to be as precise as possible for the focus of sonication to create a cavity suitable for transplantation. The anaesthetised rat's breathing diaphragm motion can displace the focal area of the sonication. The probe we had used had a wide base and centring the wide convex part of the probe on the small rat liver with the breathing motion can create motion artefact that would result in distorted lesions. In our experiment this could have moved the focal area from the thickest part of the rat liver to the thinner peripheral area in the right lobe thus resulting in the traverse of the energy through the full length of the liver. The shape of the

transduces and the probe also affects the positioning. The convex shape of the probe and the size mismatch also makes accurate positioning difficult. This could have been circumvented by using a more canonical shaped probe to facilitate a more accurate positioning. This simple adjustment can make a significant change to the outcome. Given the puncture of the liver capsule, this means the required powers must be re-calculated. During a preliminary test phase, prior to the actual experiment described above, we used the same parameters on fresh exsanguinated discarded rats ($N = 5$) to assess the depth of penetration and accuracy of parameters. These rats were already dead and hence the sonication was carried a short period after sacrifice of the animals. In none of these rats the parameters we used caused any puncture of the liver capsule. There was a noticeable difference between the dead rats and the live rats used in our experiment. There was slightly more thickness to the livers of the dead rats compared to the live rats we used in our experiments. We assumed the thickness of the livers are going to be the same and hence no adjustment was made to the parameters used. Needs to focus on the data on success of histotripsy and safety in controls.

The puncture in the liver capsule is related to the parameter used and the thickness of the organ. The puncture of the liver capsule can create major problems post sonication. It can be a source of un-controlled bleeding; however, this did not occur in any of the experimental rats. Most of the punctured capsules had minor bleeding which had stopped after small amount of pressure had been applied. Another problem a breached capsule can cause is wash away of the transplanted cells after its injection in the cavity. This would be more pronounced if bleeding of any degree were to happen. In fact, the lack of an identifiable cell population in the cavity in the histological analysis of the punctured livers could partly be explained by this. However, if the cells were washed away from the liver

cavity, the expectation is for an island of these cells to be seen in the peritoneum elsewhere. This was not the case neither on gross examination nor histological analysis.

7.8.3 Feasibility and safety of 3D Hep implantation:

This study demonstrated that 3D hepatocyte transplantation is technically feasible, with no evidence of acute toxicity. However, post-implantation histological analysis revealed no detectable transplanted cells, suggesting challenges with cell survival, immune rejection, or implantation technique. Histotripsy's immunogenic effects (355, 492, 493), while beneficial in oncological applications, may exacerbate rejection risks.

An important aspect of the experiment to consider which maybe the explanation for the absence of the implanted cells post analysis is the immunological aspect of the histotripsy. The animals were not immunosuppressed post transplantation; therefore, immunological rejection is a plausible explanation for the disappearing 3D Heps. Histotripsy is known to elicit local and systemic immune reaction following sonication (493-499). Indeed, it has been shown that sonication with histotripsy can result in a stronger infiltration of CD4 and CD8 T cells and NK cells in histotripsy-treated area (497). In experimental models, histotripsy results in release of DAMP molecules as well as release of pro-inflammatory cytokines which can result in recruitment of further immune cells to the site of sonication (493, 497). Debris released in the core of the lesion have a role in immunogenicity and the subsequent immune cells recruitment to the site. An intense immune response may prove detrimental to the existence of the implanted hepatocytes. The 3D hepatocytes themselves are recognised as foreign and can elicit an immune response without the exaggerated effect of histotripsy.

The effect of the histotripsy in heightening the immune response in the local area of the transplanted cells may mean the cells are more prone to immune rejection. This is a strong possibility and a reasonable explanation for the lack of observation of the 3DHeps

histologically. To avoid problems with rejection, it may require animals to be immune suppressed prior to sonication.

7.8.4 Evaluation of recovery and cause of post procedure termination

(n=1):

One subject experienced prolonged recovery and required early termination due to systemic complications. This highlights the importance of monitoring physiological responses to identify any unintended effects of histotripsy or cell implantation. We did not perform autopsy as the animal was not preserved after termination to facilitate this.

7.8.5 Weight gain as surrogate of recovery

Weight gain served as an indirect marker of recovery and health post-surgery. Animals in both control and experimental groups exhibited significant weight gain over time, with no major differences between the groups, indicating general recovery from the procedure. Not only this could be an indirect surrogate marker of health of the rats after the procedure, but it can also highlight their metabolic state, and their body requirement post operatively. The significant difference from base line and day 9 and day 29 highlights the highlight the immunohumoral changes that can happen after an insult of surgery (500). The increased body metabolism post-surgery can lead to increased oral intake of the animals with consequential weight gain. More so, this could partly be in keeping with the increased hypertrophy of the liver noted post sonication. The observation of the liver hypertrophy at postmortem examination for all the rats is an important finding. The response to the sonication injury is hypertrophy of the liver and could contribute to a slight degree of weight gain. Future studies should aim to correlate these findings more objectively by assessing biochemical and radiological changes in the post operative period.

In the context of histotripsy and cell implantation studies, animals in both control and experimental groups have exhibited significant weight gain over time, with no major differences between the groups. This suggests that the procedures do not adversely affect the general recovery and well-being of the subjects. Consistent weight gain indicates effective recovery and the absence of systemic adverse effects.

7.8.6 Tissue sampling, variability, liver and other organ injury, possibility of immune response

Our analysis of the livers histologically showed no evidence of implanted cells. We have also analysed other organs that looked suspicious to have cells deposited there but their histological analysis did not confirm this. Lack of implanted cells across every tissue examined makes the case for a systemic immune response very strong. Hence future implantation should be with immunosuppression cover as well as appropriate anti-microbials to avoid infection.

Another limitation of the current study was the delivery of the cells. The pre-filled syringe proved too difficult to precisely deliver the cell load in the cavity. On one occasion the needle resulted in a slight bleeding in the cavity which meant delay in the delivery of the cells in the cavity which was already disturbed by a blood clot. The presence of blood clot and bleeding may not be in favour of successful engraftment. Future cell delivery must be with a smaller hypodermic needle to ensure minimal secondary damage to the cavity.

7.8.7 Implanted cell detection discussion

Despite efforts to detect implanted 3D hepatocytes, studies have reported no evidence of transplanted cells in histological or biochemical assays post-implantation. This underscores the challenges of cell retention and survival in an immunocompetent host.

As mentioned above, future experiments should consider immunosuppressive strategies to mitigate rejection and enhance the detectability and functionality of implanted cells. Additionally, employing advanced imaging and molecular techniques may improve the tracking and assessment of implanted cell viability and integration (382).

7.8.8 Implication for future studies, technique and assessment modification.

We are planning a repeat experiment in a smaller number of rat models with modification of the transducer head, slight adjustment to the parameters and an improved cell delivery to provide evidence of successful cell implantation in the cavity generated. For future larger animal studies this method requires imaging guidance for identification of lesion location and accurate delivery of the cells. Lastly, immunocompromised animals should be considered to assess the feasibility of 3D Hep implantation in the rodent models.

Overall:

While our initial experiments focused on ECM decellularization for cell implantation, we shifted towards creating cavities that support a niche environment for engraftment. We found that the ECM core was disrupted under our parameters, with collagen matrix breakdown. However, this disruption, combined with cell suspension, may promote engraftment of implanted cells although further work is required to demonstrate the mechanistic pathways. Further optimisation of histotripsy parameters and cell delivery is needed to improve graft attachment and regeneration.

References

1. Ramachandran P, Matchett KP, Dobie R, Wilson-Kanamori JR, Henderson NC. Single-cell technologies in hepatology: new insights into liver biology and disease pathogenesis. *Nature Reviews Gastroenterology & Hepatology*. 2020.
2. Chary A, Holodniy M. Recent advances in hepatitis C virus treatment: review of HCV protease inhibitor clinical trials. *Rev Recent Clin Trials*. 2010;5(3):158-73.
3. Riazi K, Azhari H, Charette JH, Underwood FE, King JA, Afshar EE, et al. The prevalence and incidence of NAFLD worldwide: a systematic review and meta-analysis. *The Lancet Gastroenterology & Hepatology*. 2022;7(9):851-61.
4. Martin Blachier HL, Markus Peck-Radosavljevic, Dominique-Charles Valla, Françoise Roudot-Thoraval. The Burden of liver disease in Europe: A review of available epidemiological data. *EASL; 2013. Report No.: 978-2-8399-1176-4*.
5. Zatonski WA, Sulkowska U, Manczuk M, Rehm J, Boffetta P, Lowenfels AB, et al. Liver cirrhosis mortality in Europe, with special attention to Central and Eastern Europe. *European addiction research*. 2010;16(4):193-201.
6. Roehlen N, Crouchet E, Baumert TF. Liver Fibrosis: Mechanistic Concepts and Therapeutic Perspectives. *Cells*. 2020;9(4).
7. Wong MCS, Huang J. The growing burden of liver cirrhosis: implications for preventive measures. *Hepatol Int*. 2018;12(3):201-3.
8. Peck-Radosavljevic M, Angeli P, Cordoba J, Farges O, Valla D. Managing complications in cirrhotic patients. *United European gastroenterology journal*. 2015;3(1):80-94.
9. Froghi S, Froghi F, Davidson BR. Surgery in Liver Disease. In: Radu-Ionita F, Pyrsopoulos NT, Jinga M, Tintoiu IC, Sun Z, Bontas E, editors. *Liver Diseases: A Multidisciplinary Textbook*. Cham: Springer International Publishing; 2020. p. 769-83.
10. Asrani SK, Devarbhavi H, Eaton J, Kamath PS. Burden of liver diseases in the world. *Journal of Hepatology*. 2019;70(1):151-71.
11. Liu Y-B, Chen M-K. Epidemiology of liver cirrhosis and associated complications: Current knowledge and future directions. *World Journal of Gastroenterology*. 2022;28(41):5910-30.
12. Schuppan D, Afdhal NH. Liver cirrhosis. *The Lancet*. 2008;371(9615):838-51.
13. Koo S, Sharp L, Hull M, Rushton S, Neilson LJ, McPherson S, et al. Uncovering undiagnosed liver disease: prevalence and opportunity for intervention in a population attending colonoscopy. *BMJ Open Gastroenterol*. 2021;8(1).
14. Hazeldine S, Hydes T, Sheron N. Alcoholic liver disease - the extent of the problem and what you can do about it. *Clin Med (Lond)*. 2015;15(2):179-85.
15. Zhai M, Long J, Liu S, Liu C, Li L, Yang L, et al. The burden of liver cirrhosis and underlying etiologies: results from the global burden of disease study 2017. *Aging*. 2021;13(1):279-300.
16. Huang DQ, Terrault NA, Tacke F, Gluud LL, Arrese M, Bugianesi E, et al. Global epidemiology of cirrhosis — aetiology, trends and predictions. *Nature Reviews Gastroenterology & Hepatology*. 2023;20(6):388-98.
17. Rockey DC, Caldwell SH, Goodman ZD, Nelson RC, Smith AD. Liver biopsy. *Hepatology*. 2009;49(3):1017-44.
18. Poynard T, Bedossa P, Opolon P. Natural history of liver fibrosis progression in patients with chronic hepatitis C. The OBSVIRC, METAVIR, CLINIVIR, and DOSVIRC groups. *Lancet*. 1997;349(9055):825-32.

19. Schwantes-An TH, Darlay R, Mathurin P, Masson S, Liangpunsakul S, Mueller S, et al. Genome-wide Association Study and Meta-analysis on Alcohol-Associated Liver Cirrhosis Identifies Genetic Risk Factors. *Hepatology*. 2021;73(5):1920-31.
20. Zhang J, Wang H, Liu J, Fu L, Peng S. ANXA1 is identified as a key gene associated with high risk and T cell infiltration in primary sclerosing cholangitis. *Human Genomics*. 2023;17(1):86.
21. Scorza M, Elce A, Zarrilli F, Liguori R, Amato F, Castaldo G. Genetic diseases that predispose to early liver cirrhosis. *Int J Hepatol*. 2014;2014:713754.
22. Burdelski M, Rogiers X. Liver transplantation in metabolic disorders. *Acta Gastroenterol Belg*. 1999;62(3):300-5.
23. Hansen K, Horslen S. Metabolic liver disease in children. Liver transplantation : official publication of the American Association for the Study of Liver Diseases and the International Liver Transplantation Society. 2008;14(5):713-33.
24. Zou YG, Wang H, Li WW, Dai DL. Challenges in pediatric inherited/metabolic liver disease: Focus on the disease spectrum, diagnosis and management of relatively common disorders. *World J Gastroenterol*. 2023;29(14):2114-26.
25. Manns MP, Maasoumy B. Breakthroughs in hepatitis C research: from discovery to cure. *Nature Reviews Gastroenterology & Hepatology*. 2022;19(8):533-50.
26. Shiffman M, Ramesh S, Shiffman ML. What Is the Likelihood That My Patient With Chronic Hepatitis C Will Develop Cirrhosis, Hepatocellular Carcinoma, and/or Hepatic Decompensation? Thorofare, New Jersey :: SLACK; 2024. 3-6 p.
27. Tada T, Toyoda H, Yasuda S, Kumada T, Kurisu A, Ohisa M, et al. Long-term prognosis of liver disease in patients with eradicated chronic hepatitis C virus: An analysis using a Markov chain model. *Hepatology Research*. 2020;50(8):936-46.
28. Kwon JA, Dore GJ, Hajarizadeh B, Alavi M, Valerio H, Grebely J, et al. Australia could miss the WHO hepatitis C virus elimination targets due to declining treatment uptake and ongoing burden of advanced liver disease complications. *PloS one*. 2021;16(9):e0257369.
29. Topi S, Gaxhja E, Charitos IA, Colella M, Santacroce L. Hepatitis C Virus: History and Current Knowledge. *Gastroenterology Insights*. 2024;15(3):676-707.
30. Yu L. Pathogenesis of Liver Injury and Hepatic Failure. In: Li L, editor. *Artificial Liver*. Singapore: Springer Nature Singapore; 2021. p. 105-66.
31. Berggren KA, Suzuki S, Ploss A. Animal Models Used in Hepatitis C Virus Research. *International Journal of Molecular Sciences*. 2020;21(11):3869.
32. Lee MJ. A review of liver fibrosis and cirrhosis regression. *jptm*. 2023;57(4):189-95.
33. Barry AE, Baldeosingh R, Lamm R, Patel K, Zhang K, Dominguez DA, et al. Hepatic Stellate Cells and Hepatocarcinogenesis. *Frontiers in Cell and Developmental Biology*. 2020;8.
34. Kamm DR, McCommis KS. Hepatic stellate cells in physiology and pathology. *J Physiol*. 2022;600(8):1825-37.
35. Friedman SL. Hepatic Stellate Cells: Protean, Multifunctional, and Enigmatic Cells of the Liver. *Physiological Reviews*. 2008;88(1):125-72.
36. Brandão DF, Ramalho LNZ, Ramalho FS, Zucoloto S, Martinelli ADLC, Castro E Silva OD. Liver cirrhosis and hepatic stellate cells. *Acta Cirurgica Brasileira*. 2006;21(suppl 1):54-7.
37. Pakshir P, Noskovicova N, Lodyga M, Son DO, Schuster R, Goodwin A, et al. The myofibroblast at a glance. *Journal of Cell Science*. 2020;133(13):jcs227900.

38. Tang Y, Zhang Q, Zhu Y, Chen G, Yu F. Low concentrations of bilirubin inhibit activation of hepatic stellate cells in vitro. *Molecular Medicine Reports*. 2017;15(4):1647-53.
39. Liu XY, Liu RX, Hou F, Cui LJ, Li CY, Chi C, et al. Fibronectin expression is critical for liver fibrogenesis in vivo and in vitro. *Mol Med Rep*. 2016;14(4):3669-75.
40. Geremias AT, Carvalho MA, Borojevic R, Monteiro AN. TGF β 1 and PDGF AA override Collagen type I inhibition of proliferation in human liver connective tissue cells. *BMC Gastroenterology*. 2004;4(1).
41. Graf F, Horn P, Ho AD, Boutros M, Maercker C. The extracellular matrix proteins type I collagen, type III collagen, fibronectin, and laminin 421 stimulate migration of cancer cells. *The FASEB Journal*. 2021;35(7):e21692.
42. Moriya K, Bae E, Honda K, Sakai K, Sakaguchi T, Tsujimoto I, et al. A Fibronectin-Independent Mechanism of Collagen Fibrillogenesis in Adult Liver Remodeling. *Gastroenterology*. 2011;140(5):1653-63.
43. Huang E, Peng N, Xiao F, Hu D, Wang X, Lu L. The Roles of Immune Cells in the Pathogenesis of Fibrosis. *Int J Mol Sci*. 2020;21(15).
44. Wynn TA, Vannella KM. Macrophages in Tissue Repair, Regeneration, and Fibrosis. *Immunity*. 2016;44(3):450-62.
45. Braga TT, Agudelo JS, Camara NO. Macrophages During the Fibrotic Process: M2 as Friend and Foe. *Front Immunol*. 2015;6:602.
46. Wynn TA, Barron L. Macrophages: master regulators of inflammation and fibrosis. *Semin Liver Dis*. 2010;30(3):245-57.
47. Rauchenwald T, Handle F, Connolly CE, Degen A, Seifarth C, Hermann M, et al. Preadipocytes in human granulation tissue: role in wound healing and response to macrophage polarization. *Inflammation and Regeneration*. 2023;43(1).
48. Wang X, Zhou J, Li X, Liu C, Liu L, Cui H. The Role of Macrophages in Lung Fibrosis and the Signaling Pathway. *Cell Biochemistry and Biophysics*. 2024;82(2):479-88.
49. Shan Z, Ju C. Hepatic Macrophages in Liver Injury. *Frontiers in Immunology*. 2020;11.
50. Weiskirchen R, Tacke F. Cellular and molecular functions of hepatic stellate cells in inflammatory responses and liver immunology. *Hepatobiliary Surg Nutr*. 2014;3(6):344-63.
51. Świdarska M, Jaroszewicz J, Stawicka A, Parfieniuk-Kowerda A, Chabowski A, Flisiak R. The interplay between Th17 and T-regulatory responses as well as adipokines in the progression of non-alcoholic fatty liver disease. *Clinical and Experimental Hepatology*. 2017;3(3):127-34.
52. Nati M, Haddad D, Birkenfeld AL, Koch CA, Chavakis T, Chatzigeorgiou A. The role of immune cells in metabolism-related liver inflammation and development of non-alcoholic steatohepatitis (NASH). *Reviews in Endocrine and Metabolic Disorders*. 2016;17(1):29-39.
53. Feldman M. <Sleisenger and Fordtran's Gastrointestinal and Liver Disease Pathophysiology, Diagnosis, Management>: Elsevier; 2016.
54. Jagdish RK, Roy A, Kumar K, Premkumar M, Sharma M, Rao PN, et al. Pathophysiology and management of liver cirrhosis: from portal hypertension to acute-on-chronic liver failure. *Frontiers in Medicine*. 2023;10.
55. Groszmann RJ, Abraldes JG. Portal Hypertension: From Bedside to Bench. *Journal of Clinical Gastroenterology*. 2005;39(4).

56. Loureiro-Silva MR, Cadelina GW, Groszmann RJ. Deficit in nitric oxide production in cirrhotic rat livers is located in the sinusoidal and postsinusoidal areas. *Am J Physiol Gastrointest Liver Physiol*. 2003;284(4):G567-74.
57. Shah V, Toruner M, Haddad F, Cadelina G, Papapetropoulos A, Choo K, et al. Impaired endothelial nitric oxide synthase activity associated with enhanced caveolin binding in experimental cirrhosis in the rat. *Gastroenterology*. 1999;117(5):1222-8.
58. McConnell M, Iwakiri Y. Biology of portal hypertension. *Hepatology International*. 2018;12(1):11-23.
59. Iwakiri Y, Shah V, Rockey DC. Vascular pathobiology in chronic liver disease and cirrhosis - current status and future directions. *J Hepatol*. 2014;61(4):912-24.
60. Rothermund L, Leggewie S, Schwarz A, Thöne-Reinecke C, Cho JJ, Bauer C, et al. Regulation of the hepatic endothelin system in advanced biliary fibrosis in rats. *Clin Chem Lab Med*. 2000;38(6):507-12.
61. Bhunchet E, Fujieda K. Capillarization and venularization of hepatic sinusoids in porcine serum-induced rat liver fibrosis: a mechanism to maintain liver blood flow. *Hepatology*. 1993;18(6):1450-8.
62. Dill MT, Rothweiler S, Djonov V, Hlushchuk R, Tornillo L, Terracciano L, et al. Disruption of Notch1 induces vascular remodeling, intussusceptive angiogenesis, and angiosarcomas in livers of mice. *Gastroenterology*. 2012;142(4):967-77. e2.
63. D'Amico G, Garcia-Tsao G, Pagliaro L. Natural history and prognostic indicators of survival in cirrhosis: A systematic review of 118 studies. *Journal of Hepatology*. 2006;44(1):217-31.
64. Hacking C. Cirrhosis 2 Jun 2024 [Available from: <https://dx.doi.org/10.53347/rID-1131>].
65. Liu X, Tan SBM, Awiwi MO, Jang H-J, Chernyak V, Fowler KJ, et al. Imaging Findings in Cirrhotic Liver: Pearls and Pitfalls for Diagnosis of Focal Benign and Malignant Lesions. *Radiographics*. 2023;43(9):e230043.
66. Ferenci P. Hepatic encephalopathy. *Gastroenterology Report*. 2017;5(2):138-47.
67. Islam R, Kundu S, Jha SB, Rivera AP, Flores Monar GV, Islam H, et al. Cirrhosis and Coagulopathy: Mechanisms of Hemostasis Changes in Liver Failure and Their Management. *Cureus*. 2022;14(4):e23785.
68. Drolz A, Horvatits T, Roedl K, Rutter K, Staufer K, Kneidinger N, et al. Coagulation parameters and major bleeding in critically ill patients with cirrhosis. *Hepatology*. 2016;64(2):556-68.
69. Tripodi A, Primignani M, Mannucci PM. Abnormalities of hemostasis and bleeding in chronic liver disease: the paradigm is challenged. *Internal and Emergency Medicine*. 2010;5(1):7-12.
70. Caldwell SH, Hoffman M, Lisman T, Macik BG, Northup PG, Reddy KR, et al. Coagulation disorders and hemostasis in liver disease: pathophysiology and critical assessment of current management. *Hepatology*. 2006;44(4):1039-46.
71. Rijken DC, Lijnen HR. New insights into the molecular mechanisms of the fibrinolytic system. *J Thromb Haemost*. 2009;7(1):4-13.
72. Lisman T, Leebeek FW, Mosnier LO, Bouma BN, Meijers JC, Janssen HL, et al. Thrombin-activatable fibrinolysis inhibitor deficiency in cirrhosis is not associated with increased plasma fibrinolysis. *Gastroenterology*. 2001;121(1):131-9.
73. Colucci M, Binetti BM, Branca MG, Clerici C, Morelli A, Semeraro N, et al. Deficiency of thrombin activatable fibrinolysis inhibitor in cirrhosis is associated with increased plasma fibrinolysis. *Hepatology*. 2003;38(1):230-7.
74. Pose E, Piano S, Juanola A, Ginès P. Hepatorenal Syndrome in Cirrhosis. *Gastroenterology*. 2024;166(4):588-604.e1.

75. Luo X, Yu J. Letter to the Editor: Regarding terlipressin-related patient outcomes in hepatorenal syndrome-acute kidney injury. *Hepatology*. 2024;80(5).
76. Peluso L, Savi M, Coppalini G, Veliaj D, Villari N, Albano G, et al. Management of hepatorenal syndrome and treatment-related adverse events. *Current Medical Research and Opinion*. 2024;40(7):1155-62.
77. Jung C-Y, Chang JW. Hepatorenal syndrome: Current concepts and future perspectives. *Clinical and Molecular Hepatology*. 2023;29(4):891-908.
78. Barreto R, Elia C, Solà E, Moreira R, Ariza X, Rodríguez E, et al. Urinary neutrophil gelatinase-associated lipocalin predicts kidney outcome and death in patients with cirrhosis and bacterial infections. *J Hepatol*. 2014;61(1):35-42.
79. Qasim A, Jyala A, Shrivastava S, Allena N, Ghazanfar H, Bhatt V, et al. Hepatopulmonary Syndrome: A Comprehensive Review. *Cureus*. 2024;16(7):e65204.
80. Skelly MM, James PD, Ryder SD. Findings on liver biopsy to investigate abnormal liver function tests in the absence of diagnostic serology. *Journal of Hepatology*. 2001;35(2):195-9.
81. Neuberger J, Patel J, Caldwell H, Davies S, Hebditch V, Hollywood C, et al. Guidelines on the use of liver biopsy in clinical practice from the British Society of Gastroenterology, the Royal College of Radiologists and the Royal College of Pathology. *Gut*. 2020;69(8):1382-403.
82. Khalifa A, Lewin DN, Sasso R, Rockey DC. The Utility of Liver Biopsy in the Evaluation of Liver Disease and Abnormal Liver Function Tests. *American Journal of Clinical Pathology*. 2021;156(2):259-67.
83. Sharma P. Value of Liver Function Tests in Cirrhosis. *Journal of Clinical and Experimental Hepatology*. 2022;12(3):948-64.
84. Stravitz RT, Ilan Y. Potential use of metabolic breath tests to assess liver disease and prognosis: has the time arrived for routine use in the clinic? *Liver International*. 2017;37(3):328-36.
85. Luerken L, Dollinger M, Goetz A, Utpatel K, Doppler MC, Weiss JB, et al. Diagnostic Accuracy of Indocyanine Green Clearance Test for Different Stages of Liver Fibrosis and Cirrhosis. *Diagnostics (Basel)*. 2023;13(16).
86. Cirrhosis | Radiology Reference Article | Radiopaedia.org.
87. Schwoppe RB, Katz M, Russell T, Reiter MJ, Lisanti CJ. The many faces of cirrhosis. *Abdominal Radiology*. 2020;45(10):3065-80.
88. de Lédinghen V, Vergniol J. Transient elastography (FibroScan). *Gastroenterol Clin Biol*. 2008;32(6 Suppl 1):58-67.
89. Berzigotti A, Tsochatzis E, Boursier J, Castera L, Cazzagon N, Friedrich-Rust M, et al. EASL Clinical Practice Guidelines on non-invasive tests for evaluation of liver disease severity and prognosis – 2013; 2021 update. *Journal of Hepatology*. 2021;75(3):659-89.
90. Friedrich-Rust M, Poynard T, Castera L. Critical comparison of elastography methods to assess chronic liver disease. *Nature Reviews Gastroenterology & Hepatology*. 2016;13(7):402-11.
91. Berzigotti A. Non-invasive evaluation of portal hypertension using ultrasound elastography. *J Hepatol*. 2017;67(2):399-411.
92. Ferraioli G, Barr RG, Berzigotti A, Sporea I, Wong VWS, Reiberger T, et al. WFUMB Guideline/Guidance on Liver Multiparametric Ultrasound: Part 1. Update to 2018 Guidelines on Liver Ultrasound Elastography. *Ultrasound in Medicine & Biology*. 2024;50(8):1071-87.
93. De Franchis R. Expanding consensus in portal hypertension. *Journal of Hepatology*. 2015;63(3):743-52.

94. Barr RG, Wilson SR, Rubens D, Garcia-Tsao G, Ferraioli G. Update to the Society of Radiologists in Ultrasound Liver Elastography Consensus Statement. *Radiology*. 2020;296(2):263-74.
95. Chowdhury AB, Mehta KJ. Liver biopsy for assessment of chronic liver diseases: a synopsis. *Clinical and Experimental Medicine*. 2022;23(2):273-85.
96. Nallagangula KS, Nagaraj SK, Venkataswamy L, Chandrappa M. Liver Fibrosis: A Compilation on the Biomarkers Status and Their Significance During Disease Progression. *Future Sci OA*. 2018;4(1):FSO250.
97. Standish RA, Cholongitas E, Dhillon A, Burroughs AK, Dhillon AP. An appraisal of the histopathological assessment of liver fibrosis. *Gut*. 2006;55(4):569-78.
98. Lo RC, Kim H. Histopathological evaluation of liver fibrosis and cirrhosis regression. *Clinical and Molecular Hepatology*. 2017;23(4):302-7.
99. Brol MJ, Drebber U, Luetkens JA, Odenthal M, Trebicka J. “The pathogenesis of hepatic fibrosis: basic facts and clinical challenges”—assessment of liver fibrosis: a narrative review. *Digestive Medicine Research*. 2022;5.
100. Desmet VJ, Knodell RG, Ishak KG, Black WC, Chen TS, Craig R, Kaplowitz N, Kiernan TW, Wollman J. Formulation and application of a numerical scoring system for assessing histological activity in asymptomatic chronic active hepatitis [Hepatology 1981;1:431–435]. *Journal of Hepatology*. 2003;38(4):382-6.
101. Braticevici CF, Papacoea R, Tribus L, Badarau A. Can we replace liver biopsy with non-invasive procedures? *Liver biopsy*. 2011;6:225-40.
102. Mansour A, Watson W, Shayani V, Pickleman J. Abdominal operations in patients with cirrhosis: still a major surgical challenge. *Surgery*. 1997;122(4):730-5; discussion 5-6.
103. Kamath PS, Wiesner RH, Malinchoc M, Kremers W, Therneau TM, Kosberg CL, et al. A model to predict survival in patients with end-stage liver disease. *Hepatology*. 2001;33(2):464-70.
104. Bhangui P, Laurent A, Amathieu R, Azoulay D. Assessment of risk for non-hepatic surgery in cirrhotic patients. *Journal of Hepatology*. 2012;57(4):874-84.
105. Northup PG, Wanamaker RC, Lee VD, Adams RB, Berg CL. Model for End-Stage Liver Disease (MELD) predicts nontransplant surgical mortality in patients with cirrhosis. *Ann Surg*. 2005;242(2):244-51.
106. Rahbari NN, Reissfelder C, Koch M, Elbers H, Striebel F, Buchler MW, et al. The predictive value of postoperative clinical risk scores for outcome after hepatic resection: a validation analysis in 807 patients. *Ann Surg Oncol*. 2011;18(13):3640-9.
107. Befeler AS, Palmer DE, Hoffman M, Longo W, Solomon H, Di Bisceglie AM. The safety of intra-abdominal surgery in patients with cirrhosis: Model for end-stage liver disease score is superior to child-turcotte-pugh classification in predicting outcome. *Archives of Surgery*. 2005;140(7):650-4.
108. Balogh J, Victor D, Asham EH, Burroughs SG, Boktour M, Saharia A, et al. Hepatocellular carcinoma: a review. *Journal of Hepatocellular Carcinoma*. 2016;Volume 3:41-53.
109. Schuppan D, Pinzani M. Anti-fibrotic therapy: lost in translation? *J Hepatol*. 2012;56 Suppl 1:S66-74.
110. Tannapfel A, Dienes HP, Lohse AW. The indications for liver biopsy. *Dtsch Arztebl Int*. 2012;109(27-28):477-83.
111. Shan L, Wang F, Zhai D, Meng X, Liu J, Lv X. New Drugs for Hepatic Fibrosis. *Frontiers in Pharmacology*. 2022;13.

112. Tan Z, Sun H, Xue T, Gan C, Liu H, Xie Y, et al. Liver Fibrosis: Therapeutic Targets and Advances in Drug Therapy. *Frontiers in Cell and Developmental Biology*. 2021;9.
113. Ciardullo S, Muraca E, Vergani M, Invernizzi P, Perseghin G. Advancements in pharmacological treatment of NAFLD/MASLD: a focus on metabolic and liver-targeted interventions. *Gastroenterology Report*. 2023;12.
114. Zhang CY, Liu S, Yang M. Treatment of liver fibrosis: Past, current, and future. *World J Hepatol*. 2023;15(6):755-74.
115. Qiu J, Ozawa M, Terasaki PI. Liver transplantation in the United States. *Clin Transpl*. 2005;17-28.
116. EASL Clinical Practice Guidelines: Liver transplantation. *J Hepatol*. 2016;64(2):433-85.
117. Rana A, Ackah RL, Webb GJ, Halazun KJ, Vierling JM, Liu H, et al. No Gains in Long-term Survival After Liver Transplantation Over the Past Three Decades. *Ann Surg*. 2019;269(1):20-7.
118. Nicolas CT, Hickey RD, Chen HS, Mao SA, Lopera Higueta M, Wang Y, et al. Concise Review: Liver Regenerative Medicine: From Hepatocyte Transplantation to Bioartificial Livers and Bioengineered Grafts. *Stem Cells*. 2017;35(1):42-50.
119. Collin De L'Hortet A, Takeishi K, Guzman-Lepe J, Handa K, Matsubara K, Fukumitsu K, et al. Liver-Regenerative Transplantation: Regrow and Reset. *American Journal of Transplantation*. 2016;16(6):1688-96.
120. Dueland S, Syversveen T, Solheim JM, Solberg S, Grut H, Bjørnbeth BA, et al. Survival Following Liver Transplantation for Patients With Nonresectable Liver-only Colorectal Metastases. *Ann Surg*. 2020;271(2):212-8.
121. Tandon R, Froghi S. Artificial liver support systems. *J Gastroenterol Hepatol*. 2021;36(5):1164-79.
122. Vimalasvaran S, Nulty J, Dhawan A. Cellular Therapies in Pediatric Liver Diseases. *Cells*. 2022;11(16):2483.
123. Huebert RC, Rakela J. Cellular therapy for liver disease. *Mayo Clin Proc*. 2014;89(3):414-24.
124. Hughes RD, Mitry RR, Dhawan A. Hepatocyte transplantation for metabolic liver disease: UK experience. *J R Soc Med*. 2005;98(8):341-5.
125. Dhawan A, Mitry RR, Hughes RD. Hepatocyte transplantation for liver-based metabolic disorders. 2006;29(2-3):431-5.
126. Fox IJ. Hepatocyte Transplantation. *Gastroenterol Hepatol (N Y)*. 2014;10(9):594-6.
127. Pietrosi G, Vizzini G, Gerlach J, Chinnici C, Luca A, Amico G, et al. Phases I-II Matched Case-Control Study of Human Fetal Liver Cell Transplantation for Treatment of Chronic Liver Disease. *Cell Transplant*. 2015;24(8):1627-38.
128. Wang F, Zhou L, Ma X, Ma W, Wang C, Lu Y, et al. Monitoring of intrasplenic hepatocyte transplantation for acute-on-chronic liver failure: a prospective five-year follow-up study. *Transplant Proc*. 2014;46(1):192-8.
129. Christ B, Dollinger MM. The generation of hepatocytes from mesenchymal stem cells and engraftment into the liver. *Curr Opin Organ Transplant*. 2011;16(1):69-75.
130. Nicolas CT, Wang Y, Nyberg SL. Cell therapy in chronic liver disease. *Curr Opin Gastroenterol*. 2016;32(3):189-94.
131. Peggy Stock BC. Hepatocyte Transplantation. Peggy Stock BC, editor: Humana New York, NY; 27 June 2018.

132. Nguyen MP, Jain V, Dhawan A. Human Hepatocyte Transplantation. In: Shapiro R, Sarwal MM, Raina R, Sethi SK, editors. *Pediatric Solid Organ Transplantation: A Practical Handbook*. Singapore: Springer Nature Singapore; 2023. p. 473-95.
133. Nulty J, Anand H, Dhawan A. Human Hepatocyte Transplantation: Three Decades of Clinical Experience and Future Perspective. *Stem Cells Translational Medicine*. 2024;13(3):204-18.
134. Drosos I, Kolios G. Stem cells in liver regeneration and their potential clinical applications. *Stem Cell Rev Rep*. 2013;9(5):668-84.
135. Gilgenkrantz H, Collin de l'Hortet A. Understanding Liver Regeneration: From Mechanisms to Regenerative Medicine. *The American journal of pathology*. 2018;188(6):1316-27.
136. Ezquer F, Bruna F, Calligaris S, Conget P, Ezquer M. Multipotent mesenchymal stromal cells: A promising strategy to manage alcoholic liver disease. *World J Gastroenterol*. 2016;22(1):24-36.
137. Alfaifi M, Eom YW, Newsome PN, Baik SK. Mesenchymal stromal cell therapy for liver diseases. *J Hepatol*. 2018;68(6):1272-85.
138. Amer ME, El-Sayed SZ, El-Kheir WA, Gabr H, Gomaa AA, El-Noomani N, et al. Clinical and laboratory evaluation of patients with end-stage liver cell failure injected with bone marrow-derived hepatocyte-like cells. *Eur J Gastroenterol Hepatol*. 2011;23(10):936-41.
139. Amin MA, Sabry D, Rashed LA, Aref WM, el-Ghobary MA, Farhan MS, et al. Short-term evaluation of autologous transplantation of bone marrow-derived mesenchymal stem cells in patients with cirrhosis: Egyptian study. *Clin Transplant*. 2013;27(4):607-12.
140. Andreone P, Catani L, Margini C, Brodosi L, Lorenzini S, Sollazzo D, et al. Reinfusion of highly purified CD133+ bone marrow-derived stem/progenitor cells in patients with end-stage liver disease: A phase I clinical trial. *Dig Liver Dis*. 2015;47(12):1059-66.
141. El-Ansary M, Abdel-Aziz I, Mogawer S, Abdel-Hamid S, Hammam O, Teaema S, et al. Phase II trial: undifferentiated versus differentiated autologous mesenchymal stem cells transplantation in Egyptian patients with HCV induced liver cirrhosis. *Stem Cell Rev Rep*. 2012;8(3):972-81.
142. Jang YO, Kim YJ, Baik SK, Kim MY, Eom YW, Cho MY, et al. Histological improvement following administration of autologous bone marrow-derived mesenchymal stem cells for alcoholic cirrhosis: a pilot study. *Liver international : official journal of the International Association for the Study of the Liver*. 2014;34(1):33-41.
143. Mohamadnejad M, Alimoghaddam K, Bagheri M, Ashrafi M, Abdollahzadeh L, Akhlaghpour S, et al. Randomized placebo-controlled trial of mesenchymal stem cell transplantation in decompensated cirrhosis. *Liver international : official journal of the International Association for the Study of the Liver*. 2013;33(10):1490-6.
144. Mohamadnejad M, Vosough M, Moossavi S, Nikfam S, Mardpour S, Akhlaghpour S, et al. Intraportal Infusion of Bone Marrow Mononuclear or CD133+ Cells in Patients With Decompensated Cirrhosis: A Double-Blind Randomized Controlled Trial. *Stem Cells Transl Med*. 2016;5(1):87-94.
145. Nikeghbalian S, Pournasr B, Aghdami N, Rasekhi A, Geramizadeh B, Hosseini Asl SM, et al. Autologous transplantation of bone marrow-derived mononuclear and CD133(+) cells in patients with decompensated cirrhosis. *Arch Iran Med*. 2011;14(1):12-7.

146. Park CH, Bae SH, Kim HY, Kim JK, Jung ES, Chun HJ, et al. A pilot study of autologous CD34-depleted bone marrow mononuclear cell transplantation via the hepatic artery in five patients with liver failure. *Cytotherapy*. 2013;15(12):1571-9.
147. Peng L, Xie DY, Lin BL, Liu J, Zhu HP, Xie C, et al. Autologous bone marrow mesenchymal stem cell transplantation in liver failure patients caused by hepatitis B: short-term and long-term outcomes. *Hepatology*. 2011;54(3):820-8.
148. Salama H, Zekri AR, Ahmed R, Medhat I, Abdallah el S, Darwish T, et al. Assessment of health-related quality of life in patients receiving stem cell therapy for end-stage liver disease: an Egyptian study. *Stem Cell Res Ther*. 2012;3(6):49.
149. Spahr L, Chalandon Y, Terraz S, Kindler V, Rubbia-Brandt L, Frossard JL, et al. Autologous bone marrow mononuclear cell transplantation in patients with decompensated alcoholic liver disease: a randomized controlled trial. *PloS one*. 2013;8(1):e53719.
150. Zhang Z, Lin H, Shi M, Xu R, Fu J, Lv J, et al. Human umbilical cord mesenchymal stem cells improve liver function and ascites in decompensated liver cirrhosis patients. *J Gastroenterol Hepatol*. 2012;27 Suppl 2:112-20.
151. Gómez-Aristizábal A, Keating A, Davies JE. Mesenchymal Stromal Cells as Supportive Cells for Hepatocytes. *Molecular Therapy*. 2009;17(9):1504-8.
152. Fitzpatrick E, Wu Y, Dhadda P, Hughes RD, Mitry RR, Qin H, et al. Coculture with mesenchymal stem cells results in improved viability and function of human hepatocytes. *Cell Transplant*. 2015;24(1):73-83.
153. Alwahsh SM, Rashidi H, Hay DC. Liver cell therapy: is this the end of the beginning? *Cell Mol Life Sci*. 2018;75(8):1307-24.
154. Kulkarni S, Rudnick DA. Induced Pluripotent Stem Cell-Derived Hepatocytes and Precision Medicine in Human Liver Disease. *J Pediatr Gastroenterol Nutr*. 2018;66(5):716-9.
155. Kuse Y, Taniguchi H. Present and Future Perspectives of Using Human-Induced Pluripotent Stem Cells and Organoid Against Liver Failure. *Cell Transplant*. 2019;28(1_suppl):160S-5S.
156. Vosough M, Moslem M, Pournasr B, Baharvand H. Cell-based therapeutics for liver disorders. *Br Med Bull*. 2011;100:157-72.
157. Rashid ST, Corbineau S, Hannan N, Marciniak SJ, Miranda E, Alexander G, et al. Modeling inherited metabolic disorders of the liver using human induced pluripotent stem cells. *J Clin Invest*. 2010;120(9):3127-36.
158. Hosseini V, Maroufi NF, Saghati S, Asadi N, Darabi M, Ahmad SNS, et al. Current progress in hepatic tissue regeneration by tissue engineering. *Journal of translational medicine*. 2019;17(1):383.
159. Tahara S, Sharma S, De Faria FCC, Sarchet P, Tomasello L, Rentsch S, et al. Comparison of three-dimensional cell culture techniques of dedifferentiated liposarcoma and their integration with future research. *Frontiers in Cell and Developmental Biology*. 2024;12.
160. Kreß S, Almeria C, Nebel S, Faust D, Kasper C. Application of Scaffold-Free 3D Models. In: Kasper C, Egger D, Lavrentieva A, editors. *Basic Concepts on 3D Cell Culture*. Cham: Springer International Publishing; 2021. p. 147-74.
161. Torok E, Lutgehetmann M, Bierwolf J, Melbeck S, Dullmann J, Nashan B, et al. Primary human hepatocytes on biodegradable poly(l-lactic acid) matrices: a promising model for improving transplantation efficiency with tissue engineering. *Liver transplantation : official publication of the American Association for the Study of Liver Diseases and the International Liver Transplantation Society*. 2011;17(2):104-14.

162. Yuan J, Li W, Huang J, Guo X, Li X, Lu X, et al. Transplantation of human adipose stem cell-derived hepatocyte-like cells with restricted localization to liver using acellular amniotic membrane. *Stem Cell Res Ther.* 2015;6:217.
163. Wang Y-N, Khokhlova TD, Buravkov S, Chernikov V, Kreider W, Partanen A, et al. Mechanical decellularization of tissue volumes using boiling histotripsy. *Physics in Medicine & Biology.* 2018;63(23):235023.
164. Collin de l'Hortet A, Takeishi K, Guzman-Lepe J, Handa K, Matsubara K, Fukumitsu K, et al. Liver-Regenerative Transplantation: Regrow and Reset. *Am J Transplant.* 2016;16(6):1688-96.
165. Hu H, Gehart H, Artegiani B, C LO-I, Dekkers F, Basak O, et al. Long-Term Expansion of Functional Mouse and Human Hepatocytes as 3D Organoids. *Cell.* 2018;175(6):1591-606 e19.
166. Wu LJ, Chen ZY, Wang Y, Zhao JG, Xie XZ, Chen G. Organoids of liver diseases: From bench to bedside. *World J Gastroenterol.* 2019;25(16):1913-27.
167. Takebe T, Sekine K, Enomura M, Koike H, Kimura M, Ogaeri T, et al. Vascularized and functional human liver from an iPSC-derived organ bud transplant. *Nature.* 2013;499(7459):481-4.
168. Mitragotri S. Healing sound: the use of ultrasound in drug delivery and other therapeutic applications. *Nat Rev Drug Discov.* 2005;4(3):255-60.
169. Koneru J, Alaparathi R, Yalamanchali S, Reddy R. Therapeutic ultrasound - The healing sound and its applications in oral diseases: The review of literature. *Journal of Orofacial Sciences.* 2012;4(1):3-6.
170. Coussios C.C. RRA. Applications of Acoustics and Cavitation to Noninvasive Therapy and Drug Delivery. *Annual Review of Fluid Mechanics.* 2008;40(1):395-420.
171. Illing RO, Kennedy JE, Wu F, ter Haar GR, Protheroe AS, Friend PJ, et al. The safety and feasibility of extracorporeal high-intensity focused ultrasound (HIFU) for the treatment of liver and kidney tumours in a Western population. *British journal of cancer.* 2005;93:890-5.
172. Leighton TG. What is ultrasound ? *Progress in Biophysics & Molecular Biology.* 2007;93:3-83.
173. Dalecki D. Mechanical bioeffects of ultrasound. *Annu Rev Biomed Eng.* 2004;6:229-48.
174. Facciorusso A, Serviddio G, Muscatiello N. Local ablative treatments for hepatocellular carcinoma: An updated review. *World J Gastrointest Pharmacol Ther.* 2016;7(4):477-89.
175. Rokhina EV, Lens P, Virkutyte J. Low-frequency ultrasound in biotechnology: state of the art. *Trends in Biotechnology.* 2009;27:298-306.
176. She WH, Cheung TT, Jenkins CR, Irwin MG. Clinical applications of high-intensity focused ultrasound. *Hong Kong Med J.* 2016;22(4):382-92.
177. Robertson VJ, Baker KG. A review of therapeutic ultrasound: effectiveness studies. *Phys Ther.* 2001;81(7):1339-50.
178. Diana M, Schiraldi L, Liu YY, Memeo R, Mutter D, Pessaux P, et al. High intensity focused ultrasound (HIFU) applied to hepato-bilio-pancreatic and the digestive system-current state of the art and future perspectives. *Hepatobiliary Surg Nutr.* 2016;5(4):329-44.
179. Tomizawa M, Shinozaki F, Motoyoshi Y, Sugiyama T, Yamamoto S, Sueishi M. Sonoporation: Gene transfer using ultrasound. *World journal of methodology.* 2013;3:39-44.

180. Tyler WJ, Tufail Y, Finsterwald M, Tauchmann ML, Olson EJ, Majestic C. Remote excitation of neuronal circuits using low-intensity, low-frequency ultrasound. *PloS one*. 2008;3.
181. Wu F, Wang ZB, Cao YD, Chen WZ, Bai J, Zou JZ, et al. A randomised clinical trial of high-intensity focused ultrasound ablation for the treatment of patients with localised breast cancer. *British journal of cancer*. 2003;89:2227-33.
182. Ahmadi F, McLoughlin IV, Chauhan S, ter-Haar G. Bio-effects and safety of low-intensity, low-frequency ultrasonic exposure. *Prog Biophys Mol Biol*. 2012;108(3):119-38.
183. Mendiratta-Lala M, Wiggermann P, Pech M, Serres-Créixams X, White SB, Davis C, et al. The #HOPE4LIVER Single-Arm Pivotal Trial for Histotripsy of Primary and Metastatic Liver Tumors. *Radiology*. 2024;312(3):e233051.
184. FDA U. FDA approves first MRI-guided focused ultrasound device to treat essential tremor: FDA; July 11, 2016 [Available from: <https://www.fda.gov/news-events/press-announcements/fda-approves-first-mri-guided-focused-ultrasound-device-treat-essential-tremor>].
185. Foundation F. FDA Approves Focused Ultrasound Treatment for Parkinson's Disease Focused Ultrasound Foundation4 November 2021 [Available from: <https://www.fusfoundation.org/posts/fda-approves-focused-ultrasound-treatment-for-parkinsons-disease/>].
186. Excellence NifHaC. Ultrasound-guided highintensity transcutaneous focused ultrasound for symptomatic uterine fibroids. NICE, guidance Ip; 24 July 2019.
187. Excellence NifHaC. Focal therapy using high-intensity focused ultrasound for localised prostate cancer 05 April 2023 [Available from: <https://www.nice.org.uk/guidance/ipg756>].
188. Excellence NifHaC. EXOGEN ultrasound bone healing system for long bone fractures with non-union or delayed healing: NICE; 09 January 2013 [updated 08 October 2019. Available from: <https://www.nice.org.uk/Guidance/MTG12>].
189. Izadifar Z, Izadifar Z, Chapman D, Babyn P. An Introduction to High Intensity Focused Ultrasound: Systematic Review on Principles, Devices, and Clinical Applications. *Journal of Clinical Medicine*. 2020;9(2):460.
190. Hedrick WR. Ultrasound physics and instrumentation: St. Louis, Mo. : Elsevier Mosby; 2005. 445 pages p.
191. Kremkau FW. Diagnostic ultrasound : principles and instruments: St. Louis, Mo. : Elsevier Saunders; 2006. 521 pages p.
192. Baker KG, Robertson VJ, Duck FA. A review of therapeutic ultrasound: biophysical effects. *Phys Ther*. 2001;81(7):1351-8.
193. ter Haar G. Therapeutic ultrasound. *Eur J Ultrasound*. 1999;9(1):3-9.
194. Johns LD. Nonthermal Effects of Therapeutic Ultrasound: The Frequency Resonance Hypothesis. *Journal of Athletic Training*. 2002;37(3):293-9.
195. O'Daly BJ, Morris E, Gavin GP, O'Byrne JM, McGuinness GB. High-power low-frequency ultrasound: A review of tissue dissection and ablation in medicine and surgery. *Journal of Materials Processing Technology*. 2008;200:38-58.
196. Tachibana K. Emerging technologies in therapeutic ultrasound: thermal ablation to gene delivery. (0914-7470 (Print)).
197. Maloney E, Hwang JH. Emerging HIFU applications in cancer therapy. *International Journal of Hyperthermia*. 2015;31(3):302-9.
198. Lindstrom PA. Prefrontal ultrasonic irradiation-a substitute for lobotomy. *AMA Arch Neurol Psychiatry*. 1954;72(4):399-425.

199. Fry WJ, Barnard JW, Fry EJ, Krumins RF, Brennan JF. Ultrasonic lesions in the mammalian central nervous system. *Science*. 1955;122(3168):517-8.
200. Bachu VS, Kedda J, Suk I, Green JJ, Tyler B. High-Intensity Focused Ultrasound: A Review of Mechanisms and Clinical Applications. *Ann Biomed Eng*. 2021;49(9):1975-91.
201. Hectors SJCG, Jacobs I, Moonen CTW, Strijkers GJ, Nicolay K. MRI methods for the evaluation of high intensity focused ultrasound tumor treatment: Current status and future needs. *Magnetic Resonance in Medicine*. 2016;75(1):302-17.
202. Hectors SJCG, Jacobs I, Strijkers GJ, Nicolay K. Multiparametric MRI Analysis for the Identification of High Intensity Focused Ultrasound-Treated Tumor Tissue. *PloS one*. 2014;9(6):e99936.
203. Van Leenders GJLH, Beerlage HP, Ruijter ET, de la Rosette JJMCH, van de Kaa CA. Histopathological changes associated with high intensity focused ultrasound (HIFU) treatment for localised adenocarcinoma of the prostate. *Journal of Clinical Pathology*. 2000;53(5):391-4.
204. Zhou Y-F. High intensity focused ultrasound in clinical tumor ablation. *World Journal of Clinical Oncology*. 2011;2(1):8.
205. Robertson VJ, Ward AR. Dangers in extrapolating in vitro uses of therapeutic ultrasound. *Phys Ther*. 1996;76(1):78-9.
206. Ramirez A, Schwane JA, McFarland C, Starcher B. The effect of ultrasound on collagen synthesis and fibroblast proliferation in vitro. *Med Sci Sports Exerc*. 1997;29(3):326-32.
207. Bahbah N, Novell A, Bouakaz A, Djelouah H. Linear and nonlinear characterization of microbubbles and tissue using the Nakagami statistical model. *Ultrasonics*. 2017;76:200-7.
208. Constans C, Deffieux T, Pouget P, Tanter M, Aubry JF. A 200 - 1380 kHz Quadrifrequency Focused Ultrasound Transducer For Neurostimulation In Rodents And Primates: Transcranial In Vitro Calibration And Numerical Study Of The Influence Of Skull Cavity. *IEEE transactions on ultrasonics, ferroelectrics, and frequency control*. 2017.
209. Daeichin V, van Rooij T, Skachkov I, Ergin B, Specht PA, Lima A, et al. Microbubble composition and preparation for high-frequency contrast-enhanced ultrasound imaging: in vitro and in vivo evaluation. *IEEE transactions on ultrasonics, ferroelectrics, and frequency control*. 2016.
210. Fix SM, Novell A, Yun Y, Dayton PA, Arena CB. An evaluation of the sonoporation potential of low-boiling point phase-change ultrasound contrast agents in vitro. *J Ther Ultrasound*. 2017;5:7.
211. Roessler FC, Wang Z, Schumacher S, Ohlrich M, Kaps M, Menciassi A, et al. In Vitro Examination of the Thrombolytic Efficacy of Desmoteplase and Therapeutic Ultrasound Compared with rt-PA. *Ultrasound Med Biol*. 2015;41(12):3233-40.
212. Wylie MP, McGuinness GB, Gavin GP. Therapeutic ultrasound angioplasty: the risk of arterial perforation. An in vitro study. *Conference proceedings : Annual International Conference of the IEEE Engineering in Medicine and Biology Society IEEE Engineering in Medicine and Biology Society Annual Conference*. 2009;2009:282-5.
213. Arnal B, Baranger J, Demene C, Tanter M, Pernot M. In vivo real-time cavitation imaging in moving organs. *Phys Med Biol*. 2017;62(3):843-57.
214. Chen R, Paeng DG, Lam KH, Zhou Q, Shung KK, Matsuoka N, et al. In vivo Sonothrombolysis of Ear Marginal Vein of Rabbits Monitored with High-frequency Ultrasound Needle Transducer. *Journal of medical and biological engineering*. 2013;33(1):103-10.

215. Goertz DE, Thind AS, Karshafian R, Ladouceur M, Whyne CM, Foster FS, et al. In vivo feasibility study of ultrasound potentiated collagenase therapy of chronic total occlusions. *Ultrasonics*. 2014;54(1):20-4.
216. Huang JJ, Shi YQ, Li RL, Hu A, Zhou HS, Cheng Q, et al. Angiogenesis effect of therapeutic ultrasound on ischemic hind limb in mice. *American journal of translational research*. 2014;6(6):703-13.
217. King RL, Brown JR, Pauly KB. Localization of ultrasound-induced in vivo neurostimulation in the mouse model. *Ultrasound Med Biol*. 2014;40(7):1512-22.
218. Lu ZY, Li RL, Zhou HS, Huang JJ, Qi J, Su ZX, et al. Rescue of hypertension-related impairment of angiogenesis by therapeutic ultrasound. *American journal of translational research*. 2016;8(7):3087-96.
219. Nabili M, Shenoy A, Chawla S, Mahesh S, Liu J, Geist C, et al. Ultrasound-enhanced ocular delivery of dexamethasone sodium phosphate: an in vivo study. *J Ther Ultrasound*. 2014;2:6.
220. Pacella JJ, Brands J, Schnatz FG, Black JJ, Chen X, Villanueva FS. Treatment of microvascular micro-embolization using microbubbles and long-tone-burst ultrasound: an in vivo study. *Ultrasound Med Biol*. 2015;41(2):456-64.
221. Vlaisavljevich E, Kim Y, Allen S, Owens G, Pelletier S, Cain C, et al. Image-guided non-invasive ultrasound liver ablation using histotripsy: feasibility study in an in vivo porcine model. *Ultrasound Med Biol*. 2013;39(8):1398-409.
222. Yariv I, Lipovsky A, Gedanken A, Lubart R, Fixler D. Enhanced pharmacological activity of vitamin B(1)(2) and penicillin as nanoparticles. *Int J Nanomedicine*. 2015;10:3593-601.
223. Draper DO, Sunderland S, Kirkendall DT, Ricard M. A comparison of temperature rise in human calf muscles following applications of underwater and topical gel ultrasound. *The Journal of orthopaedic and sports physical therapy*. 1993;17(5):247-51.
224. Rimington SJ, Draper DO, Durrant E, Fellingham G. Temperature changes during therapeutic ultrasound in the precooled human gastrocnemius muscle. *Journal of athletic training*. 1994;29(4):325-7.
225. Abbas S, Peng P. Basic Principles and Physics of Ultrasound. In: Peng P, Finlayson R, Lee SH, Bhatia A, editors. *Ultrasound for Interventional Pain Management: An Illustrated Procedural Guide*. Cham: Springer International Publishing; 2020. p. 1-31.
226. Yetik H, Ariyurek C, Bozkurt A, Ergun AS, editors. Frequency optimization in high intensity focused ultrasound. 2014 IEEE International Ultrasonics Symposium; 2014 3-6 Sept. 2014.
227. Key R. Ultrasound Properties: Radiolog Key; [Available from: <https://radiologykey.com/ultrasound-10/>].
228. Rahimian S, Tavakkoli J. Estimating dynamic changes of tissue attenuation coefficient during high-intensity focused ultrasound treatment. *Journal of therapeutic ultrasound*. 2013;1(1):14.
229. Gallo JA, Draper DO, Brody LT, Fellingham GW. A comparison of human muscle temperature increases during 3-MHz continuous and pulsed ultrasound with equivalent temporal average intensities. *The Journal of orthopaedic and sports physical therapy*. 2004;34(7):395-401.
230. Doan N, Reher P, Meghji S, Harris M. In vitro effects of therapeutic ultrasound on cell proliferation, protein synthesis, and cytokine production by human fibroblasts, osteoblasts, and monocytes. *Journal of Oral and Maxillofacial Surgery*. 1999;57(4):409-19.

231. Sklar LR, El Tal AK, Kerwin LY. Use of Transcutaneous Ultrasound for Lipolysis and Skin Tightening: A Review. *Aesthetic Plastic Surgery*. 2014;38(2):429-41.
232. Chetverikova EP, Pashovkin TN, Rosanova NA, Sarvazyan AP, Williams AR. Interaction of therapeutic ultrasound with purified enzymes in vitro. *Ultrasonics*. 1985;23(4):183-8.
233. Wu J-p, Yu J, Fowlkes JB, Liang P, Nolsøe CP. US-guided ablation of tumors – where is it used and how did we get there. *Med-X*. 2023;1(1):5.
234. Aubry JF, Pauly KB, Moonen C, Haar G, Ries M, Salomir R, et al. The road to clinical use of high-intensity focused ultrasound for liver cancer: technical and clinical consensus. *J Ther Ultrasound*. 2013;1:13.
235. Ellens N, Hynynen K. Frequency considerations for deep ablation with high-intensity focused ultrasound: A simulation study. *Med Phys*. 2015;42(8):4896-10.
236. Habibi M, Berger RD, Calkins H. Radiofrequency ablation: technological trends, challenges, and opportunities. *EP Europace*. 2020;23(4):511-9.
237. Jiao J, Wu F, Zou J, Li F, Liu F, Zhao X, et al. [Effect of ablations by pulsed versus continuous high-intensity focused ultrasound on isolated perfused porcine liver]. *Nan fang yi ke da xue xue bao = Journal of Southern Medical University*. 2013;33(2):230-4.
238. Guan L, Xu G. Destructive effect of HIFU on rabbit embedded endometrial carcinoma tissues and their vascularities. *Oncotarget*. 2017.
239. Einhorn TA, Gerstenfeld LC. Fracture healing: mechanisms and interventions. *Nat Rev Rheumatol*. 2015;11(1):45-54.
240. Speed Ca. Therapeutic ultrasound in soft tissue lesions. *Rheumatology (Oxford, England)*. 2001;40:1331-6.
241. Shek SY, Yeung CK, Chan JC, Chan HH. Efficacy of high-intensity focused ultrasonography for noninvasive body sculpting in Chinese patients. *Lasers in surgery and medicine*. 2014;46(4):263-9.
242. Suh DH, Choi JH, Lee SJ, Jeong KH, Song KY, Shin MK. Comparative histometric analysis of the effects of high-intensity focused ultrasound and radiofrequency on skin. *Journal of cosmetic and laser therapy : official publication of the European Society for Laser Dermatology*. 2015;17(5):230-6.
243. Yang K-H, Parvizi J, Wang S-J, Lewallen DG, Kinnick RR, Greenleaf JF, et al. Exposure to low-intensity ultrasound increases aggrecan gene expression in a rat femur fracture model. *Journal of Orthopaedic Research*. 1996;14(5):802-9.
244. Vachaparambil KJ, Einarsrud KE. Explanation of Bubble Nucleation Mechanisms: A Gradient Theory Approach. *Journal of The Electrochemical Society*. 2018;165(10):E504-E12.
245. de Andrade MO, Haqshenas R, Pahk KJ, Saffari N. Mechanisms of nuclei growth in ultrasound bubble nucleation. *Ultrason Sonochem*. 2022;88:106091.
246. Bui TQ, Ngo HT, Tran HT. Surface-protective assistance of ultrasound in synthesis of superparamagnetic magnetite nanoparticles and in preparation of mono-core magnetite-silica nanocomposites. *Journal of Science: Advanced Materials and Devices*. 2018;3(3):323-30.
247. Yeats E, Lu N, Sukovich JR, Xu Z, Hall TL. Soft Tissue Aberration Correction for Histotripsy Using Acoustic Emissions From Cavitation Cloud Nucleation and Collapse. *Ultrasound in Medicine & Biology*. 2023.
248. Bader KB, Vlaisavljevich E, Maxwell AD. For Whom the Bubble Grows: Physical Principles of Bubble Nucleation and Dynamics in Histotripsy Ultrasound Therapy. *Ultrasound in medicine & biology*. 2019;45(5):1056-80.

249. Crum LA, Fowlkes JB. Acoustic cavitation generated by microsecond pulses of ultrasound. *Nature*. 1986;319(6048):52-4.
250. Stewart HG SM. An Overview Of Ultrasound: Theory, Measurement, Medical Applications, and Biological Effects. 1982:82–8190.
251. Khokhlova TD, Canney MS, Khokhlova VA, Sapozhnikov OA, Crum LA, Bailey MR. Controlled tissue emulsification produced by high intensity focused ultrasound shock waves and millisecond boiling. *The Journal of the Acoustical Society of America*. 2011;130(5):3498-510.
252. Vlaisavljevich E, Lin K-W, Warnez MT, Singh R, Mancina L, Putnam AJ, et al. Effects of tissue stiffness, ultrasound frequency, and pressure on histotripsy-induced cavitation bubble behavior. *Physics in Medicine & Biology*. 2015;60(6):2271.
253. Carroll D ML, Hacking C, et al. Ultrasound Attenuation Radiopedia10 Apr 2019 [updated 3 Jun 2024].
254. Pahk KJ, G  lat P, Kim H, Saffari N. Bubble dynamics in boiling histotripsy. *Ultrasound in Medicine & Biology*. 2018;44(12):2673-96.
255. Xu Z, Hall TL, Vlaisavljevich E, Lee FT. Histotripsy: the first noninvasive, non-ionizing, non-thermal ablation technique based on ultrasound. *International Journal of Hyperthermia*. 2021;38(1):561-75.
256. Maxwell AD, Cain CA, Hall TL, Fowlkes JB, Xu Z. Probability of cavitation for single ultrasound pulses applied to tissues and tissue-mimicking materials. *Ultrasound in medicine & biology*. 2013;39(3):449-65.
257. Vlaisavljevich E, Maxwell A, Mancina L, Johnsen E, Cain C, Xu Z. Visualizing the Histotripsy Process: Bubble Cloud–Cancer Cell Interactions in a Tissue-Mimicking Environment. *Ultrasound in Medicine & Biology*. 2016;42(10):2466-77.
258. WL N. Physical mechanisms for biological effects of ultrasound. 1978:78-8062.
259. Wu J. Acoustic Streaming and Its Applications. *Fluids*. 2018;3(4):108.
260. Miller DL. Overview of experimental studies of biological effects of medical ultrasound caused by gas body activation and inertial cavitation. *Prog Biophys Mol Biol*. 2007;93(1-3):314-30.
261. Burks SR, Nguyen BA, Tebebi PA, Kim SJ, Bresler MN, Ziadloo A, et al. Pulsed Focused Ultrasound Pretreatment Improves Mesenchymal Stromal Cell Efficacy in Preventing and Rescuing Established Acute Kidney Injury in Mice. *STEM CELLS*. 2015;33(4):1241-53.
262. Dyson M, Suckling J. Stimulation of tissue repair by ultrasound: a survey of the mechanisms involved. *Physiotherapy*. 1978;64(4):105-8.
263. ter Haar GR. High intensity focused ultrasound for the treatment of tumors. *Echocardiography*. 2001;18(4):317-22.
264. Khokhlova VA, Fowlkes JB, Roberts WW, Schade GR, Xu Z, Khokhlova TD, et al. Histotripsy methods in mechanical disintegration of tissue: Towards clinical applications. *International Journal of Hyperthermia*. 2015;31(2):145-62.
265. Vlaisavljevich E, Lin KW, Maxwell A, Warnez MT, Mancina L, Singh R, et al. Effects of ultrasound frequency and tissue stiffness on the histotripsy intrinsic threshold for cavitation. *Ultrasound Med Biol*. 2015;41(6):1651-67.
266. Duc NM, Keserci B. Emerging clinical applications of high-intensity focused ultrasound. *Diagnostic and Interventional Radiology*. 2019;25(5):398-409.
267. Sharma S, Pandey S. Treatment of essential tremor: current status. *Postgrad Med J*. 2020;96(1132):84-93.
268. Jagannathan J, Sanghvi NT, Crum LA, Yen C-P, Medel R, Dumont AS, et al. HIGH-INTENSITY FOCUSED ULTRASOUND SURGERY OF THE BRAIN. *Neurosurgery*. 2009;64(2):201-11.

269. Elias WJ, Lipsman N, Ondo WG, Ghanouni P, Kim YG, Lee W, et al. A Randomized Trial of Focused Ultrasound Thalamotomy for Essential Tremor. *New England Journal of Medicine*. 2016;375(8):730-9.
270. Martínez-Fernández R, Máñez-Miró JU, Rodríguez-Rojas R, Del Álamo M, Shah BB, Hernández-Fernández F, et al. Randomized Trial of Focused Ultrasound Subthalamotomy for Parkinson's Disease. *New England Journal of Medicine*. 2020;383(26):2501-13.
271. Sastre-Bataller I, Campins-Romeu M, Marcos-Carrión A, Gutiérrez-Martín A, Conde-Sardón R, Losada-López M, et al. Gait Function after High-Intensity Focused Ultrasound Thalamotomy for Essential Tremor: Searching for Technique Optimization. *Stereotactic and Functional Neurosurgery*. 2023;101(1):12-21.
272. Zhang M, Rodrigues A, Zhou Q, Li G. Focused ultrasound: growth potential and future directions in neurosurgery. *Journal of Neuro-Oncology*. 2022;156(1):23-32.
273. Quadri SA, Waqas M, Khan I, Khan MA, Suriya SS, Farooqui M, et al. High-intensity focused ultrasound: past, present, and future in neurosurgery. *Neurosurgical Focus*. 2018;44(2):E16.
274. Foundation FU. Focused Ultrasound Now FDA Approved to Treat Essential Tremor Patients' Second Side 5 January 2023 [Available from: <https://www.fusfoundation.org/posts/focused-ultrasound-now-fda-approved-to-treat-essential-tremor-patients-second-side/#:~:text=The%20US%20Food%20and%20Drug,million%20individuals%20in%20the%20US>].
275. Lipsman N, Mainprize TG, Schwartz ML, Hynynen K, Lozano AM. Intracranial Applications of Magnetic Resonance-guided Focused Ultrasound. *Neurotherapeutics*. 2014;11(3):593-605.
276. Meng Y, Goubran M, Rabin JS, McSweeney M, Ottoy J, Pople CB, et al. Blood-brain barrier opening of the default mode network in Alzheimer's disease with magnetic resonance-guided focused ultrasound. *Brain*. 2023;146(3):865-72.
277. Afif S, Rehan ST, Ul Hussain H, Islam MS. Low-intensity focused ultrasound, a novel approach to epilepsy treatment in developing countries. *Brain and Behavior*. 2023;13(1).
278. Krishna V, Mindel J, Sammartino F, Block C, Dwivedi AK, Jamie J, et al. A phase 1 open-label trial evaluating focused ultrasound unilateral anterior thalamotomy for focal onset epilepsy. *Epilepsia*. 2023.
279. Ali Nasser Hamad Alshareef (1)* HAHA, Ismael Meshal Aboud Alshareef (3), Aboud Meshal Aboud Alshareef (3), Ali Mana Mohsen Alsharif (4), Ali Mohammad Sultan Al Sharif (5), Abdullah Huseen Hamad Al Sharief (4), Abdullah Nasser Hamad Alsharif (4). Application of New Ultrasound Technology in Spinal Cord Injury: A Systematic Review. *Annals of Clinical and Analytical Medicine*. 2022;10(1):586-92.
280. Roberts JW, Powlovich L, Sheybani N, LeBlang S. Focused ultrasound for the treatment of glioblastoma. *J Neurooncol*. 2022;157(2):237-47.
281. Englander ZK, Wei H-J, Pouliopoulos AN, Bendau E, Upadhyayula P, Jan C-I, et al. Focused ultrasound mediated blood-brain barrier opening is safe and feasible in a murine pontine glioma model. *Scientific Reports*. 2021;11(1):6521.
282. Cohen-Inbar O, Xu Z, Sheehan JP. Focused ultrasound-aided immunomodulation in glioblastoma multiforme: a therapeutic concept. *Journal of therapeutic ultrasound*. 2016;4(1):2.
283. Burgess A, Huang Y, Waspe AC, Ganguly M, Goertz DE, Hynynen K. High-Intensity Focused Ultrasound (HIFU) for Dissolution of Clots in a Rabbit Model of Embolic Stroke. *PloS one*. 2012;7(8):e42311.

284. Gerhardson T, Sukovich JR, Chaudhary N, Chenevert TL, Ives K, Hall TL, et al. Histotripsy Clot Liquefaction in a Porcine Intracerebral Hemorrhage Model. *Neurosurgery*. 2020;86(3):429-36.
285. Sukovich JR, Cain CA, Pandey AS, Chaudhary N, Camelo-Piragua S, Allen SP, et al. In vivo histotripsy brain treatment. *Journal of Neurosurgery*. 2019;131(4):1331-8.
286. Tharkar P, Varanasi R, Wong WSF, Jin CT, Chrzanowski W. Nano-Enhanced Drug Delivery and Therapeutic Ultrasound for Cancer Treatment and Beyond. *Frontiers in Bioengineering and Biotechnology*. 2019;7.
287. Qin P, Han T, Yu ACH, Xu L. Mechanistic understanding the bioeffects of ultrasound-driven microbubbles to enhance macromolecule delivery. *Journal of Controlled Release*. 2018;272:169-81.
288. Yuksel Durmaz Y, Vlaisavljevich E, Xu Z, Elsayed M. Development of Nanodroplets for Histotripsy-Mediated Cell Ablation. *Molecular Pharmaceutics*. 2014;11(10):3684-95.
289. Hu L, Batheja P, Meidan V, Michniak-Kohn BB. CHAPTER 4 - Iontophoretic Transdermal Drug Delivery. In: Kulkarni VS, editor. *Handbook of Non-Invasive Drug Delivery Systems*. Boston: William Andrew Publishing; 2010. p. 95-118.
290. Jangjou A, Meisami AH, Jamali K, Niakan MH, Abbasi M, Shafiee M, et al. The promising shadow of microbubble over medical sciences: from fighting wide scope of prevalence disease to cancer eradication. *Journal of Biomedical Science*. 2021;28(1).
291. Kong C, Chang WS. Preclinical Research on Focused Ultrasound-Mediated Blood-Brain Barrier Opening for Neurological Disorders: A Review. *Neurol Int*. 2023;15(1):285-300.
292. Hsiao YH, Kuo SJ, Tsai HD, Chou MC, Yeh GP. Clinical Application of High-intensity Focused Ultrasound in Cancer Therapy. *J Cancer*. 2016;7(3):225-31.
293. Sehmbi AS, Froghi S, Oliveira de Andrade M, Saffari N, Fuller B, Quaglia A, et al. Systematic review of the role of high intensity focused ultrasound (HIFU) in treating malignant lesions of the hepatobiliary system. *HPB (Oxford)*. 2021;23(2):187-96.
294. Campbell WA, Makary MS. Advances in Image-Guided Ablation Therapies for Solid Tumors. *Cancers*. 2024;16(14):2560.
295. Numata K, Wang F. New developments in ablation therapy for hepatocellular carcinoma: combination with systemic therapy and radiotherapy. *Hepatobiliary Surgery and Nutrition*. 2022;11(5):766-9.
296. Izzo F, Granata V, Grassi R, Fusco R, Palaia R, Delrio P, et al. Radiofrequency Ablation and Microwave Ablation in Liver Tumors: An Update. *The Oncologist*. 2019;24(10):e990-e1005.
297. Bhansali AP, Gwinn RP. Ablation: Radiofrequency, Laser, and HIFU. In: Pouratian N, Sheth SA, editors. *Stereotactic and Functional Neurosurgery: Principles and Applications*. Cham: Springer International Publishing; 2020. p. 223-33.
298. Lynne Eldridge M. Stereotactic Body Radiotherapy (SBRT) Side Effects and More verywellhealthNovember 14, 2024 [updated November 14, 2024. Available from: https://www.verywellhealth.com/what-is-sbrrt-2249187?utm_source=chatgpt.com.
299. Haar GT, Coussios C. High intensity focused ultrasound: physical principles and devices. *Int J Hyperthermia*. 2007;23(2):89-104.
300. Cheung TT, Poon RT, Jenkins CR, Chu FS, Chok KS, Chan AC, et al. Survival analysis of high-intensity focused ultrasound therapy vs. transarterial chemoembolization for unresectable hepatocellular carcinomas. *Liver international : official journal of the International Association for the Study of the Liver*. 2014;34(6):e136-43.

301. Zhu H, Zhou K, Zhang L, Jin C, Peng S, Yang W, et al. High intensity focused ultrasound (HIFU) therapy for local treatment of hepatocellular carcinoma: role of partial rib resection. *European journal of radiology*. 2009;72(1):160-6.
302. Zhang L, Zhu H, Jin C, Zhou K, Li K, Su H, et al. High-intensity focused ultrasound (HIFU): effective and safe therapy for hepatocellular carcinoma adjacent to major hepatic veins. *European radiology*. 2009;19(2):437-45.
303. Numata K, Fukuda H, Ohto M, Itou R, Nozaki A, Kondou M, et al. Evaluation of the therapeutic efficacy of high-intensity focused ultrasound ablation of hepatocellular carcinoma by three-dimensional sonography with a perflubutane-based contrast agent. *European journal of radiology*. 2010;75(2):e67-75.
304. Jin C, Zhu H, Wang Z, Wu F, Chen W, Li K, et al. High-intensity focused ultrasound combined with transarterial chemoembolization for unresectable hepatocellular carcinoma: long-term follow-up and clinical analysis. *European journal of radiology*. 2011;80(3):662-9.
305. Wang Y, Wang W, Tang J. Ultrasound-guided high-intensity focused ultrasound treatment for needle-track seeding of hepatocellular carcinoma: preliminary results. *Int J Hyperthermia*. 2010;26(5):441-7.
306. Ng KK, Poon RT, Chan SC, Chok KS, Cheung TT, Tung H, et al. High-intensity focused ultrasound for hepatocellular carcinoma: a single-center experience. *Ann Surg*. 2011;253(5):981-7.
307. Xu G, Luo G, He L, Li J, Shan H, Zhang R, et al. Follow-up of high-intensity focused ultrasound treatment for patients with hepatocellular carcinoma. *Ultrasound Med Biol*. 2011;37(12):1993-9.
308. Cheung TT, Chok KS, Lo RC, Sharr WW, Chan SC, Poon RT, et al. High-intensity focused ultrasound ablation as a bridging therapy for hepatocellular carcinoma patients awaiting liver transplantation. *Hepatobiliary Pancreat Dis Int*. 2012;11(5):542-4.
309. Fukuda H, Numata K, Nozaki A, Morimoto M, Kondo M, Tanaka K, et al. Findings of multidetector row computed tomography of HCCs treated by HIFU ablation. *European journal of radiology*. 2012;81(3):e239-43.
310. Leslie T, Ritchie R, Illing R, Ter Haar G, Phillips R, Middleton M, et al. High-intensity focused ultrasound treatment of liver tumours: post-treatment MRI correlates well with intra-operative estimates of treatment volume. *The British journal of radiology*. 2012;85(1018):1363-70.
311. Kim J, Chung DJ, Jung SE, Cho SH, Hahn ST, Lee JM. Therapeutic effect of high-intensity focused ultrasound combined with transarterial chemoembolisation for hepatocellular carcinoma <5 cm: comparison with transarterial chemoembolisation monotherapy--preliminary observations. *The British journal of radiology*. 2012;85(1018):e940-6.
312. Ni S, Liu L, Shu Y. Sequential transcatheter arterial chemoembolization, three-dimensional conformal radiotherapy, and high-intensity focused ultrasound treatment for unresectable hepatocellular carcinoma patients. *J Biomed Res*. 2012;26(4):260-7.
313. Cheung TT, Chu FS, Jenkins CR, Tsang DS, Chok KS, Chan AC, et al. Tolerance of high-intensity focused ultrasound ablation in patients with hepatocellular carcinoma. *World journal of surgery*. 2012;36(10):2420-7.
314. Chan AC, Cheung TT, Fan ST, Chok KS, Chan SC, Poon RT, et al. Survival analysis of high-intensity focused ultrasound therapy versus radiofrequency ablation in the treatment of recurrent hepatocellular carcinoma. *Ann Surg*. 2013;257(4):686-92.
315. Cheung TT, Fan ST, Chu FS, Jenkins CR, Chok KS, Tsang SH, et al. Survival analysis of high-intensity focused ultrasound ablation in patients with small hepatocellular carcinoma. *HPB (Oxford)*. 2013;15(8):567-73.

316. Fukuda H, Numata K, Nozaki A, Kondo M, Morimoto M, Maeda S, et al. High-intensity focused ultrasound ablation assisted using color Doppler imaging for the treatment of hepatocellular carcinomas. *Abdominal imaging*. 2013;38(6):1263-8.
317. Cheung TT, Fan ST, Chan SC, Chok KS, Chu FS, Jenkins CR, et al. High-intensity focused ultrasound ablation: an effective bridging therapy for hepatocellular carcinoma patients. *World J Gastroenterol*. 2013;19(20):3083-9.
318. Wang S, Yang C, Zhang J, Kong XR, Zhu H, Wu F, et al. First experience of high-intensity focused ultrasound combined with transcatheter arterial embolization as local control for hepatoblastoma. *Hepatology*. 2014;59(1):170-7.
319. Zhu J, Zhu H, Mei Z, Jin C, Ran L, Zhou K, et al. High-intensity focused ultrasound ablation for treatment of hepatocellular carcinoma and hypersplenism: preliminary study. *Journal of ultrasound in medicine : official journal of the American Institute of Ultrasound in Medicine*. 2013;32(10):1855-62.
320. Chok KS, Cheung TT, Lo RC, Chu FS, Tsang SH, Chan AC, et al. Pilot study of high-intensity focused ultrasound ablation as a bridging therapy for hepatocellular carcinoma patients wait-listed for liver transplantation. *Liver transplantation : official publication of the American Association for the Study of Liver Diseases and the International Liver Transplantation Society*. 2014;20(8):912-21.
321. Zhang Q, Bian SQ, Lv W, Kou D, Hu HL, Guo SS, et al. Observation of efficacy of TACE combined with HIFU on patients with middle-advanced liver cancer. *Eur Rev Med Pharmacol Sci*. 2019;23(3 Suppl):239-46.
322. Luo Y, Jiang Y. Comparison of Efficiency of TACE plus HIFU and TACE alone on Patients with Primary Liver Cancer. *J Coll Physicians Surg Pak*. 2019;29(5):414-7.
323. Zhang Y, Zhao J, Guo D, Zhong W, Ran L. Evaluation of short-term response of high intensity focused ultrasound ablation for primary hepatic carcinoma: utility of contrast-enhanced MRI and diffusion-weighted imaging. *European journal of radiology*. 2011;79(3):347-52.
324. Vidal-Jove J, Serres X, Vlaisavljevich E, Cannata J, Duryea A, Miller R, et al. First-in-man histotripsy of hepatic tumors: the THERESA trial, a feasibility study. *International Journal of Hyperthermia*. 2022;39(1):1115-23.
325. Nishikawa H, Osaki Y. Comparison of high-intensity focused ultrasound therapy and radiofrequency ablation for recurrent hepatocellular carcinoma. *Hepatobiliary Surg Nutr*. 2013;2(3):168-70.
326. Khokhlova TD, Hwang JH. HIFU for Palliative Treatment of Pancreatic Cancer. *Adv Exp Med Biol*. 2016;880:83-95.
327. Thudium M, Bette B, Tonguc T, Ghaei S, Conrad R, Becher MU, et al. Multidisciplinary management and outcome in pancreatic cancer patients treated with high-intensity focused ultrasound. *International Journal of Hyperthermia*. 2020;37(1):456-62.
328. Wu F. High intensity focused ultrasound: a noninvasive therapy for locally advanced pancreatic cancer. *World J Gastroenterol*. 2014;20(44):16480-8.
329. Wang K, Zhu H, Meng Z, Chen Z, Lin J, Shen Y, et al. Safety evaluation of high-intensity focused ultrasound in patients with pancreatic cancer. *Onkologie*. 2013;36(3):88-92.
330. Sung HY, Jung SE, Cho SH, Zhou K, Han JY, Han ST, et al. Long-term outcome of high-intensity focused ultrasound in advanced pancreatic cancer. *Pancreas*. 2011;40(7):1080-6.
331. Dababou S, Marrocchio C, Rosenberg J, Bitton R, Pauly KB, Napoli A, et al. A meta-analysis of palliative treatment of pancreatic cancer with high intensity focused ultrasound. *Journal of therapeutic ultrasound*. 2017;5(1):9.

332. Strunk HM, Henseler J, Rauch M, Mücke M, Kukuk G, Cuhls H, et al. Clinical Use of High-Intensity Focused Ultrasound (HIFU) for Tumor and Pain Reduction in Advanced Pancreatic Cancer. *Rofo*. 2016;188(07):662-70.
333. Nikfarjam M, Muralidharan V, Christophi C. Mechanisms of focal heat destruction of liver tumors. *J Surg Res*. 2005;127(2):208-23.
334. Wheatley DN, Kerr C, Gregory DW. Heat-induced damage to HeLa-S3 cells: correlation of viability, permeability, osmosensitivity, phase-contrast light-, scanning electron- and transmission electron-microscopical findings. *Int J Hyperthermia*. 1989;5(2):145-62.
335. Ning Z, Xie J, Chen Q, Zhang C, Xu L, Song L, et al. <p>HIFU is safe, effective, and feasible in pancreatic cancer patients: a monocentric retrospective study among 523 patients</p>. *OncoTargets and Therapy*. 2019;Volume 12:1021-9.
336. Fergadi MP, Magouliotis DE, Rountas C, Vlychou M, Athanasiou T, Symeonidis D, et al. A meta-analysis evaluating the role of high-intensity focused ultrasound (HIFU) as a fourth treatment modality for patients with locally advanced pancreatic cancer. *Abdominal Radiology*. 2022;47(1):254-64.
337. Lynch J. Tumor-destroying soundwaves receive FDA approval for liver treatment in humans Michigan University October 9, 2023 [Available from: https://www.michiganmedicine.org/health-lab/tumor-destroying-soundwaves-receive-fda-approval-liver-treatment-humans?utm_source=chatgpt.com].
338. Khokhlova TD, Schade GR, Wang Y-N, Buravkov SV, Chernikov VP, Simon JC, et al. Pilot in vivo studies on transcutaneous boiling histotripsy in porcine liver and kidney. *Scientific Reports*. 2019;9(1).
339. Xu Z, Khokhlova TD, Cho CS, Khokhlova VA. Histotripsy: A Method for Mechanical Tissue Ablation with Ultrasound. *Annual Review of Biomedical Engineering*. 2024;26(Volume 26, 2024):141-67.
340. Wang Y-N, Khokhlova TD, Buravkov S, Chernikov V, Kreider W, Partanen A, et al. Mechanical decellularization of tissue volumes using boiling histotripsy. *Physics in Medicine & Biology*. 2018;63(23):235023.
341. Vlaisavljevich E, Greve J, Cheng X, Ives K, Shi J, Jin L, et al. Non-Invasive Ultrasound Liver Ablation Using Histotripsy: Chronic Study in an In Vivo Rodent Model. *Ultrasound in medicine & biology*. 2016;42(8):1890-902.
342. Bawiec CR, Khokhlova TD, Sapozhnikov OA, Rosnitskiy PB, Cunitz BW, Ghanem MA, et al. A Prototype Therapy System for Boiling Histotripsy in Abdominal Targets Based on a 256-Element Spiral Array. *IEEE transactions on ultrasonics, ferroelectrics, and frequency control*. 2021;68(5):1496-510.
343. Vlaisavljevich E, Owens G, Lundt J, Teofilovic D, Ives K, Duryea A, et al. Non-Invasive Liver Ablation Using Histotripsy: Preclinical Safety Study in an In Vivo Porcine Model. *Ultrasound Med Biol*. 2017;43(6):1237-51.
344. Wang Y-N, Khokhlova TD, Buravkov S, Chernikov V, Kreider W, Partanen A, et al. Mechanical decellularization of tissue volumes using boiling histotripsy. *Physics in medicine and biology*. 2018;63(23):235023-.
345. Joung C, Heo J, Pahk KJ, Pahk K. Boiling histotripsy exhibits anti-fibrotic effects in animal models of liver fibrosis. *Scientific Reports*. 2024;14(1):15099.
346. Khokhlova TD, Wang Y-N, Simon JC, Cunitz BW, Starr F, Paun M, et al. Ultrasound-guided tissue fractionation by high intensity focused ultrasound in an in vivo porcine liver model. *Proceedings of the National Academy of Sciences*. 2014;111(22):8161-6.
347. Heo J, Joung C, Pahk K, Pahk KJ. Investigation of the long-term healing response of the liver to boiling histotripsy treatment in vivo. *Scientific Reports*. 2022;12(1).

348. Pahk KJ, Mohammad GH, Malago M, Saffari N, Dhar DK. A Novel Approach to Ultrasound-Mediated Tissue Decellularization and Intra-Hepatic Cell Delivery in Rats. *Ultrasound Med Biol*. 2016;42(8):1958-67.
349. Lu P, Takai K, Weaver VM, Werb Z. Extracellular matrix degradation and remodeling in development and disease. *Cold Spring Harb Perspect Biol*. 2011;3(12).
350. Daley WP, Peters SB, Larsen M. Extracellular matrix dynamics in development and regenerative medicine. *Journal of Cell Science*. 2008;121(3):255-64.
351. Hynes RO. The extracellular matrix: not just pretty fibrils. *Science*. 2009;326(5957):1216-9.
352. Lopez JI, Mouw JK, Weaver VM. Biomechanical regulation of cell orientation and fate. *Oncogene*. 2008;27(55):6981-93.
353. Cui N, Hu M, Khalil RA. Biochemical and Biological Attributes of Matrix Metalloproteinases. Elsevier; 2017. p. 1-73.
354. Wang Y-N, Khokhlova T, Maxwell A, Kreider W, Partanen A, Farr N, et al. Tissue decellularization with boiling histotripsy and the potential in regenerative medicine. *The Journal of the Acoustical Society of America*. 2014;136(4):2278-.
355. Hendricks-Wenger A, Hutchison R, Vlaisavljevich E, Allen IC. Immunological Effects of Histotripsy for Cancer Therapy. *Frontiers in Oncology*. 2021;11.
356. Nam GH, Pahk KJ, Jeon S, Park HJ, Kim GB, Oh SJ, et al. Investigation of the Potential Immunological Effects of Boiling Histotripsy for Cancer Treatment. *Advanced Therapeutics*. 2020;3(8):1900214.
357. Julier Z, Park AJ, Briquez PS, Martino MM. Promoting tissue regeneration by modulating the immune system. *Acta Biomater*. 2017;53:13-28.
358. Simon JC, Sapozhnikov OA, Wang YN, Khokhlova VA, Crum LA, Bailey MR. Investigation into the mechanisms of tissue atomization by high-intensity focused ultrasound. *Ultrasound Med Biol*. 2015;41(5):1372-85.
359. Khokhlova TD, Schade GR, Wang YN, Buravkov SV, Chernikov VP, Simon JC, et al. Pilot in vivo studies on transcutaneous boiling histotripsy in porcine liver and kidney. *Sci Rep*. 2019;9(1):20176.
360. Khokhlova TD, Wang YN, Simon JC, Cunitz BW, Starr F, Paun M, et al. Ultrasound-guided tissue fractionation by high intensity focused ultrasound in an in vivo porcine liver model. *Proc Natl Acad Sci U S A*. 2014;111(22):8161-6.
361. Kim Y, Vlaisavljevich E, Owens GE, Allen SP, Cain CA, Xu Z. In vivo transcostal histotripsy therapy without aberration correction. *Phys Med Biol*. 2014;59(11):2553-68.
362. Longo KC, Knott EA, Watson RF, Swietlik JF, Vlaisavljevich E, Smolock AR, et al. Robotically Assisted Sonic Therapy (RAST) for Noninvasive Hepatic Ablation in a Porcine Model: Mitigation of Body Wall Damage with a Modified Pulse Sequence. *Cardiovasc Intervent Radiol*. 2019;42(7):1016-23.
363. Kim Y, Fifer CG, Gelehrter SK, Owens GE, Berman DR, Vlaisavljevich E, et al. Developmental impact and lesion maturation of histotripsy-mediated non-invasive tissue ablation in a fetal sheep model. *Ultrasound Med Biol*. 2013;39(6):1047-55.
364. Kim Y, Gelehrter SK, Fifer CG, Lu JC, Owens GE, Berman DR, et al. Non-invasive pulsed cavitation ultrasound for fetal tissue ablation: feasibility study in a fetal sheep model. *Ultrasound Obstet Gynecol*. 2011;37(4):450-7.
365. Vlaisavljevich E, Greve J, Cheng X, Ives K, Shi J, Jin L, et al. Non-Invasive Ultrasound Liver Ablation Using Histotripsy: Chronic Study in an In Vivo Rodent Model. *Ultrasound Med Biol*. 2016;42(8):1890-902.

366. Vlaisavljevich E, Kim Y, Owens G, Roberts W, Cain C, Xu Z. Effects of tissue mechanical properties on susceptibility to histotripsy-induced tissue damage. *Physics in medicine and biology*. 2014;59(2):253-70.
367. Smolock AR, Cristescu MM, Vlaisavljevich E, Gendron-Fitzpatrick A, Green C, Cannata J, et al. Robotically Assisted Sonic Therapy as a Noninvasive Nonthermal Ablation Modality: Proof of Concept in a Porcine Liver Model. *Radiology*. 2018;287(2):485-93.
368. Pahk KJ, de Andrade MO, G  lat P, Kim H, Saffari N. Mechanical damage induced by the appearance of rectified bubble growth in a viscoelastic medium during boiling histotripsy exposure. *Ultrason Sonochem*. 2019;53:164-77.
369. Worlikar T, Vlaisavljevich E, Gerhardson T, Greve J, Wan S, Kuruvilla S, et al. Histotripsy for Non-Invasive Ablation of Hepatocellular Carcinoma (HCC) Tumor in a Subcutaneous Xenograft Murine Model. Conference proceedings : Annual International Conference of the IEEE Engineering in Medicine and Biology Society IEEE Engineering in Medicine and Biology Society Annual Conference. 2018;2018:6064-7.
370. Lundt JE, Allen SP, Shi J, Hall TL, Cain CA, Xu Z. Non-invasive, Rapid Ablation of Tissue Volume Using Histotripsy. *Ultrasound Med Biol*. 2017;43(12):2834-47.
371. Rog CJ, Alassas M, Ong E. Histotripsy—A Novel and Intriguing Technique of Liver Ablation. *JAMA Surgery*. 2024.
372. Soneson JE. A User-Friendly Software Package for HIFU Simulation. *AIP Conference Proceedings*. 2009;1113(1):165-9.
373. de Andrade MO, Haqshenas SR, Pahk KJ, Saffari N. The effects of ultrasound pressure and temperature fields in millisecond bubble nucleation. *Ultrason Sonochem*. 2019;55:262-72.
374. Canney MS, Bailey MR, Crum LA, Khokhlova VA, Sapozhnikov OA. Acoustic characterization of high intensity focused ultrasound fields: A combined measurement and modeling approach. *The Journal of the Acoustical Society of America*. 2008;124(4):2406-20.
375. Pahk KJ, G  lat P, Sinden D, Dhar DK, Saffari N. Numerical and Experimental Study of Mechanisms Involved in Boiling Histotripsy. *Ultrasound in medicine & biology*. 2017;43(12):2848-61.
376. Pahk KJ, de Andrade MO, G  lat P, Kim H, Saffari N. Mechanical damage induced by the appearance of rectified bubble growth in a viscoelastic medium during boiling histotripsy exposure. *Ultrasonics Sonochemistry*. 2019;53:164-77.
377. Pahk KJ, G  lat P, Sinden D, Dhar DK, Saffari N. Numerical and Experimental Study of Mechanisms Involved in Boiling Histotripsy. *Ultrasound Med Biol*. 2017;43(12):2848-61.
378. Khokhlova TD, Canney MS, Khokhlova VA, Sapozhnikov OA, Crum LA, Bailey MR. Controlled tissue emulsification produced by high intensity focused ultrasound shock waves and millisecond boiling. *J Acoust Soc Am*. 2011;130(5):3498-510.
379. Ferro A, Mestre T, Carneiro P, Sahumbaiev I, Seruca R, Sanches JM. Blue intensity matters for cell cycle profiling in fluorescence DAPI-stained images. *Laboratory Investigation*. 2017;97(5):615-25.
380. Meny  rt O, Harami-Papp H, Sukumar S, Sch  fer R, Magnani L, de Barrios O, et al. Guidelines for the selection of functional assays to evaluate the hallmarks of cancer. *Biochimica et Biophysica Acta (BBA) - Reviews on Cancer*. 2016;1866(2):300-19.
381. Lucendo-Villarin B, Rashidi H, Alhaque S, Fischer L, Meseguer-Ripolles J, Wang Y, et al. Serum Free Production of Three-dimensional Human Hepatospheres from Pluripotent Stem Cells. *Journal of Visualized Experiments*. 2019(149).

382. Rashidi H, Khalil A, Froghi S, Hall A, Gelat P, Davidson B, et al. The safety and efficacy of Ultrasound Histotripsy and human pluripotent stem cell-derived hepatic spheroid implantation as a potential therapy for treatment of congenital metabolic liver disease: assessment in an immunocompetent rodent model. *bioRxiv*. 2024:2024.11.08.622652.
383. Rashidi H, Luu N-T, Alwahsh SM, Ginai M, Alhaque S, Dong H, et al. 3D human liver tissue from pluripotent stem cells displays stable phenotype in vitro and supports compromised liver function in vivo. *Archives of Toxicology*. 2018;92(10):3117-29.
384. W.W R. Development and translation of histotripsy: Current status and future directions. *Current Opinion in Urology*. 2014.
385. Pahk KJ, Mohammad GH, Malago M, Saffari N, Dhar DK. A Novel Approach to Ultrasound-Mediated Tissue Decellularization and Intra-Hepatic Cell Delivery in Rats. *Ultrasound in Medicine and Biology*. 2016.
386. He M, Callanan A. Comparison of methods for whole-organ decellularization in tissue engineering of bioartificial organs. 2013.
387. Gilpin A, Yang Y. Decellularization Strategies for Regenerative Medicine: From Processing Techniques to Applications. *BioMed Research International*. 2017;2017:1-13.
388. Miles CA, Bailey AJ. Thermal denaturation of collagen revisited. *Proceedings / Indian Academy of Sciences*. 1999;111(1):71-80.
389. de Andrade MO, Haqshenas SR, Pahk KJ, Saffari N. The effects of ultrasound pressure and temperature fields in millisecond bubble nucleation. *Ultrasonics Sonochemistry*. 2019.
390. Maxwell A, Sapozhnikov O, Bailey M, Crum L, Xu Z, Fowlkes B, et al. Disintegration of Tissue Using High Intensity Focused Ultrasound: Two Approaches That Utilize Shock Waves. *Acoustics Today*. 2012.
391. Khokhlova TD, Canney MS, Khokhlova VA, Sapozhnikov OA, Crum LA, Bailey MR. Controlled tissue emulsification produced by high intensity focused ultrasound shock waves and millisecond boiling. *The Journal of the Acoustical Society of America*. 2011.
392. Garczyńska K, Tzschätzsch H, Assili S, Kühl AA, Häckel A, Schellenberger E, et al. Effect of Post-mortem Interval and Perfusion on the Biophysical Properties of ex vivo Liver Tissue Investigated Longitudinally by MRE and DWI. *Frontiers in Physiology*. 2021;12.
393. Greiner C, Grainger S, Farrow S, Davis A, Su JL, Saybolt MD, et al. Robust quantitative assessment of collagen fibers with picrosirius red stain and linearly polarized light as demonstrated on atherosclerotic plaque samples. *PloS one*. 2021;16(3):e0248068.
394. Wang Y-N, Khokhlova T, Maxwell A, Kreider W, Partanen A, Farr N, et al. Tissue decellularization with boiling histotripsy and the potential in regenerative medicine. *The Journal of the Acoustical Society of America*. 2014.
395. Pahk KJ, de Andrade MO, Glat P, Kim H, Saffari N. Mechanical damage induced by the appearance of rectified bubble growth in a viscoelastic medium during boiling histotripsy exposure. *Ultrasonics Sonochemistry*. 2019.
396. Guyette JP, Gilpin SE, Charest JM, Tapias LF, Ren X, Ott HC. Perfusion decellularization of whole organs. *Nature Protocols*. 2014;9(6):1451-68.
397. Hillebrandt K, Polenz D, Butter A, Tang P, Reutzel-Selke A, Andreou A, et al. Procedure for Decellularization of Rat Livers in an Oscillating-pressure Perfusion Device. *J Vis Exp*. 2015(102):e53029.
398. Struecker B, Hillebrandt KH, Voithl R, Butter A, Schmuck RB, Reutzel-Selke A, et al. Porcine liver decellularization under oscillating pressure conditions: a technical

refinement to improve the homogeneity of the decellularization process. *Tissue Eng Part C Methods*. 2015;21(3):303-13.

399. Willemse J, Verstegen MMA, Vermeulen A, Schurink IJ, Roest HP, van der Laan LJW, et al. Fast, robust and effective decellularization of whole human livers using mild detergents and pressure controlled perfusion. *Mater Sci Eng C Mater Biol Appl*. 2020;108:110200.

400. Khokhlova TD, Wang YN, Simon JC, Cunitz BW, Starr F, Paun M, et al. Ultrasound-guided tissue fractionation by high intensity focused ultrasound in an in vivo porcine liver model. *Proceedings of the National Academy of Sciences of the United States of America*. 2014.

401. Keikhosravi A, Shribak M, Conklin MW, Liu Y, Li B, Loeffler A, et al. Real-time polarization microscopy of fibrillar collagen in histopathology. *Scientific Reports*. 2021;11(1).

402. Rojkind M, Giambrone M-A, Biempica L. Collagen Types in Normal and Cirrhotic Liver. *Gastroenterology*. 1979;76(4):710-9.

403. Rojkind M, Martinez-Palomo A. Increase in type I and type III collagens in human alcoholic liver cirrhosis. *Proceedings of the National Academy of Sciences*. 1976;73(2):539-43.

404. Seyer JM, Hutcheson ET, Kang AH. Collagen polymorphism in normal and cirrhotic human liver. *Journal of Clinical Investigation*. 1977;59(2):241-8.

405. Best SL, Liu Y, Keikhosravi A, Drifka CR, Woo KM, Mehta GS, et al. Collagen organization of renal cell carcinoma differs between low and high grade tumors. *BMC Cancer*. 2019;19(1):490.

406. Provenzano PP, Inman DR, Eliceiri KW, Knittel JG, Yan L, Rueden CT, et al. Collagen density promotes mammary tumor initiation and progression. *BMC Med*. 2008;6:11.

407. Cicchi R, Massi D, Sestini S, Carli P, De Giorgi V, Lotti T, et al. Multidimensional non-linear laser imaging of Basal Cell Carcinoma. *Opt Express*. 2007;15(16):10135-48.

408. Ekataksin W, Wake K. Liver units in three dimensions: I. Organization of argyrophilic connective tissue skeleton in porcine liver with particular reference to the "compound hepatic lobule". *Am J Anat*. 1991;191(2):113-53.

409. Lattouf R, Younes R, Lutomski D, Naaman N, Godeau G, Senni K, et al. Picrosirius red staining: a useful tool to appraise collagen networks in normal and pathological tissues. *J Histochem Cytochem*. 2014;62(10):751-8.

410. Whittaker P, Kloner RA, Boughner DR, Pickering JG. Quantitative assessment of myocardial collagen with picrosirius red staining and circularly polarized light. *Basic Research in Cardiology*. 1994;89(5):397-410.

411. Vogel B, Siebert H, Hofmann U, Frantz S. Determination of collagen content within picrosirius red stained paraffin-embedded tissue sections using fluorescence microscopy. *MethodsX*. 2015;2:124-34.

412. Provenzano PP, Cuevas C, Chang AE, Goel VK, Von Hoff DD, Hingorani SR. Enzymatic targeting of the stroma ablates physical barriers to treatment of pancreatic ductal adenocarcinoma. *Cancer Cell*. 2012;21(3):418-29.

413. Arun Gopinathan P, Kokila G, Jyothi M, Ananjan C, Pradeep L, Humaira Nazir S. Study of Collagen Birefringence in Different Grades of Oral Squamous Cell Carcinoma Using Picrosirius Red and Polarized Light Microscopy. *Scientifica (Cairo)*. 2015;2015:802980.

414. Bordoloi B, Siddiqui S, Jaiswal R, Tandon A, Jain A, Chaturvedi R. A quantitative and qualitative comparative analysis of collagen fibers to determine the role of connective

- tissue stroma in oral squamous cell carcinoma using special stains and polarized microscopy. *J Oral Maxillofac Pathol.* 2020;24(2):398.
415. López De Padilla CM, Coenen MJ, Tovar A, De la Vega RE, Evans CH, Müller SA. Picrosirius Red Staining: Revisiting Its Application to the Qualitative and Quantitative Assessment of Collagen Type I and Type III in Tendon. *Journal of Histochemistry & Cytochemistry.* 2021;69(10):633-43.
 416. Hussey GS, Dziki JL, Badylak SF. Extracellular matrix-based materials for regenerative medicine. *Nature Reviews Materials.* 2018;3(7):159-73.
 417. Hall TL, Fowlkes JB, Cain CA, editors. Imaging feedback of tissue liquefaction (histotripsy) in ultrasound surgery. *IEEE Ultrasonics Symposium*, 2005; 2005 18-21 Sept. 2005.
 418. Canney MS, Khokhlova VA, Bessonova OV, Bailey MR, Crum LA. Shock-Induced Heating and Millisecond Boiling in Gels and Tissue Due to High Intensity Focused Ultrasound. *Ultrasound in Medicine & Biology.* 2010;36(2):250-67.
 419. Eranki A, Farr N, Partanen A, V. Sharma K, Chen H, Rossi CT, et al. Boiling histotripsy lesion characterization on a clinical magnetic resonance imaging-guided high intensity focused ultrasound system. *PloS one.* 2017;12(3):e0173867.
 420. Khokhlova TD, Haider YA, Maxwell AD, Kreider W, Bailey MR, Khokhlova VA. Dependence of Boiling Histotripsy Treatment Efficiency on HIFU Frequency and Focal Pressure Levels. *Ultrasound Med Biol.* 2017;43(9):1975-85.
 421. Worlikar T, Vlasisavljevich E, Gerhardson T, Greve J, Wan S, Kuruvilla S, et al. Histotripsy for Non-Invasive Ablation of Hepatocellular Carcinoma (HCC) Tumor in a Subcutaneous Xenograft Murine Model. *Annu Int Conf IEEE Eng Med Biol Soc.* 2018;2018:6064-7.
 422. Pahk KJ, Shin C-H, Bae IY, Yang Y, Kim S-H, Pahk K, et al. Boiling Histotripsy-induced Partial Mechanical Ablation Modulates Tumour Microenvironment by Promoting Immunogenic Cell Death of Cancers. *Scientific Reports.* 2019;9(1).
 423. Dubinsky TJ, Khokhlova TD, Khokhlova V, Schade GR. Histotripsy: The Next Generation of High-Intensity Focused Ultrasound for Focal Prostate Cancer Therapy. *Journal of Ultrasound in Medicine.* 2020;39(6):1057-67.
 424. Sehmbi AS, Froghi S, Oliveira De Andrade M, Saffari N, Fuller B, Quaglia A, et al. Systematic review of the role of high intensity focused ultrasound (HIFU) in treating malignant lesions of the hepatobiliary system. *HPB.* 2021;23(2):187-96.
 425. Pitt WG, Hussein GA, Staples BJ. Ultrasonic drug delivery--a general review. *Expert Opin Drug Deliv.* 2004;1(1):37-56.
 426. Singh MP, Sethuraman SN, Miller C, Malayer J, Ranjan A. Boiling histotripsy and in-situ CD40 stimulation improve the checkpoint blockade therapy of poorly immunogenic tumors. *Theranostics.* 2021;11(2):540-54.
 427. Simon JC, Sapozhnikov OA, Khokhlova VA, Wang Y-N, Crum LA, Bailey MR. Ultrasonic atomization of tissue and its role in tissue fractionation by high intensity focused ultrasound. *Physics in medicine and biology.* 2012;57(23):8061-78.
 428. Simon JC, Sapozhnikov OA, Wang Y-N, Khokhlova VA, Crum LA, Bailey MR. Investigation into the Mechanisms of Tissue Atomization by High-Intensity Focused Ultrasound. *Ultrasound in Medicine & Biology.* 2015;41(5):1372-85.
 429. Vlasisavljevich E, Xu Z, Arvidson A, Jin L, Roberts W, Cain C. Effects of Thermal Preconditioning on Tissue Susceptibility to Histotripsy. *Ultrasound in medicine & biology.* 2015;41(11):2938-54.
 430. Macoskey JJ, Zhang X, Hall TL, Shi J, Beig SA, Johnsen E, et al. Bubble-Induced Color Doppler Feedback Correlates with Histotripsy-Induced Destruction of Structural Components in Liver Tissue. *Ultrasound Med Biol.* 2018;44(3):602-12.

431. Ntonas A, Katsourakis A, Galanis N, Filo E, Noussios G. Comparative Anatomical Study Between the Human and Swine Liver and Its Importance in Xenotransplantation. *Cureus*. 2020.
432. Wang YN, Khokhlova T, Bailey M, Hwang JH, Khokhlova V. Histological and biochemical analysis of mechanical and thermal bioeffects in boiling histotripsy lesions induced by high intensity focused ultrasound. *Ultrasound Med Biol*. 2013;39(3):424-38.
433. Rai R, Richardson C, Flecknell P, Robertson H, Burt A, Manas DM. Study of apoptosis and heat shock protein (HSP) expression in hepatocytes following radiofrequency ablation (RFA). *J Surg Res*. 2005;129(1):147-51.
434. Luo W, Zhou X, Gong X, Zheng M, Zhang J, Guo X. Study of sequential histopathologic changes, apoptosis, and cell proliferation in rabbit livers after high-intensity focused ultrasound ablation. *Journal of ultrasound in medicine : official journal of the American Institute of Ultrasound in Medicine*. 2007;26(4):477-85.
435. Khokhlova VA, Fowlkes JB, Roberts WW, Schade GR, Xu Z, Khokhlova TD, et al. Histotripsy methods in mechanical disintegration of tissue: towards clinical applications. *Int J Hyperthermia*. 2015;31(2):145-62.
436. Tang J, Godlewski G, Rouy S, Delacrétaiz G. Morphologic changes in collagen fibers after 830 nm diode laser welding. *Lasers in surgery and medicine*. 1997;21(5):438-43.
437. Tang J, Zeng F, Savage H, Ho PP, Alfano RR. Laser irradiative tissue probed in situ by collagen 380-nm fluorescence imaging. *Lasers in surgery and medicine*. 2000;27(2):158-64.
438. Singh S, Siriwardana PN, Johnston EW, Watkins J, Bandula S, Illing R, et al. Perivascular extension of microwave ablation zone: demonstrated using an ex vivo porcine perfusion liver model<sup/>. *Int J Hyperthermia*. 2018;34(7):1114-20.
439. Iansante V, Mitry RR, Filippi C, Fitzpatrick E, Dhawan A. Human hepatocyte transplantation for liver disease: current status and future perspectives. *Pediatric Research*. 2018;83(1-2):232-40.
440. Dhawan A, Puppi J, Hughes RD, Mitry RR. Human hepatocyte transplantation: current experience and future challenges. *Nature Reviews Gastroenterology & Hepatology*. 2010;7(5):288-98.
441. Hughes RD, Mitry RR, Dhawan A, Lehec SC, Girlanda R, Rela M, et al. Isolation of hepatocytes from livers from non-heart-beating donors for cell transplantation. *2006;12(5):713-7*.
442. Allen KJ, Soriano HE. Liver cell transplantation: The road to clinical application. *Journal of Laboratory and Clinical Medicine*. 2001;138(5):298-312.
443. Fisher RA, Strom SC. Human Hepatocyte Transplantation: Worldwide Results. *Transplantation*. 2006;82(4):441-9.
444. Puppi J, Strom SC, Hughes RD, Bansal S, Castell JV, Dagher I, et al. Improving the Techniques for Human Hepatocyte Transplantation: Report from a Consensus Meeting in London. *Cell Transplantation*. 2012;21(1):1-10.
445. Mitry RR, Hughes RD, Dhawan A. Progress in human hepatocytes: isolation, culture & cryopreservation. *Seminars in Cell & Developmental Biology*. 2002;13(6):463-7.
446. Kegel V, Deharde D, Pfeiffer E, Zeilinger K, Seehofer D, Damm G. Protocol for Isolation of Primary Human Hepatocytes and Corresponding Major Populations of Non-parenchymal Liver Cells. *J Vis Exp*. 2016(109):e53069.
447. Yu Y, Fisher JE, Lillegard JB, Rodysill B, Amiot B, Nyberg SL. Cell therapies for liver diseases. *Liver transplantation : official publication of the American Association*

- for the Study of Liver Diseases and the International Liver Transplantation Society. 2012;18(1):9-21.
448. Pahk KJ, G  lat P, Kim H, Saffari N. Bubble dynamics in boiling histotripsy. *Ultrasound in Medicine and Biology*. 2018;44(12):2673-96.
 449. Pahk KJ, Mohammad GH, Malago M, Saffari N, Dhar DK. A Novel Approach to Ultrasound-Mediated Tissue Decellularization and Intra-Hepatic Cell Delivery in Rats. *Ultrasound in Medicine & Biology*. 2016;42(8):1958-67.
 450. Berry MN. HIGH-YIELD PREPARATION OF ISOLATED RAT LIVER PARENCHYMAL CELLS: A Biochemical and Fine Structural Study. *The Journal of Cell Biology*. 1969;43(3):506-20.
 451. Zhao L-Y, Liu S, Chen Z-G, Zou J-Z, Wu F. Cavitation enhances coagulated size during pulsed high-intensity focussed ultrasound ablation in an isolated liver perfusion system. *International Journal of Hyperthermia*. 2017;33(3):343-53.
 452. Cosgrove D, Lassau N. Imaging of perfusion using ultrasound. *Eur J Nucl Med Mol Imaging*. 2010;37 Suppl 1:S65-85.
 453. Dijkmans PA, Juffermans LJM, Musters RJP, van Wamel A, ten Cate FJ, van Gilst W, et al. Microbubbles and ultrasound: from diagnosis to therapy. *European Journal of Echocardiography*. 2004;5(4):245-6.
 454. Khokhlova TD, Schade GR, Wang Y-N, Buravkov SV, Chernikov VP, Simon JC, et al. Pilot in vivo studies on transcutaneous boiling histotripsy in porcine liver and kidney. *Scientific Reports*. 2019;9(1):20176.
 455. Panconesi R, Flores Carvalho M, Mueller M, Meierhofer D, Dutkowski P, Muiesan P, et al. Viability Assessment in Liver Transplantation—What Is the Impact of Dynamic Organ Preservation? *Biomedicines*. 2021;9(2):161.
 456. Venema LH, Brat A, Moers C, t Hart NA, Ploeg RJ, Hannaert P, et al. Effects of Oxygen During Long-term Hypothermic Machine Perfusion in a Porcine Model of Kidney Donation After Circulatory Death. *Transplantation*. 2019;103(10):2057-64.
 457. Vlaisavljevich E, Cain CA, Xu Z, editors. The effect of histotripsy on tissues with different mechanical properties. 2011 IEEE International Ultrasonics Symposium; 2011 18-21 Oct. 2011.
 458. Vlaisavljevich E, Kim Y, Owens G, Roberts W, Cain C, Xu Z. Effects of tissue mechanical properties on susceptibility to histotripsy-induced tissue damage. *Physics in Medicine and Biology*. 2014;59(2):253-70.
 459. Schurink IJ, Willemse J, Verstegen MMA, Laan LJW, Jonge J. Long-Term Perfusion of the Liver Outside the Body: Warming Up for <i>Ex Vivo</i> Therapies? *Hepatology*. 2020;72(4):1485-7.
 460. Hafez, T.; Fuller, B.J.; Ch9 Organ Preservation for Transplantation in *Advances in Biopreservation*. Boca Raton: CRC Press. Baust JE, Baust, J. (Ed.). editor: Taylor & Francis; 2007.
 461. Drochmans P. Isolation and subfractionation on ficoll gradients of adult rat hepatocytes. Size, morphology, and biochemical characteristics of cell fractions. 1975;66(1):1-22.
 462. Lee SML, Schelcher C, Demmel M, Hauner M, Thasler WE. Isolation of Human Hepatocytes by a Two-step Collagenase Perfusion Procedure. *Journal of Visualized Experiments*. 2013(79).
 463. Hameed AM, Laurence JM, Lam VWT, Pleass HC, Hawthorne WJ. A systematic review and meta-analysis of cold in situ perfusion and preservation of the hepatic allograft: Working toward a unified approach. *Liver transplantation : official publication of the American Association for the Study of Liver Diseases and the International Liver Transplantation Society*. 2017;23(12):1615-27.

464. Cabral F, Miller CM, Kudrna KM, Hass BE, Daubendiek JG, Kellar BM, et al. Purification of Hepatocytes and Sinusoidal Endothelial Cells from Mouse Liver Perfusion. *Journal of Visualized Experiments*. 2018(132).
465. Shulman M, Nahmias Y. Long-Term Culture and Coculture of Primary Rat and Human Hepatocytes. Humana Press; 2012. p. 287-302.
466. Wang G, Zheng Y, Wang Y, Cai Z, Liao N, Liu J, et al. Co-culture system of hepatocytes and endothelial cells: two in vitro approaches for enhancing liver-specific functions of hepatocytes. *Cytotechnology*. 2018;70(4):1279-90.
467. Seo W. Hepatic non-parenchymal cells: Master regulators of alcoholic liver disease? *World Journal of Gastroenterology*. 2016;22(4):1348.
468. Krause P, Saghatolislam F, Koenig S, Unthan-Fechner K, Probst I. Maintaining Hepatocyte Differentiation in vitro through Co-Culture with Hepatic Stellate Cells. *In Vitro Cellular & Developmental Biology Animal*. 2009;45(5/6):205-12.
469. Bhatia SN, Balis UJ, Yarmush ML, Toner M. Effect of cell–cell interactions in preservation of cellular phenotype: cocultivation of hepatocytes and nonparenchymal cells. *The FASEB Journal*. 1999;13(14):1883-900.
470. Thomas RJ, Bhandari R, Barrett DA, Bennett AJ, Fry JR, Powe D, et al. The Effect of Three-Dimensional Co-Culture of Hepatocytes and Hepatic Stellate Cells on Key Hepatocyte Functions in vitro. *Cells Tissues Organs*. 2005;181(2):67-79.
471. Kolios G. Role of Kupffer cells in the pathogenesis of liver disease. *World Journal of Gastroenterology*. 2006;12(46):7413.
472. McQuitty CE, Williams R, Chokshi S, Urbani L. Immunomodulatory Role of the Extracellular Matrix Within the Liver Disease Microenvironment. *Frontiers in Immunology*. 2020;11.
473. Abbas N, Getachew A, You K, Shah Z, Chen Y, Tao J, et al. Kupffer cells mediate the recruitment of hepatic stellate cells into the localized liver damage. *Biochemical and Biophysical Research Communications*. 2020;529(2):474-9.
474. Cheng Q-N, Yang X, Wu J-F, Ai W-B, Ni Y-R. Interaction of non-parenchymal hepatocytes in the process of hepatic fibrosis (Review). *Mol Med Rep*. 2021;23(5):364.
475. !!! INVALID CITATION !!! (45-47).
476. Goulet F, Normand C, Morin O. Cellular interactions promote tissue-specific function, biomatrix deposition and junctional communication of primary cultured hepatocytes. 1988;8(5):1010-8.
477. Willebrords J, Crespo Yanguas S, Maes M, Decrock E, Wang N, Leybaert L, et al. Structure, Regulation and Function of Gap Junctions in Liver. *Cell Communication & Adhesion*. 2015;22(2-6):29-37.
478. Vinken M, Papeleu P, Snykers S, De Rop E, Henkens T, Chipman JK, et al. Involvement of Cell Junctions in Hepatocyte Culture Functionality. *Critical Reviews in Toxicology*. 2006;36(4):299-318.
479. Buyl K, De Kock J, Bolleyn J, Rogiers V, Vanhaecke T. Measurement of Albumin Secretion as Functionality Test in Primary Hepatocyte Cultures. *Methods Mol Biol*. 2015;1250:303-8.
480. WOODS RJ, FULLER BJ, ATTENBURROW VD, NUTT LH, HOBBS KEF. FUNCTIONAL ASSESSMENT OF HEPATOCYTES AFTER TRANSPLANTATION INTO RAT SPLEEN. *Transplantation*. 1982;33(2):123-6.
481. Raper SE, Grossman M, Rader DJ, Thoene JG, Clark BJ, Kolansky DM, et al. Safety and Feasibility of Liver-Directed Ex Vivo Gene Therapy for Homozygous Familial Hypercholesterolemia. 1996;223(2):116-26.
482. Li H, Zhang L. Liver regeneration microenvironment of hepatocellular carcinoma for prevention and therapy. *Oncotarget*. 2017;8(1):1805-13.

483. Michalopoulos GK, Bhushan B. Liver regeneration: biological and pathological mechanisms and implications. *Nat Rev Gastroenterol Hepatol*. 2021;18(1):40-55.
484. Zhang J, Zhao X, Liang L, Li J, Demirci U, Wang S. A decade of progress in liver regenerative medicine. *Biomaterials*. 2018;157:161-76.
485. Nicolas CT, Wang Y, Nyberg SL. Cell therapy in chronic liver disease. *Current Opinion in Gastroenterology*. 2016:1.
486. Dwyer BJ, Macmillan MT, Brennan PN, Forbes SJ. Cell therapy for advanced liver diseases: Repair or rebuild. *Journal of Hepatology*. 2021;74(1):185-99.
487. Becker FF. RESTORATION OF LIVER MASS FOLLOWING PARTIAL HEPATECTOMY: "SURGICAL HEPARTROPHY". I. INFLUENCE OF BLOOD FLOW. *Am J Pathol*. 1963;43(3):497-510.
488. Michalopoulos GK. Liver regeneration. *Journal of Cellular Physiology*. 2007;213(2):286-300.
489. Rashidi H, Hay DC. Serum-Free Production of Three-Dimensional Hepatospheres from Pluripotent Stem Cells. New York, NY: Springer US. p. 1-12.
490. Hendricks-Wenger A, Arnold L, Gannon J, Simon A, Singh N, Sheppard H, et al. Histotripsy Ablation in Preclinical Animal Models of Cancer and Spontaneous Tumors in Veterinary Patients: A Review. *IEEE transactions on ultrasonics, ferroelectrics, and frequency control*. 2022;69(1):5-26.
491. Froghi S, de Andrade MO, Hadi LM, Gelat P, Rashidi H, Quaglia A, et al. Liver Ultrasound Histotripsy: Novel Analysis of the Histotripsy Site Cell Constituents with Implications for Histotripsy Application in Cell Transplantation and Cancer Therapy. *Bioengineering (Basel)*. 2023;10(2).
492. Osada T, Jiang X, Zhao Y, Chen M, Kreager BC, Wu H, et al. The use of histotripsy as intratumoral immunotherapy beyond tissue ablation—the rationale for exploring the immune effects of histotripsy. *International Journal of Hyperthermia*. 2023;40(1):2263672.
493. Pahk KJ, Shin CH, Bae IY, Yang Y, Kim SH, Pahk K, et al. Boiling Histotripsy-induced Partial Mechanical Ablation Modulates Tumour Microenvironment by Promoting Immunogenic Cell Death of Cancers. *Sci Rep*. 2019;9(1):9050.
494. Hendricks-Wenger A, Hutchison R, Vlaisavljevich E, Allen IC. Immunological Effects of Histotripsy for Cancer Therapy. *Front Oncol*. 2021;11:681629.
495. Pepple AL, Guy JL, McGinnis R, Felsted AE, Song B, Hubbard R, et al. Spatiotemporal local and abscopal cell death and immune responses to histotripsy focused ultrasound tumor ablation. *Frontiers in Immunology*. 2023;14.
496. Nam G-H, Pahk KJ, Jeon S, Park H-J, Kim GB, Oh SJ, et al. Investigation of the Potential Immunological Effects of Boiling Histotripsy for Cancer Treatment. *Advanced Therapeutics*. 2020;3(8):1900214.
497. Osada T, Jiang X, Zhao Y, Chen M, Kreager BC, Wu H, et al. The use of histotripsy as intratumoral immunotherapy beyond tissue ablation—the rationale for exploring the immune effects of histotripsy. *International Journal of Hyperthermia*. 2023;40(1).
498. Hendricks AD, Sereno J, Gannon J, Zeher A, Brock RM, Betiel-White N, et al. Histotripsy ablation stimulates the innate immune system and modulates anti-tumor immunity in pancreatic cancer. *The Journal of Immunology*. 2021;206(1_Supplement):56.05-56.05.
499. Ho YJ, Li JP, Fan CH, Liu HL, Yeh CK. Ultrasound in tumor immunotherapy: Current status and future developments. *J Control Release*. 2020;323:12-23.

500. Lo T, Rudge EJM, Chase RP, Subramaniam R, Heshmati K, Lucey EM, et al. Early changes in immune cell metabolism and function are a hallmark of sleeve gastrectomy: a prospective human study. medRxiv. 2020.

Supplement 1

	Duty								Intra		Large portal tract	Large hepatic vein
	Power	cycle	Tissue SR	Cavity	Burn mark	Septa snap	Septa loos	Subcapsular	parenchymal	Gap		
NP	50p		1% Liver	Available	Available	Present	Confluent	Present	Present			
NP	50p		1% Liver	Available	Available	Absent	Focal	Present	Absent			
P	50p		1% Liver	Available	Available	Absent	Confluent	Not assessable	Present			
P	50p		1% Liver	Available	Available	Present	Confluent	Present	Present			
P	50p		1% Liver	Available	Available	Absent	Confluent	Not assessable	Present	Present	Present	Present
										Not	Not	
P	50p		1% Liver	Available	Available	Absent	Absent	Absent	Absent	Not applicable	applicable	applicable
											Not	
P	50p		1% Liver	Available	Available	Present	Confluent	Not assessable	Present	Absent	Present	applicable
P	50p		1% Liver	Available	Available	Absent	Confluent	Absent	Present	Present	Present	Present
P	50p		1% Liver	Available	Available	Empty foci	Focal	Not assessable	Present	Present	Present	Present
											Not	
P	50p		1% Liver	Available	Available	Absent	Absent	Absent	Absent	Absent	Absent	applicable
P	50p		1% Liver	Available	Available	Absent	Confluent	Present	Present	Present	Present	Involved
											Not	
P	50p		1% Liver	Available	Available	Absent	Absent	Absent	Absent	Absent	Absent	applicable Present
P	50p		1% Liver	Available	Available	Absent	Confluent	Absent	Present	Present	Present	Absent
											Not	
P	50p		1% Liver	Available	Available	Present	Patchy	Absent	Present	Absent	Present	applicable Absent
					Minute single						Not	
P	50p		1% Liver	Available	Available	cavity	Absent	Absent	Absent	Absent	Absent	applicable Present
											Not	
P	50p		1% Liver	Available	Available	Absent	Absent	Absent	Absent	Absent	Absent	applicable Present
P	50p		1% Liver	Available	Available	Present	Confluent	Absent	Present	Present	Present	Absent Involved
											Not	
P	50p		1% Liver	Available	Available	Present	Patchy	Absent	Present	Absent	Present	applicable Absent
											Not	
P	50p		1% Liver	Available	Available	Absent	Absent	Absent	Absent	Absent	Absent	applicable Absent
					Small cavities							
					subcapsular to							
					intraperenchymal							
P	50p		1% Liver	Available	Available	? Real	Patchy	Present	Present	Present	Present	Absent
P	50p		1% Liver	Available	Available	Present	Patchy	Absent	Present	Present	Present	Absent
											Not	
P	50p		1% Liver	Available	Available	Present	Absent	Present	Absent	Absent	Absent	applicable Absent
											Not	
P	100p		1% Liver	Available	Available	Present	Absent	Absent	Present	Absent	Absent	applicable Absent

P	50p	1.50% Liver	Available	Available	Absent	Absent	Absent	Absent	Absent	Absent	Not applicable	Not Absent
P	50p	1% Liver	Available	Available	Absent	Focal	Absent	Present	Absent	Present	Not applicable	Not Absent
NP	50p	1% Liver	Available	Available	Absent	Confluent	Present	Present	Absent	Present	Not applicable	Not Absent
NP	150p	1% Liver	Available	Available	Absent	Absent	Absent	Absent	Absent	Absent	Not applicable	Not Absent
P	50p	1.50% Liver	Available	Available	Present	Absent	Present	Absent	Present	Absent	Not applicable	Not Absent
P	150p	1.50% Liver	Available	Available	Present	Focal	Present	Present	Absent	Present	Not applicable	Present
P	150P	1% Liver	Available	Available	Present	Absent	Absent	Absent	Absent	Present	Not applicable	Not Absent
P	100p	1% Liver	Available	Available	Present	Absent	Absent	Present	Absent	Present	Not applicable	Not Absent
P	150p	1% Liver	Available	Available	Present	Focal	Present	Present	Absent	Present	Not applicable	Not Absent
NP	50p	1.50% Liver	Available	Available	Present	Absent	Present	Absent	Absent	Present	Not applicable	Present
P	150p	1% Liver	Available	Available	Present	Focal	Present	Present	Absent	Present	Not applicable	Present
P	150p	1% Liver	Available	Available	Present	Confluent	Present	Present	Absent	Present	Not applicable	Present
P	150p	1.50% Liver	Available	Available	Present	Focal	Present	Present	Absent	Present	Not applicable	Not Absent
P	50p	1% Liver	Available	Available	Present	Confluent	Present	Present	Present	Present	Present	Absent
P	100p	1% Liver	Available	Available	Present	Confluent	Present	Present	Absent	Present	Not applicable	Not Absent
P	50p	1% Liver	Available	Available	Present	Absent	Present	Absent	Present	Absent	Not applicable	Not Absent
P	150p	1% Liver	Available	Available	Absent	Absent	Absent	Absent	Absent	Absent	Not applicable	Present
P	100p	1.50% Liver	Available	Available	Present	Absent	Present	Absent	Present	Present	Absent	Present
P	100p	1% Liver	Available	Available	Absent	Confluent	Present	Present	Absent	Present	Not applicable	Not Absent
P	150p	1% Liver	Available	Available	Absent	Confluent	Present	Present	Absent	Present	Not applicable	Not Absent
P	50p	1% Liver	Available	Available	Present	Confluent	Present	Present	Absent	Present	Not applicable	Not Absent
P	150p	1% Liver	Available	Available	Present	Absent	Present	Absent	Absent	Present	Not applicable	Not Absent
P	50p	1.50% Liver	Available	Available	Present	Confluent	Present	Present	Absent	Present	Not applicable	Present

P	50p	1.50% Liver	Available	Available	Absent	Absent	Absent	Absent	Absent	Absent	Not applicable	Absent
P	50p	1% Liver	Available	Available	Absent	Absent	Absent	Absent	Absent	Absent	Not applicable	Absent
P	100p	1% Liver	Available	Available	Present	Confluent	Present	Present	Present	Present	Present	Present
P	100p	1% Liver	Available	Available	Present	Absent	Present	Absent	Absent	Present	Not applicable	Absent
NP	100p	1% Liver	Available	Available	Present	Patchy	Present	Present	Absent	Present	Not applicable	Absent
P	150p	1.50% Liver	Available	Available	Present	Absent	Present	Absent	Present	Present	Absent	Absent
P	150p	1.50% Liver	Available	Available	Present	Confluent	Present	Present	Absent	Present	Not applicable	Present
P	50p	1% Liver	Available	Available	Present	Absent	Present	Absent	Absent	Present	Not applicable	Absent
P	150p	1% Liver	Available	Available	Present	Confluent	Present	Present	Absent	Present	Not applicable	Absent
P	150p	1% Liver	Available	Available	Absent	Absent	Absent	Absent	Absent	Absent	Not applicable	Absent
P	150p	1% Liver	Available	Available	Absent	Confluent	Absent	Present	Absent	Present	Not applicable	Absent
NP	150p	1% Liver	Available	Available	Present	Absent	Present	Absent	Present	Present	Absent	Absent
NP	150p	1% Liver	Available	Available	Absent	Confluent	Present	Present	Absent	Absent	Not applicable	Absent
P	150p	1% Liver	Available	Available	Present	Absent	Present	Absent	Absent	Present	Not applicable	Absent
NP	50p	1% Liver	Available	Available	Present	Absent	Present	Absent	Absent	Absent	Not applicable	Absent
NP	50p	1% Liver	Available	Available	Absent	Absent	Absent	Absent	Absent	Absent	Not applicable	Absent
P	50p	1% Liver	Available	Available	Present	Absent	Present	Present	Absent	Present	Not applicable	Absent
NP	50p	1% Liver	Available	Available	Absent	Absent	Absent	Absent	Absent	Absent	Not applicable	Absent
P	50p	1% Liver	Available	Available	Present	Confluent	Present	Present	Absent	Present	Not applicable	Absent
NP	50p	1% Liver	Available	Available	Track like injury	Absent	Absent	Present	Absent	Present	Not applicable	Absent
P	50p	1% Liver	Available	Available	Absent	Absent	Absent	Absent	Absent	Absent	Not applicable	Absent
P	50p	1% Liver	Available	Available	Tissue cracks	Absent	Present	Absent	Present	Present	Absent	Absent
NP	50p	1% Liver	Available	Available	Present	Absent	Present	Absent	Present	Present	Absent	Absent
P	50p	1% Liver	Available	Available	Present	Focal	Present	Present	Absent	Present	Not applicable	Absent
NP	50p	1% Liver	Available	Available	Track like injury	Absent	Present	Present	Absent	Present	Not applicable	Absent

P	50p	1% Liver	Available	Available	Present	Absent	Present	Present	Present	Present	Absent	Absent
NP	50p	1% Liver	Available	Available	Present	Confluent	Present	Present	Absent	Present	Not applicable	Absent
P	50p	1% Liver	Available	Available	Present	Absent	Present	Absent	Present	Present	Absent	Absent
P	50p	1% Liver	Available	Available	Present	Absent	Present	Absent	Present	Present	Absent	Absent
NP	50p	1% Liver	Available	Available	Present	Focal	Present	Present	Present	Present	Absent	Absent
P	50p	1% Liver	Available	Available	Present	Absent	Present	Absent	Absent	Present	Not applicable	Absent
NP	50p	1% Liver	Available	Available	Absent	Absent	Absent	Absent	Absent	Absent	Not applicable	Absent
NP	50p	1% Liver	Available	Available	Present	Absent	Present	Absent	Present	Absent	Not applicable	Absent
P	50p	1% Liver	Available	Available	Present	Absent	Present	Absent	Present	Absent	Not applicable	Absent
P	50p	1% Liver	Available	Available	Absent	Absent	Absent	Absent	Absent	Absent	Not applicable	Absent
NP	50p	1% Liver	Available	Available	Absent	Absent	Absent	Absent	Absent	Absent	Not applicable	Absent
P	50p	1% Liver	Available	Available	Present	Absent	Present	Absent	Present	Present	Absent	Absent
P	50p	1% Liver	Available	Available	Present	Absent	Present	Absent	Present	Present	Absent	Absent
P	50p	1% Liver	Available	Available	Present	Absent	Absent	Absent	Present	Absent	Not applicable	Absent
P	50p	1% Liver	Available	Available	Present	Confluent	Present	Present	Present	Present	Absent	Absent
P	50p	1% Liver	Available	Available	Present	Patchy	Present	Present	Present	Present	Absent	Absent
P	50p	1% Liver	Available	Available	Present	Confluent	Present	Present	Absent	Present	Not applicable	Absent
P	50p	1% Liver	Available	Available	Present	Absent	Absent	Absent	Absent	Present	Not applicable	Absent
P	50p	1% Liver	Available	Available	Present	Absent	Present	Absent	Absent	Present	Not applicable	Absent

Table 18 – Supplementary data of the 91 histology slides reviewed by the expert pathologist as a second review with observations as noted above. The table marks presence or absence of the named histological features on H&E slides. P: perfused, NP: non-perfused; P in the power column refers to pulse duration.

Supplement 2

Parameter	Value
Label	Label1
Mode	Luminescence
Attenuation	AUTOMATIC
Color for OD2 Attenuation	
Integration Time	1000 ms
Settle Time	0 ms
Part of Plate	A1-H4
Start Time	23/12/2019 17:17:42
End Time	23/12/2019 17:18:38
Temperature	22.3 °C

<>	1	2	3	4
A	3	0	2	9
B	8	25	5	24
C	2	23	7	22
D	10	26	5	28
E	7	29	7	15
F	4	30	10	24
G	5	8	11	11
H	0	8	0	1

Table 19 – Incubation raw data for cell culture work and cell titre glow

Supplement 3

Animal Number:	Day 0	Day 9	Day 16	Day 23	Day 29	
1	264	266				Mid
2	252	277				Mid
3	270	285				Mid
4	255	284				Mid
5	271	286				Mid
6	276	285	316	335.1	353	Full
7	259					
8	278	291	322	343.3	364	Full
9	267	204				Mid
10	222	234				Mid
11	261	280	319	330.5	348	Full
12	243	263	282	295.9	308	Full
13	272	290	326	352.4	376.5	Full
14	265	286	321	342.6	363	Full
15	242	264	296	325.7	349.1	Full
16	260	289	312	330.5	344.9	Full

Table 20 - Animal weight during different time interval in both the mid and full termination group.

Appendix 1. Manuscripts published during the time of PhD.

Published manuscripts:

Arjan S. Sehmbi, **Saied Froghi** et al, Systematic review of the role of high intensity focused ultrasound (HIFU) in treating malignant lesions of the hepatobiliary system, HPB, Volume 23, Issue 2, 2021, Pages 187-196, <https://doi.org/10.1016/j.hpb.2020.06.013>.

Tandon R, **Froghi S**. Artificial liver support systems. J Gastroenterol Hepatol. 2021 May;36(5):1164-1179. doi: 10.1111/jgh.15255. Epub 2020 Oct 3. PMID: 32918840.

Froghi, S., Grant, C.R., Tandon, R. *et al*. New Insights on the Role of TRP Channels in Calcium Signalling and Immunomodulation: Review of Pathways and Implications for Clinical Practice. *Clinic Rev Allerg Immunol* 60, 271–292 (2021). <https://doi.org/10.1007/s12016-020-08824-3>

Froghi, S.; de Andrade, M.O.; Hadi, L.M.; Gelat, P.; Rashidi, H.; Quaglia, A.; Fuller, B.; Saffari, N.; Davidson, B. Liver Ultrasound Histotripsy: Novel Analysis of the Histotripsy Site Cell Constituents with Implications for Histotripsy Application in Cell Transplantation and Cancer Therapy. *Bioengineering* **2023**, *10*, 276. <https://doi.org/10.3390/bioengineering10020276>

Froghi, S.; Hall, A.; Hanafi Bin Jalal, A.; Andrade, M.O.d.; Mohammad Hadi, L.; Rashidi, H.; G  lat, P.; Saffari, N.; Davidson, B.; Quaglia, A. Ultrasound Histotripsy on a Viable Perfused Whole Porcine Liver: Histological Aspects, Including 3D Reconstruction of the Histotripsy Site. *Bioengineering* **2023**, *10*, 278. <https://doi.org/10.3390/bioengineering10030278>

Hassan Rashidi, Amjad Khalil, **Saied Froghi**, Andrew Hall, Pierre Gelat, Brian Davids on, Alberto Quaglia, Nader Saffari; The safety and efficacy of Ultrasound Histotripsy and

human pluripotent stem cell-derived hepatic spheroid implantation as a potential therapy for treatment of congenital metabolic liver disease: assessment in an immunocompetent rodent model

bioRxiv 2024.11.08.622652; doi: <https://doi.org/10.1101/2024.11.08.622652>

Book chapters:

1. Chapter 13: Liver Ischaemia-Reperfusion Injury
Froghi F, **Froghi S**, Davidson B.
Springer Publication. 10 Jan 2020. p129-141. Liver Diseases: A Multidisciplinary Textbook.
2. Chapter 70: Surgery in Liver Disease
Froghi S, Froghi F, Davidson B.
Springer Publication. 10 Jan 2020. p769-783. Liver Diseases: A Multidisciplinary Textbook.
3. Liver Transplantation for Malignancy Other than Hepatocellular Carcinoma
Saied Froghi, Alejandro Ramirez-Del Val, Brian R Davidson; 2023; Textbook of Liver Transplantation Volume: 1; Pages: 758-786; Publisher: PARAS Medical Publishers
4. Sriskanthanathan, A., Avini, E., Scott, A., Avini, A., **Froghi, S.**, 2024. Regenerative Strategies in Biliary Tree Development in Health and Disease. In: Rezaei, N. (Ed.), Comprehensive Hematology and Stem Cell Research, vol. 4, pp. 123–134. US: Elsevier. <https://dx.doi.org/10.1016/B978-0-443-15717-2.00089-5>. ISBN: 9780443157172 © 2024 Elsevier Inc.

Published abstracts:

Artificial liver support systems.

Tandon R, Froghi S.

J Gastroenterol Hepatol. 2021 May;36(5):1164-1179. doi: 10.1111/jgh.15255. Epub 2020 Oct 3.

PMID: 32918840

Froghi S, Sehmbi AS, Andrade MD, *et al*

P189 Role of high intensity focused ultrasound (HIFU) in treating cancerous lesions of the hepatobiliary system

Gut 2021;**70**:A141.

Froghi S, Andrade MD, Hadi LM, *et al* P190 Proof of concept & novel technique of cell harvest using histotripsy: implications in cell transplantation *Gut* 2021;70:A141-A142.